PROCEEDINGS OF THE

Japan-Bangladesh Joint Seminar on Advances in Bridge Engineering

WITH SPECIAL ATTENTION TO STEEL & COMPOSITE CONSTRUCTION

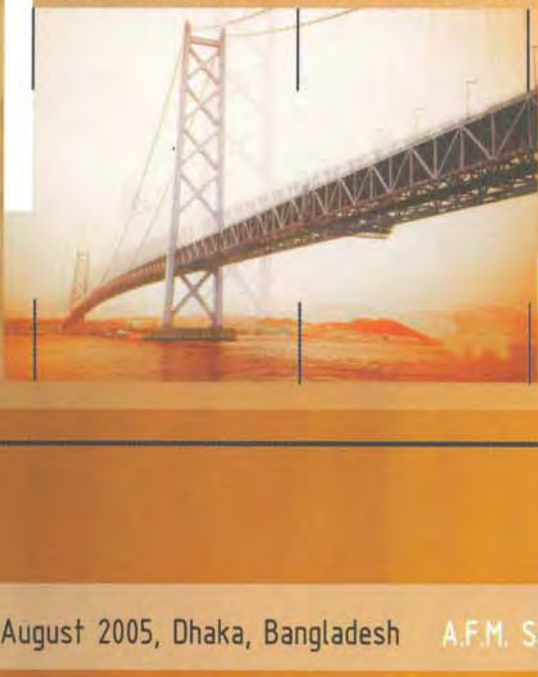

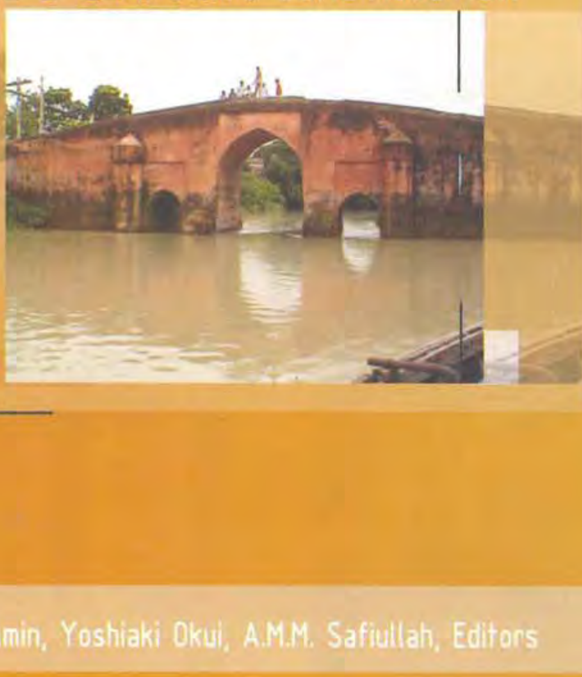

10 August 2005, Dhaka, Bangladesh

A.F.M. Saiful Amin, Yoshiaki Okui, A.M.M. Safiullah, Editors

Organized by

JSCE 社団法人 土木学会
JAPAN SOCIETY OF CIVIL ENGINEERS

Civil Engineering Division
Institution of Engineers, Bangladesh

Committee of Steel Structures
Japan Society of Civil Engineers

In association with

Jamuna Multipurpose Bridge Authority
Government of the Peoples' Republic of Bangladesh

Roads and Highways Department
Government of the Peoples' Republic of Bangladesh

Proceedings of the Japan-Bangladesh Joint Seminar on Advances in Bridge Engineering

Proceedings of the Japan-Bangladesh Joint Seminar on Advances in Bridge Engineering

Editors

Dr. A.F.M. Saiful Amin
Assistant Professor
Department of Civil Engineering
Bangladesh University of Engineering and Technology, Dhaka 1000, Bangladesh

Dr. Yoshiaki Okui
Associate Professor
Department of Civil & Environmental Engineering, Saitama University
255 Shimo Okubo, Saitama 338-8570, Japan

Dr. A.M.M. Safiullah
Professor
Department of Civil Engineering
Bangladesh University of Engineering and Technology, Dhaka 1000, Bangladesh

Organized by

JSCE 社団法人 土木学会
JAPAN SOCIETY OF CIVIL ENGINEERS

Civil Engineering Division
Institution of Engineers, Bangladesh

Committee of Steel Structures
Japan Society of Civil Engineers

In association with

Jamuna Multipurpose Bridge Authority
Government of the Peoples' Republic of Bangladesh

Roads and Highways Department
Government of the Peoples' Republic of Bangladesh

Dhaka, Bangladesh
10 August 2005

Jointly Published by:

Civil Engineering Division, The Institution of Engineers, Bangladesh.
Committee on Steel Structures, Japan Society of Civil Engineers.

August, 2005

Cover design: Masuque Hossain Tonmoy and Mostafizur Rahman

ISBN: 984-32-2520-6

Disclaimer

The texts and figures of the papers compiled in this volume were set individually by the concerned authors. The ideas or views expressed in the papers included in this volume are of individual authors. In no way these are of the Institution of Engineers, Bangladesh or the Japan Society of Civil Engineers or the Editors or the institutions to which they belong to.

On the front cover page

Left: The Akashi Kaikyo Bridge (AKB) is a three-span, two-hinged stiffening girder system suspension bridge that spans the Akashi Strait between Maiko, Tarumi-ward in Kobe, and Matsuho, on Awaji Island. After various investigations including aerodynamic tests on large scale three dimensional prototypes, actual construction of the bridge began in May 1988, and took a total of ten years. The AKB was opened to traffic on April 5, 1998. The AKB become the longest suspension bridges in the world, surpassing the Humber Bridge (England, 1,410 meter center span) by 581 meters. Although in primary design the AKB was 3,910 meters long overall, with a center span of 1,990 meters, it was extended 1 meter by the Great Hanshin Earthquake (January 17, 1995). Source: Honshu-Shikoku Bridge Authority, Japan.

Right: The photo depicts one of the known oldest bridges of Bangladesh. It is a masonry bridge built in the 17th century during Mughal period over the Mir Kadim Canal, Munshigonj, Dhaka Division. The bridge has a center arch of 4.3m span and 8.5m in height above the bed of the canal with two side arches of 2.2m span each and 5.2m high. The piers are 1.8m thick. The wings are straight back and the whole length of the bridge is 52.7m. Source: Dani, A.H. (1961). Muslim Architecture in Bengal, Asiatic Society of Pakistan Publication No. 7, Dacca. Courtesy: Engr. Emdadul Huq, Retd. Additional Chief Engineer, Public Work Department, Bangladesh. Photo: Dr. Engr. A.F.M. Saiful Amin, BUET.

Printed in Bangladesh at Tamanna Printers Pvt. Limited.

Preface

The Institution of Engineers, Bangladesh (IEB) and Japan Society of Civil Engineers (JSCE) have made an agreement of cooperation five years ago. However, there were not many opportunities for us to contact with each other on technical issues. This is for the first time, the Civil Engineering Division, IEB; is going to jointly organize a seminar on bridge engineering with Committee of Steel Structures. JSCE. The Roads and Highways Department and Jamuna Multipurpose Bridge Authority of the Government of the Peoples' Republic of Bangladesh have extended their full support for the event.

In Bangladesh, bridges form a vital component of communication infrastructure. The geographical location also puts Bangladesh in an important location to contribute in regional cooperation through participation in Asian highway network. To this end, considerable efforts were given over the last decades to construct a nationwide uninterrupted road and rail network. This drive resulted in construction of remarkable bridges over some of the major rivers and tributaries. A number of moderate to large bridge projects are now on the feasibility/design/construction phase. Steps have been taken to construct flyovers and footbridges in urban areas to aid commuter movement. On this backdrop, there exists a need to update the knowledgebase of the academicians, designers and construction industry of the country working in the field of bridge engineering by exchanging ideas and sharing the individual experiences. The seminar is expected to initiate the transfer of sustainable technologies regarding economic design, construction, use and maintenance of bridges in Bangladesh.

This proceeding contains papers contributed for the seminar by specialists from Japan and Bangladesh. The papers have been grouped into four topics of bridge engineering: Geotechnical aspects; Steel, composite bridges and advanced materials; Structural dynamics; and Instrumentation and monitoring. In order to enhance regional cooperation, the seminar aims to generate discussions on the necessity and format of a unified Bridge Code for Asian countries.

In recent years, every structural engineer in the world recognizes the importance of the international code, and is interested in the code such as ISO. We hope and trust that this seminar will be the first step to make the model code for bridges accepted in Bangladesh and Japan, and to lead to the Asian code.

We express our heartiest gratitude to Committee of Steel Structures, JSCE to initiate this program and for their active support without which this seminar could not have been possible. Also we take this opportunity to express our gratitude to the Roads and Highways Department, the Jamuna Bridge Authority, the IEB and the Civil Engineering Division of IEB to extend their full support for this event. Finally it goes without saying that the sincere hard work put in by the contributing authors deserves our praise and gratitude.

Finally, we would like to refer to the sayings of famous scientist, Sir Isaac Newton, who lamented:

Men Build Too Many Walls Not Enough Bridges

We hope this seminar will not only talk about bridges but also be able to bring the two Societies JSCE and IEB closer and build a bridge of eternal friendship between the two peoples for a world of peace and stability. This may be a very small step towards this goal, but a certain one.

A.F.M. Saiful Amin
Yoshiaki Okui
A.M.M. Safiullah

Dhaka
10 August 2005

Contents

Japan-Bangladesh Joint Seminar on Advances in Bridge Engineering ISBN: 984-32-2520-6
Dhaka, Bangladesh. 10 August 2005

Identification of dynamic parameters of the Jamuna Multipurpose Bridge in ambient transverse vibration

R. Ahsan[1*], T.M. Al-Hussaini[1], M.A. Ansary[1], M.M. Rahman[2]

[1]*Department of Civil Engineering*
Bangladesh University of Engineering and Technology, Dhaka 1000, Bangladesh.
[2]*Bangladesh Water Development Board*

Abstract

Jamuna Multipurpose Bridge, located in a seismically active region, is the most important bridge in Bangladesh. The bridge has been instrumented with sensors to monitor its behaviour. The present paper analyses ambient vibration of the pier-deck system in transverse direction and compares the recorded vibration with an SDOF model in frequency domain. The frequency spectrum of the response of the pier-deck system in ambient vibration suggests that the actual behaviour of the system is more like a Two Degree of Freedom system. An analytical model of the TDOF system is then developed in the paper and the predominant frequency of the ambient vibration of the deck is explained.

1. Introduction

The 4.8 km long Jamuna Multipurpose Bridge over the mighty Jamuna river has established the long cherished road link between the East and West of Bangladesh. The bridge site location map is shown in Fig.1. The bridge is located in a seismically active region and has been designed to resist dynamic forces due to earthquakes with peak ground acceleration as high as 0.2g [1]. JMB is the first bridge in the country where seismic pintles have been used. The pintles act as an isolation device for protection against earthquakes [2]. The bridge has also been instrumented with accelerometers [3]. The present study is aimed at identifying the dynamic parameters of the bridge in transverse vibration from the recorded data. A number of schemes for identification of the dynamic parameters of bridges have been developed in recent years [4,5]. The schemes are intended for particular applications depending on the type of bridge, nature

* Email: raquibahsan@ce.buet.ac.bd

of excitation or kind of isolation devices. In the present study dynamic parameters of the Jamuna Bridge in transvers vibration have been identified for ambient vibration. Since the study deals with low amplitude ambient vibration the effect of isolation devices is negligible. However the dynamic parameters obtained from the study are helpful in studying the behaviour of the bridge when isolation devices come into effect.

2. Bridge description

The bridge is slightly curved in plan. The main bridge is about 4.8 km long, prestressed concrete box-girder type, and consists of 47 nearly equal spans of 99.375 m. plus two smaller end spans of 64.6875 m. The main bridge is supported by twenty-one 3-pile piers and twenty-nine 2-pile piers. There are 128 m long road approach viaducts at both ends of the main bridge. There are six hinges (expansion joints) that separate the main bridge structure into seven modules (two end modules, four 7-span module and a 6-span module in the middle). For seismic protection of the Jamuna bridge, seismic protection devices consisting of steel pin dissipating elements and shock transmitter units have been placed in between the girders and the piers. Salient features of the bridge are shown in Table 1.

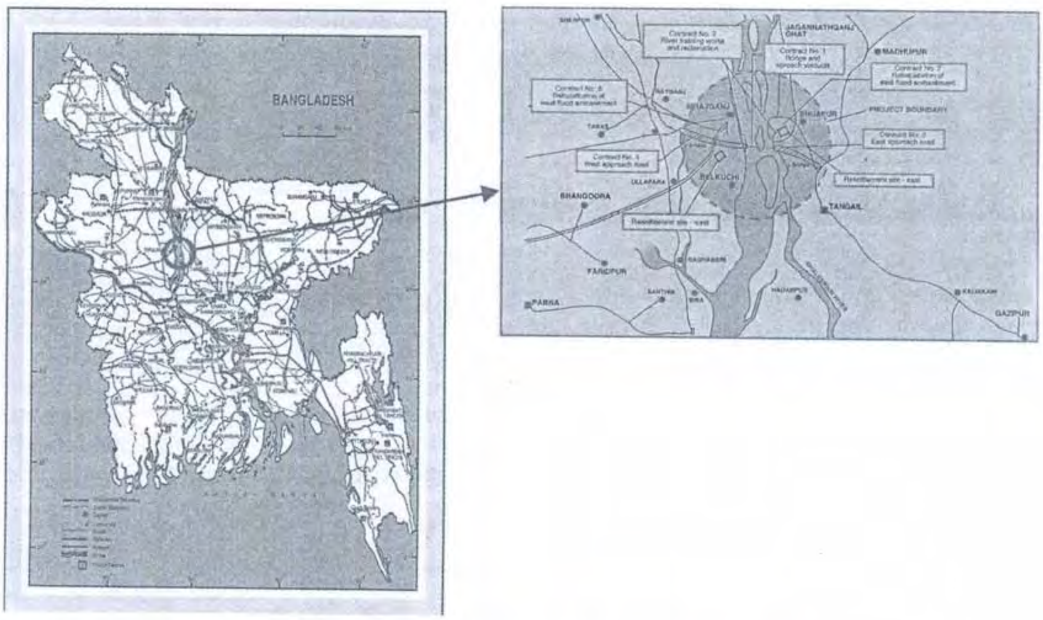

Fig. 1. Location of the Jamuna Multipurpose bridge

2.1 Pile configuration

The substructure of each module consists of three 3-pile piers and three or four 2-pile piers for the six and seven span modules respectively. The foundations consist of driven tubular steel piles, filled with concrete. Pile diameters are 3.15m for the 2-pile piers and 2.50m for the 3-pile piers, and toe levels vary from -70.Om PWD (Public Works Datum) to -82.0m PWD, with a head level of +11m PWD. The thickness of the steel tube varies along the length of the pile. Pile caps are of precast reinforced concrete shell with in-situ reinforced concrete infill construction. They have a base level of +11.0 m PWD, and so the piles are embedded some 7m within the caps. The pile caps carry pier stems which in turn support the bearings. Figure 2 shows the general arrangement of piles.

Table 1. Salient features of the bridge

Length of bridge	4.8 km
Length of viaduct of each side	128.0 m
Width of bridge	18.5 m
Number of spans	47+2
Length of each span	99.375 m
Length of end span	64.6875 m
Number of lanes	4
Number of rail-lines	1
3 Pile Pier (2500 mm OD)	21
2 Pile Pier (3150 mm OD)	29
Number of Total Piers	50
Number of Total Piles	121
Tubular steel Pile Thickness	40mm to 60mm
Average Length of Pile	83.0 m (72 m below river bed level)
Box girder segment length	4.0 m
Absolute rake of Pile (Batter Pile)	1 : 6
Pier Stem height	2.72m to 12.04m

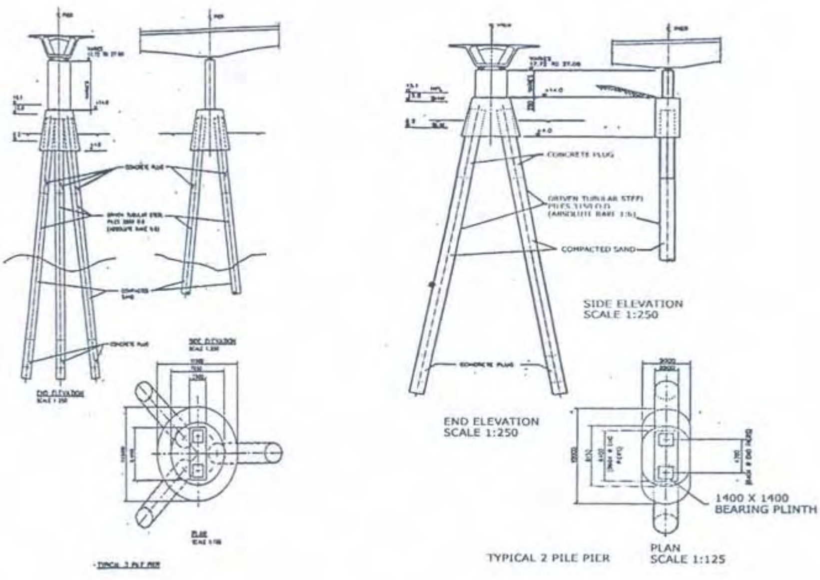

(a) (b)

Fig. 2. General arrangement of piles (a) Three pile pier (b) Two pile pier

2.2 Pier stem

The height of pier stem varies from 2.72m to 13.05m and is constructed of reinforced concrete. Figures 3 and 4 show the cross-section and elevation of the pier stem respectively. The hollow section of pier stem is filled with concrete up to 3m of ifs height. The cross-sectional properties of hollow and solid sections are given in Table 2.

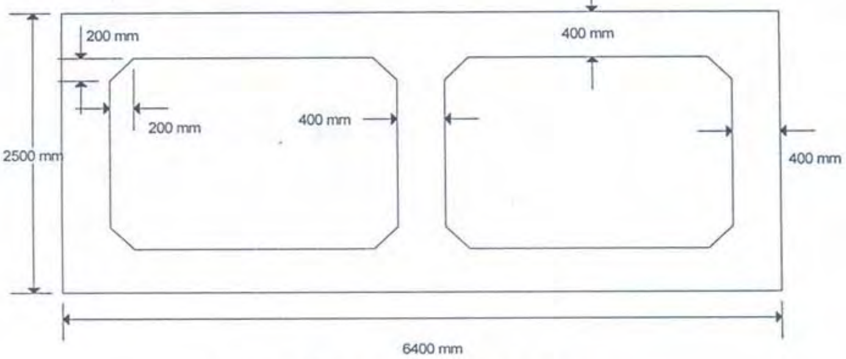

Fig. 3. Cross- section of pier stem

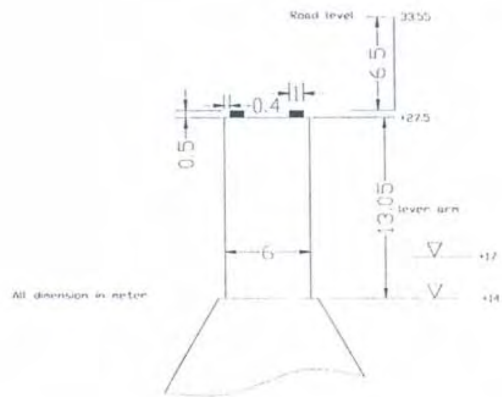

Fig. 4. Elevation of pier stem

Table 2. Cross sectional properties of pier stem

Section Type	Area, m^2	Moment of Inertia (longitudinal), m^4	Moment of Inertia (Transverse), m^4
Hollow	6.84	5.85	38.42
Solid	15.0	7.81	45.0

2.3 *Deck configuration*

The deck is of prestressed post-tensioned concrete segmental construction, with a varying depth single box section (Fig. 5). Spans cantilevering out from the piers are joined by an in-situ closure at mid-span. The width of the box-section is the same for all sections which is 18.5m but the depth varies from 6.5m at the pier top to 3.25m at midspan. Accordingly, area and moment of inertia both in longitudinal and transverse direction vary along the span.

3. Seismicity of bridge site

Professor Bolt in his report [6] on Seismicity Studies for Jamuna Bridge, Bangladesh, mentioned that the adopted site of the bridge (24.42°N, 89.75°E) could experience shaking from both great and moderate-sized distant earthquakes and from moderate near-site earthquakes during the lifetime (considered as 100 years) of the bridge structure. According to Bolt [5], only one seismic source needs to be considered in postulating strong ground shaking at the Jamuna Bridge site: Zone D at a distance of 25 to 50 km. The design peak ground acceleration is 0.2g. Bolt [6] mentioned that his work had been hampered by the lack of recordings from seismographic stations in the region. He recommended that several strong motion accelerometers should be installed near the bridge structure so that any local shaking can be measured accurately.

4. Instrumentation plan

It was planned to instrument one of the seven modules of the bridge and also to install a few sensors at the abutment. The seven-span module next to the west-end module (designated as Module 1 in the bridge design) was chosen because of its proximity to the most likely source of a major earthquake. The bridge is designed for a peak ground acceleration of 0.2g due to a 7.0 magnitude earthquake in the Bogra fault zone, which is about 25 to 40 kms from the west end of the bridge. Besides, six free field stations, three on each side of the Jamuna River, were to be setup to measure the ground motions. The stations are 70 to 90 km apart from one another forming an equilateral triangle as closely as possible on both sides of the bridge.

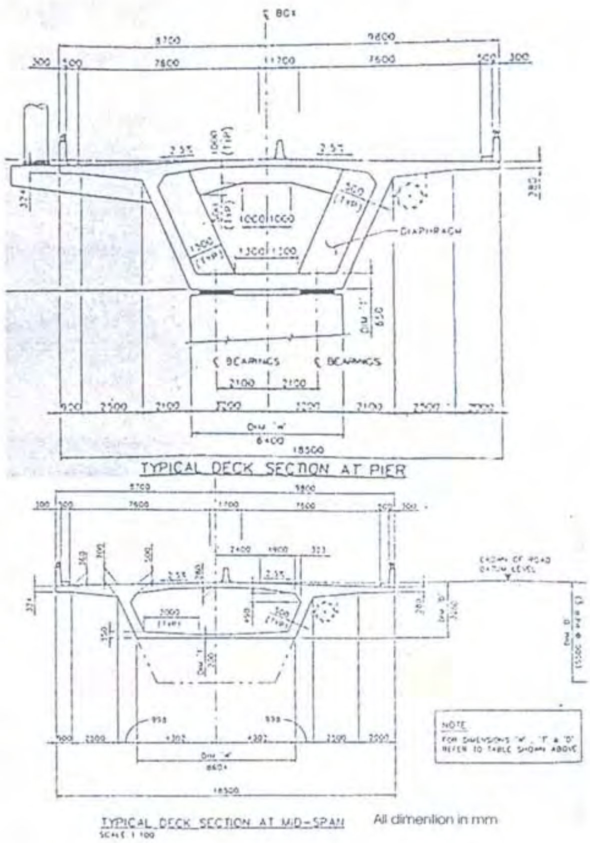

Fig. 5. Typical deck cross sections

In addition, one borehole sensor was to be placed at the West End of the bridge. There was also provision for a portable free field station to be placed at any suitable location, which could be moved if necessary.

Two triaxial, one biaxial and five uniaxial accelerometer (Model Episensor) sensors and three displacement sensors were installed on Module 1 of the bridge structure. There are thus sixteen channels of data. These data are fed to three digital K2 data recorders labelled Jamuna, Meghna and Surma. Each K2 recorder can support up to six channels of data. It was decided to place the three recorders and the communication enclosure close to one another within the box girder deck (Fig.6) near Pier P10.

All the sensors were placed in their designated positions and each of them connected to one particular channel of a recorder. These were connected to one communication enclosure for data transfer to the Data control centre server through the 2.4 GHz wireless radio and antenna hoisted on a lamp post of the bridge (Fig.7). The system was set at UTC time through a GPS.

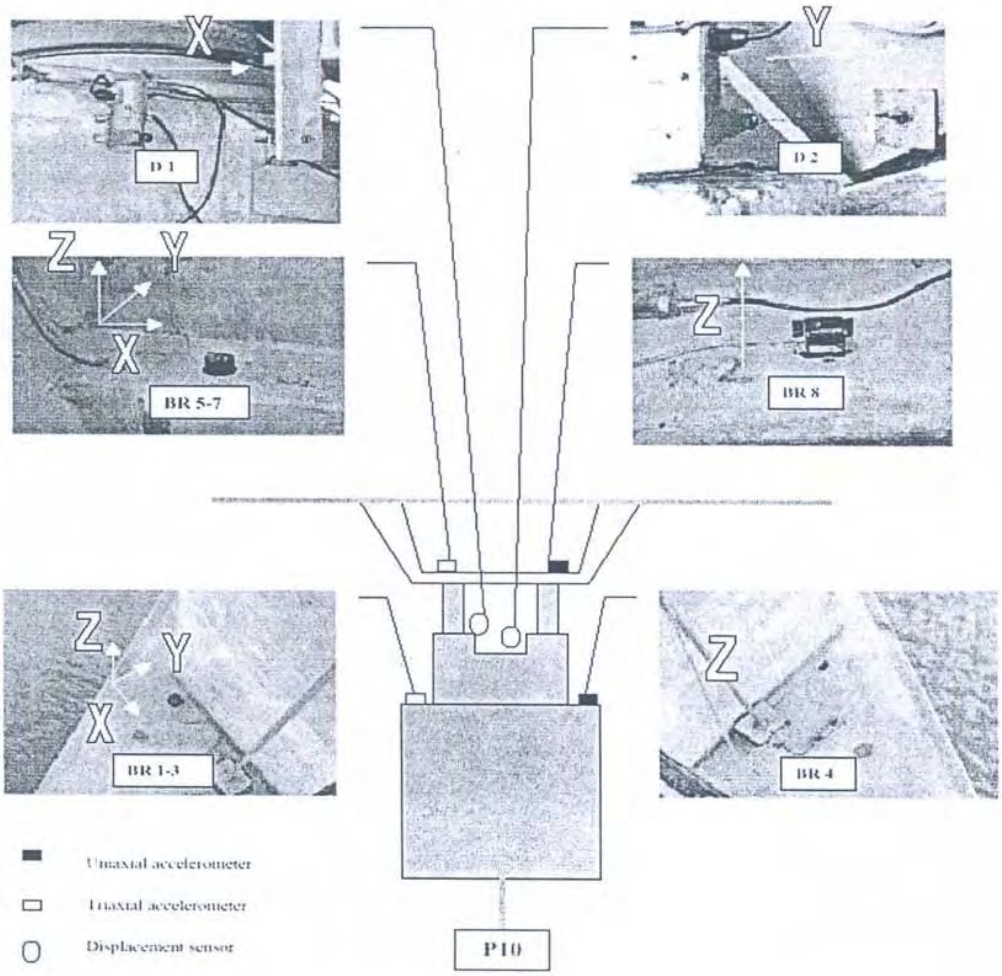

Fig. 6. Location of various accelerometer and displacement sensors at pile and pier.

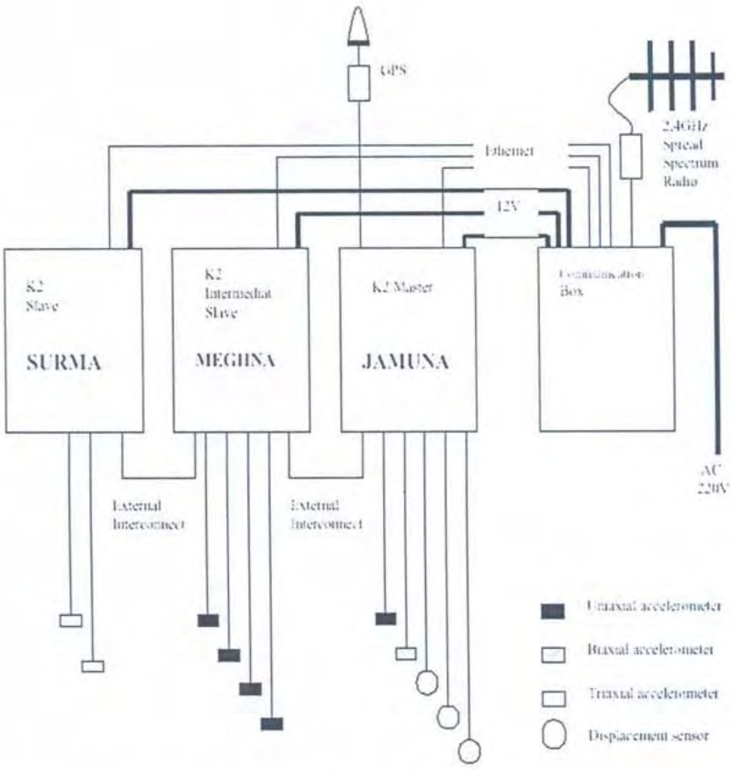

Fig. 7. Connectivity among the sensors

5. Ambient vibration of the pier-deck system

Ambient vibration of the bridge is being constantly monitored with the installed sensors. Vibration of the bridge during train and road traffic movement is also being consciously recorded. A typical example of transverse vibration of pile-cap at BR1-X and corresponding vibration in the box-girder cum deck at BR5-X is shown in Figures 8 and 9. The Fourier spectrums of these noise data of ambient vibration are shown in Figures 10 and 11. From Fig. 10 the predominant frequency of the input motion can be found approximately 1.58 Hz. In addition to this frequency, the major contribution in the deck vibration comes from the frequency level 1.37Hz and a secondary contribution from 1.1 Hz, as can be seen from Fig. 11.

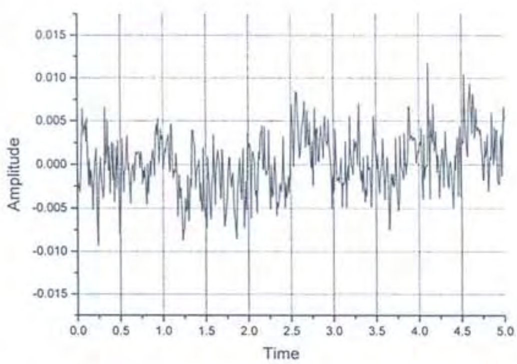

Fig. 8. Amplitude VS Time (without traffic BR_1X)

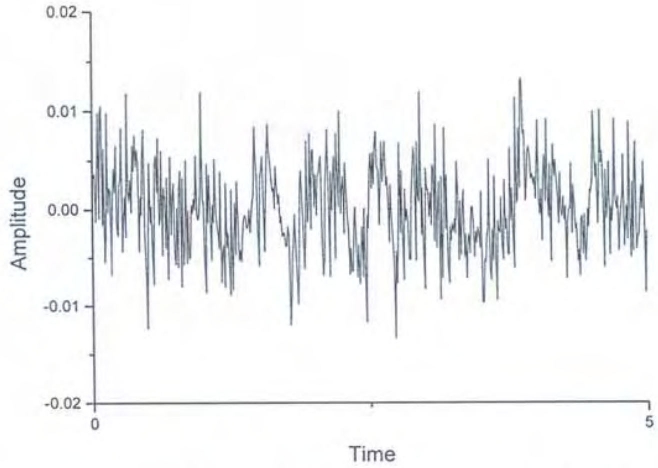

Fig. 9. Amplitude VS Time (without traffic BR_5X)

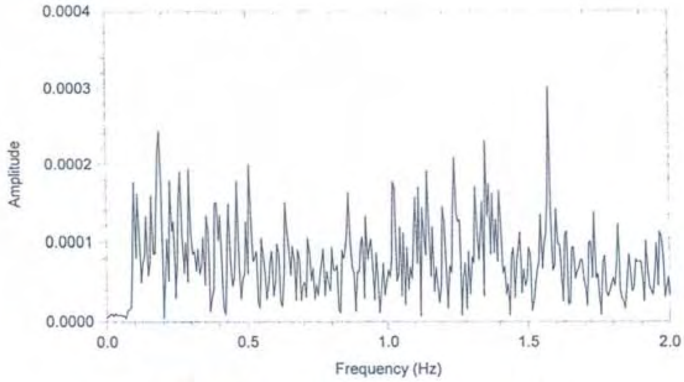

Fig. 10. FFT of BR_1X (without traffic)

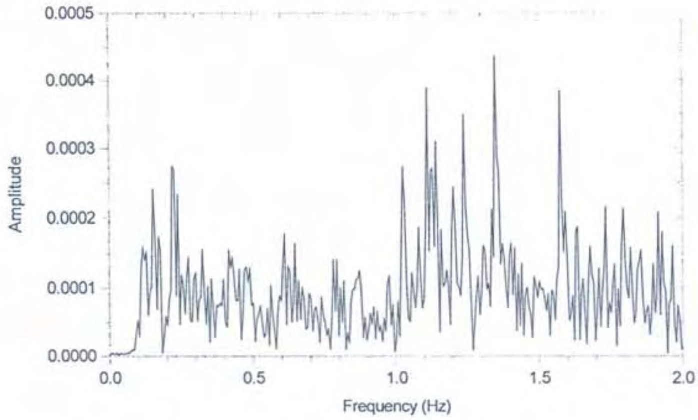

Fig. 11. FFT of BR_5X (without traffic)

5.1 SDOF model

In order to understand the dynamics of the system, at first, a Single Degree of Freedom system of the pier and deck is studied. For the SDOF system, a 100m segment of deck is considered on a single pier and the planer curvature of the bridge is ignored. Although, the depth of the deck varies parabolically along the length, for simplicity, here a linear variation is assumed (Fig. 12). Instead of the complicated cross-section of the original deck a simplified cross-section is assumed for calculation (Fig. 13). The mass of the deck of a 100m segment is found to be 1.095×10^5 slug. Assuming a linear shape function of the pier, the total lumped mass of the SDOF system can be thought of deck mass plus one-third of the pier mass, which amounts to 2.304×10^5 slug.

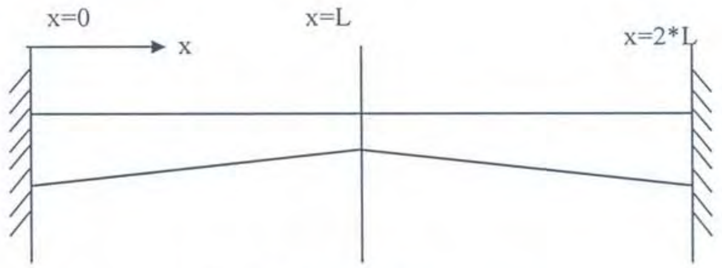

Fig. 12. Simplified deck profile

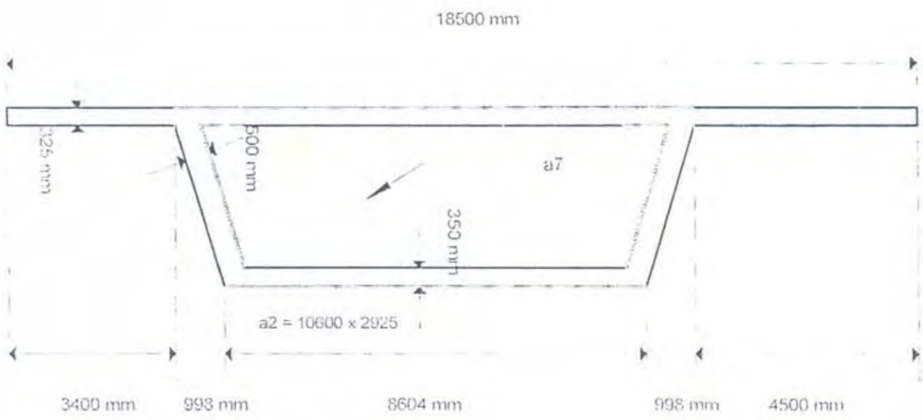

Fig. 13. Simplified deck cross-section at mid-span

The stiffness of the pier is calculated $1.055*10^7$ lb/in assuming the pier to act like a cantilever. Contribution of the deck stiffness is taken into account assuming that the 100m segment of the deck is fixed on both ends. The total stiffness of the system becomes 1.67×10^7 lb/in. Hence the natural frequency of the SDOF model is 1.08 Hz which is very close to the secondary peak of the Fourier spectrum of the deck vibration (Fig. 11).

5.2 TDOF model

Although the SDOF model explains the secondary frequency of 1.1Hz, it fails to reflect the predominant frequency of 1.37Hz. From Fig. 11, three distinct peaks can be observed. One of which, 1.58 Hz, is the contribution of the forcing frequency of the ambient input vibration as seen in Fig. 10. The two peaks suggest that the pier-deck system can be better simulated with a Two Degree of Freedom system (as shown in Fig. 14). The governing equations of motion of the system are as follows.

Considering equilibrium of mass m_1,

$$m_1\ddot{u}_1 + (k_1 + k_2)u_1 - k_2u_2 + (c_1 + c_2)\dot{u}_1 - c_2\dot{u}_2 = -m_1\ddot{u}_g \tag{1}$$

Considering equilibrium of mass m_2,

$$m_2\ddot{u}_2 - k_2u_1 + k_2u_2 - c_2\dot{u}_1 + c_2\dot{u}_2 = -m_2\ddot{u}_g \tag{2}$$

For undamped condition (c=0), Fourier transformation of Equations (1) and (2) yiled,

$$(k_1 + k_2 - m_1\omega^2)\hat{u}_1 - k_2\hat{u}_2 + m_1\hat{\ddot{u}}_g = 0 \tag{3}$$

$$-k_2\hat{u}_1 + (k_2 - m_2\omega^2)\hat{u}_2 + m_2\hat{\ddot{u}}_g = 0 \tag{4}$$

Thus, from equations (3) and (4)

$$\frac{\hat{u}_1}{-k_2m_2 - m_1k_2 + m_1m_2\omega^2} = \frac{\hat{u}_2}{-m_1k_2 - m_2k_1 - m_2k_2 + m_1m_2\omega^2}$$

$$= \frac{\hat{\ddot{u}}_g}{k_1k_2 - k_1m_2\omega^2 + k_2{}^2 - k_2m_2\omega^2 - k_2m_1\omega^2 + m_1m_2\omega^4 - k_2{}^2}$$

i.e., the transfer functions are $\dfrac{\hat{u}_1}{\hat{\ddot{u}}_g} = \dfrac{\omega^2 - \dfrac{k_2}{m_1} - \dfrac{k_2}{m_2}}{\omega^4 - \omega^2\left(\dfrac{k_1}{m_1} + \dfrac{k_2}{m_1} + \dfrac{k_2}{m_2}\right) + \dfrac{k_1}{m_1}\cdot\dfrac{k_2}{m_2}}$

and $\dfrac{\hat{u}_2}{\hat{\ddot{u}}_g} = \dfrac{\omega^2 - \left(\dfrac{k_1}{m_1} + \dfrac{k_2}{m_2} + \dfrac{k_2}{m_1}\right)}{\omega^4 - \omega^2\left(\dfrac{k_1}{m_1} + \dfrac{k_2}{m_1} + \dfrac{k_2}{m_2}\right) + \dfrac{k_1}{m_1}\cdot\dfrac{k_2}{m_2}}$.

For resonance, $\dfrac{\hat{u}_1}{\hat{\ddot{u}}_g} = \dfrac{\hat{u}_2}{\hat{\ddot{u}}_g} = \infty$. Therefore, the denominator of the transfer functions,

$$\omega^4 - \omega^2\left(\frac{k_1}{m_1} + \frac{k_2}{m_1} + \frac{k_2}{m_2}\right) + \frac{k_1}{m_1}\cdot\frac{k_2}{m_2} = 0 \tag{5}$$

Solving the above equation for ω, the predominant frequencies of a TDOF system can be calculated.

Now for the pier deck stiffness, for the pier stiffness k_1, mass m_1 will be the deck mass and one-third of the pier mass, i.e., 2.23x10^5 slug. For the deck stiffness k_2, mass m_2 will be one-third of the deck mass 7.3x10^4 slug.

The frequency parameters of Eq. (5) are calculated, $\dfrac{k_1}{m_1} = 74.07$, $\dfrac{k_2}{m_2} = 0.27$ and $\dfrac{k_2}{m_1} = 0.09$.

From Eq. (5), $\omega^2 = \begin{Bmatrix} 74.16 \\ 0.27 \end{Bmatrix}$.

Ignoring the long period vibration, $\omega = 8.61$ radian/sec or $f = 1.37$ Hz which coincides with the predominant frequency of the ambient vibration of the deck (Fig. 11).

6. Conclusions

The ambient vibration of the pier-deck system of the Jamuna Bridge was studied in this paper. The bridge is instrumented with accelerometers at different locations. The time-history records from the pile-cap and the deck of a particular pier location were studied in the paper. Two dominant frequencies were observed in the frequency spectrum of the deck vibration. The pier deck system was modeled both as an SDOF system and a TDOF system. The higher of the dominant frequencies corresponds to a predominant frequency of the TDOF system and the lower one corresponds to the SDOF system.

Acknowledgement

The authors gratefully acknowledge the Jamuna Multipurpose Bridge Authority for sponsoring the Jamuna Multipurpose Bridge Seismic Instrumentation Project. The authors also thank Mr. Moniruzzaman, Mr. A.B.M. Mahibul Alaam and Mr. Shariful Huq for their assistance in the present work.

References

[1] Bolt, B.A (1987) 'Site Specific Seismicity Study of Seismic Intensity and Ground Motion Parameter for Proposed Jamuna Bridge, Bangladesh' Report prepared for seismic design of Jamuna Bridge.

[2] BUET (2001) 'Invitation for Proposals for Supply and Installation of Seismic Instruments for Bangabandhu (Jamuna Multipurpose) Bridge', report submitted to JMBA.

[3] BUET (2003) 'Final Report: Installation Phase, Jamuna Multipurpose Bridge Seismic Instrumentation Project', report submitted to JMBA.

[4] Peng C.Y. (1987) 'Generalized model identification of linear and non-linear dynamic systems' Report no. EERL 87-5, EERI, Caltech.

[5] Lus H., Betti R., Yu J. and De Angelis M. (2004) 'Investigation of a system identification methodology in the context of the ASCE Benchmark Problem,' Journal of Engineering Mechanics, ASCE.

[6] Bolt, Bruce A. (1987). "Site Specific Study of Seismic Intensity and Ground Motion Parameters for Proposed Jamuna River Bridge, Bangladesh". Jamuna Multipurpose Bridge Authority, Govt. of the People's Republic of Bangladesh, pp. 1-36.

Japan-Bangladesh Joint Seminar on Advances in Bridge Engineering
Dhaka, Bangladesh. 10 August 2005

ISBN: 984-32-2520-6

Vibration serviceability requirement in the design of arch-supported suspended footbridge

A.F.M. Saiful Amin*, Tahsin Reza Hossain, Alamgir Habib

Department of Civil Engineering
Bangladesh University of Engineering and Technology,Dhaka 1000, Bangladesh.

Abstract

Several cases of vibration serviceability problems with footbridges have been reported in the recent past from all over the world. In these cases, the respective designs failed to consider the so called 'footfall action mechanism' where human movement induces large amplitude lateral vibrations in the deck system. This prompted the code authorities to revise the code provisions for this class of bridges. According to the revised code provisions (BS 5400: Part 2, amended vide BD 37/01 on August 2001), the footbridges need to satisfy the vibration serviceability requirements indicated by the eigen frequencies of the system for first horizontal mode (1.5 Hz) and first vertical mode (5 Hz). With this background, the paper presents the design steps that were followed in a recent footbridge project in Bangladesh. In the design process, parametric studies were carried out to study the effect of different geometric parameters on the eigen frequencies of the bridge deck system. The study clearly shows that for addressing the problem, the lateral dynamic stability of the deck system can be effectively improved by increasing the lateral stiffness of the deck system. The lateral stiffening of the supporting system of the deck, two double curved arches in this case, further improves the performance. Attempts are also made to explore the possibility of improving the vertical dynamic stability of the system by incorporating additional deck-lake bed ties.

1. Introduction

Footbridges are now becoming an integral part of the of modern city infrastructures. These bridges allow safe transfer of pedestrians over the urban roads, city waterways or highways by providing a segregated grade separated transportation facility in walking mode. Furthermore, in some applications, the bridges of this class also connect urban installations at different elevations. In the current trend, the architects, in the design process carefully consider the aesthetic appeal of these bridges to maintain a harmony with the surrounding infrastructure of the neighbourhood while the structural engineers

* Email: samin@ce.buet.ac.bd

follow the current design codes to ensure the stability, safety and durability of the structure. The construction of 332m long three-span Millennium bridge having a notable architectural appearance built over the Thames at London is a recent example. However, on the eventful opening day of the bridge with a large crowd trying to use it, the Millennium Bridge oscillated significantly due to vibration induced by pedestrian movement. On the eve of a new millennium, the event made the scientific and engineering community over the world realize the necessity to further sharpen their views about the nature that interacts with our built environment. The dynamic stability of the structures due to human movement induced vibration came into focus. Following that event, several studies have been carried out that led to significant modifications of the code provisions for the footbridges. Nevertheless, the efforts of the architects and structural engineers in coming up with new and innovative designs have not ceased in the recent days. Very recently, a similar footbridge has been designed and constructed over the Crescent Lake at Dhaka, Bangladesh by considering the recently improved code provisions. This paper discusses different intrinsic aspects of the analysis and design of the bridge from the structural engineers' viewpoint.

2. Pedestrian-induced lateral vibration problem

2.1 Early case studies

Early technical information regarding human movement induced lateral vibration is known from the work of Bachmann (1992). It presents several valuable case studies and reports serviceability problems due to vibration in footbridges. In one case, vertical vibration problem occurred in a steel bridge that had a fundamental frequency of about 4 Hz. In addition, Bachmann (1992) records the report of having lateral vibration problem in another case of 110m long steel footbridge that had the frequency in the lowest lateral mode in the range of about 1.1 Hz. However, his work could not explain the cause that triggered such a phenomena.

2.2 Identification of the footfall action mechanism

The credit of the identification of the mechanism of synchronized footfall action goes to the work of Fujino et al. (1992 and 1993). The work was initially based on addressing the lateral vibration problem of T-bridge (Toda Park Bridge, Toda City, Japan), a pedestrian cable stayed bridge that was completed in 1989. Immediately after it was opened, the bridge suffered from lateral vibration induced by high number of pedestrians trying to pass over it in a peak-time. The detail study done by Y. Fujino and his associates mentions that people usually walk with a frequency of about 2 Hz, it is not commonly known but about 10% of the vertical loading works laterally when people walk (Nakamura and Fujino 2002). The gravity of center of human body moves laterally when person steps with his right and left foot in turn, which induces this lateral dynamic force. The frequency of this lateral dynamic force is about 1 Hz. So he mentions that the lateral dynamic forces induced by pedestrians can be a resonant force for the bridge-deck system whose natural frequencies are closer to this frequency (1 Hz).

However, all these works and reports were mainly available in the scientific and technical literatures and the professional design engineers were unaware of such problems as the design codes did not take these works into consideration. The problem struck once again in the Millennium bridge London, UK on its opening day (June 2000).

2.3 The problem with the Millennium Bridge, London, UK

In September 1996, a design competition was organized by the *Financial Times* newspaper in association with the London Borough of Southwark to design a new footbridge across the River Thames. The design of the present three span Millennium Bridge won the competition. The lengths of the three spans are 81m for the north span, 144m for the main span between the piers and 108m for the south span. The structural form of the bridge is a shallow suspension bridge, where the cables are as much as possible (Dallard et al. 2001a,b) below the level of the bridge deck to free the views from the deck. On the opening day (10 June 2000), the bridge experienced unexpected excessive lateral vibrations when pedestrians with a maximum density of 1.3 and 1.5 persons per square meter tried to cross the bridge. The movement took place at the south span at a frequency of about 0.8 Hz, at central span at frequencies just under 0.5Hz and at the north span just over 1 Hz. The number of pedestrians allowed onto the bridge was reduced on 11 June 2000 and movement occurred more rarely. On 12 June it was decided to close the bridge and it had to be retrofitted before opening to the traffic once again.

3. Recent codes on pedestrian bridges

Following the incident of the Millennium Bridge, London, the engineering community started to appreciate the necessity of revising existing codes for pedestrian bridges and take the vibration serviceability problem into consideration. This led to some major code revisions.

The recent code (BS 5400: Part 2, amended vide BD 37/01 on August 2001) states that for pedestrian bridge superstructures for which the fundamental natural frequency of vibration exceeds 5 Hz for the unloaded bridge in the vertical direction and 1.5 Hz for the loaded bridge in the horizontal direction, the vibration serviceability requirement is deemed to be satisfied. However, in the cases where these conditions are not satisfied, the code suggests for field vibration tests for determining the maximum acceleration of movement. The method for estimation procedures must have to be agreed upon with a competent authority.

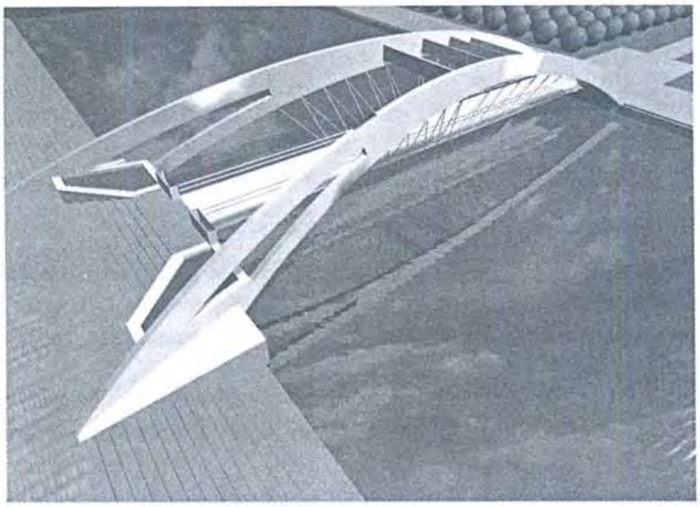

Fig. 1. A three dimensional view of the bridge as per initial architectural design

4. Architectural design and structural solution strategy in Crescent lake bridge

The study of the dynamic behavior of the arch-supported suspended-span footbridge presented in this paper originates from a development project initiated by the Public Works Department (PWD), Government of the Peoples' Republic of Bangladesh. The footbridge was constructed over the Crescent Lake, Dhaka, Bangladesh to facilitate movement of the pedestrians from adjacent roads to the nearby Mausoleum Complex of former Bangladesh President. Since the footbridge was to be constructed within the Master Plan area of well-known Bangladesh National Parliament Building Complex designed by famous Architect Louis Isadore Kahn, the architectural design of the footbrdige needed to be in harmony with the masterpiece creation of Architect Kahn. With this motivation, the architectural drawing suggested the construction of the pedestrian bridge with a special physical system where the hanging steel-framed deck (57.3m in length) fitted with tampered glass panels gets its support from two shallow reinforced concrete arches through hangers made of cables. The arches are connected at the top through reinforced concrete and steel ties. The arches have curvatures both in plan and elevation and are supported on 90 piles to bear the large lateral thrusts. Figure 1 presents a complete three dimensional view of the bridge as per the initial architectural design.

In such a system presented in Figure 1, the lateral and vertical stabilities of the arches and the deck system were considered to be quite vital. Hence, based on the conceptual design, a structural solution strategy had to be drawn so that the dynamic stability of the arch-deck system of the bridge can be ensured in accrodance with the recent code requirements mentioned in Section 3. To this end, fundamental natural frequencies of the bridge for a number of stiffening systems are considered. To identify the most effective stiffening system, a parametric study has been conducted to ascertain the major geometric parameters that govern the dynamic stability of the bridge system. Based on this parametric study, an arch-deck system that meets the most recent code requirements for eigen frequencies has been determined. Final part of the paper gives results obtained from a number of trial systems that can provide a better dynamic performance.

5. Finite element model of the bridge

In order to perform static and dynamic analysis of the arch-deck system, the three dimensional finite element model of the arches was developed using Strand Version 6.1- a general purpose finite element software. The arches were idealized as 3-dimensional beam. The supporting steel hangers that connect the steel girder with the arch were modeled as link (tension-compression) elements. The bridge girder made of steel sections was modeled as 3-dimensional beam elements. In order to check the design adequacy of the bridge, the available design codes/guides were consulted to ascertain the self weight of the bridge, the expected pedestrian load and the expected wind load on the arch and deck system. Within this notion, different geometric arrangements of deck, tie and bracing system were considered. Figures 2 and 3 presents two of these arrangements while the further details of all the options are presented in Section 6.

After modeling the arch, hangers and the deck system, the arch was analyzed for dead loads, live loads due to pedestrians and lateral wind forces. In general, for the design loads and assigned sections, the model was found to be numerically adequate. In view of the code requirements, the models developed here are used in the following Sections to study the dynamic stability of the system under pedestrian movement.

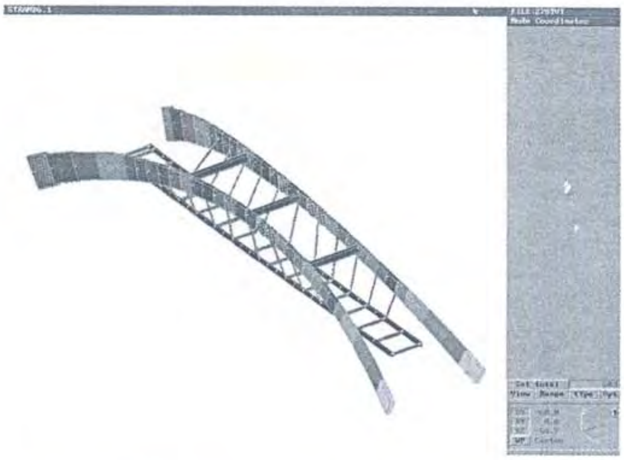

Fig. 2. Finite element model of the footbridge (Option B, Table 1)

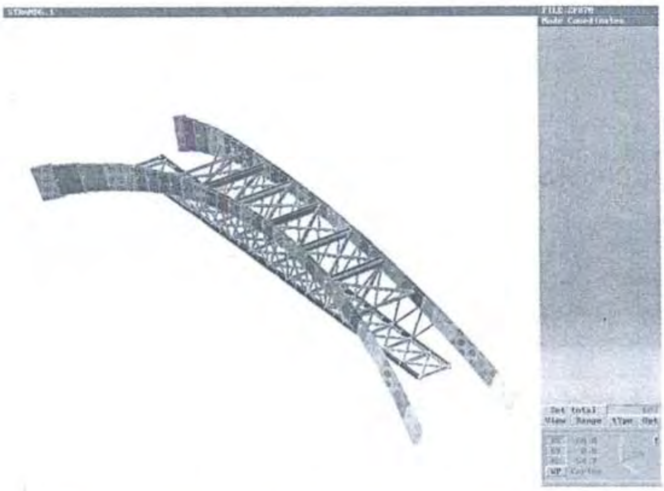

Fig. 3. Finite element model of the footbridge (Option E, Table 1)

6. Dynamic stability of the arch-deck system

6.1 Eigenvalue analysis

The recent code requirements regarding the vibration serviceability requirements are presented in Section 3. Section 4 has provided an overview of the structural system of the bridge. There it is observed that to achieve an adequate system, the fundamental vibration modes and natural frequencies of the structure with different stiffening systems need to be studied in details. Once studied, this would reveal the performance of the structural system against pedestrian movement. To this end, a parametric study was carried out to investigate the effect of different stiffening systems on the vibration modes and the fundamental natural frequencies of the arch-deck system using the developed finite element model (Section 5). Eigenvalues were calculated up to five modes for eleven possible combination options for choosing the most suitable arch-deck system. Among the eleven options, first five options (A-E) are based on the variation of the hanger system, deck width, deck bracings and number of ties connecting the arches at top as presented in Table 1. In addition, another six options (F-K) consisting of connecting the bridge deck with lake bed through different tie arrangements are presented in Table 2 and Figure 5. These cases have been considered to explore the possibility of further improving the dynamic performance of the system in accordance with the stipulated code requirements.

Table 1
Different options of arch-deck system considered for eigenvalue analysis

	Hanger system		Deck width		Deck bracings		Ties between arches at overhead locations		
	Straight	Inclined	4.27m	7.9m	Yes	No	3 RCC ties	5 RCC ties	5 RCC ties, 7 steel ties and bracings
A	O			O		O	O		
B	O		O			O	O		
C	O		O		O		O		
D		O	O		O			O	
E		O	O		O				O

Table 2
Different deck-lake bed tie arrangements trial systems

	Deck-lake bed tie number						
	1	2	3	4	5	6	7
F	O						
G				O			
H	O			O			
I			O	O	O		
J		O	O	O	O	O	O
K	O	O	O	O	O	O	O

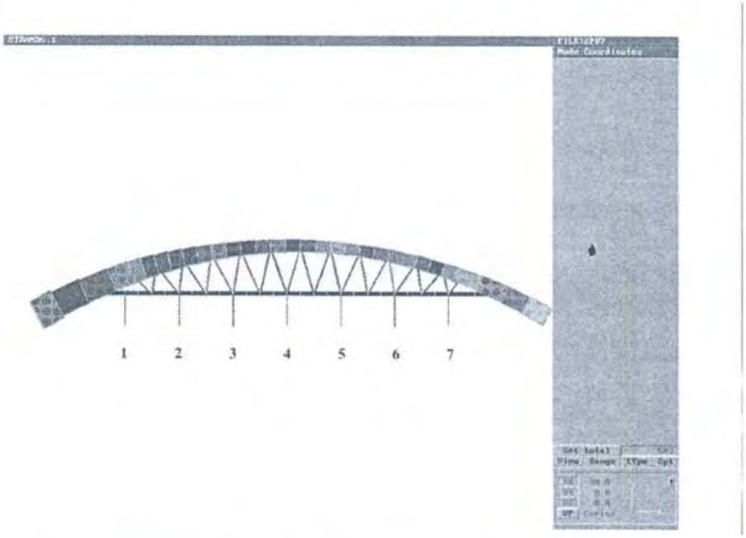

Fig. 4. Numbering scheme for deck-lake bed tie arrangement options

6.2 Mode shapes ascertained from the modal analysis

Figure 5 presents the typical mode shape for the first horizontal mode as computed for Option A or B. However, with the addition of deck bracings, the lateral stiffness of the deck system is increased. Due to this change, no true horizontal mode shape for the lowest frequency could be obtained. Rather it takes a complex mode shape, a horizontal sway coupled with a torsional mode. Figure 6 delineates the fact. However, there was no change in the mode shape for horizontal mode in options (F-K) of adding ties between the deck and lake bed. Figure 7 presents a typical shape.

In spite of changing geometric configurations, in all cases it was possible to obtain a true vertical mode shape. Figure 8 presents a typical shape.

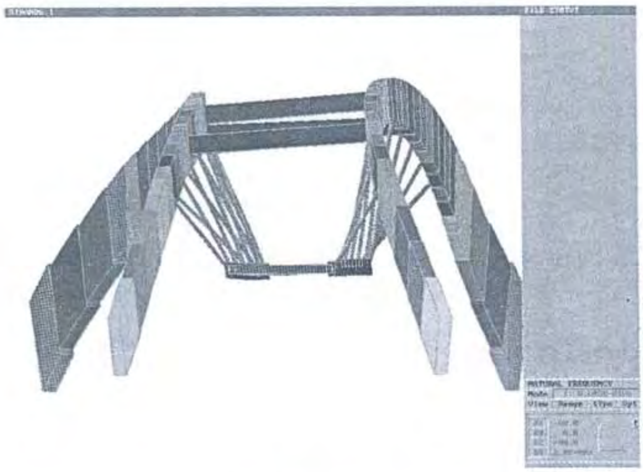

Fig. 5. First horizontal mode of vibration in the deck system for Option B

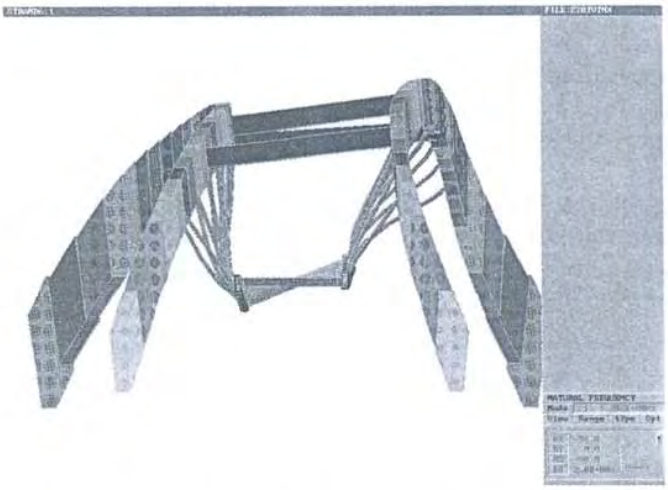

Fig. 6. First horizontal mode of vibration in the deck system for Option C

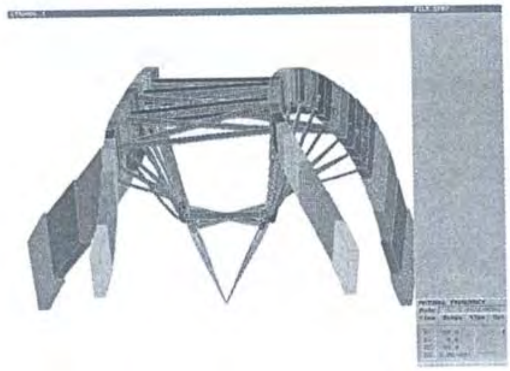

Fig. 7. First horizontal mode of vibration in the deck system for Option K

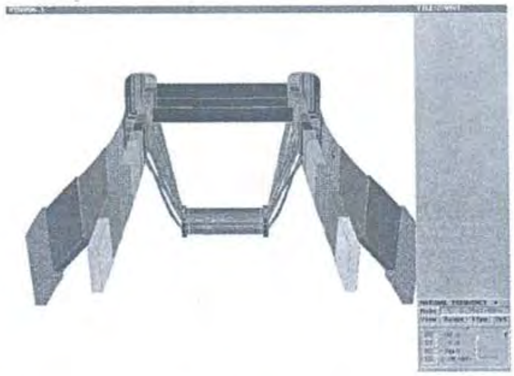

Fig. 8. Typical first vertical mode of vibration in the deck system for all options

6.3 Eigenvalues computed from the finite element model

The eigenvalues determined from the finite element model for first horizontal mode and first vertical mode are presented in Figure 9 in relation to the code recommended values. By comparing the computed eigenvalues for different cases, it is evident that the dynamic stability of the system expressed in terms of eigen frequencies improves for the following changes in the model geometry:

1. Decrease of deck width (Option B)
2. Increase of the lateral stiffness of the deck system by adding additional cross-bracings (Option C)
3. Adoption of inclined hangers instead of straight vertical hangers (Option D, E)
4. Increase the number of ties and cross bracings between the arches at the top (Option D, E)
5. Incorporating additional ties between the deck and lake bed (Option F-K)

Among all the eleven cases presented in Figure 9, it is clear that the dynamic stability of system can be improved if proper attention is paid to the above mentioned aspects. As a matter of fact, the first three aspects indicated above increases the lateral stiffness of the deck while the fourth aspect increases the lateral stiffness of the supporting arches. The fifth option attempts to increase the vertical stiffness of the deck. However, when compared with the code requirements, it is evident that the lateral stiffness of the system indicated by the frequency of the first horizontal mode can be attained in all the options above Option D whereas none of the cases could satisfy the vertical stiffness requirement indicated by the frequency of the first vertical mode. When compared between the cases, it is evident that the Option K with the deck connected to the lake-bed at seven different locations (Fig. 4) give the best possible performance in the light of the code but at the cost of aesthetic beauty.

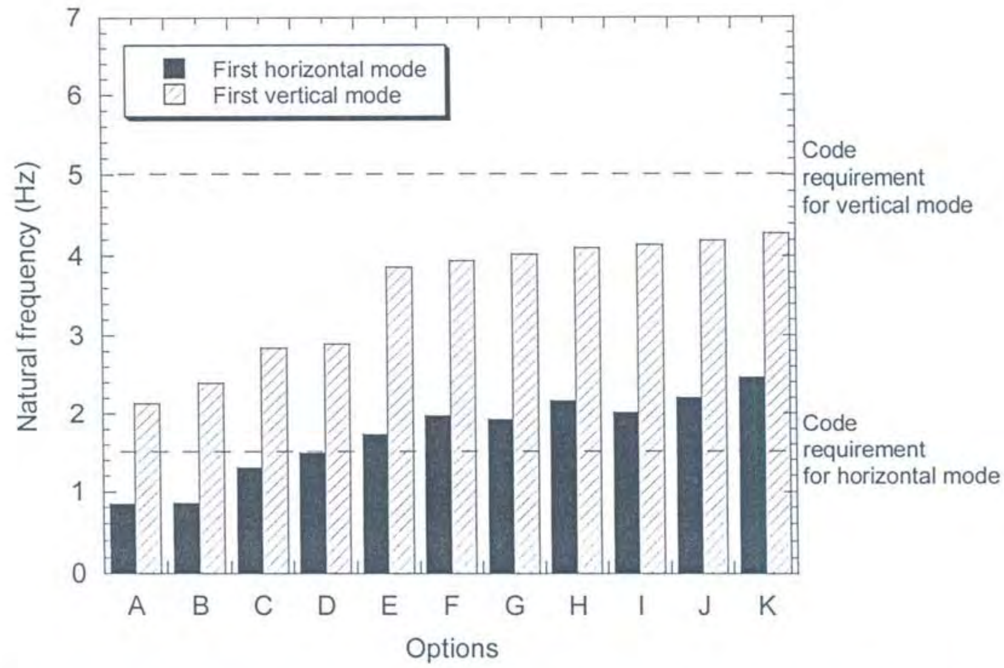

Fig. 10. Eigen frequencies determined for different Options and presented against the code requirements.

With a view to preserving the architectural view of the project to the best possible way, it was decided to go for constructing the bridge along with a provision of installing the deck-lake bed ties and perform a field test on the completed bridge without installing the ties. To this end, a field test involving an adequate number of volunteers crossing the bridge in both arbitrary and regular fashions was performed. The perception of users on its use was noted to have a more clear understanding of the behavior of the completed bridge under dynamic excitation. During the field test, the bridge was found to perform well and no perceivable vibration problem took place. The bridge was opened to pedestrian traffic.

7. Conclusions

In accordance with the recent code provisions, the footbridges need to meet the vibration serviceability requirements. To this end, in the recently completed Crescent lake footbridge project in Dhaka, Bangladesh, detail eigenvalue analyses were carried out on different finite element models with varied geometric parameters. The parametric study shows the necessity of having a careful consideration in choosing a geometric configuration that is most stable from vibration serviceability viewpoint. Furthermore, it is clear that a design not even completely satisfying the code stipulated eigen frequency(s) may also perform satisfactorily in the field level. However, in such cases, a full scale field test should be carefully performed before opening the facility to the traffic and in the event of failure of satisfying the performance requirements in field tests, the designer must maintain other clear provisions in his design for improving the system performance through adjustments in the field level.

References

Bachmann, H. (1992). Case-studies of structures with man-induced vibrations, J. Engineering Mechanics, 118, 631-647.

British Standard 5400: Part 2 (2002). Design Manual for Roads and Bridges, Highways Agency, London: The Stationary Office, February 2002. (Reference of amendment: BD 37/01 August 2001).

Dallard, P., Fitzpatrick, A.J., Flint, A., Bourva, S.L., Low, A., Smith, R.M.R., Willford, (2001a). The London Millennium Footbridge , The Structural Engineer, 79, 17-33.

Dallard, P., Fitzpatrick, T., Flint, A., Low, A., Smith, R.R., Willford, M., Roche, M. (2001b). London millennium bridge: Pedestrian-induced lateral vibration, J. Bridge Engineering, 6, 412-417.

Fujino, Y., Pacheco, B.M., Nakamura, S. and Warnitchai, P. (1993). Synchronization of human walking observed during lateral vibration of a congested pedestrian bridge, Earthquake Engineering and Structural Dynamics, 22, 741-758.

Fujino, Y., Sun, L., Pacheco, B.M. and Chaiseri, P. (1992). Tuned liquid damper (TLD) for suppressing horizontal motion of structures, *J. Engineering Mechanics, ASCE,* 118, 2017-2030.

Nakamura, S and Fujino, Y. (2002). Lateral vibration on a Pedestrian Cable Stayed Bridge, Structural Engineering International, 12, 295-300.

Japan-Bangladesh Joint Seminar on Advances in Bridge Engineering ISBN: 984-32-2520-6
Dhaka, Bangladesh. 10 August 2005

A cyclic model for pressure insensitive soil

M.R. Hossain[1], M.S.A. Siddiquee[1*], F. Tatsuoka[2]

[1]*Department of Civil Engineering*
Bangladesh University of Engineering and Technology, Dhaka 1000, Bangladesh
[2]*Tokyo University of Science, Noda shi, Chiba, Japan*

Abstract

Geotechnical structures usually undergo cyclic loading during its lifetime of service. Bridge piers, abutments are very susceptible to cyclic loading. It has been a long standing problem to solve the cyclic loading phenomena by a reasonably accurate cyclic model. In this paper, a novel cyclic model is developed by extending the one-dimensional Masing's rule to general stress-space (3D). The cyclic behavior is simulated by introducing a new framework in which the origin of the stress-strain space is shifted to the instantaneous stress point while the direction of the loading is reversed. A hyperbolic growth function for isotropic strain hardening is used and Rowe's stress-dilatancy is implemented for the material with slight modification for cyclic loading. No new concept for hardening is introduced here, but the old isotropic hardening rule is applied in an efficient manner to simulate the behavior of material under cyclic loading.

Keywords: cyclic loading, elastoplastic model, Masing's rule.

1. Introduction

Soils are often subjected to transient and cyclic loading such as that induced by road traffic or by wind and wave action on bridges. Earthquakes provide additional examples of transient loading. To understand more deeply the response of soil to such loading it is necessary to account for its changing properties in the course of cyclic deformation and its inelastic behavior resulting in progressive dilation and associated pore pressure change.

Starting from pioneering work by Druker and Prager (1952), various improvements, extensions and alternative soil plasticity theories have been proposed. In this process the second author has proposed a novel model for the monotonic loading of geomaterial and implemented the model for multi-element FE code (Siddiquee 1994). The cyclic evaluation of the material is modeled through kinematic hardening, isotropic hardening

* Email: sid@ce.buet.ac.bd

or a combination of both. The cyclic evaluation of extended Masing behavior is very difficult to model through the kinematic hardening (Hossain 2005, Montáns 2000).

Masing's rule states that the unloading curve keeps a homological ratio of two to monotonic one. It has been experimentally observed that this rule holds closely in most materials. The extension of this rule, also observed in most materials, is that the modeling process takes place through the initial monotonic curve or through previous reloading ones when they are intersected. The numerical simulation of this rule from isotropic and kinematic hardening requires difficult-to-obtain variable combinations of both hardening types.

The objective of the present study is therefore to develop a method to simulate the cyclic stress-strain relation of sand subjected to irregular cyclic loading history. The proposed model has the advantage that it has a direct relevance to Masing's rule. The cycle will close and the monotonic curve will be recovered after the previous threshold has been surpassed. The computational cost will be substantially smaller than that of traditional multi-surface models and the accuracy will usually be better.

2. Formulation of the constitutive relation

An isotropic strain hardening single surface model is formulated within a new framework to simulate the cyclic behavior of geo-material. Hardening part of the model is achieved through a hyperbolic equation, which can model the non-linear stress-strain relationship. The cyclic behavior is simulated by introducing a new framework in which the origin of the stress-strain space is shifted to the instantaneous stress point while the direction of the loading is reversed. Then the yield surface again grows isotropically from the new origin.

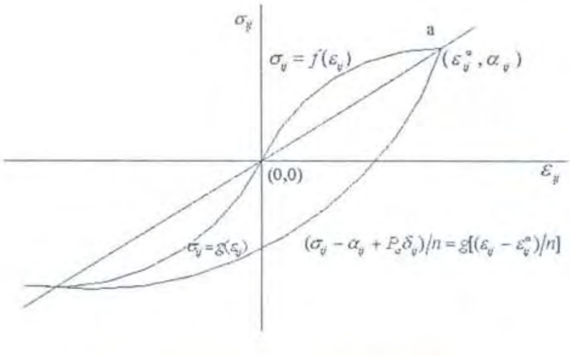

Fig. 1. Framework for cyclic loading

Here during loading the stress state moves from the origin to the point 'a' where $\sigma_{ij}=\alpha_{ij}$ for a corresponding strain ε_{ij}^{a} following a loading curve $\sigma_{ij}=f(\varepsilon_{ij})$. Now when the unloading starts the origin is shifted to α_{ij} and the direction of the stress tensor σ_{ij} and strain tensor ε_{ij} is reversed. Now all the calculation is made from the new origin and yield surface grows isotropically from it. And the unloading curve follows the equation $(\sigma_{ij}-\alpha_{ij}+P_a\delta_{ij})/n=g[(\varepsilon_{ij}-\varepsilon_{ij}^{a})/n]$ where n is ratio between unloading curve to the unloading skeleton curve. It is obtained by using a proportionality rule where a straight line is drawn from the point of stress reversal passing the origin O to intersect the unloading skeleton curve and thus finds the value of n. If the loading and unloading skeleton curves are similar in shape, n is equal to two, which is stated by Masing's rule. If the confining pressure at O is P_0 and at Point a it is $P_0+\Delta P$, then set P_a as $P_0-\Delta P$. This confining pressure ensures a smooth connection between the unloading curve and the unloading skeleton curve.

When the unloading curve intersects the unloading skeleton curve, origin is restored to the original position and the stress-strain relationship is found by the hyperbolic relationship of $\sigma_{ij}=g(\varepsilon_{ij})$. Thus a close hysteretic stress-strain relation is found giving the most accurate material response. Now by employing the drag rule we can simulate the increase in stress amplitude for same strain value during cyclic loading.

3. Yield function and plastic potential

Any strain-hardening model needs the description of a set of continuous yield and plastic potential surface (in case of non associative flow rule). As in this study mostly granular material will be dealt with, so the yield function will follow the material suitability. All point differentiable smooth Druker-Prager failure criteria for yield function is chosen. The yield function (f) and plastic potential function (ϕ) are given by,

$$f=\eta I_1+\sqrt{J_{2D}} \tag{1}$$

$$\phi=\xi I_1+\sqrt{J_{2D}} \tag{2}$$

where,

$$\eta=\frac{2\sin\varphi_{mob}}{\sqrt{3}(3-\sin\varphi_{mob})} \tag{3}$$

$$\xi=\frac{2\sin\psi}{\sqrt{3}(3-\sin\psi)} \tag{4}$$

φ_{mob} = Mobilized angle of friction, ψ = Angle of dilatancy

4. The growth function

The growth function (Tanaka) expressed as follows was used,

$$\eta=\left[\frac{2\sqrt{\kappa\kappa_f}}{\kappa+\kappa_f}\right]^m\eta_p \qquad (\kappa\le\kappa_f) \tag{5}$$

where m and κ are material constants and η_p is the value of η at the peak state.

5. Modification of the original Masing's rule

Here $\tau=f(\gamma)$ represents the primary loading and unloading curves that are symmetric about the origin i.e., $f(-\gamma)=-f(\gamma)$. When the loading direction is reversed at point 'a' (τ_a,γ_a), the unloading curve is given as: $(\tau-\tau_a)/n=f[(\gamma-\gamma_a)/n]$

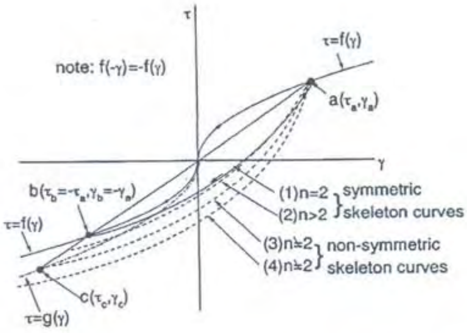

Fig. 2. Schematic diagram explaining proportional rule (Tatsuaka et al., 1999)

where n=2. In this case, the unloading curve joins the unloading skeleton curve at the symmetric point 'b' (τ_b, γ_b) with $\tau_b = -\tau_a$ and $\gamma_b = -\gamma_a$. On the other hand, many experimental results show that the unloading curve from point 'a' does not join the skeleton curve at point 'b'. In addition, the primary loading and unloading curves could be largely non-symmetric. In this case, two different functions $\tau = f(\gamma)$ and $\tau = g(\gamma)$ should be assigned for loading and unloading curves. It could be assumed that the unloading curve from point 'a' in this case is given as,

$$(\tau - \tau_a)/n = g[(\gamma - \gamma_a)/n]$$

where point 'c' (τ_c, γ_c)= intersection of straight line passing the reversing Point a and the origin and the unloading primary curve $\tau = g(\gamma)$. For unloading curve to join the primary unloading curve at point 'c', the power n should be equal to $-(\tau - \tau_c)/\tau_c (\geq 0)$, which is usually different from two and may not be constant during cyclic loading. The value of n is determiner by proportional rule (Tatsuaka et al. 1999, 2003).

For the current model the relation ship between η and the plastic hardening parameter κ is used because the η-κ relations are much more symmetric and simpler to model with. Now, by moving the origin to the point of reversal for the unloading curve we get,

$$\eta = n \left[\frac{2\sqrt{\frac{\kappa \kappa_f}{n}}}{\frac{\kappa}{n} + \kappa_f} \right]^m \eta_p \tag{6}$$

where κ is calculated from the new origin.

6. Modeling hysteretic stress-strain relationship (proportional rule)

The proportional rule consists of external and internal rules. Upon the reversal of loading direction, either external or internal rule is chosen for a given loading history based on the largeness of the current value of κ relative to instantaneous maximum and minimum value of κ as κ_{max} and κ_{min}. To keep continuity between external rule and internal rule, it is assumed that a pair of points having coordinates κ_{max} and κ_{min} is always located on opposite side of the origin O on a straight line passing the origin. The meaning of K_{min} and K_{max} is explained below:

1. Suppose that loading starts from the origin and continue until Point A. At Point A, K_{max} = the maximum value of K ever achieved by loading = K_A. Accordingly, K_{max} at Point B (located along the first unloading curve from Point A) = K_A. When the current K value becomes larger than the previous value of κ_{max} (i.e., when $K > K_{max} = K_A$), the previous value of κ_{max} is replaced by the instantaneous κ value.

2. The K_{min} value is defined as the smaller value of (a) the smallest value of K ever attained during unloading and (b) the K value at the intersection of the straight line starting from the point of K_{max} and passing the origin O with the unloading skeleton curve $\eta = g(\kappa)$. The κ_{min} value of Point B = K_C (K at Point C), corresponding to Point A.

3. The κ_{max} value is defined as larger value of (a) the largest value of K ever attained by loading and (b) the value of K at the intersection of the straight line starting from the point of κ_{min} and passing the origin O with the loading skeleton curve $\eta = f(\kappa)$.

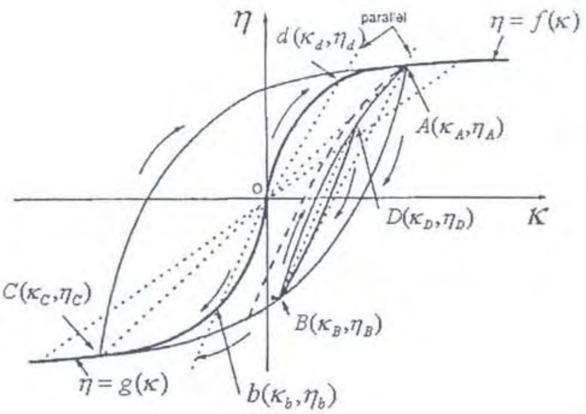

Fig. 3. Details of proportional rule

The rules to obtain the hysteretic stress-strain relationship for cyclic loading are described below, referring to Figs. 3 and 4:

1. Stress-strain curves for reloading and so on are obtained as follows:

   - When unloading is reversed to reloading while renewing the κ_{min} value to the instantaneous plastic strain K, the reloading curve is obtained by following external rule.

- When unloading is reversed to reloading with $\kappa_{\max} \geq \kappa \geq \kappa_{\min}$ maintaining the previous $\kappa_{\max}$ and $\kappa_{\min}$, the reloading curve is obtained by following the internal rule, and
- When the loading is continued while renewing the $\kappa_{\max}$ value to instantaneous plastic strain K, the loading curve $\eta = f(\kappa)$ is followed.

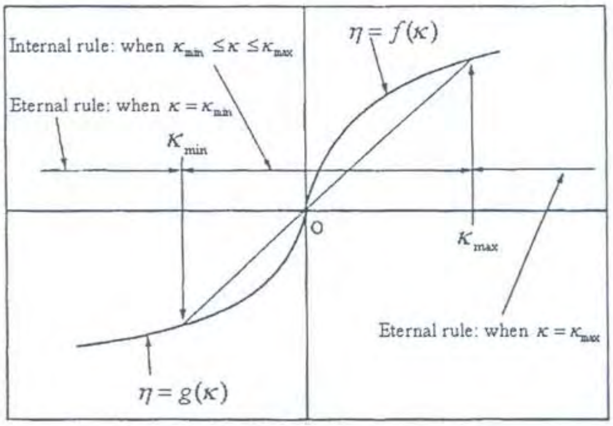

Fig. 4. Rule to choose either external or internal rule for given instantaneous plastic strain K

2. Stress-strain curves for unloading and so on are obtained as follows:

- When loading is reversed to unloading while renewing the $K_{\max}$ value to the instantaneous plastic strain K, the unloading curve is obtained by following external rule,
- When loading is reversed to unloading with $\kappa_{\max} \geq \kappa \geq \kappa_{\min}$ maintaining the previous $\kappa_{\max}$ and $\kappa_{\min}$, the unloading curve is obtained by following the internal rule, and
- When the unloading is continued while renewing the $\kappa_{\min}$ value to instantaneous plastic strain K, the unloading skeleton curve $\eta = g(\kappa)$ is followed.

The rules are described below more specifically referring to Fig 3.

1. During the first primary loading from origin O (κ_0, η_0), where $\kappa_{\max} = \kappa_{\min} = 0$, until point 'A', always $\kappa_{\max} = K$ and the stress-strain curve follows the loading skeleton curve $\eta = f(\kappa)$. At point 'A' (κ_A, η_A), we have $\kappa_{\max} = \kappa_A$ and $\kappa_{\min} = \kappa_C$.

2. When loading is reversed at point 'A', the unloading curve bound for point 'C' is obtained by following the external rule (with $\kappa_{\max} = \kappa_A$) and using the known unloading skeleton curve $\eta = g(\kappa)$ and the coordinate at point 'C' (κ_C, η_C) as:

$$\frac{\eta-\eta_A}{n_1}=g\left(\frac{\kappa-\kappa_A}{n_1}\right) \tag{7.a}$$

$$n_1=\frac{(-\eta_C)+\eta_A}{(-\eta_C)}=\frac{(-\kappa_C)+\kappa_A}{(-\kappa_C)} \quad (\geq 0) \tag{7.b}$$

3. When unloading continues passing point 'C', the stress-strain curve follows the unloading skeleton curve $\eta=g(\kappa)$ with $\kappa_{\max}$ = instantaneous κ.

4. Here, the target plastic strain κ_{target} is introduced, which is defined the value of κ at that point for which the stress-strain curve is bound after the loading direction is reversed. For unloading and reloading curves following the external rule, κ_{target} is equal to $\kappa_{\min}$ and $\kappa_{\max}$, respectively. In Fig. 3 κ_{target} for the unloading curve starting from point 'A' bound for point 'C' is $\kappa_{\min}=\kappa_C$.

5. In Fig. 3, when unloading is reversed to reloading at point 'B', where κ is between $\kappa_{\min}=\kappa_C$ and $\kappa_{\max}=\kappa_A$, the reloading curve is obtained by following internal rule. The target point is assumed to be the same with the latest previous reversing point before point 'B' (i.e., point 'A'). Then, this reloading curve is obtained by scaling the loading skeleton curve as:

$$\frac{\eta-\eta_B}{n_2}=f\left(\frac{\kappa-\kappa_B}{n_2}\right) \tag{8.a}$$

$$n_2=\frac{\eta_A-\eta_B}{\eta_d}=\frac{\kappa_A-\kappa_B}{\kappa_d} \quad (\geq 0) \tag{8.b}$$

where point 'd' (κ_d,η_d) = intersection of the straight line starting from the origin O while parallel to the straight line between points 'B' and 'A' with the loading skeleton curve $\eta=f(\kappa)$.

6. In Fig. 3 when the loading direction is reversed at point 'D', the re-unloading branch, which is bound for the latest previous point (i.e., point 'B'), is obtained by EQ. 7(a), but using another scaling factor n_3 given below,

$$n_3=\frac{(-\eta_C)+\eta_A}{(-\eta_C)}\frac{\eta_D-\eta_B}{\eta_A-\eta_B}=\frac{(-\kappa_C)+\kappa_A}{(-\kappa_C)}\frac{\kappa_D-\kappa_B}{\kappa_A-\kappa_B} \quad (\geq 0) \tag{9}$$

At point 'B', the re-unloading curve does not smoothly rejoin the previous unloading curve $A\rightarrow B\rightarrow C$. The unloading curve beyond point 'B' follows the curve $A\rightarrow B\rightarrow C$.

7. When following the internal rule, the κ_{target} value is always equal to the κ value at the latest previous reversing point (before the current revsing point). For example, κ_{target} is $\kappa_A=\kappa_{\max}$ for the reloading branch $B\rightarrow A$ and κ_B for the re-unloading branch $D\rightarrow B$.

8. Whenever the previous reversing point is passed, all the memory of previous cyclic loading history is erased. So, the reloading curve beyond Point B is bound for point 'A', not for point 'D'.

7. Stress-dilatancy relations (flow rule)

To convert the $\eta \sim \kappa$ relation into a $\sigma_v \sim \varepsilon_v$ relation, a flow rule, such as stress-dilatancy relation becomes necessary. The dilatancy behavior of sand has been studied by many researchers (Bolton, M. D., 1986, Tatsuoka, F., 1987). But for present study Rowe's stress-dilatancy relation is used. The Rowe's stress-dilatancy relation for plane strain condition is:

$$R = -KD \tag{10}$$

where,

$$R = \frac{\sigma_1}{\sigma_3} = \frac{1+\sin\varphi_{mob}}{1-\sin\varphi_{mob}}$$

$$K = \left(\frac{\sigma_1}{\sigma_3}\right)_{\varphi=\varphi_r} = \frac{1+\sin\varphi_r}{1-\sin\varphi_r}$$

$$D = -\frac{d\varepsilon_3^p}{d\varepsilon_1^p}$$

φ_r = Residual angle of friction

Considering the plastic potential as Druker-Prager and a non-associated flow rule, it can be written,

$$\phi = \frac{1}{3}(\sigma_1 - \sigma_3) + \frac{1}{2}(\sigma_1 + \sigma_3)\sin\psi \tag{11}$$

From the definition of dilatancy angle the following relation can be obtained:

$$d\varepsilon_3^p = -\frac{1+\sin\psi}{1-\sin\psi} \tag{12}$$

Substituting eqn. 12, R and K into eqn. 10, the following equation can be obtained:

$$\frac{1+\sin\psi}{1-\sin\psi} = \frac{(1+\sin\varphi_{mob})(1+\sin\varphi_r)}{(1-\sin\varphi_{mob})(1-\sin\varphi_r)}$$

Solving, $$\sin\psi = \frac{\sin\varphi_{mob} - \sin\varphi_r}{1-\sin\varphi_{mob}\sin\varphi_r} \tag{13}$$

Substituting eqn. 3 and eqn. 13 into eqn. 4, we get,

$$\xi = \frac{\sqrt{3}(\eta - \eta_r)}{\sqrt{3} + 3\eta_r - 6\sqrt{3}\eta\eta_r} \tag{14}$$

where,

$$\eta_r = \frac{2\sin\varphi_r}{\sqrt{3}(3-\sin\varphi_r)}$$

This is the stress-dilatancy relation for loading and unloading skeleton curves. For loading and unloading curves, using eqn. 6, the stress-dilatancy relation becomes,

$$\xi = \frac{\sqrt{3}(\eta - n\eta_r)}{\sqrt{3} + 3n\eta_r - 6\sqrt{3}n\eta\eta_r} \tag{15}$$

7.1 *Material parameters*

A hypothetical material is chosen to simulate the drained cyclic plane strain test results. In the following table the material parameters listed:

Table 1. Material parameters

Parameters	Symbol	Values
Elastic Shear modulus	G_e	7120 KPa
Elastic bulk modulus	K_e	25000 KPa
Peak Strength (Loading)	φ_{pl}	15°
Peak Strength (Unloading)	φ_{pu}	15°
Residual Strength (Loading)	φ_{rl}	12°
Residual Strength (Unloading)	φ_{ru}	12°
Cumulative Peak Plastic Strain (Loading)	κ_{fl}	0.1
Cumulative Peak Plastic Strain (Unloading)	κ_{fu}	0.1
Power of Hyperbolic Hardening Relation (Loading)	m_l	0.6
Power of Hyperbolic Hardening Relation (Unloading)	m_u	0.6

8. Results and discussions

To simulate the cyclic behavior of sand under plane strain condition, a hypothetical cyclic displacement is applied to a quadrilateral element. As a result, we found the stress-strain relationship of the sand undergoing cyclic loading. The results are plotted for various well-known relations. For each load step $1e^{-5}$ mm/mm strain is applied in the σ_1 direction and corresponding stress and strain matrix is found. From the total stress and strain matrix we found various required parameters. A set of results are simulated here. The graphs and their significances are stated below.

In Fig. 5 shear strain γ is plotted against the load steps. Thus we can visualize the cyclic behavior of strain applied.

In Fig. 6 the cumulative plastic strain (κ) is plotted against the load step. Here we can see the accumulated plastic strain in loading direction is recovered in the reversed loading direction.

In Fig. 7 the $\eta \sim \kappa$ relationship under cyclic loading is presented. Here, the η grows hyperbolically as plastic shear strain accumulates. It follows the Masing's rule and forms a closed loop.

In Fig. 8 the $R \sim \kappa$ relationship under cyclic loading is illustrated. Here, the $R = \sigma_1/\sigma_3$ is the stress ratio. It is also a measure of the shear stress applied and have a value equal to

1 when $\sigma_1 = \sigma_3$. Its behavior also completely follows the Masing's rule and forms a closed loop.

In Fig. 9 the $R \sim \gamma$ relationship under cyclic loading is plotted. It is similar to the $R \sim \kappa$ relationship.

In Fig. 10 the $\varepsilon_v \sim \gamma$ relationship under cyclic loading is demonstrated. The volumetric strain accumulation here follows the Rowe's stress-dilatancy relationship.

In Fig. 11 volumetric strain ε_v is plotted against the load steps. Thus we can visualize the cyclic behavior of the volumetric strain.

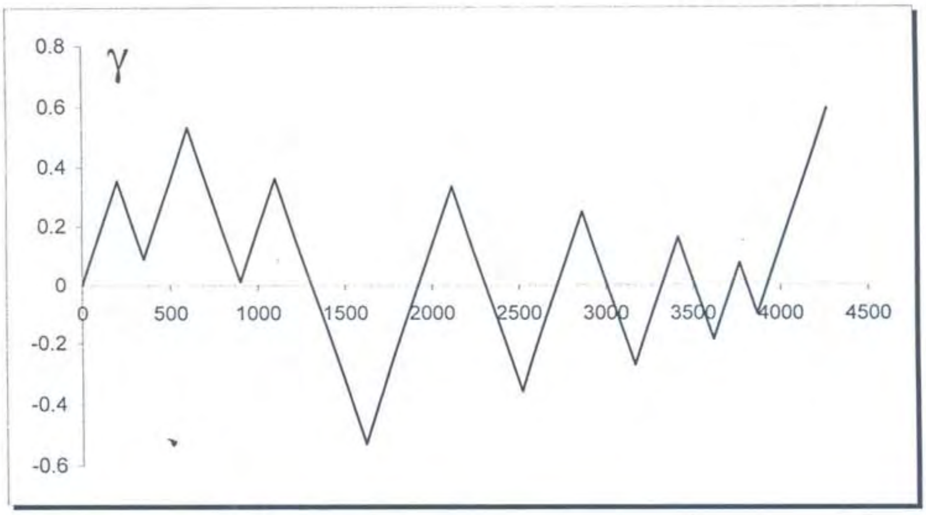

Fig. 5. Shear strain γ vs. load steps

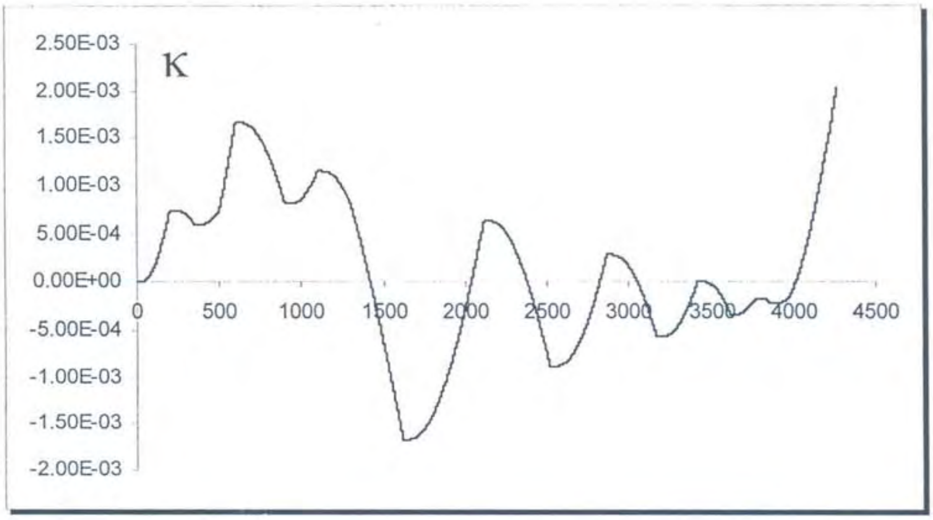

Fig. 6. Cumulative plastic strain K vs. load steps

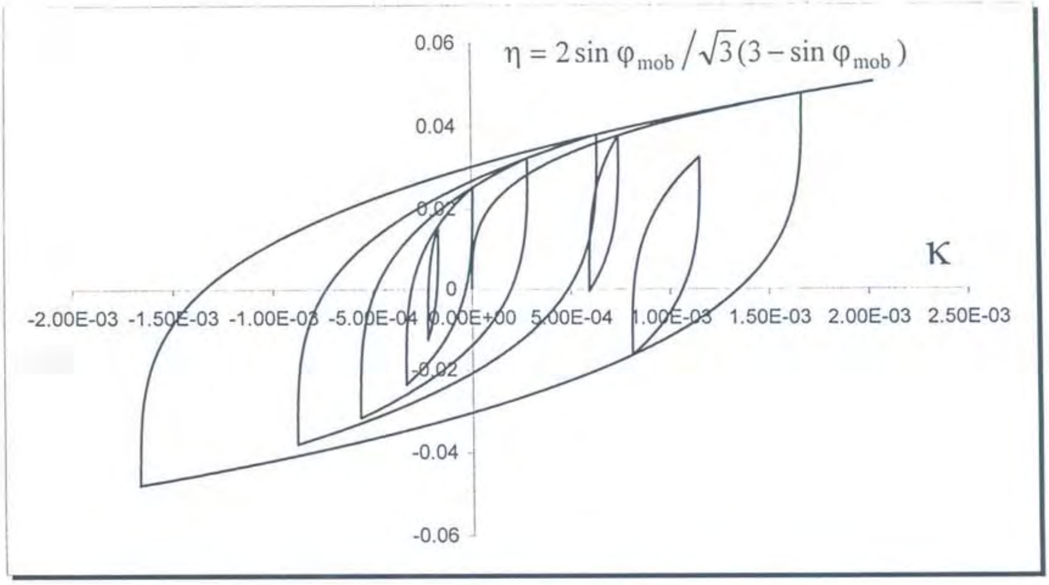

Fig. 7. $\eta \sim \kappa$ curve

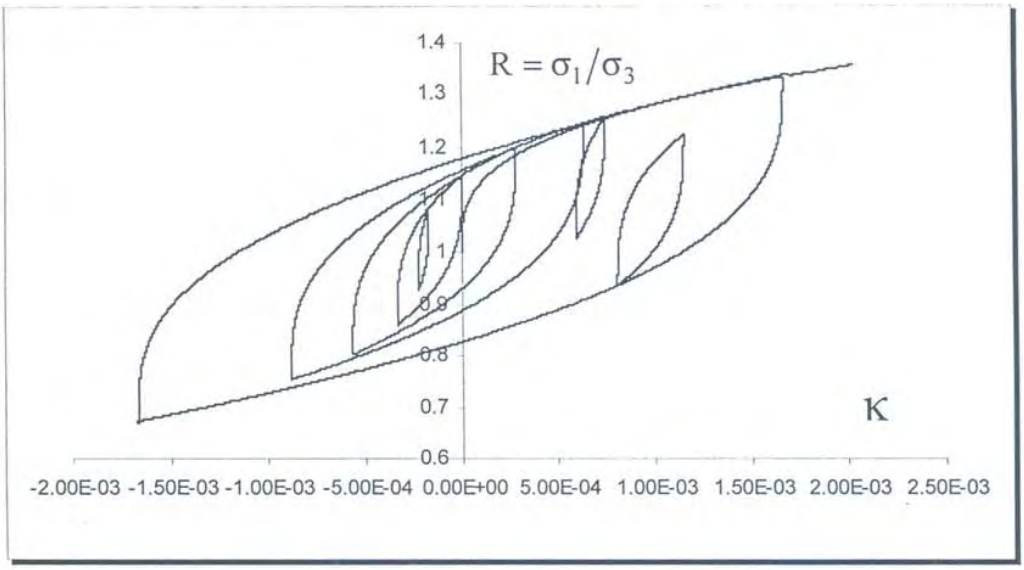

Fig. 8. Stress ratio R vs. cumulative plastic strain κ

9. Conclusions

The following conclusion can be drawn from the results simulated by the model,

1. The relationship between stress ratio $R = \sigma_1/\sigma_3$ and shear strain $\gamma = \varepsilon_1 - \varepsilon_3$ obtained from the drained cyclic plane strain test on a hypothetical pressure independent material performed at a constant σ_3 is rather symmetric to the about the neutral axis of $R = 0$.

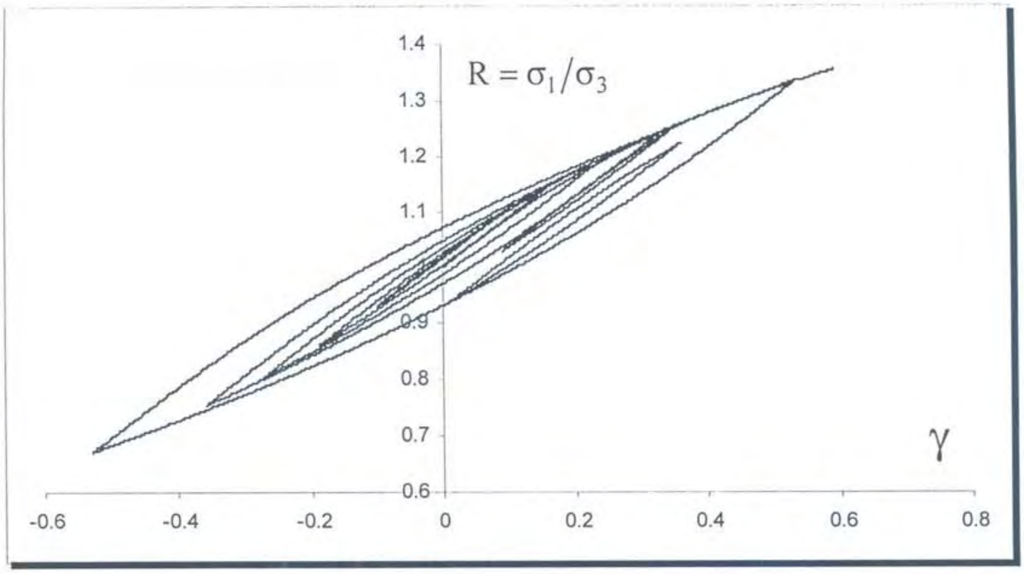

Fig. 9. Stress ratio R vs. shear strain γ

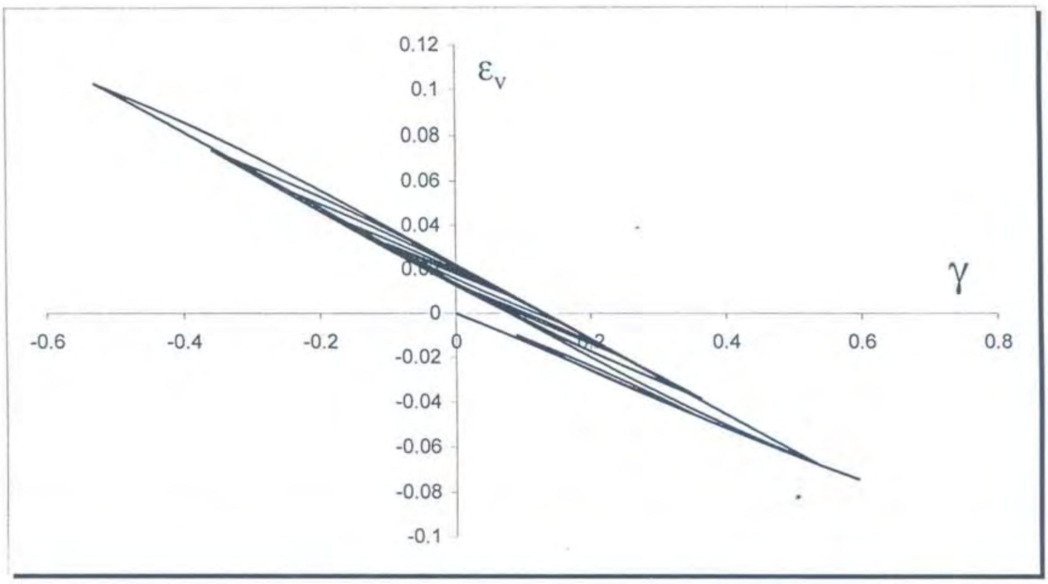

Fig. 10. Volumetric strain ε_v vs. shear strain γ

2. The hyperbolic relationship (Tanaka) could simulate to a reasonable accuracy those $\eta \sim \kappa$ relations. So, the simulated $\eta \sim \kappa$ relations can be used as the skeleton curves in the simulation of the cyclic plane strain stress-strain behavior.

3. The proportional rule consisting of external and internal rule (Tatsuoka et al. 2003) formulated by modifying the original Masing's rule is used here. The proportional rule is more flexible and more general to simulate stress-strain relations of sand under various cyclic loading conditions, in particular when the

primary loading and unloading stress-strain relations are not symmetric about the neutral axis.

4. After necessary modification, the Rowe's stress-dilatancy relation could reasonably simulate the flow characteristics in cyclic plane strain loading.

5. Finally, the proposed framework can be well integrated with the finite element method (FEM) to solve the boundary value problems subjected to cyclic loadings.

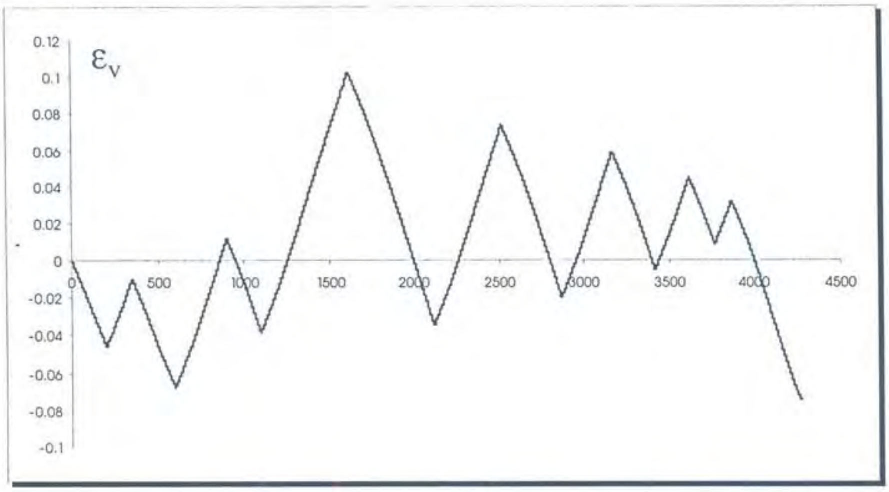

Fig. 11. Volumetric strain ε_v vs. load steps

The model proposed here can well simulate the cyclic behavior of a hypothetical material, which is pressure independent. Thus, the model is a complete model for pressure independent material and with further modification it should be applied to pressure dependent materials. Also introducing the drag rule it will simulate the cyclic stress-strain behavior in which the stress amplitude increases at a decreasing rate during cyclic loading with constant strain amplitude.

References

Bolton, M.D. (1986). "The strength and dilatancy of sands", *Geotechnique*, 36, No. 1, 65-78.

Hossain, M.R. (2005). "FE Modeling of the Stress-Strain Behavior of Sand in cyclic Plane Strain Loading", B. Sc. Engg. Thesis, Bangladesh University of Engineering and Technology.

Montáns, F. J. (2000). "Bounding surface plasticy model with extended Masing's behavior", *Comput. Methods Appl. Mech. Engrg.*, 182, 135-162.

Siddiquee, M.S.A. (1994). "FEM simulations of deformation and failure of stiff geomaterials based on element test results", D.Eng. dissertation, The University of Tokyo, Japan.

Tanaka, T., "Elasto-plastic strain hardening-softening soil model with shear banding".

Tatsuoka, F. (1987). "Discussion" on "The strength and dilatancy of sands", by Bolton, M.D., *Geotechnique*, 37, No. 2, 219-226.

Tatsuoka, F., Jardine, R.J., Lo Presti, D.C.F., Di Benedetto, H., and Kodaka, T. (1999). "Characterizing the pre-failure deformation properties of geomaterials, Theme Lecture", *Proc. 14th ICSMFE*, Hamburg, 1997, 4, 2129-2164.

Tatsuoka, F., Masuda, T., Siddiquee, M.S.A., and Koseki, J. (2003). "Modeling the stress-strain relation of sand in cyclic plane strain loading", *J. Geotech. Geoenv. Engrg., ASCE*, May, 450-467.

Japan-Bangladesh Joint Seminar on Advances in Bridge Engineering ISBN: 984-32-2520-6
Dhaka, Bangladesh. 10 August 2005

A nonlinear model for soft rock and its application in bridge pier settlement calculation

M.S. Islam[1], M.S.A. Siddiquee[1*], F. Tatsuoka[2]

[1]*Department of Civil Engineering*
Bangladesh University of Engineering and Technology, Dhaka 1000, Bangladesh
[2]*Tokyo University of Science, Noda shi, Chiba, Japan*

Abstract

A phenomenological model has been developed for soft rock based on the results of a series of triaxial compression (TC) tests conducted on Kobe sandstone with a very high measurement precision. From the analysis and interpretation of the test results, it has been found that small strain Young's modulus (E^e) is a function of the major principal stress. E^e for elastic strains of soft rock is assumed to be cross-anisotropic. A damage function has been used to derive the appropriate elastic Young's modulus when subjected to shear loading. As the basic stress-strain relation, the relationship between the tangent modulus and the shear stress level is used. The differential form of which is subsequently integrated by a 4th order Runge-Kutta solver to obtain the stress-strain relation. The model of soft rock considered an isotropic hardening elasto-plastic FEM solver which takes into account the pressure sensitivity, cross-anisotropy, degradation of Young's modulus with the degree of mobilized shear stress and the nonlinearity of the shear stress-shear strain relationship. This model is successfully calibrated with Akashi gravel and applied in the simulation for the settlement of Akashi-Kaikyo bridge piers. The simulations were carried out for both drained and undrained condition by changing the Poisson's ratio. The layering informations beneath the foundations were used in the FEM simulation. The use of very accurate Young's modulus from the field shear wave velocity test was the key to the successful simulation of the settlement under bridge pier foundations.

Keywords: FEM, model, soft rock and simulation.

1. Introduction

In recent years, since increasing number of foundations have been placed on soft rock, it becomes of great importance to evaluate mechanical properties of soft rocks accurately. General aspects and engineering characteristics of soft rocks in Japan were reported by different researchers such as Aki et al. (1979). Numerous failure criteria for foundation

* Email: sid@ce.buet.ac.bd

satiability analyses or elastic-plastic finite element analyses have also been proposed. As concerns relationships between the confining pressure and strength of soft rocks, power function models were proposed by Hobbs (1966), Yoshinaka and Yamabe (1980) and Adachi and Ogawa (1980). It is reasonable that linear equations such as the Mohr-Coulomb's failure criterion are not suitable for soft rocks. But instead, non-linear equations as a power function may better describe the failure model for soft rocks. In this context, a general methodology for modelling the stress-strain relationship for soft rock has been developed.

The modeling has been carried out by mathematical formulation of the stress-strain relations obtained by a long-term element test programme at the Institute of Industrial Science (IIS), University of Tokyo, Japan. (Hayano et. al., 1997; Jiang et al., 1998; Kohata et al., 1997, Tatsuoka and Kohata, 1995; Tatsuoka and Kim, 1995 and Tatsuoka et al., 1995). The model is derived from the laboratory triaxial compression (TC) test results. All the tests were equipped with Local Deformation Transducers (LDT) to obtain stress-strain relations at small strains free from the effect of bedding error (Goto et. al., 1999). Elastic deformation parameters, the Young's modulus, were obtained from small unloading-reloading cycles applied during the TC testing. The model considers the pressure level-dependency of elastic Young's modulus, stress system-induced anisotropy, non-linearity of stress-strain relations, damage to micro-structures by shearing while based on field Young's modulus (E_f) from in-situ shear wave velocity measurements. The mentioned soft rock model is developed basically from the TC test data of Kobe sandstone. Finite Element Method (FEM) is used to simulate the settlement under the pier foundations of Akashi-Kaikyo Bridge. During the FEM simulation of the settlement of the pier 2P, of the Akashi-Kaikyo Bridge in Japan, it was found that there is a layer of Akashi-gravel at the top. However, available TC test data for Akashi gravel was limited. In the absence of availability of adequate test data on Akashi gravel, the soft rock model developed in this study is calibrated for the Akashi gravel to simulate the pier 2P's behaviour with layering information. This paper deals with the development of the model for the particular soft rock. Application of this model to simulate the settlements of the pier of the Akashi-Kaikyo Bridge in Japan has been presented.

2. Properties of Akashi sandstone

Wet density of the Akashi sandstone ranges from 1.99 to 2.19 g/cm^3 with an average value of 2.09 g/cm^3 (Kashima et al., 1995). The measured wet density is smaller than the actual density because of water loss in the samples during sampling. The calculated saturated density varies in a small range from 2.10 to 2.20 g/cm^3 as compared to the wet density. Grain size distributions of this sand are also available in Kashima et al. (1995). The maximum diameter (D_{max}) ranges from 36 to 136 mm and a diameter at 60% finer (D_{60}) ranges from 0.70 to 19.00 mm. The Akashi sanstone is mostly classified into gravel with fines based on Japanese Soil Classification. The coefficient of uniformity generally exceeds 10. Gravel shape is mainly subangular and subrounded. The formation contains 20 to 30% of decomposed gravel.

3. Constitutive model

An elasto-plastic isotropic hardening model is employed here for the soft rock. The plastic part is modeled by a non-associated flow rule based on a generalized Mohr-Coulomb yield function along with a Drucker-Prager type plastic potential function. As the basic stress-strain relation, the relationship between the tangent shear modulus and the shear stress level is used (hence called "plasticity function"), the differential form of which is subsequently integrated by a 4th order Runge-Kutta solver to obtain the stress-strain relation. A damage function is used to describe the degradation of Young's modulus due to micro-cracking that develops with the increase in shear stress. However, unlike the constitutive relations for sand, the constitutive relations for soft rock does not include softening, shear banding and strength anisotropy. The model traces the stress-strain relation up to the peak.

3.1 Young's modulus

From the triaxial compression (TC) test results (Hayano et. al., 1997; Jiang and Kohata. 1998; Jiang et al., 1998; Kohata et al., 1997), it has been observed that small strain Young's modulus (E^e) for elastic major principal strain is a function of the major principal stress, i.e., $E^e = f(\sigma_1)$. Figure 1 shows the variation of E_{max} ($=E^e$) with confining pressure (σ_l) for Kobe sandstone. It is seen that E_{max} increases with the increase of σ_1. The plot also shows an apparent linear relation signifying a power law dependence of E^e on σ_1. In Figure 1, E_0^e is the value of Young's Modulus at zero confining pressure.

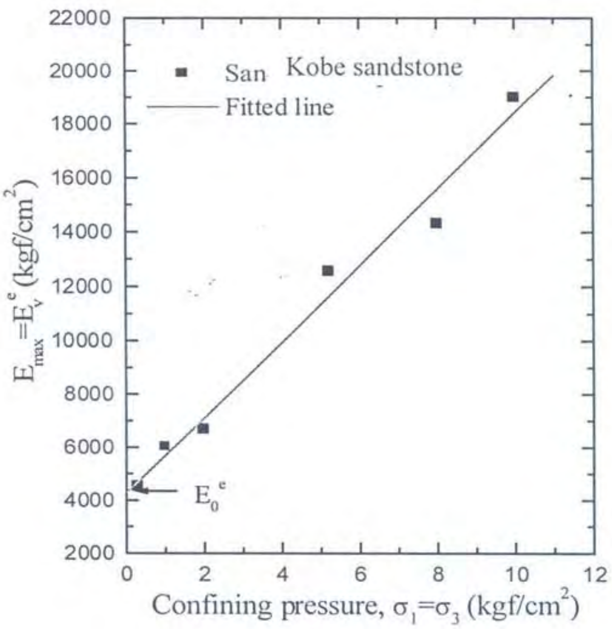

Fig. 1. Variation of $E_{max}(E^e)$ with $\sigma_1 = \sigma_3$.

3.2 Cross-anisotropy

The Young's modulus E^e for elastic strains of soft rock is assumed to be cross-anisotropic. From the test results it was seen that the Young's modulus, E^e for elastic strains of Kobe sandstone can be reasonably assumed to be cross-anisotropic (Hoque and Tatsuoka, 1998) under axially symmetric stress conditions (stress system-induced anisotropy). This feature is modeled as described in Eq. 1.

$$E_v^e = E_0^e + a\sigma_v^b, \quad E_h^e = E_0^e + a\sigma_h^b \tag{1}$$

where, E^e_v and E^e_h are the Young's moduli for elastic normal strains in the vertical and horizontal directions, respectively. E^e_0 is the value of Young's modulus at zero confining pressure (Fig. 1).

As the material has a cohesion, E^e_0 is a non-zero value. From Eq. (1), $E^e_v = E^e_h = E^e_0$ is obtained when $\sigma_v = \sigma_h$, namely inherent isotropy is assumed for elasticity. From the energy conservation law, the following relationships are obtained;

$$\nu_{hv}^e = \nu_0^e \alpha, \; \nu_{vh}^e = \nu_0^e \alpha^{-1} \tag{2}$$

where, $\alpha = \sqrt{E_h^e / E_v^e}$, ν_{hv}^e = Poisson's ratio for the deformation from horizontal to vertical directions (vice versa for ν_{vh}) and ν^e_0 is the Poisson's ratio for elastic strains under isotropic stress conditions. In the same way, the shear modulus G^e_{hv} for elastic shear strains is derived as described in Eq. 3.

$$G_{hv}^e = E_{45}^e / 2(1 + \nu_0^e)$$

$$E_{45}^e = E_0^e + a\{0.5(\sigma_v + \sigma_h)\}^b \tag{3}$$

where, G^e_{hv} is cross anisotropic shear modulus in h ~ v plane and E^e_{45} is cross anisotropic Young's modulus at an angle 45° with h ~ v plane. E^e_0 is isotropic Young's modulus, σ_v is current vertical stress component and σ_h is current horizontal stress component, respectively. E^e_{45} is E^e when the direction of σ_1 is at 45° relative to the vertical.

3.3 Damage function

The concept of the damage function is developed due to the experimental evidence of the deterioration of the material strength, reflected in the continuous reduction of equivalent Young's modulus E^e when compared to E_{max} under an identical σ_1, depending on the amplitude of shear stress. The evaluation of the damage function was necessary for the following two cases.

3.3.1 Elastic modulus

An empirical model was developed for the Kobe sandstone based on the results for consolidated drained triaxial compression (TC) tests measuring axial strain locally. The core samples tested were obtained by block sampling from the bottom of the excavation to a depth of 61 m for pier 1A of Akashi-Kaikyo Bridge (Kohata et al., 1994).

At a depth of 61m, four plate loading tests using a rigid 60 cm-diameter plate were performed. Figure 2 shows the variation of different Young's Moduli with depth. The initial Young's moduli, E_{max} defined at axial strains less than about 0.001 % in the TC tests performed at an confining pressure equal to the original in-situ effective overburden pressure are only slightly smaller than the Young's moduli E_f from field shear wave velocities. The difference is due partly to the drained condition in the TC tests compared to the undrained condition in the seismic survey (thus by the factor of (1+0.2)/(1+0.46), in which 0.2 and 0.46 are drained and undrained Poisson's ratios, respectively). The difference is also due partly to the effects of inevitable sample disturbance.

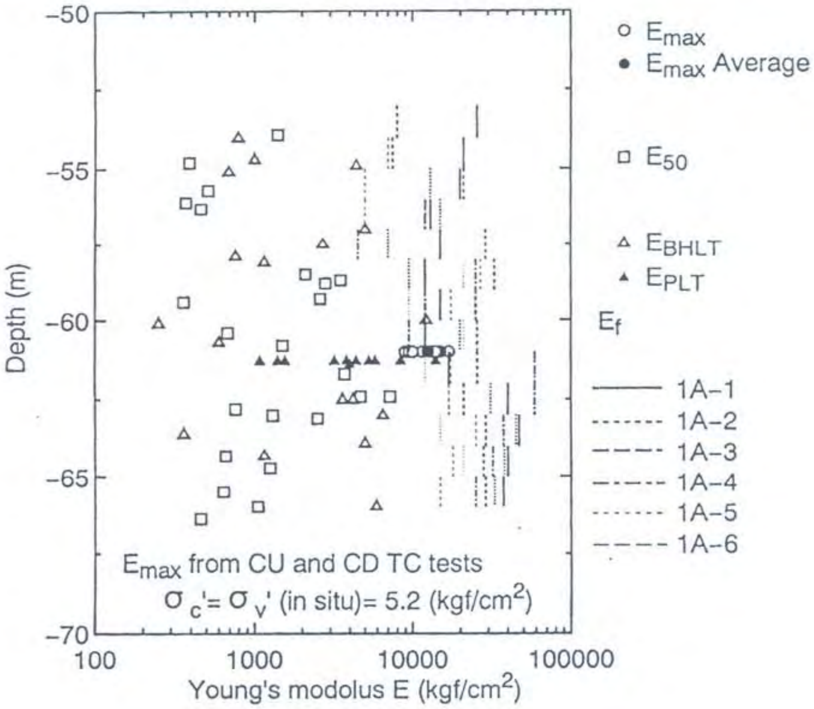

Fig. 2. Variation of Young's moduli with depth (E_f: from shear wave velocity measurements, E_{max} from local axial strains by LDT, E_{50} from unconfined compression tests with external axial strains, E_{BHLT}: from bore hole loading test, E_{PLT}: from plate loading test).

As also presented in Kohata et al. (1994), the Young's modulus, E_{eq} for elastic axial strains measured in small unload/reload cycles during triaxial compression is primarily a function of the axial stress σ_l, exhibiting cross-anisotropy. However, with shearing E_{eq} becomes noticeably smaller than E_{max} ($=E_v{}^e$ under isotropic stress conditions) measured at the same axial stress (σ_l). The variation of equivalent Young's modulus determined from the slope of the unloading-relaoding curve E_{eq} and maximum Young's modulus obtained from the beginning part of the shearing by monotonic loading, E_{max} for the same σ_1 is plotted in Figure 3. In this Figure, m is defined as stated in Eq. 4.

$$\frac{E_{eq}}{E_{max}} = E_0^e + a\sigma_1^m \tag{4}$$

Comparing Eq. 1 and 4, we can find that m =b. Figure 3 describes the relationships between E_{max}, E_{eq} and σ_1 for different m values i.e., 0, 0.5 and 0.7. In this figure, E_{max} is denoted as $E^e(\sigma_1)$. As this reduction in E_{eq} can be considered due to the damage to the micro-structure by shear deformation, the relation between the ratio $E_{eq}/E^e(\sigma_1)$ and the shear stress level q/q_{max} is defined as the damage function f_d^e as stated in Eq. 5.

$$E_{eq}(\sigma_1) = E^e(\sigma_1) \cdot f_d^e(\tau/\tau_{max}) \tag{5}$$

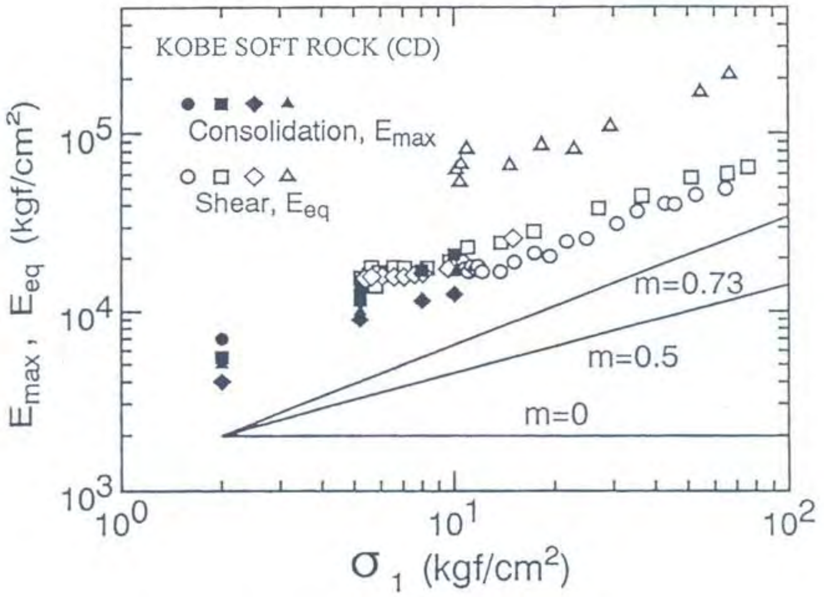

Fig. 3. Variation of E_{max} and E_{eq} with σ_1.

where, E_{eq} is Equivalent Young's modulus determined from small amplitude cyclic-loading test, σ_1 is major principal stress and τ/τ_{max} is relative mobilized shear stress which is equal to q/q_{max}.

The variation of $E_{eq}/E^e(\sigma_1)$ with q/q_{max} for Akashi-gravel is presented in Figure 4. For the first approximation, the average relationship for E_{eq} and q/q_{max} can be modeled by a simple hyperbolic function as described in Eq. 6.

Function-1

$$f_d^e\left(\frac{\tau}{\tau_{max}}\right) = \frac{1}{1 + 2.75 \cdot (\tau/\tau_{max})} \tag{6}$$

The average relation can be also modeled more precisely by the following Eq. 7.

Function-2

$$\left.\begin{aligned}(\tau/\tau_{\max}) \le 0.137, \quad & f_d^e\left(\frac{\tau}{\tau_{\max}}\right) = \frac{1-0.15*(\tau/\tau_{\max})^{0.15}}{1+(\tau/\tau_{\max})^{0.25}} \\ (\tau/\tau_{\max}) > 0.137, \quad & f_d^e\left(\frac{\tau}{\tau_{\max}}\right) = 0.5519\end{aligned}\right\} \tag{7}$$

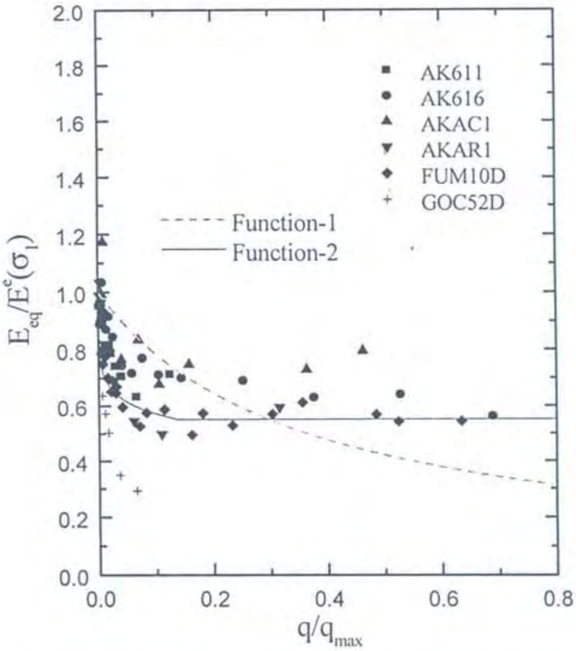

Fig. 4. Decrease in E_{eq} with shear stress level (Akashi sandstone).

For the model, the relationship between $E^e(\sigma_1)$ and τ_{max} was obtained by averaging the TC test results. These relationships are described in Eq. 8.

$$\begin{aligned}E_{\max} &= 4276.28 + 1413.56\sigma_1 \\ \tau_{\max} &= 39.03 + 1.33\sigma_3\end{aligned} \tag{8}$$

in which E^e, τ_{max}, σ_1 and σ_3 are in kgf/cm^2. The damaged shear modulus G_{eq} for elastic strains is obtained as $E_{eq}(\sigma_1)/\{2(1 + \nu^e)\}$, in which ν^e is the Poisson's ratio for elastic strains assumed to be equal to 0.2 and 0.46 for drained and undrained conditions, respectively.

3.3.2 *Plasticity function*

For the undrained TC tests, the tangent shear modulus G_{tan} can be obtained from the relationship between the deviator stress and the locally measuring axial strain, since the shear strain, γ is obtained as $\gamma = (3/2)\varepsilon_1$. On the other hand, for the drained TC tests, the available raw data of the drained TC tests are locally and externally measured axial strains, and externally measured volumetric strains obtained from the amount of the pore water expelled from or soaked into a specimen. So the bedding error was first determined in the axial direction, i.e., ε_1 as a function of σ_1. The same amount of correction for ε_1 was applied to the recorded volumetric strain, ε_v as a correction factor for the calculation of radial strain in order to determine the maximum shear strain, i.e.,

$$\text{Correct } \gamma = (\varepsilon_1)_{\text{locally measured}} - (\varepsilon_3)_{\text{corrected}} \tag{9}$$

where,

$$(\varepsilon_3)_{corrected} = \frac{3}{2}(\varepsilon_1)_{locally\ measured} - \frac{1}{2}(\varepsilon_v)_{corrected}$$

$$(\varepsilon_v)_{\text{corrected}} = (\varepsilon_v)_{\text{measured}} - \{(\Delta\varepsilon_1)_{\text{BE}} \text{ as a function of } \sigma_1\}$$

This shear strain is used to calculate G_{tan} from the results of the undrained TC tests. The value of G_{tan} for ε_1 in the vertical direction is normalized by respective G_{max} (calculated from the experimental Young's modulus, $E^e(\sigma_1)$ and an assumed Poisson's ratio of 0.2 for drained tests and 0.46 for the undrained tests, respectively). The tangent shear modulus G_{tan} for total shear strains measured during the TC tests on Akashi sandstone divided by $G^e(\sigma_I) = E^e/\{2(1 + \nu^e)\}$ are plotted against q/q_{max} in Figure 5.

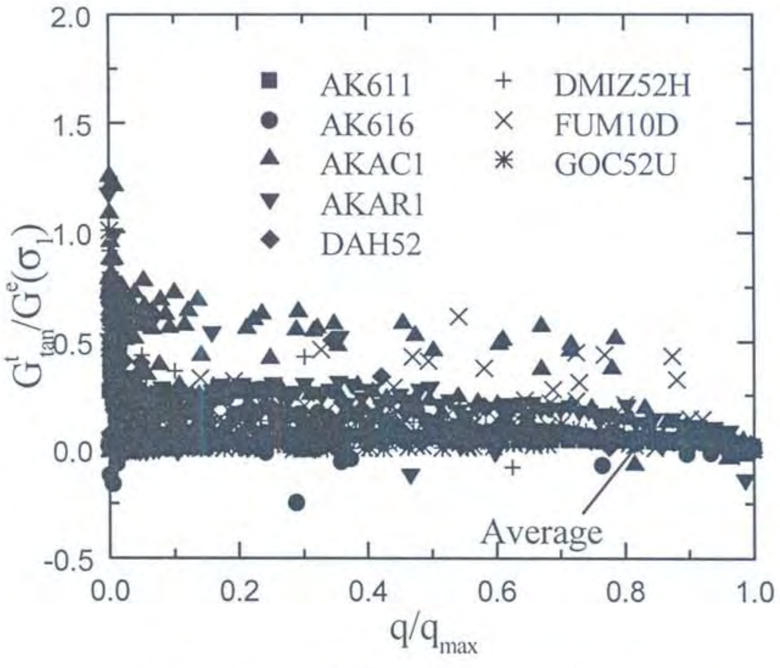

Fig. 5. $G^t_{tan}/G^e(\sigma)$ versus q/q_{max} (Akashi sandstone).

Here, in choosing the plasticity function that it was the function that starts from 1.0 when q/q_{max} is 0 and it is 0.0 when q/q_{max} is 1.0. It is seen from the Figure 5 that the function drops sharply at the beginning, followed by a flat part, which characterizes a S-shape stress-strain curve. This trend is believed to be linked to such a physical meaning as the opening of the micro cracks due to the initial shear loading stage. Subsequently, the ratio, $G_{tan}/G^e(\sigma_1)$ rises a little and again drops towards zero as q/q_{max} approaches 1.0. A systematic difference between the drained and undrained conditions was not found. To express the peculiar behavior that the ratio decreases very sharply with q/q_{max} at the initial stage followed by a slight increase and a subsequent gradual decrease to zero, the following Eq. (10) was chosen, while the parameters were obtained by non-linear regression of the data.

$$G_{tan}^t(\sigma_1) = G^e(\sigma_1) \cdot h^g(\tau/\tau_{max}) \tag{10}$$

$$h^g(y) = \frac{1 - y + c(y^2 - y) + d(y^3 - y)}{1 + by} \tag{11}$$

where, $y = \tau/\tau_{max}$, b=9674, c=778 and d=-2740. The plasticity function h^g is equal to the damage function for G_{eq} times the ratio "damaged elastic shear strain increment"/"total shear strain increment".

4. FEM implementation

In this research, classical non-associated elasto-plastic isotropically hardening non-linear Finite Element Method (FEM) is used. In order to capture the basic behaviour of soft rock, Mohr-Coulomb type of yield function and Druker-prager type of plastic potential is used. A four noded iso-parametric element was used with 1-point integration. The probable hour-glass mode was prevented (Flanagan and Belytschko, 1981). A highly optimized non-linear equation solver, Dynamic Relaxation (DR) (Tanaka and Kawamoto, 1988) is used to solve the nonlinear equations, resulting from the material nonlinearity. Integration of the elasto-plastic equations was performed by means of a return mapping scheme (Ortiz and Simo, 1986). Selectively reduced integration (reduced integration on shear terms) was used to reduce the shear locking near incompressible situation. Dilatency is implemented via modified Rowe's stress-dilatency relation. General elasto-palstic frame work of the model is described below:

This is essentially an elasto-plastic isotropic strain hardened analysis with non-associated flow rule (Eq. 12).

$$\phi = \alpha I_1 + \frac{1}{g(\theta)}\sqrt{J_2} - K = 0 \tag{12}$$

where, $g(\theta) = \dfrac{3 - \sin\phi_{mob}}{2\sqrt{3}\cos\theta - 2\cos\theta\sin\phi_{mob}}$ and $\alpha = \dfrac{2\sin\phi_{mob}}{\sqrt{3}(3 - \sin\phi_{mob})}$

where, J_1 is 1st stress invariant, J_2 is 2nd invariant of deviatoric stress, K is cohesion terms, θ is Load angle, and ϕ_{mob} is mobilized angle of internal friction.

The original Rowe's stress-dilatancy relation was modified to define the plastic potential as stated in Eq. 13.

$$\psi = \alpha' I_1 + \sqrt{J_2} - K = 0 \tag{13}$$

where, $\alpha' = \dfrac{2 \sin \psi}{\sqrt{3}(3 - \sin \psi)}$, $\sin\psi = \dfrac{\sin\phi_{mob} - \sin\phi_r}{1 - \sin\phi_{mob}\sin\phi_r}$ and ϕ_{mob} is mobilized angle of internal friction and ψ is mobilized angle of dilatancy.

The evolution of the yield function is modeled as described in Eq. 14 (Tanaka and Kawamoto, 1988).

$$\alpha = \int(\kappa) \tag{14}$$

where, $\kappa = \int d\varepsilon^P$ and $d\varepsilon^P = [2(de^P_{11})^2 + 2\,(de^P_{22})^2 + 2\,(de^P_{33})^2 + (d\gamma^P_{11})^2 + (d\gamma^P_{23})^2 + (d\gamma^P_{31})^2]^{1/2}$

$de^P_{ij} \sim d\gamma^P_{ij}$ are the deviatoric components of plastic strain increments, κ = plasticity parameter (internal variable).

5. Verification of FEM formulation

The model thus developed in this study has been used to simulate the actual settlement measured under the piers of the Akashi-Kaikyo Bridge in Japan. Figure 6 shows the detail layout of the bridge. The bridge is for 6-lane highway with the design speed of 100 km/hr. On April 5, 1998, the Akashi-Kaikyo Bridge was completed and opened to traffic. The bridge, which links Kobe city and Awajshima Island both in Hyogo Prefecture, has main span of 1991 m and a total length of 3911 m and thus becomes the world's largest suspension bridge. The construction work of the bridge foundations has been finished successfully in 1993, which started 20 years before with an investigation of laying the foundation of bridge-pier and keeping it in-place against very strong sea current. The bridge rested on two huge anchors and other two pier foundations. The two middle piers were named as 2P and 3P. The caissons of the piers were constructed elsewhere and tugged by boats to the place of the bridge foundation. The places of the pier foundations were first excavated to some depth (15 to 20 m) and then the caissons were sunk by pouring water inside. Then the inside was filled by underwater concreting. Namely, first the outer chamber of the pier caisson is filled with concrete and then the main body was filled with concrete. The base rock beneath the straits is granite, on which Kobe formation (alternating layers of sand stone and mud-stone in the Miocene), Akashi formation (semi consolidated sand and gravel layer in the late Pliocene and the early Pleistocene) and the Alluvium layer are deposited.

5.1 Simulation using laboratory test data

The FEM simulation followed the sequence of excavation and concrete filling. Two series of analysis were performed. In the first series, the simulation was performed based on the model described in article 3, which has been calibrated only by the results of laboratory TC tests data of the undisturbed samples of sedimentary soft rock obtained at the site of anchor 1A, and those of Akashi gravel obtained at the site of Pier 2P. In the second series, another set of simulations were carried out by using the maximum Young's modulus obtained from field shear wave velocity in each layer.

At the pier 2P, there is a thin weak layer of Akashi gravel which is also modeled using the same approach as of the Kobe soft rock. Only a difference is the lack of the damage function for the Young's modulus for the gravel. In the FEM simulation, the sequence of ground excavation and footing construction analysis was begun by removing all the elements to be excavated and then applying the self weights of concrete under sea water each by each layer while iterating the solution for equilibrium. Figure 7 shows the FEM idealization of the pier sites 2P and 3P. Figure 8 shows the meshes used for the analysis of 2P and 3P pier foundations.

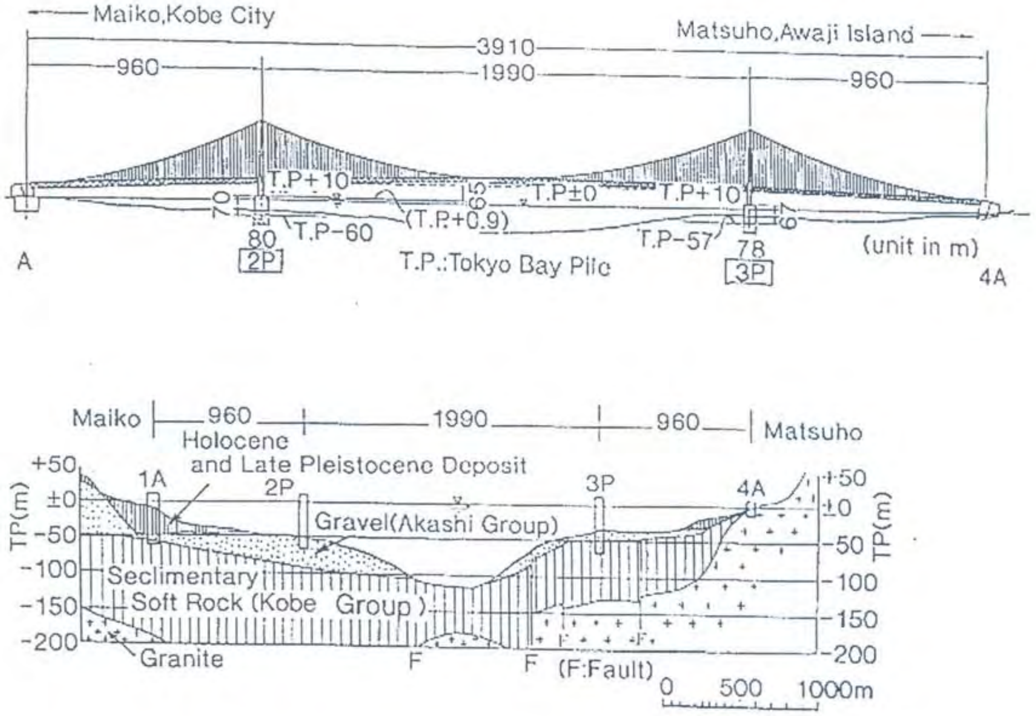

Fig. 6. Details layout of Akashi-Kaikyo Bridge piers.

The analysis was carried out under axisymmetric loading conditions. Figure 9 shows the simulated load-displacement curves for 2P and 3P pier foundations, which include the measured load-settlement curve. As it can be seen that the FEM simulations were done separately for two different conditions using (a) a drained Poisson's ratio, v=0.2 and (b) an Undrained Poisson's ratio, v=0.46. It can be observed from the Figure 9 that the measured load-settlement data lies close to the undrained solution. The comparison between the FEM simulation and the measured behavior suggests that the construction was not slow enough to allow fully drained conditions, and if the construction would have taken considerably long time, extra settlement due to consolidation would have resulted. In any case, it can be said that as a whole the simulated results were quite close to the measured data. Detail settlement profile are calculated at five load levels along the central line of the pier foundations as marked 1 to 5 on Figure 9. The details of the results are available in Siddiquee (1994).

5.2 *Simulation using the field data*

Below each of the two piers, there were several layers of the same material, which have different shear wave velocity values, i.e., different shear modulus values. This information was used to determine the elastic Young's modulus as closely as possible to the field Young's modulus. This goal is attained by the following method. First, the overburden pressure, σ_{v0} at the central depth of each layer and its field Young's modulus, E_{f0} were obtained. Then using the equations for the Young's modulus variation found from TC tests data (Eq. 8), the elastic Young's modulus E^e was obtained as described in Eq. 15.

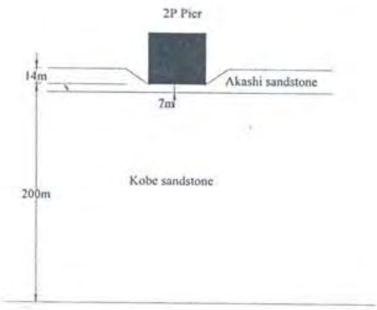

Fig. 7. FEM idealization of 2P and 3P pier site (using laboratory test data).

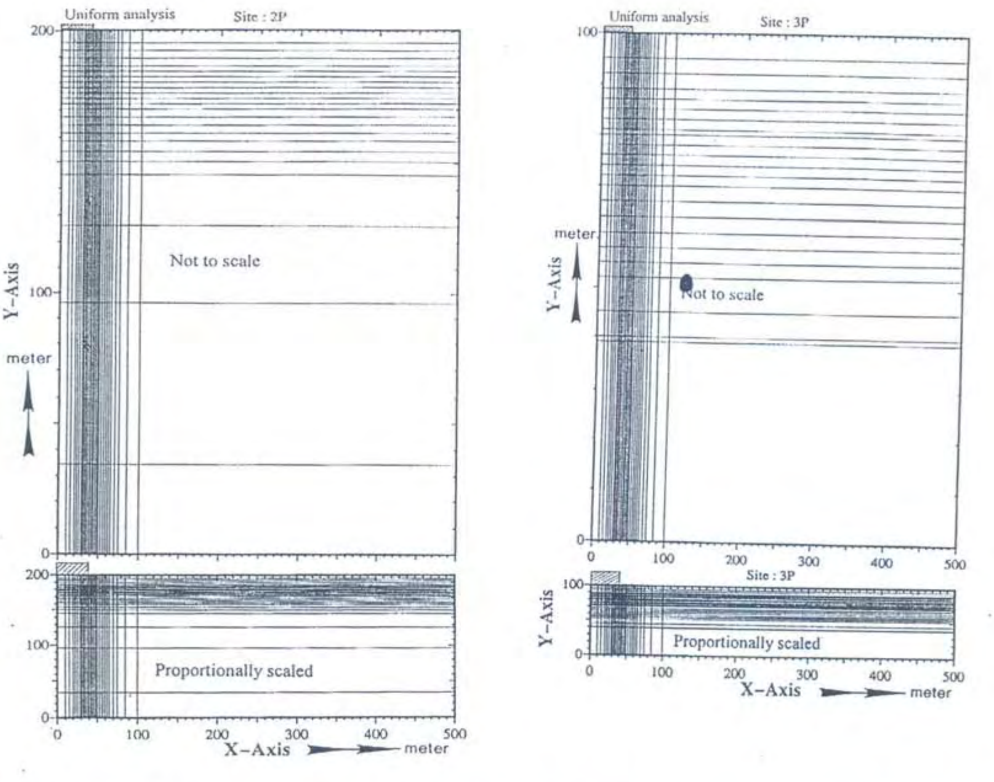

Fig. 8. Mesh used in the FEM simulation of settlement of Akashi-Kaikyo Bridge pier 2P and 3P.

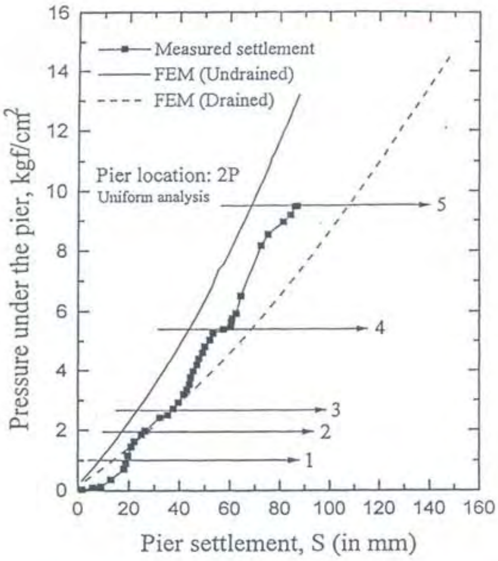

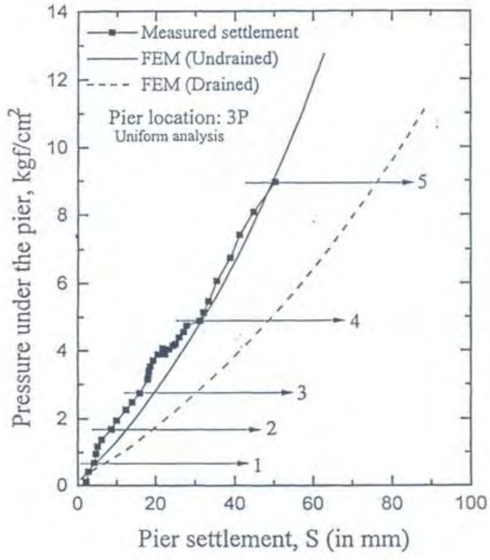

Fig. 9. Load-settlement curves of the Akashi-Kaikyo Bridge pier foundations 2P and 3P.

$$E^{e} = E_{f0} + \text{Constant} \cdot (\sigma_{c} - \sigma_{v0}) \tag{15}$$

where, E^e is elastic Young's modulus, E_{f0} is the Young's modulus at the top layer, σ_c is the confining stress at current layer and σ_{v0} is confining stress at top layer. In the above equation, the rate of the increase in the Young's modulus obtained from TC test data ("Constant" in Eq. 15) and the basic field Young's modulus E_{f0} from the field shear wave velocity data are used. The layering information at the pier 2P and 3P are provided in Figure 10 and Tables 1 and 2.

Table 1. Layer information for the pier 2P (depth of excavation = 14m)

Layer name	Layer thickness (m)	γ_{sat} (t/m^3)	V_s (m/s)	Poisson's ratio, ν	Calculated σ_{v0} (kgf/cm^2)	Calculated E_{f0} (kgf/cm^2)
A_k	7	1.96	360	0.47	0.651	2592.0
K_{2p-1}	32	2.15	450	0.44	3.360	4442.6
K_{2p-2}	28	2.27	720	0.44	6.840	12007.8
K_{2p-3}	30	2.24	710	0.43	10.770	11522.2
K_{2p-4}	62	2.28	880	0.43	16.870	18016.6
Gr'	34	2.35	1100	0.45	24.150	29015.3

In Tables 1 and 2 the layer thickness values are calculated from the bottom of each pier foundation. The diameter of the pier foundation is 80 m and 78 m for 2P and 3P, respectively. Figure 11 shows the FEM mesh used here in this layered soil analysis to accommodate the layers in such a way that the mesh size changes smoothly.

Figure 12 shows the simulated load-displacement curves (Siddique, 1995; Siddique at al., 1994 and 1995) for both 2P and 3P pier foundations containing the measured load-settlement data.

Table 2. Layer information for the pier 3P (depth of excavation = 19m)

Layer name	Layer thickness (m)	γ_{sat} (t/m^3)	V_s (m/s)	Poisson's ratio, ν	Calculated σ_{v0} (kgf/cm^2)	Calculated E_{f0} (kgf/cm^2)
K_{3p-2}	9	2.27	470	0.47	1.736	5111.7
K_{2p-3}	14	2.34	560	0.47	4.585	7488.0
K_{2p-4}	6	2.34	590	0.47	5.895	8311.0
K_{2p-5}	12	2.20	450	0.48	6.480	4545.9
K_{2p-6}	1	2.36	730	0.46	8.046	12833.1
Gr'	29	2.35	860	0.45	10.626	17735.3

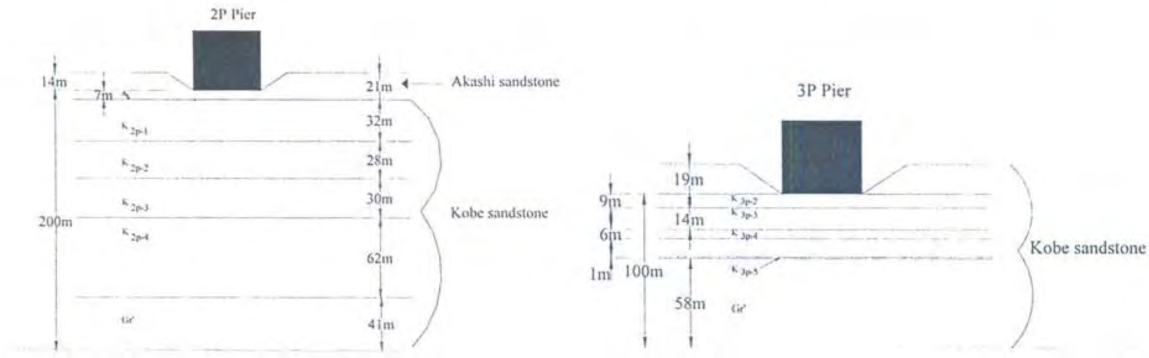

Fig.10. Layer information for the pier 2P and 3P as used in the FEM discretization.

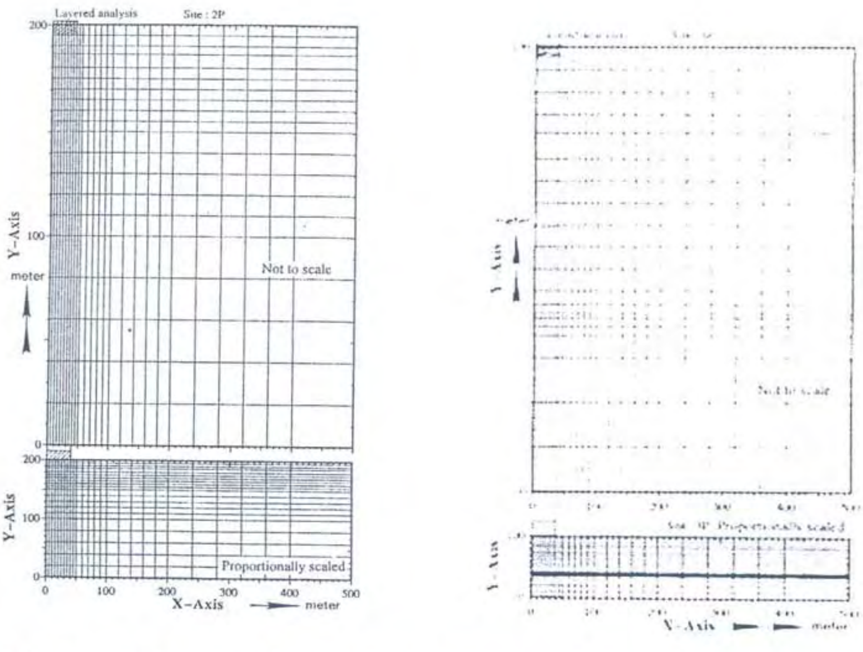

Fig. 11. Mesh used in the FEM simulation of settlement of Akashi-Kaikyo bridge pier 2P and 3P.

The simulations were performed for two drainage conditions varying the Poison's ratio as (a) fully drained condition by applying a Poisson's ratio, ν=0.2 and (b) fully undrained condition with a Poisson's ratio of ν=0.46. The results are expected to be stiffer than the previous simulation considering only the same models as to Young's modulus for each soil or rock type containing several layers. Because the shear modulus obtained from the shear wave velocity at these layers are in general greater than its corresponding values obtained at the stress values of layer mid height from the empirical equation for E_{max} versus σ_v based on the laboratory test data. But some of the layers at greater depths actually had values of shear modulus E_{f0} from the field seismic survey, which are lower than the values based on Eq. 8. This situation resulted in a relatively softer response in the simulation of 2P-pier foundation. Detail settlement profile are calculated at five load levels along the central line of the pier foundations as marked 1 to 5 on Figure 12. The details of the results are available in Siddiquee (1994).

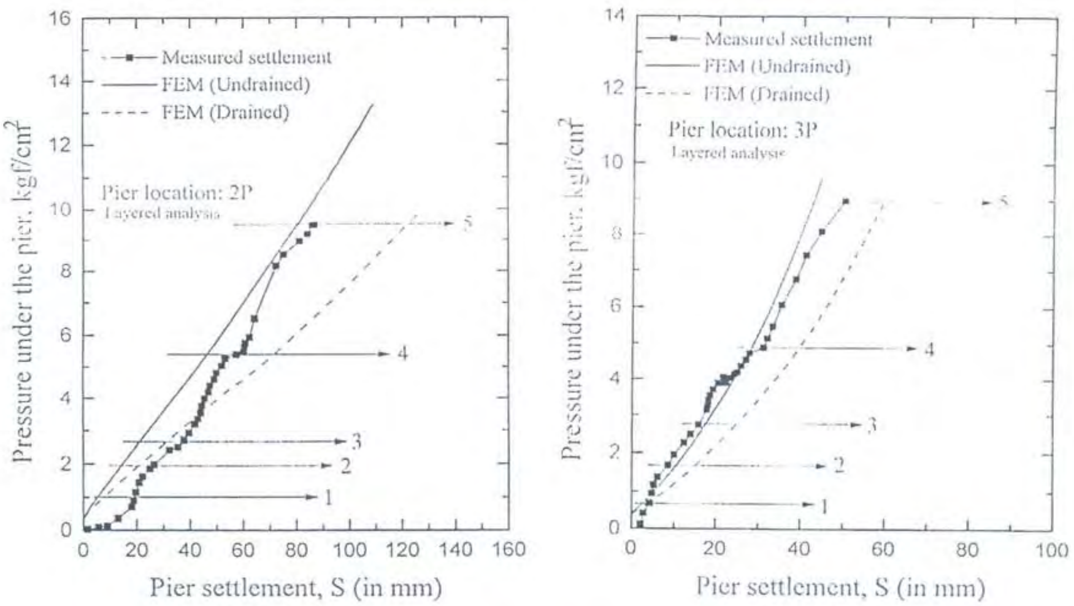

Fig. 12. Load-settlement curves of the Akashi-Kaikyo bridge pier foundation 2P and 3P.

6. Conclusions

A novel model has been developed for soft rock based on the laboratory test results. This model is successfully used for simulating the settlement of the bridge pier foundations. A continuum approach has been devised to model stiff geomaterials by masking the effect of micro-cracks through the introduction of a damage function. Pressure level dependency, cross anisotropy and nonlinearity contributed towards the realistic simulation of the load-settlement behavior of the Akashi-Kaikyo Bridge piers. It is shown that field seismic survey data can be used directly to model such materials as soft rock.

The small strain Young's modulus E^e is a function of the major and minor principal stresses. The small strain Young's modulus E^e of soft rock is assumed to be cross-anisotropic as interpreted from the TC test results. A damage function has been devised to derive the appropriate elastic Young's modulus when subjected to shear loading. The plasticity has been modelled by tangential Young's modulus/tangential shear modulus, whichever available. The tangential shear modulus is further decomposed into two components. One part grows with major principal stress and another part decreases with increasing mobilized shear stress.

Settlement under the piers of the Akashi-Kaikyo Bridge has been simulated successfully using the developed model and the field modulus. The simulation of the settlement of the piers under drained and undrained condition has been carried out. It has been found that simulation in drained condition is closer to the actual settlement record.

References

Adachi, T., Ogawa, T., 1980. Mechanical properties and failure criterion of soft sedimentary rock. Journal of Geotechnical Engineering, JSCE 295, 51-63 (in Japanese).

Aki, K., Adachi, T., Nishi, K., 1979. Time dependent characteristics and constitutive equations of soft rock (porus tuff). J. Geotec. Engg., JSCE 282, 75-96 (in Japanese).

Flanagan, D. P., Belytschko, T., 1981. A uniform strain hexahedron and quadrilateral with orthogonal hourglass control. International Journal of Numerical Methods in Engineering 17, 679-706.

Goto, S., Burland, J. B., Tatsuoka, F., 1999. Non-linear soil model with various strain levels and its application to axisymmetric excavation problem. Soils and Foundations 39 (4), 111-119.

Hayano, K., Sato, T., Tatsuoka, F., 1997. Deformation characteristics of a sedimentary softrock from triaxial compression tests using rectangular prism specimens. Geotechnique, 47 (3), 439-449.

Hobbs, D.W., 1966. A study of behaviour of broken rock under triaxial compression and its application to Mine Roadways. Int. J. Rock Mech., Mining Sci. 3, 11-14.

Hoque, E., and Tatsuoka, F. 1998. Anisotropy in the elastic deformation of materials. Soils and Foundations 38(1), 163-179.

Jiang,G.L., Kohata,Y., Sunaga, M., 1998. Some factors affecting deformation characteristics at small strains of a sandy gravel. Journal of Railway Technical Research Institute 12 (4), 49-54 (in Japanese).

Kashima, S., Yamamoto, S., Takahashi, M. Sasao, Yamada, S., 1995. Large scale sampling of Akashi gravelly layer and its mechanical property. Rock Foundation, Yoshinaka & Kikuchi (eds.), Balkema, Rotterdam.

Kohata, Y., Tatsuoka, F., Dong, J., Teachavorasinskun, S., Mizumoto, K., 1994. Stress states affecting elastic deformation moduli of geomaterials. Proc. of Int. Symp. on Prefailure Deformation Characteristics of Geomaterials, IS-Hokkaido, '94, Balkema, 1, 3-9.

Kohata,Y., Tatsuoka,F., Wang,L., Jiang,G.L., Hoque, E., Kodaka,T., 1997. Modelling the non-linear deformation properties of stiff geomaterials, Geotechnique 47 (3), 563-580.

Ortiz, M., Simo, J.C., 1986. An analysis of a new class of integration algorithms for elasto-plastic constitutive relations. International Journal of Numerical Methods in Engineering, 23, 353-366.

Siddiquee, M S.A. 1994. FEM Simulation of deformation and failure of stiff geomaterials based on element test results, Ph.D. Thesis, The University of Tokyo, Japan.

Siddiquee, M.S.A., Tatsuoka, F., Hoque, E., Tsubouchi, T., Yoshida, O., Yamamoto, S., Tanaka, T. (1994). FEM simulation of footing settlement for stiff geomaterials, Proc. of Int. Symposium Pre-Failure Deformation of Geomaterials (Shibuya et al., eds.), Balkema 1, 531-537.

Siddiquee, M.S.A., Tatsuoka,F., Kohata, Y., Yoshida, O. and Yamamoto, Y. and Tanaka, T., 1995. Settlement of a pier foundation for Akashi-Kaikyo Bridge and its numerical analysis, Proc. Int. Workshop on Rock Foundation of Large Scale Structures, Tokyo, Balkema, 413-420.

Tanaka, T., Kawamoto, O., 1988. Three dimensional finite element collapse analysis for foundations and slopes using dynamic relaxation, Proc. of Num. methods in geomechanics, Istanbul, 1213-1218.

Tatsuoka, F., Kohata,Y., 1995. Stiffness of hard soils and soft rocks in engineering applications, Keynote Lecture, Proc. of Int. Symposium Pre-Failure Deformation of Geo-materials (Shibuya et al., eds.), Balkema, 2, 947-1063.

Tatsuoka. F., Kim,Y.-S., 1995. Deformation of shear zone in sedimentary soft rock observed in triaxial compression, Localisation and Bifurcation Theory for Soils and Rocks (Chambon et al., eds.), Balkema, 181-187.

Tatsuoka.F., Lo Presti.D.C.F., Kohata.Y. 1995. Deformation characteristics of soils and soft rocks under monotonic and cyclic loads and their relationships. SOA Report, Proc. of the Third Int. Conf. on Recent Advances in Geotechnical Earthquake Engineering and Soil Dynamics. St Luis (Prakash eds.), 2, 851 -879.

Yoshinaka, R., Yamabe, T., 1980. Strength criterion of rocks, Soils and Foundation, JSSMFE, 20 (4), 113-126.

Japan-Bangladesh Joint Seminar on Advances in Bridge Engineering
Dhaka, Bangladesh. 10 August 2005

ISBN: 984-32-2520-6

Dynamic behavior of cable-stayed bridge with damping

Md. Toihidul Islam, Tanvir Manzur*, Alamgir Habib

Department of Civil Engineering, Bangladesh University of Engineering and Technology
Dhaka 1000, Bangladesh.

Abstract

Cable-stayed bridges are flexible structural systems. These flexible systems are susceptible to the dynamic effects of wind and earthquake loads. The investigation of dynamic response for long-span Cable-stayed bridges largely depends on a detailed understanding of their dynamic characteristics. With the increasing central span of modern cable-stayed bridges, the trend of the bridge to use more shallow and slender girders to meet the requirements of aerodynamics. In this case, bridge safety (strength, stiffness and stability) under severe loadings and environmental dynamic loadings such as winds and earthquakes presents increasingly important concerns in both design and construction. Damping is a solution that can be used in the long-span Cable-stayed bridges efficiently and economically to control the dynamic loadings. In this study, the dynamic analyses with damping and without damping of a number of long Cable-stayed bridges are performed. For analysis, computer software SAP2000 v 8.1.2 was used. The analysis was performed with the variation of the mass and effective stiffness of the damper, which indicates that effective stiffness of damper is important parameter and mass of damper is not significant. From the analysis, it was found that with the application of damper in the Cable-stayed bridges, response due to wind loads and earthquake loads and the natural period of the bridge can be reduced and controlled effectively and efficiently. The damping parameters that found from the analysis can be used as a guideline for using damper in the Cable-stayed bridges to get optimum results and which is also economically viable.

Keywords: cable-stayed bridge, damping, natural period, effective stiffness

1. Introduction

The problems with long span bridges such as cable stayed bridges, suspension bridges etc are that they are very flexible in nature and their dynamic properties are very difficult to evaluate. Such long span bridges need to be designed for various dynamic loads such as wind loads and earthquake loads. These loads are dynamic and their pattern cannot be

* Email: tanvirmanzur@ce.buet.ac.bd

accurately anticipated. To design for such loads the dynamic behavior of the structure must be controlled. One way to do this is to control the natural frequencies of the structure. The dynamic behavior of a cable-stayed bridge can be controlled either by increasing stiffness of the structures or using damping in the bridges. Damping is more economical solution than increasing stiffness.

This study concentrates on the dynamic analysis of cable-stayed bridges and attempts to provide the designers a set of guidelines or some other forms. From that they can get the indication of the optimum values of various parameters of a damper and their variations with different dynamic analyses like modal analysis, time history analysis and response spectrum analysis.

2. Dynamics of structure

Dynamic analysis of three-dimensional structural systems is a direct extension of static analysis. The elastic stiffness matrices are the same for both dynamic and static analysis. It is only necessary to lump the mass of the structure at the joints. The addition of inertia forces and energy dissipation forces will satisfy dynamic equilibrium. The dynamic solution for steady state harmonic loading, with and without damping, involves the same numerical effort as a static solution. Classically, there are many different mathematical methods to solve the dynamic equilibrium equations. The majority of both linear and non-linear systems can be solved with one numerical method. Energy is fundamental in dynamic analysis. At any point in time, the external work supplied to the system must be equal to the sum of the kinetic and strain energy plus the energy dissipated in the system. With respect to earthquake resistant design, effort should be given to minimize the mechanical energy in the structure. It is apparent that a rigid structure will have only kinetic energy and zero strain energy. On the other hand, a completely base isolated structure will have zero kinetic energy and zero strain energy. A structure cannot fail if it has zero strain energy.

3. Damping

In designing a cable-stayed bridge, attention should be given to the possibility of generating any of the natural periods of vibration. Due to the relatively great flexibility of cable-stayed bridges, they are more susceptible to undesirable vibrations than conventional beam structures. Therefore, because of these vibrations of cable-stayed bridges, the characteristic of damping is of great importance.

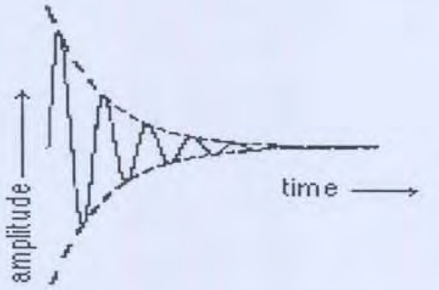

Dashed line indicates exponential decay of the amplitude.

Fig .1. Exponential damping of a sine wave.

'Damping' is a term broadly used to denote either the dissipation of energy in, and the consequent decay of, oscillation of all types, or the extent of the dissipation and decay. Damping may be defined as the inherent force that causes the gradual dying out of mechanically excited natural vibrations within a structural member and reduces the efficiency of transfer of dynamic mechanical forces through a structure.

4. Application of damper in structures

Dampers are applicable to both fixed and base isolated structures, including buildings, bridges, and lifeline equipment.

Dampers are very effective in a large building or bridge to be more survivable during an earthquake. With most structures, a relatively small amount of damping provides a large reduction in stress and deflection by dissipating energy from the structure. Like an automobile suspension, in a building where the spring forces are supplied by the building columns or base isolators which both support the building and deflect under load. It requires only a small amount of viscous damping force to reduce building deflection by a factor of two or three while simultaneously reducing overall column stresses

Dampers reduce building deflection and stress at the same time. If dampers are used to limit the deflection, it won't increase the load into the building columns. Damping reduces stress and deflection because the force from the damping is completely out of phase with stresses due to flexing of the columns. If a Damper is added to the building, damping force will drop to zero at this point of maximum deflection. This is because the damper stroking velocity goes to zero as the column reverses direction. As the building flexes back in the opposite direction, maximum damper force occurs at maximum velocity, which occurs when the column flexes through its normal, upright position. This is also the point where column stresses are at a minimum.

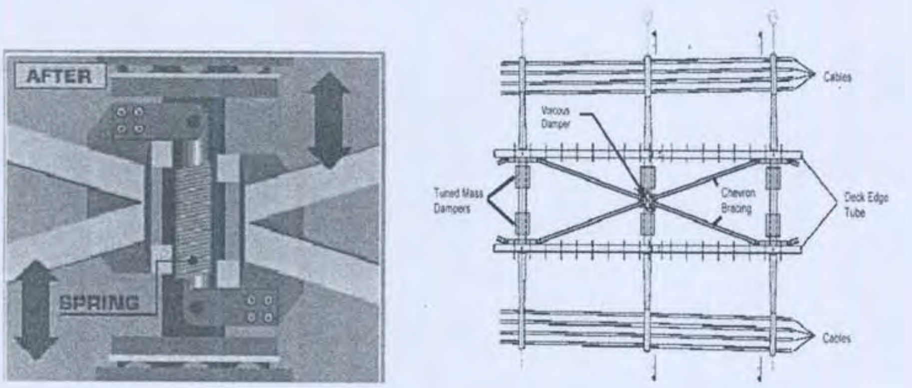

Fig. 2. Viscous and tuned mass dampers in The Millennium Bridge

A typical building normally has internal structural damping of 1 to 3 percent of critical. Optimal performance of a building with damping is achieved with damping in the range of 20 to 25 percent of critical. Experiments with building models have indicated additional improvements with damping increased to as much as 50 percent of critical, but eventually the gain goes past the point of diminishing returns from the point of damper cost.

Dampers are very effective in reducing building deflections under wind loadings without changing the stiffness of the building. In the case of tall buildings, wind motion can cause complaints of motion sickness and general discomfort from the occupants on higher floors. Dampers can reduce wind deflection by a factor of 2 or 3, greatly reducing occupant discomfort without creating localized stiff sections. New buildings designed with Dampers for mitigation of wind motion can be built with reduced lateral stiffness detailing, resulting in a less costly overall structure.

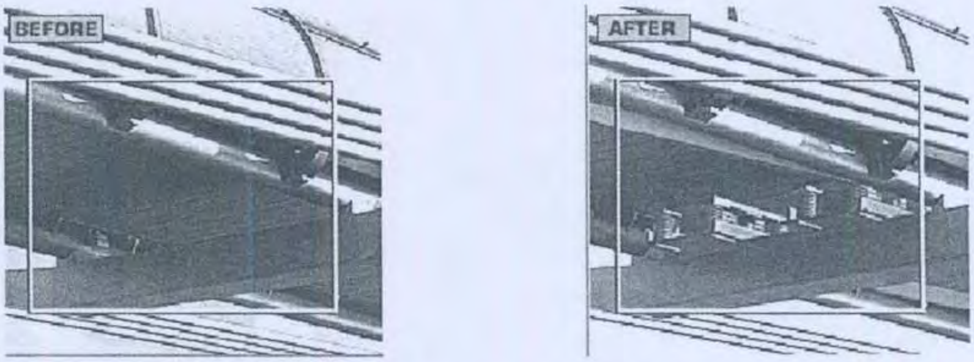

Fig. 3. Addition of tuned mass dampers in The Millennium Bridge

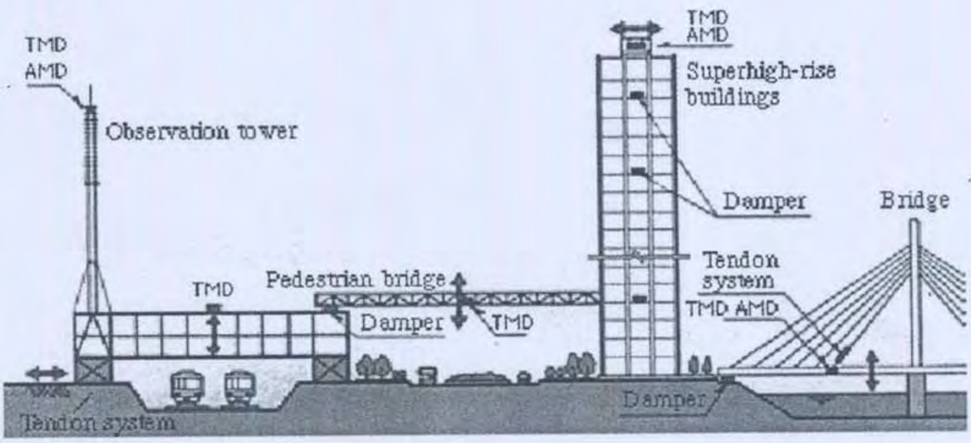

Fig. 4. A structural control device for earthquake-threatened structures

5. Methodology

In this study computer models of Cable-Stayed Bridges (Four types: Fan Type, Star Type, Radial Type and Harp Type) are developed using a specialized software (Sap2000 version 8.1.2) and a number of analyze are performed for each model with and without damping. First analysis performed is the modal analysis with damping from which optimal damping properties (mass of damper and effective stiffness of damper) are selected and these values of damping properties are used for dynamic analysis of modeled Cable-Stayed Bridges with damping. Then analyze are performed for earthquake loads (Response spectrum analysis) and wind loads (Time history analysis) for each model both without damping and with damping to study the dynamic response of cable-stayed bridge. Response-spectrum analysis is a statistical type of analysis for the determination of the likely response of a structure to seismic loading. Time-history analysis is a step-by-step analysis of the dynamical response of a structure to a specified loading that may vary with time.

For this purpose, a finite element modeling of Cable-Stayed Bridge is developed by using finite element package, SAP2000 version 8.1.2.The task of structure modeling is arguably the most difficult one facing the structural analyst, requiring critical judgment and a sound knowledge of the structural behavior of the bridge components and assemblies. Also the resulting data from the analysis must be interpreted and appraised with the discernment for use with the real structure, in order to serve as a reasonable basis for making design decisions.

- Modal analysis
- Response spectrum analysis
- Time history analysis

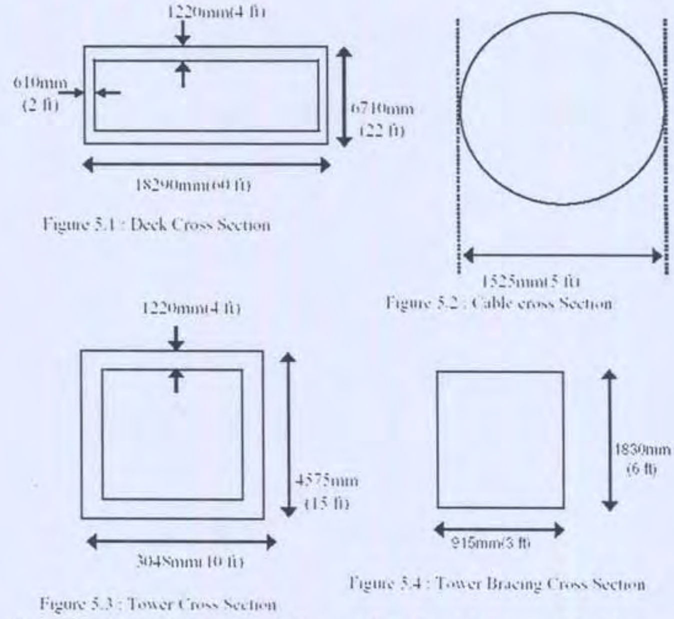

Fig. 5. Cross Sections of the modeled cable-stayed bridge

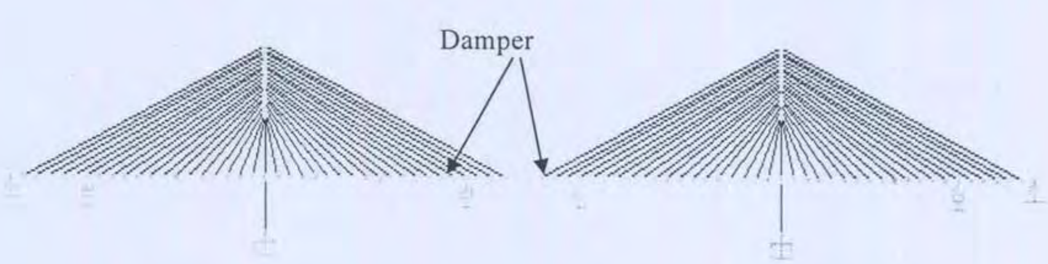

Fig. 6. Modeled cable-stayed bridge with damper

6. Analysis and results

In this study a number of Cable-stayed bridges with a constant central span 625m (2050 ft) and side span 305m(500 ft) and with different values of various parameters of damper were analyzed. For performing the analysis finite element method was used. Computer software SAP2000 was used for this modal analysis. The first 12 modes are considered in this study and mode 1 is used for analysis.

First modal analysis was performed with different values of damping parameter i.e. mass and effective stiffness of damper. Then dynamic analysis was performed for the different types of cable-stayed bridges.

After the dynamic analysis, different variations have been plotted and the effects of different variations are analyzed.

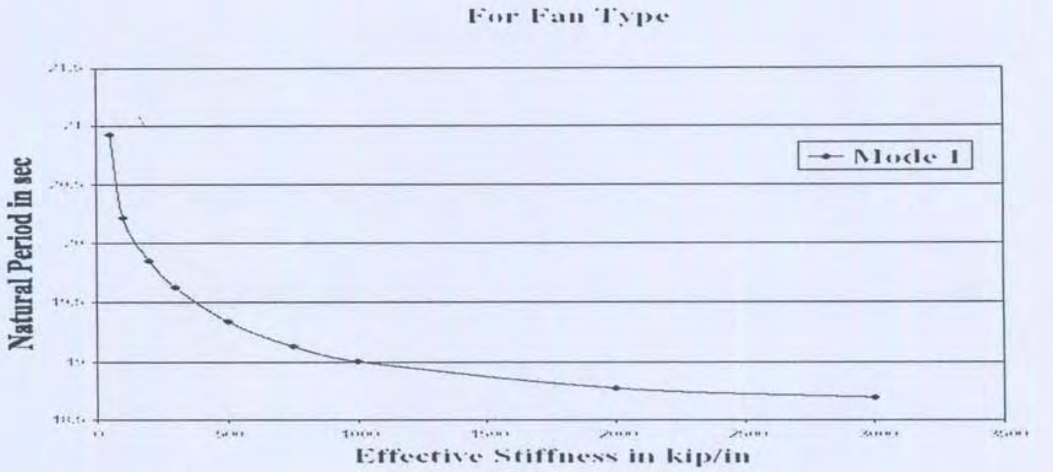

Fig. 7. Natural period vs effective stiffness of damper (for fan type)

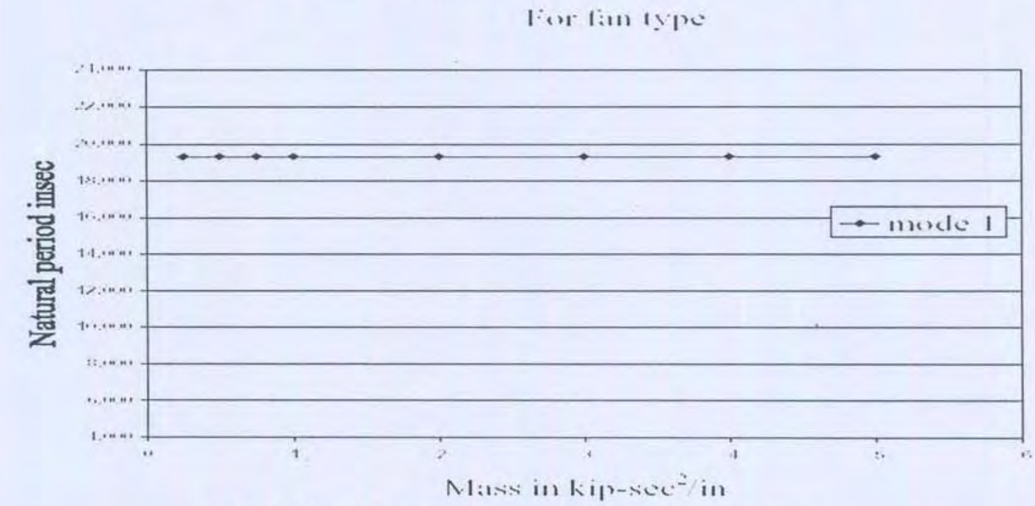

Fig. 8. Natural period vs mass of damper (for fan type)

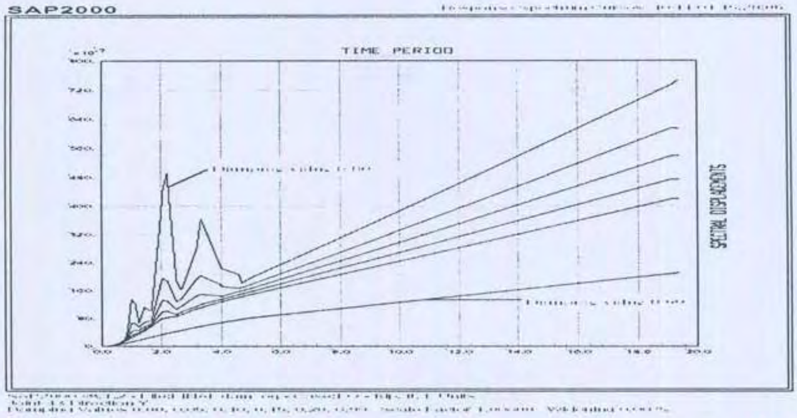

Fig. 9. Response spectrum curve (spectral displacements vs time period)

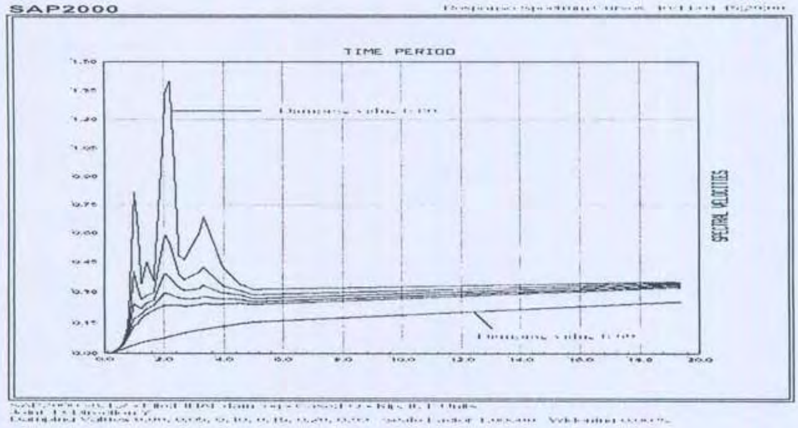

Fig.10. Response spectrum curve (spectral velocity vs time period)

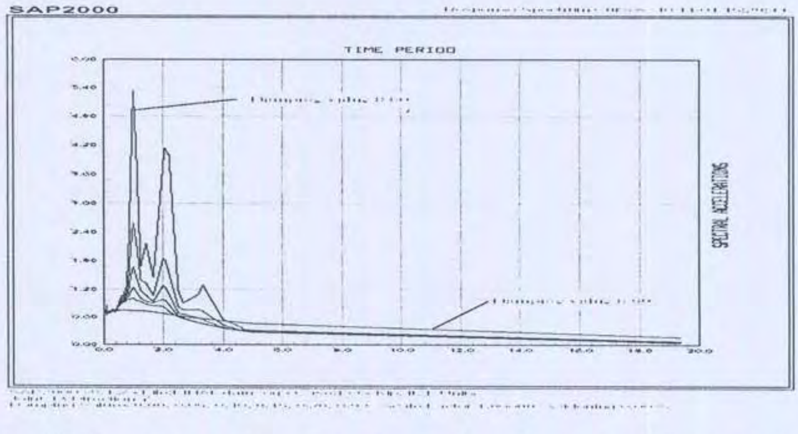

Fig. 11. Response spectrum curve (spectral accelerations vs time period)

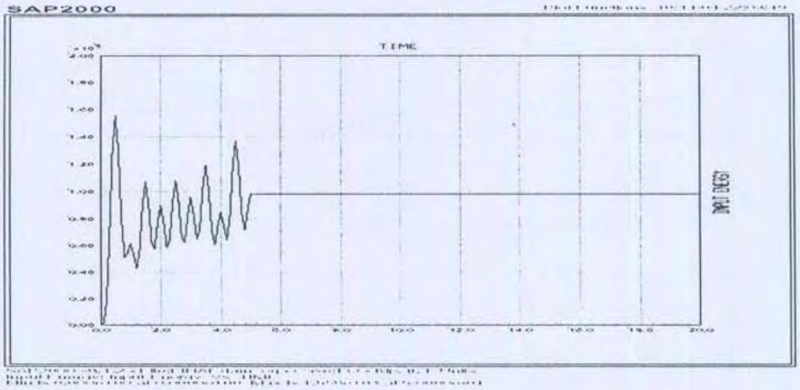

Fig. 12. Plot function analysis (input energy vs time)

Fig. 13. Plot function analysis (displacements without damping vs time)

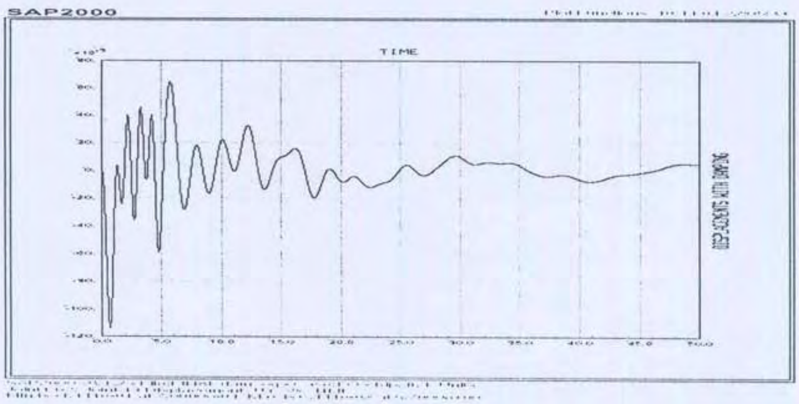

Fig. 14. Plot function analysis (displacements with damping vs time)

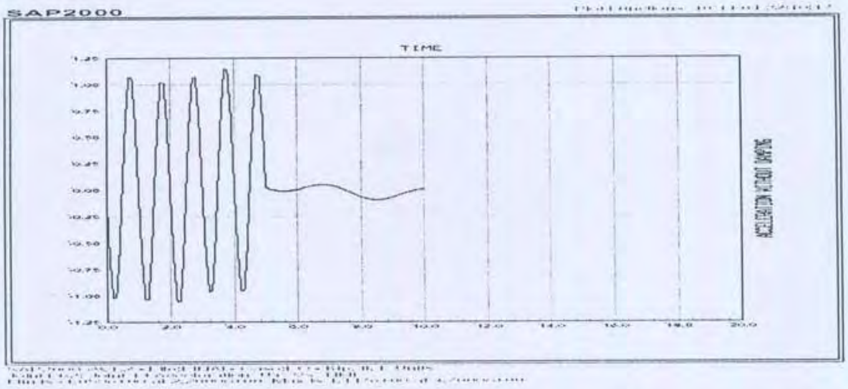

Fig. 15. Plot function analysis (acceleration without damping vs time)

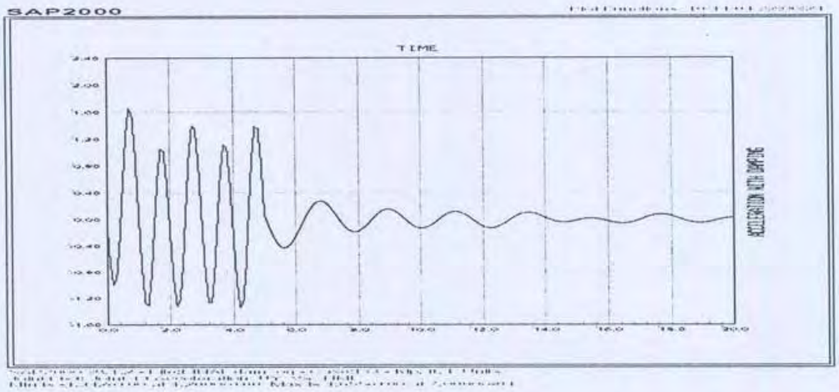

Fig. 16. Plot function analysis (acceleration without damping vs time)

6.1 Effect of effective stiffness of damper on natural period

From Fig. 7. for fan type, it can be seen that natural period decreases with effective stiffness of damper. But the decrease is nonlinear and after a certain value of effective stiffness, natural period does not decrease significantly. After the value of effective stiffness of 87.56 kN/mm (500kip/in), the change of natural period is not significant. Thus it can be concluded that effective stiffness has very significant influence on natural period of the Cable-stayed bridges and the value of effective stiffness of damper can be chosen 87.56 kN/mm (500kip/in).

6.2 Effect of mass of damper on natural period

From Fig. 8 for fan type, it would be observed that natural period shows little change with the change in mass of damper and the plotting curve is straight line i.e. mass of damper has no effect on natural period of the Cable-stayed bridges.

6.3 Response spectrum analysis

From Fig. 9, Fig. 10 and Fig. 11., representating response spectrum curve with different damping values i.e. damping ratio, it is evident that spectral displacements, spectral velocities and spectral acceleration decrease with both the time and the decreasing damping ratio. And when damping ratio is almost critical damping i.e. 100%, then spectral displacements, spectral velocities and spectral acceleration is very small and the curve is almost a straight line. From the analysis it may be said that at the damping ratio of 5% i.e.0.05., the spectral displacements, spectral velocities and spectral acceleration are almost negotiable.

6.4 Plot functions analysis

From fig. 12. it can be observed that after a certain time, input energy variations with time is constant. From fig. 13. and fig. 14., it can be said that displacements decreased significantly due to application of damper. From fig.15. and fig.16. it is evident that ground acceleration decreased substantially due to application of damper.

7. Conclusions

From the studies performed, the following conclusions are apparent:

- By proper selection of the effective stiffness of damper it is possible to significantly influence the natural periods of various types of vibration modes of the cable-stayed bridge. The value of effective stiffness of damper which gives tentative optimum solution is about 87.56 kN/mm (500kip/in).
- Prepared graphical charts for different effective stiffness of damper with natural period can be used as a guideline for selecting the tentative optimum effective stiffness of damper that required in a cable-stayed bridge.
- Dynamic response of the bridges like spectral displacements, spectral velocities, and spectral acceleration with time can be minimized and controlled effectively and efficiently by means of damping.
- The energy dissipation and variations of displacements and ground acceleration with and without damping may also be ascertained from the study.

References

Abdel-Ghaffar (1976). "Dynamic Analysis of Suspension Bridge Structures," EERL 76-01, Earthquake Engineering Research Laboratory, California Institute of Technology, Pasadena, California.

Anil K. Chopra (1995). Dynamics of Structures: Theory and Applications to Earthquake Engineering. Prentice Hall, Upper Saddle River, New Jersey.

Clough. Ray W, Penzien. J. (1993). Dynamics of Structures. McGraw-Hill. Inc

Computers and Structures, Inc. (1996). SAP2000 Analysis Reference Volume-I. Berkeley, California.

Harichandran, R.S., Hawwari, A., and Sweidan, B.N. (1996). "Response of long-span bridges to spatially varying ground motion." Journal of Structural Engineering, 122(5), 476-484.

M.S. Troitsky, DSc (1977). "Cable-Stayed bridges – An approach to Modern Bridge Design" New York, New York 10003.

Wilson, E.L., Der Kiureghian, A., and Bayo, E.P. (1981). "A Replacement for the SRSS method in seismic analysis." Earthquake Engineering and Structural Dynamics, 9, 187-194.

Wilson, E.L.(1996)."Three-Dimensional Static and Dynamic Analysis of Structures" A Physical Approach With Emphasis on Earthquake Engineering. Computers and Structures, Inc, Berkeley, California.

Japan-Bangladesh Joint Seminar on Advances in Bridge Engineering
Dhaka, Bangladesh. 10 August 2005
ISBN: 984-32-2520-6

Seismic protective systems for bridges and highway structures in Bangladesh

Asif Iqbal*

Bangladesh Consultants Limited
House 95A, Road 4, Block F, Banani, Dhaka 1213, Bangladesh.

Abstract

Mechanical equipment that is used to protect the superstructure of bridges and flyovers against earthquakes are being used in increasing numbers all over the world in recent times. They have been used in a few structures in here as well in the last few years. This paper describes the application of such devices in three major structures: Jamuna Multipurpose Bridge, Paksey Bridge and Mohakhali Flyover in Dhaka city. The concepts behind the designs and applications are explained for each case. The descriptions and working principles illustrate how the systems perform according to those concepts. Test details are provided to explain how it is assured that the devices would act exactly the way they are intended to, once they are in place.

1. Introduction

The concept of using additional devices for protection of civil engineering structures from seismic damage is around for a long time. In countries like Italy and New Zealand, that idea has been put to practice in many structures for more than thirty years now. But over the past two decades there had been tremendous developments in this area with new computational and testing facilities. Hundreds of new applications have been made during this time in road and rail bridges, viaducts and similar type of structures as well as buildings for both new construction and retrofitting of old structures.

There have been some major developments in infrastructure in Bangladesh in the past twenty years. Major bridges have been built over rivers and road networks have been improved. As the major protects have utilized modern technologies, there had been application of seismic devices in some of these bridges as the design required. Energy dissipating elements have been used in Jamuna Multipurpose Bridge where as in Paksey Bridge and Mohakhali Flyover the structures have been fitted with systems to lock-up the superstructure with the rest during an earthquake.

* E-mail: maiqbal@citechco.net

Fig. 1. Jamuna Multipurpose Bridge

2. Jamuna Multipurpose Bridge

The 4.8-km long Jamuna Multipurpose Bridge (Figure 1) is the longest bridge in Bangladesh spanning across the mighty Jamuna River. Carrying road and rail tracks, a gas pipeline and a power transmission line, the structure is of enormous economic and strategic importance.

A site-specific seismicity study concluded that earthquakes of Richter magnitude upto 7.0 may occur at the bridge location originating from the adjacent Bogra fault zone, which lies some 25 to 50 km to the northwest. The study provided a design spectrum with a peak-acceleration close to the surface of 0.2 g and a peak structural response of 0.47g. It is also estimated that the ground up to 15 m below the riverbed level may liquefy under an earthquake shaking.

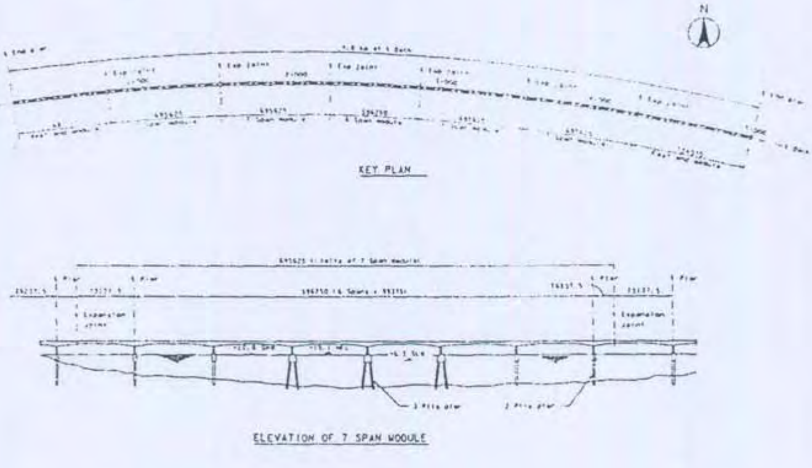

Fig. 2. Span Arrangements of Jamuna Multipurpose Bridge

The bridge consists of 47 equal spans of 99.375m each plus two end-spans each 68.375m long. The main bridge superstructure is prestressed concrete box-girders and the substructure includes 3-pile and 2-pile piers. The bridge is divided into seven modules (two end modules, four 7-span modules and a 6-span module in the middle), which means there are six expansion joints between the two ends (Figure 2).

The foundations consist of driven tubular steel piles, filled with concrete. Pile caps are of pre-cast reinforced concrete shell with in-situ reinforced concrete in-fill construction. The pile caps carry pier stems, which in turn support the bearings. The height of pier stem varies from 2.72m to 12.05m and is constructed of reinforced concrete. The deck is of prestressed post-tensioned concrete segmental construction, with a varying depth single box section.

The intention behind the seismic design of the bridge was to provide ductility to the structure. (RPT-NEDEC-BCL 1990). This way the piers and piles will not be excessively large as would be required to remain elastic during the design earthquake. But the deformations achieved because of the ductility should occur in such areas where they can be accessed and repaired. Providing metal restrainers between the deck and the top of the pier was a practical idea. The restrainer would yield to absorb energy and isolate the deck from the piers through allowing relative movements. The threshold force is also predefined from the restrainer size and material properties.

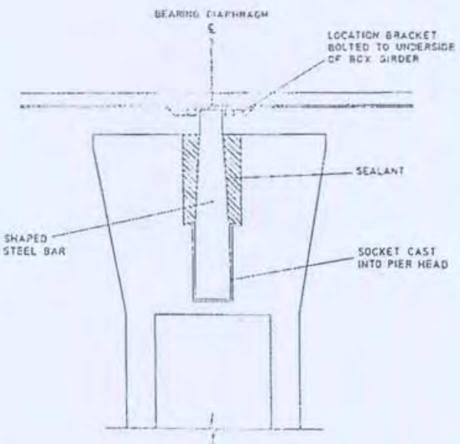

Fig. 3. Schematic drawing of seismic restrainer

A very simple type of device that had been investigated and used in real structures in New Zealand (Tyler 1978, Park and Blakeley 1978) was conceived at the preliminary stage (Figure 3). That concept was eventually applied in the bridge with some modified shape of the device.

In concept, the seismic restrainer is not much more than a mild steel bar placed vertically between the soffit of the deck and the top of the pier (Figure 3). The material is ductile and the shape is as such that the ratio of the applied bending moment to the plastic moment of resistance is normally constant over the lower third of the free height. The bar exhibits plastic deformation under stresses beyond the threshold force and the plasticity is confined to the free height because of the shape. Shear stresses in the bar are kept low intentionally by the proportions. The bar is also free to slide vertically during the elastoplastic movement so that any geometric non-linearity and subsequent instability cannot occur in the arrangement.

Figure 4 shows typical load-deflection curve of a hysteretic device. The values of the force and displacement are arbitrary and so are the numbers of cycles. It just qualitatively indicates the behaviour of the device. The area inside the curve gives the amount of energy absorbed.

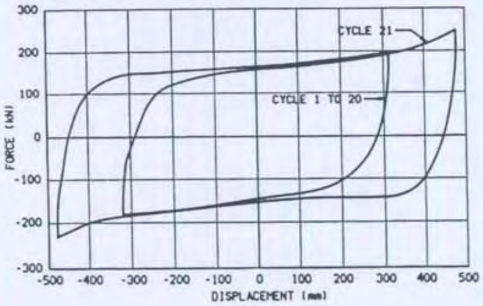

Fig. 4. Typical load-deflection curve of a steel hysteretic device

Bottom end of the device is always connected to the top of the pier. The arrangement of the connections of the top end of the devices with the superstructure depends on the location of the pier within the structure. In each module of the bridge there is a central pier, which is either the one at the centre of the module or one of the piers closest to the centre. In this pier top end of the device is connected directly to the superstructure.

In other piers of the module the connection between the top of the bar and the soffit of the deck utilizes another device called Shock Transmission Unit (STU). Practically it is nothing but a cylinder filled with viscous non-compressible fluid and a piston within. The piston is connected with a piston rod that extends out of the cylinder. The fluid inside the cylinder can slowly squeeze past the cylinder when the piston moves within the cylinder. This can happen when the piston rod is either pushed back or pulled out of the cylinder. If the movements are very slow the resistance is small but if there is any sudden movement of the piston rod the piston inside will be "locked" into position because of the viscosity of the fluid. This is why STUs are also known as Lock-Up Devices. Figure 5 shows arrangement of seismic devices in a seven-span module at both service and seismic conditions.

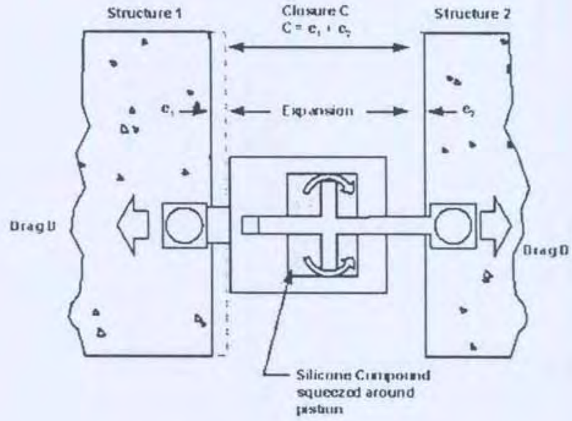

Fig. 5. Working principle of STU

At the piers other than the central pier there would be a very slow relative movement between the superstructure and the pier because of thermal changes, creep, shrinkage etc. But in the event of an earthquake there would be tendency of instantaneous relative displacement between the two. At these locations it is necessary to keep the provisions for the very slow movements but the seismic movements must be arrested. This is achieved with the STUs. The top of the seismic device is connected with deck through a STU. There will be very little force on the seismic device during the slow movements but the horizontal force will be transferred to it when the STU locks up during an earthquake.

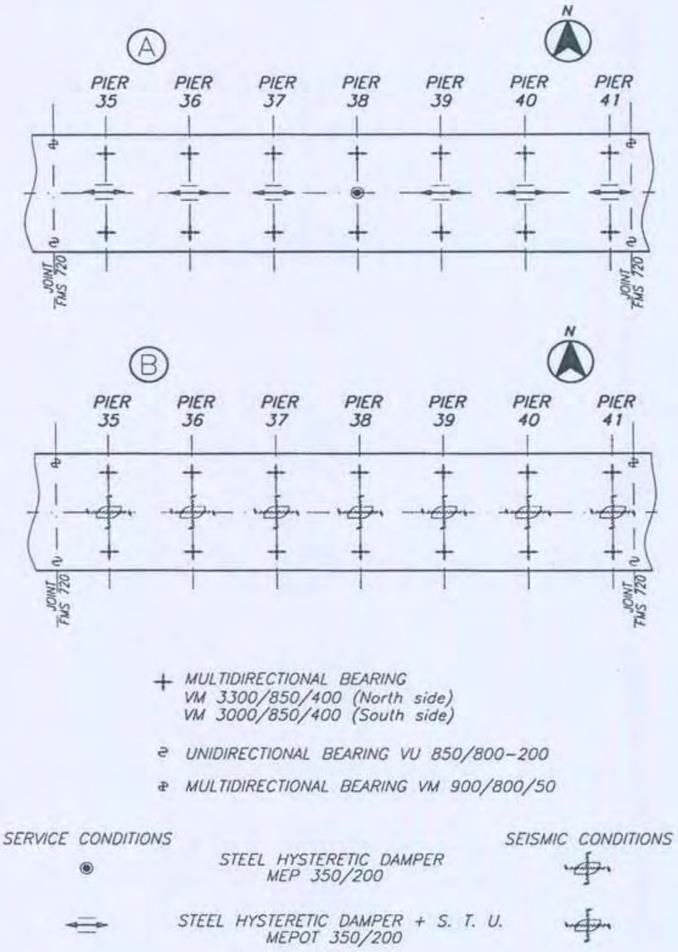

Fig. 6. Arrangement of seismic devices in a module

When the details for the actual device were worked out the single pin element was replaced by a group of 42 equal-sized pins spread across the length and the width of the device (Figure 7). The multiple-pin arrangement provided necessary redundancy as well as possible provision of maintenance and replacement.

Two types of dissipating device are used depending on the mechanism of operation. The centre of portion each module has the fixed-type, i.e., in these locations (at the 3-pile piers), there are multipin elastoplastic devices in which all horizontal movements other than those occurring in very short durations are accommodated by the elastic deformation of the pin elements. At the 2-pile piers, mobile-type devices are used that include shock transmitters with the multipin elements to allow slowly occurring movements (like the thermal expansions and contractions of the bridge superstructure) through adjustments by the shock transmitters. At sudden onset of loads, such as during an earthquake, the horizontal forces are resisted by pin elements in both the fixed and mobile-type devices. The sharing of the loads is achieved because the shock transmitter in the mobile locations locks up and transmits the loads to the pin elements. Fig. 3 shows the section of the device, which comprises of the following major components (FIP Industriale, 1996a):

- A central body with pin dissipating elements
- An upper and a lower plate, between which the pins are affixed
- A frame with two tapered faces is affixed to the superstructure. Two frames, one on either side of the central body, with an outer surfaces tapered to match the taper of the inner frame is attached to the top of the pier maintaining the required clearances for the deformation of the pins. The inner and outer frames together form a fail-safe mechanism.
- The dissipating device for the mobile locations includes a shock transmission unit made of a one-piece hydraulic cylinder that has both the end closed and a double-headed piston rod that creates two chambers within the cylinder.

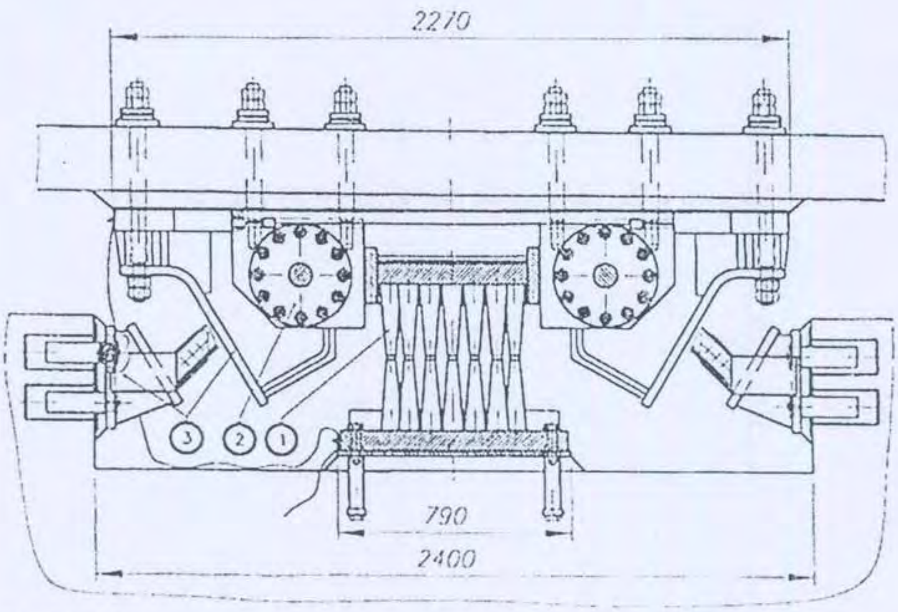

Fig. 7. Details of the energy-dissipating device: (1) pin dissipating element; (2) shock transmission unit; (3) stop-block element

The pins and the STUs are designed for a seismic load capacity of 4200 kN and displacement range of ±200 mm. The clear distance between the faces of the stop block element is 250 mm.

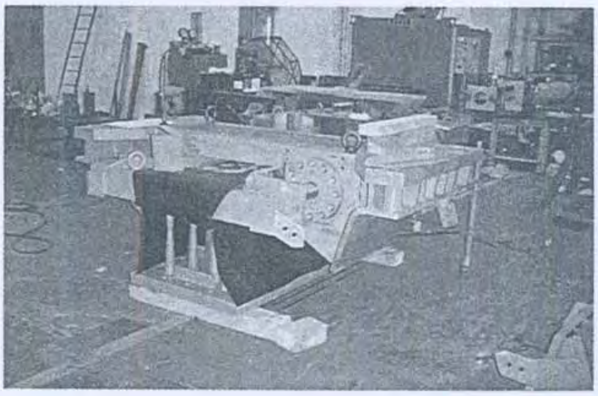

Fig. 8. View of a complete seismic device used in Jamuna Bridge

A very important step in application of any special device is testing. Since the devices vary widely in respect of material, arrangement and working principle, device-specific testing scheme and verification procedure have to be formulated.

The devices used in real structures are usually very big and it is not always possible to test the prototypes. Scaled models or smaller arrangements are used in most cases and they are believed to be representative of the full-sized devices. In case of devices for the Jamuna bridge, a 4-pin setup was tested in place of the whole device with 42 pins (FIP Industriale, 1996b). The STUs tested, however, were full-sized and with full movement capacity.

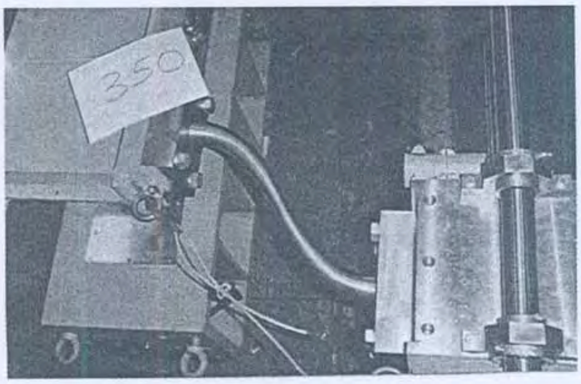

Fig. 9. Test of a steel hysteretic device

Rigorous testing protocol had been implemented for the pins and the STUs. The group of pins was tested first for 15 cycles of design displacement of 200mm each way. Then the displacement was continued until rupture of one pin at 315 mm. The tests revealed that the elastic displacement of the pins is 27mm and rest of the design displacement is plastic displacement. For the whole device the elastic force and plastic force were calculated to be 3333.75 kN and 4173.75 kN respectively. So the increase in force in the device is much less compared to the displacement after the elastic limit. That means the force transferred to the piers would be much less that it would have been if the mechanism had remained elastic.

STUs were tested through a protocol similar to that of the pins. Three sets of tests were done at 27°C, 10°C and 40°C and like the tests of the pins, each set comprised of low velocity test, high velocity test and dynamic test. The low velocity test verifies the slow movement capacity of the device as would be required for thermal change and shrinkage. The high velocity test examines the lock-up capability at sudden movements. The device is tested with sinusoidal movements in the dynamic test to verify if the lock-up mechanism holds throughout a seismic event.

In the low velocity tests the piston is moved at a rate of around 0.03 mm/sec for a stroke of 20mm for each side and 1.5 cycle in total for a total movement of 120mm. The Reaction force was measured to be 45 kN at 27°C, 70 kN at 10°C and 25 kN at 40°C and against a maximum load of 4175 kN (2.16%, 3.35% and 1.20% respectively). The small amount of reaction force means that there will be almost insignificant amount of load exerted on the substructure during the very slow thermal or other types of movements. The other point that should be noticed here is that with the increase of temperature the silicon compound inside the cylinder becomes more fluid allowing a lower reaction for slow movement.

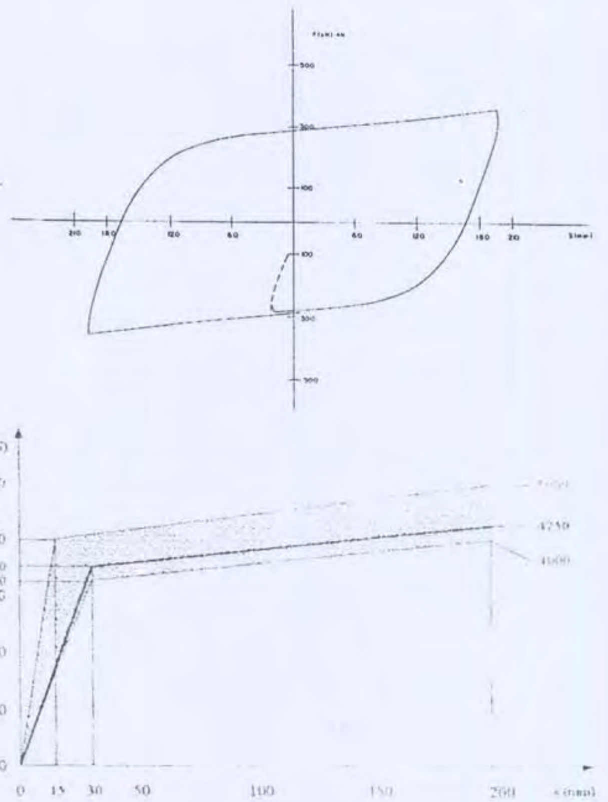

Fig. 10. (a) Load-deflection plot of 4-pin arrangement (b) nominal curve of a complete hysteretic device indicating accepted value

For the high velocity test a constant force of 22600 kN and a constant velocity of 26 mm/sec were maintained in the all the tests at three different temperatures. Displacements of the piston were 16.64 mm at 27°C, 6 mm at 10°C and 24 mm at 40°C. The tests demonstrated that the silicon compound of STU is capable of achieving the maximum reaction under impulsive shocks but with slightly increasing displacements at greater temperatures.

The dynamic test was carried out with a force of around 2000 kN in sinusoidal way and a frequency of 0.4 Hz to 0.5 Hz at 27°C, 10°C and 40°C. Pressure and displacements were measured at the 1^{st}, 10^{th} and 20^{th} cycles. That was used to calculate the ratios between the actual displacements and the stroke allowed by the STUs. At 27°C the ratio came up as 4.78% from the 1^{st} cycle, 4.72% from the 10^{th} cycle and 5.76% from the 20^{th} cycle. At 10°C they were 5.22%, 5.87% and 6.52% respectively while it was 5.22% at the 1^{st} cycle at 40°C.

It should be noted here that the displacement increases as the test progresses. This is because with the movement of the piston within the cylinder the temperature of the fluid increases reducing its own stiffness and allowing for a greater displacement. But still the STUs generally exhibit enough resistance under sustained dynamic loads.

This type of devices has been widely used in many bridges in Italy and in some other countries for more than 30 years now. The inherent concept brings in some advantages as well as possibilities of some situations that may have practical difficulties (Tsopelas and Constantinou 1994, 1997, Iqbal 2002).

The material behaviour of mild steel (Figure 10) shows that the pins remain elastic upto the elastic limit. There would be little increase of force once the yield point is crossed, but in exchange of large strains. So the maximum force transmitted to the substructure through the device can be predicted. That gives a huge advantage in designing the piers and abutments irrespective of the nature of the ground motion.

It is evident from analysis of the concept that the system is effective in reducing deck acceleration and transmission of forces to the substructure. But beyond the elastic limit the system exhibits significant permanent displacements due to lack of restoring forces within the device. Once the elastic limit of the mild steel is exceeded, the whole structure needs to be realigned externally. This is likely to be the case after a major earthquake. But there can be significant aftershocks shortly after the main event, which can add to the permanent deformations before any such work is done. Besides, some pins can fail during a major earthquake and they need to be replaced to take the device to its original stiffness level. Until that is done, the system remains at a degraded stiffness level, which can also be potentially dangerous in case there is any subsequent major earthquake.

One other concern is that the peak bearing displacement during an earthquake can exceed the design displacement. That can lead to additional forces on the superstructure due to pounding action, which means the main advantage of 'predicted' seismic forces on the pier can be rendered invalid.

Interestingly, the design philosophy of the Jamuna Bridge can be considered compatible with the next generation of codes emerging on the basis of performance-based design concept rather than conventional force-based approach (Iqbal and Al-Hussaini, 2002).

A two-level design approach is suggested for performance-based seismic design in accordance with the types of ground motion considered. A 'functional-evaluation ground motion' is a moderate earthquake that has a reasonable probability of occurrence during the lifetime of the structure. The structure should be able to resist the forces produced from this earthquake without significant damage to the basic system. A 'safety-evaluation ground motion' is the strongest possible earthquake that could ever be expected to occur at the site. Considering the low probability of that occurring it is economically justified to allow structural damage due to this type of ground motion; however, total collapse and serious damage of life and property cannot be considered acceptable.

The operational principles of elastoplastic devices are inherently organised to fit into the performance-based design approach. Forces generated by ordinary conditions like wind, braking, centrifugal actions and even minor earthquakes are resisted elastically by the steel dampers without any distress. During the design earthquake the device may exhibit elastoplastic behaviour with some permanent deformations. If necessary, the bridge superstructure will be re-centred externally and with replacement of any damaged element of the energy-dissipating device. In case of the maximum credible earthquake the steel dampers will absorb energy as much energy through yielding. If the design displacements are exceeded, there is a fail-safe mechanism in place to prevent structural collapse. Sufficient support lengths and continuity of deck should prevent total collapse.

Fig. 11. Paksey bridge

3. Paksey Bridge

The 1786m long Paksey Bridge (Figure 11) comprises of 15 typical spans of around 109.5 meters and end spans of 71.75 meters. The superstructure is of concrete box girder deck and piers are also of concrete supported by steel piles. The whole structure is one single module with continuous deck between the abutments (MM-RPT-JOC-BCL 1996).

This bridge is intended to act like an integral structure during an earthquake. That means the superstructure would be locked to the substructure at all piers. But there must be provisions for movements of the deck due to temperature changes, creep and shrinkage. This performance objective is achieved by STUs.

The deck is connected to the piers at all locations except one around the centre (Figure 12). Ideally, the centre of the deck would be restrained in both directions to the pier. Since in this case the number of spans is not even, the fixed point is at one of the two nearest piers. At all of the other piers the deck is transversely restrained and connected to the pier with STUs in the longitudinal direction. At the two ends the deck is fixed in the transverse direction with shear keys but free in the longitudinal direction.

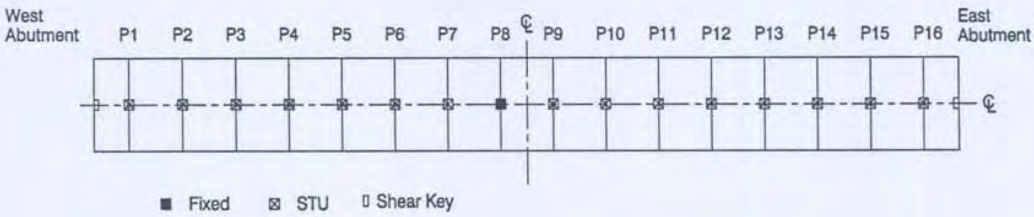

Fig. 12. Arrangement of seismic devices in Paksey bridge

The forces and movement ranges for STUs at different locations of the bridge is shown in Table 1. All the STUs at the typical piers have the same force capacity but the movement ranges are greater as they are placed outward from the fixed point. Each pier has two STUs to make up the force capacity required.

Table1. Load and displacement capacities of STUs in Paksey bridge

Location			West Abt	P1	P2	P3	P4	P5	P6	P7	P8	P9	P10	P11	P12	P13	P14	P15	P16	East Abt
Number			0	2	2	2	2	2	2	2	0	2	2	2	2	2	2	2	2	0
Design Load (kN)	ULS	Tran	14.2	14.2	14.2	14.2	14.2	14.2	14.2	14.2	14.2	14.2	14.2	14.2	14.2	14.2	14.2	14.2	14.2	14.2
		Long	-	23.0	16.7	16.7	16.7	16.7	16.7	16.7	16.7	16.7	16.7	16.7	16.7	16.7	16.7	16.7	23.0	-
Transln. (mm)	SLS	Tran	0	0	0	0	0	0	0	0	0	0	0	0	0	0	0	0	0	0
		Long	869	791	670	554	441	331	226	118	0	91	187	278	370	461	549	640	731	791

30 STUs in total, two at each pier from P1 to P7 and P9 to P16, were used with Force Capacities from 8350 kN to 11500 kN and Displacement Capacities from 100 mm to 750mm. As it is noticeable from the table, the movement ranges for piers at equal distances but on opposite side of the fixed pier are slightly different because of the asymmetric arrangement about the point-point of the whole length of the bridge. That is why the displacement capacities of STUs at similar positions at opposite sides are different in some cases. The STUs at P1 and P16 have additional force capacities because they have to resist the additional forces from the end spans.

As per the requirements, the STUs used in Paksey Bridge (Figure 13) were tested thoroughly before they were accepted (Techstar Incorporated, 2003). Each of the STUs had to go through Hydrostatic tests to test the integrity of the device, Full Cycle stroke testing to check the displacement capacities and Simulated dynamic force transfer tests to verify the operational capacity during a seismic event.

For the hydrostatic tests, all the STUs were tested for internal pressure at 150 % of the maximum computed internal pressure. The pressure was applied and kept there for a few minutes while the initial pressure and the final pressure were recorded. This is to see if the STUs leaks, because if it does then the pressure would drop. Visual inspections are also done during this time for the same reason.

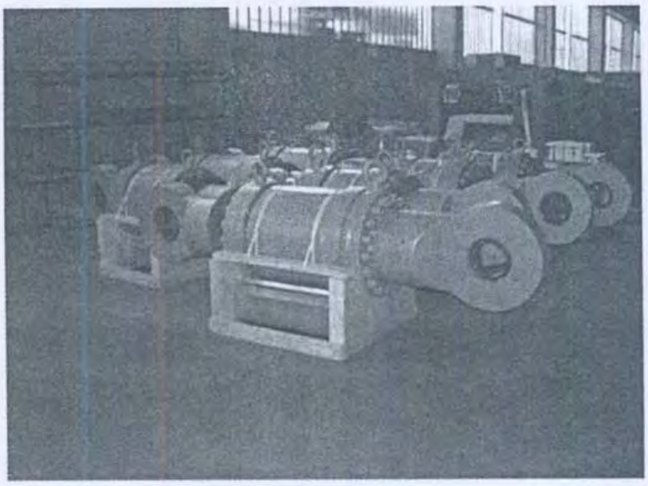

Fig. 13. View of STUs used in Paksey bridge

All the devices were tested through their full stroke. The units were tested for cycle of ±100 mm at speed of 0.05 mm per second. The number of cycles performed was such that the total movement performed was equal to 10 full strokes. For a continuous (Figure 14) plot of the load vs. time and the displacement vs. time were recorded.

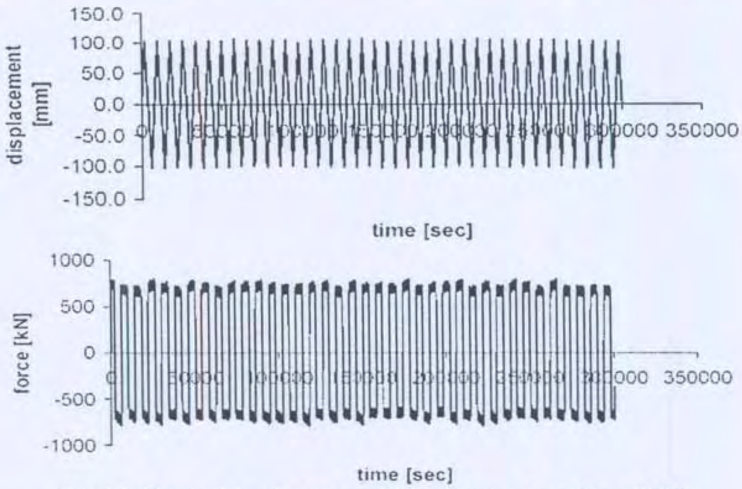

Fig.14. Typical load-time and force-time plots for a STU

Each of the STUs manufactured was tested to verify the ability to lock-up during dynamic loads. The test included application of tension and compression loads, one at a time, within less than a second and holding them for a few seconds. The loads applied, both in tension and compression, were equal to the maximum design load. Tension and compression loads were equal. For each device a continuous plot of the load vs. time and the displacement vs. time were recorded. The plots are inserted here below in Fig. 15.

The STUs used in Paksey Bridge are special both in terms of force capacity and displacement range. They would be subjected to huge forces and have to accommodate large displacements because of the arrangement and length of the bridge structure. Each of them have gone careful design and through testing to accommodate this objective.

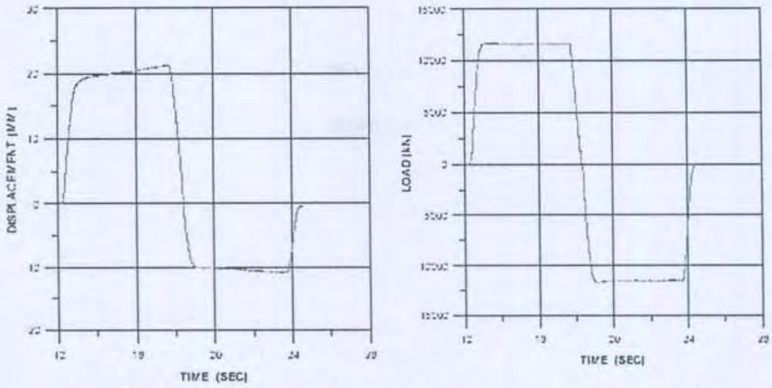

Fig. 15. Displacement-time and load-time plots for a STU

4. Mohakhali flyover

Mohakhali Flyover (Figure 16) is the first of its kind to be built in the country. This was planned as part of Dhaka Urban Transport Project to help remove traffic congestion at Mohakhali rail-crossing area of the city. The flyover is little over a kilometre long in total while the length of the structure is 687 meters. The whole structure is of concrete with the four-lane box girder deck. The structure has 19 spans in total, but they are divided into three structural modules (Figure 17). The each of the two modules at the ends are made of pre-cast segments and have the typical span length is 38 meter with around 27 meter long end spans at both ends. The module in the middle is cast in situ and has a long span of 63 meter over the railroad. The other spans in this module range from around 31 to 35 meters (DSM Consultants 2002).

Fig. 16. Mohakhali flyover

The structural arrangements of the modules determine their seismic behaviour. In each module the concrete decks are continuous from one to another. The deck is fixed with a pier near the middle of each span. There are STUs between the deck and the pier at other locations in an arrangement similar to that of Figure 18. The two ends of the structure are also connected to the abutments. During an earthquake all the STUs provide restrains in the longitudinal direction. The connections are in such a way that they are fixed in the transverse direction all the time. So the deck would be restrained at all support locations in case of a seismic event.

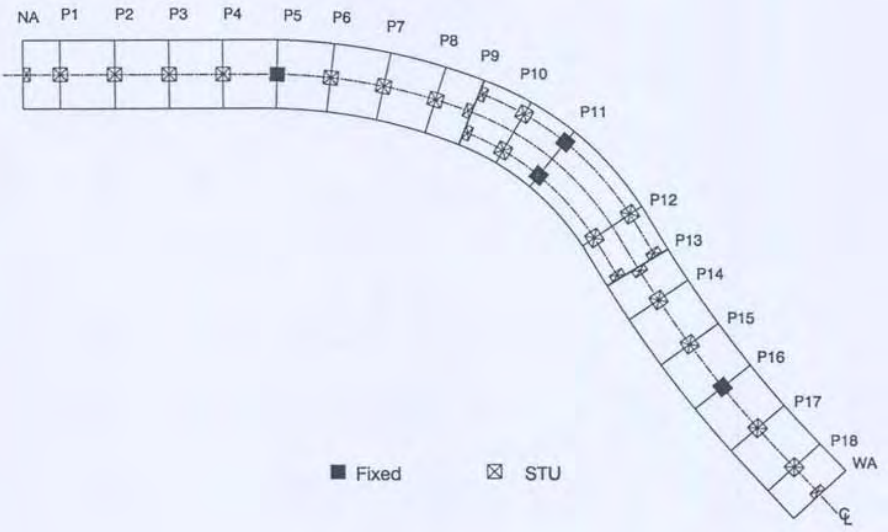

Fig. 17. Arrangement of seismic devices in Mohakhali flyover

Because of the curvature in the alignment, the orientations of the STUs are also significant. In each of the module the shear keys that produce the restrains in the typical piers are aligned towards the fixed restraint of that module.

Fig. 18. STU between the substructure and the deck

Table 2 shows the design forces and the movements at each pier location. Examining them for the proposed arrangement reveals that because more STUs are used in the module they need to be of smaller capacity in terms of both forces and movements. The two end modules have larger forces and relatively greater movement ranges.

Like most cases of this type of applications, the contractors were asked to design and work out the details of the STUs. The STUs had to be designed to operate in the temperature range of 0°C to 60°C and a relative humidity of 100 percent in addition to the movements caused by traffic and wind excitation. The device is designed to withstand the force in lateral or vertical direction generated by twice its own weight in addition to the design axial load. There should be a minimum factor of safety of 1.3 for the material yield strength and 1.4 for material ultimate tensile strength.

The operational requirements are such that the device is designed for a wind loading of 1750 kN for 100,000 cycles per year and 20 cycles of seismic loading once every 10 years. The functional life of the STUs would be 40 years but they may be maintained and repaired within this period. It should be also relatively easy to remove and replace them if that becomes necessary. But it is imperative that refurbishment would not be required before at least one maximum credible earthquake.

Table 2. Load and displacement capacities of STUs in Mohakhali flyover

Location			N. Abt	P1	P2	P3	P4	P5	P6	P7	P8	P9		P10	P11	P12	P13		P14	P15	P16	P17	P18	W. Abt
												Pre.	Situ				Situ	Pre.						
Number			1	2	2	2	2	0	2	2	2	1	4	4	0	4	4	1	2	2	0	2	2	1
Design Load (kN)	ULS	Tran	2.39	8.89	8.89	8.89	8.89	8.89	8.89	8.89	8.89	2.39	8.89	8.89	10.8	10.8	8.89	2.39	8.89	8.89	8.89	8.89	8.89	2.39
		Long	2.39	7.82	7.82	7.82	7.82	7.82	7.82	7.82	7.82	2.39	7.82	7.82	9.51	9.51	7.82	2.39	7.82	7.82	7.82	7.82	7.82	2.39
Transln. (mm)	SLS	Tran	0	0	0	0	0	0	0	0	0	0	0	0	0	0	0	0	0	0	0	0	0	0
		Long	48	38	29	20	10	0	10	20	29	38	18	9	0	18	29	29	20	10	0	10	20	29

42 STUs have been proposed in total for the whole structure. The requirements in terms of force and displacement capacities are comparable. So multiple numbers of devices with the same capacity can be used at different locations. Like the piers of the module in the middle have larger forces and four STUs are used in these locations where two are used at typical piers of other modules. Again, force capacity requirements at both ends of the modules are less and that is why only one STU is attached at these locations.

The STUs had to go through a detailed testing scheme for this structure also. A testing scheme similar to that for the STUs used in Paksey Bridge had been accepted. Hydrostatic Testing was done by 150% of maximum computed internal pressure kept for three minutes to verify the structural integrity of the high-pressure boundary. Full Cycle Stroke Testing means testing the STUs for ten complete cycles of movement at a velocity between 0.02 mm to 0.05 mm per second.

During the Full Force-Velocity Performance Testing the STUs shall have the full design force applied by piston moving at a maximum speed of 0.5 mm per second. They would be tested in both compression and tension but testing need not be cyclic. This is to see if the device can stand the pressure at this load. The deflection at which a constant stiffness is achieved is taken as lock-up deflection and corresponding force is termed lock-up force. The acceptance criteria require that the deflection from the point of lock up to the maximum test load must be less than 25 mm.

Simulated Dynamic Force Transfer Test would verify the ability of the devices to lock up during dynamic loads. The STUs would be put through both tension and compression; one at a time, within 0.5 second and the load would be sustained for 5 seconds. The force would be at least three times the lock-up force determined in the Full Force-Velocity Performance Testing but not more than the design force. Deflections during the application or reversal of forces should not exceed 25 mm. Also, the deflections due to sustained loads should not exceed 25 mm. The installation of the STUs in Mohakhali Flyover is still continued during the time of preparation of this paper.

5. Conclusion

The conceptual and design issues of application of two different types of seismic devices in three structures are presented here. It is clear that these devices are part of the whole mechanism of giving the structures protection against earthquakes. These are the first examples of such applications in this country. As the technology progresses with time people will have more confidence in them as effective in serving that purpose and more of them are likely to be used in similar structures in the near future.

Reference

Bolt, B. A. (1987), Site Specific Study of Seismic Intensity and Ground Motion Parameters for Proposed Jamuna River Bridge, Bangladesh, Report presented to Jamuna Multipurpose Bridge Authority.

DSM Consultants (2002), Mohakhali Flyover Design Report.

FIP Industriale (1996a), Technical Report on Elastoplastic Device for Seismic Protection of Jamuna Multipurpose Bridge, Padova, Italy.

FIP Industriale (1996b), Test Report on Bearings and Seismic Devices for Jamuna Multipurpose Bridge, Padova, Italy.

Iqbal, A. (2002) "Study of Seismic Isolation System of Jamuna Multipurpose Bridge, Bangladesh", Proceedings of the 15^{th} Engineering Mechanics Conference of the American Society of Civil Engineers, New York, USA.

Iqbal, A. and Al-Hussaini, T. M. (2002), "Elastoplastic Isolation System for Performance-Based Seismic Design of Bridges", Proceedings of ATC 17-2 Seminar on Response Modification Technologies for Performance-Based Seismic Design, Los Angeles, USA.

MM-RPT-JOC-BCL (1996), Paksey Bridge Design Report.

Park, R. G. and Blakeley, R. W. G. (1978), "Seismic Design of Bridges", Road Research Unit, National Roads Board, Bridge Seminar, New Zealand.

RPT-NEDECO-BCL (1990), Jamuna Bridge Project Phase II Study Design Report.

Techstar Incorporated (2003), Paksey Bridge Shock Transmission Devices Algasism Test Report, Ohio, USA.

Tyler, R. G. (1978). "Tapered Steel Energy Dissipaters for Earthquake Resistant Structures", Bulletin of the New Zealand National Society for Earthquake Engineering, Vol 11, No. 4.

Tsopelas, P. and Constantinou, M.C. (1994). NCEER-TAISEI Corporation Research Program on Sliding Seismic Isolation Systems for Bridges-Experimental and Analytical Study of a System Consisting of Lubricated PTFE Sliding Bearings and Mild Steel Dampers, Rep. No. NCEER 94-0014, National Center for Earthquake Engineering Research, State University of New York at Buffalo, New York, USA.

Tsopelas, P. and Constantinou, M.C. (1994). "Study of Elastoplastic Bridge Seismic Isolation System", ASCE Journal of Structural Engineering, 123(4), 489-498.

Japan-Bangladesh Joint Seminar on Advances in Bridge Engineering ISBN: 984-32-2520-6
Dhaka, Bangladesh. 10 August 2005

Numerical model for predicting composite behavior of stud shear connectors

Md. Khasro Miah[1], Akinori Nakajima[2], Ahsanul Kabir[*3]

[1]*Department of Civil Engineering, DUET, Gazipur, Bangladesh*
[2]*Department of Civil Engineering, Utsunomiya University, Japan*
[3]*Department of Civil Engineering, BUET, Dhaka, Bangladesh*

Abstract

The objective of this research is to study the behavior of stud shear connectors numerically and compare the numerical prediction with the experimental results to validate the numerical method. In this regard a numerical model is developed for the prediction of static behavior of the stud shear connectors, which are commonly used in the composite structure construction. The accuracy of the numerical evaluation significantly depends on the proper modeling of shear force transmission from stud shank to surrounding concrete. To attain this effectively, one-dimensional nonlinear bearing springs are employed and the characteristics of these are estimated from the bearing test of concrete. The numerical method and model proposed are validated by comparing its findings such as strain at the base and at mid height of the stud shank and slip with the experimental results.

Keywords: stud shear connector, numerical analysis, nonlinear FEA, experiment, slip, base strain

1. Introduction

Shear connectors are usually used in the composite constructions for instance steel-concrete composite girder bridge, mixed rigid bridges and steel building construction to achieve composite action of the component members. Experimental study is the key resource, which is essential to investigate the complicated behavior of the composite structure or its component. Parallel to the experimental investigation, numerical prediction bears noble achievement to justify the behavior of the composite structure. The base of the stud shank is subject to large deformation and the static as well as the fatigue failure may occur at its base. Therefore, it is important to observe the strain behavior at the base of the stud shank by both the experimental and numerical tests.

* Email: akabir@ce.buet.ac.bd

Moreover, base strain is a more appropriate measure to predict the shear force transmission through the stud shank.

To measure the base strain experimentally by employing generally used solid stud is rather impossible because of welding at the base and coating provided to protect the strain gauge. Pipe stud shear connector[1,2] is effectively used to measure the base strain experimentally. Numerical evaluation plays important role to validate the experimental results or vice versa. Incidentally, a numerical model is developed to evaluate the static responses of pipe stud shear connector. The numerical analysis can check any variation for instance geometry or material properties more easily, while experimental investigation is rather time consuming and expensive as well. Appropriate modeling of the composite system such as the shear connector, surrounding concrete and the interaction between them plays a significant role and the accuracy of the numerical analysis totally depend on how well these are modeled.

To this end, Civjan and Singh[3], Salari and Spacone[4] and Spacone and El-Tawil[5] are some of the researchers, who had investigated the shear behavior of the composite structure or its components. But the research on the behavior of the shear connector itself is quite limited. Moreover, the investigation on the base strain behavior of the stud shank either by the experiment or numerical method is almost absent, although many researchers reported some numerical results. On the other hand, Nakajima et al.[6] investigated the behavior of stud shear connectors under the pulsating and alternating load conditions numerically and compared those with the experimental results. No comparison of the strain behavior of the stud shank is available. Miah et al.[7] improved the accuracy of the strain and slip behavior of the stud shear connector based on the method proposed by Nakajima et al.[6]. The strain behavior at the base of the stud shear connector was investigated, but no comparison was made with the experimental results.

In this study, attention is paid towards the base strain behavior of the stud shear connector. Nonlinear finite element method along with Timoshenko beam theory is employed for the numerical analysis. The numerical results are compared with the experimental ones to validate the numerical formulation for the pulsating and alternating load conditions. The load condition with the compressive shear force cycles is defined as the pulsating load condition and the reversed cyclic shear force is defined as the alternating load condition.

2. Push-and pull-out test specimen

The push- and pull-out test specimen[1,2] shown in Fig. 1, is briefly introduced here and the results obtained from the test specimen are used afterward for the comparison. A pair of headed pipe studs with inside diameter 17.9mm, outside diameter 21.7mm and length 120mm was welded on the base steel plate (530mm×120mm×13mm). The size of the stud head and the welding are shown with the test specimen. Another steel plate (350mm×60mm×19mm) was welded to the base plate on the other side to increase the stiffness of the base plate and to provide sufficient resistance against plate bending. Two displacement transducers were installed to measure the slip between the concrete block and the base plate at the same level of the studs. One pair of strain gauges was installed on the inside face of the stud at the base level and another pair on the outside face at the mid height of each stud as shown in Fig. 1. The inside area of the pipe stud was then filled with cement mortar to minimize the local deformation of the pipe section during the tests.

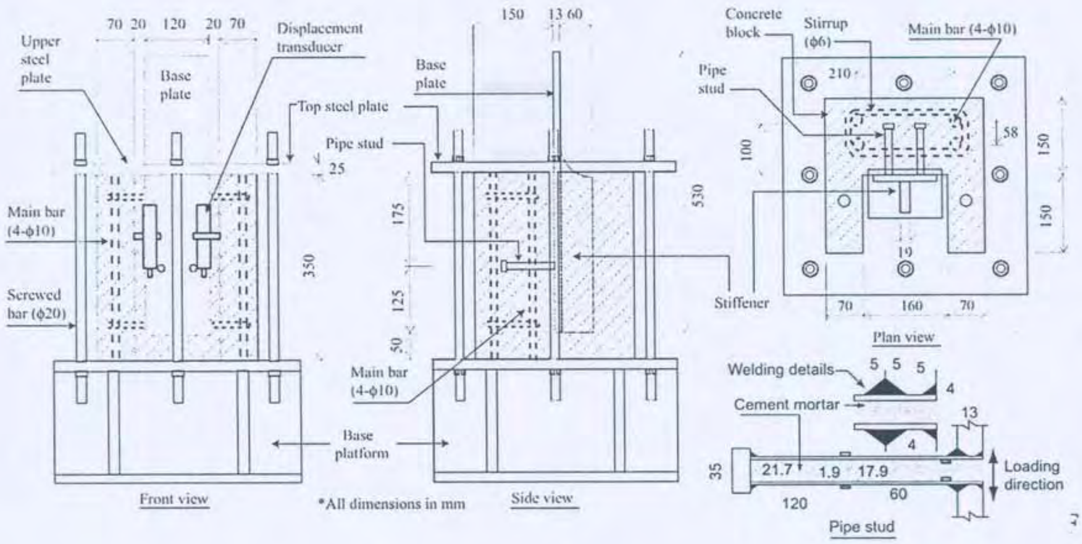

Fig. 1. Outline of test specimen

3. Bearing Test

The bearing test specimen is shown in Fig. 2 and was employed to conduct the bearing test to determine the bearing characteristics. The bearing test specimen was composed of the concrete block with the same height from the fixed end to the centerline of the stud shank of the push- and pull-out test specimen[1,2] shown in Fig. 1. A 6mm diameter rebar was welded at the inside bottom of the pipe to measure the relative displacement. The pipe was also filled with cement mortar after concreting. Two displacement transducers were placed on the top steel plate and another two were on the rebar as shown in Fig. 2 to measure the relative displacement. After a certain load level for instance 30kN, the rate of change of the rebar displacement apparently decreased. Consequently the stiffness increased with increased load levels. This was due to some set back in the experimental setup. However, for the numerical model, the initial stiffness value was used for the total loading range.

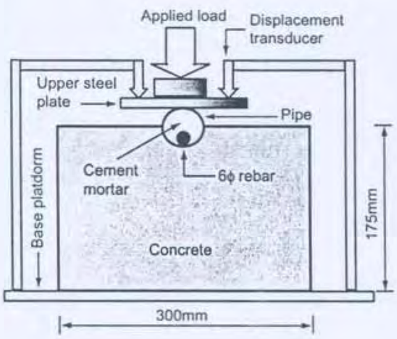

(a) Front view

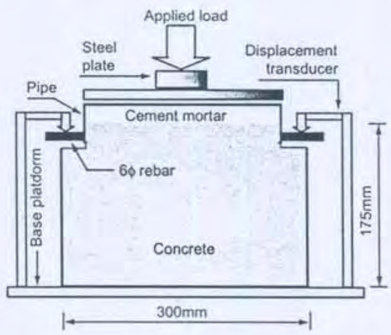

2(b) Side view

Fig. 2. Bearing test specimen

4. Analytical model

4.1 Outline of the numerical model

When the studs are employed in the steel-concrete composite structure, the applied shear force is usually transferred by the bearing force between the stud shank and the surrounding concrete across the transverse direction of the stud shank. Therefore, attention is focused on the proper modeling of the bearing force as shown in Fig. 3, which is the key resource for accurate numerical analysis to trace the mechanical behavior of the stud shear connectors.

Based on the geometry and loading symmetry, half of the specimen is modeled in this regard. The numerical model is shown in Fig. 4 including the base plate, stud and surrounding concrete. The 120mm length stud shank and 250mm length base plate are modeled as 24 and 26 beam-column elements respectively. The base plate is considered symmetrical with respect to the axis of stud shank. The effect of the stiffener is taken into account by the way of increasing the thickness of the base steel plate.

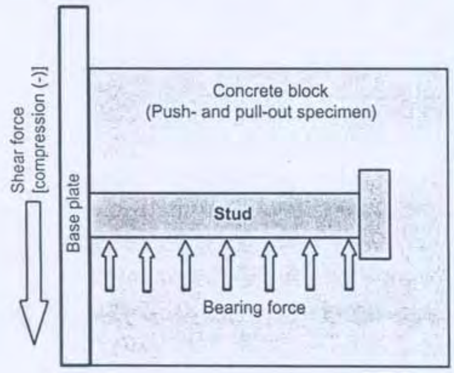

Fig. 3. Bearing force of concrete

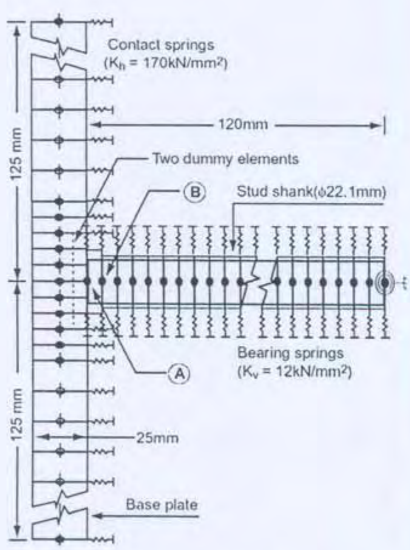

Fig. 4. Numerical model

4.2 Stud and base plate

Two-dimensional nonlinear finite element method along with Timoshenko beam model is employed for the numerical analysis of the stud and base steel plate. The base of the stud shank in the test specimen was little thicker than the diameter of stud itself due to welding. The length of the welding of 5mm with tapered section and average thickness of 2.5mm is considered in numerical analysis. The strength of the cement mortar inside of the pipe is considered in terms of increased flexural stiffness (EI) of the pipe itself. In this regard, the flexural rigidity of the pipe stud is increased by 13.5%.

The thickness of the base steel plate is assumed to be 25mm instead of 13mm in order to account for the effect of stiffener. The stud and the base plate are modeled as the beam-column element with geometrical and material nonlinearities. For geometrical nonlinearity, finite displacement and infinitesimal strain problem are taken into account since it is rational and realistic for general framed structures. The constitutive relation for the stud and base plate is shown in Fig. 5(a), which includes Von Mises yield criterion, associate flow rule and linear kinematic hardening.

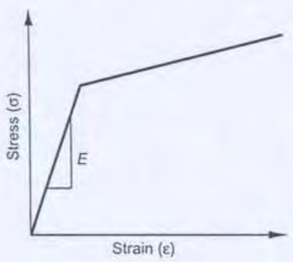

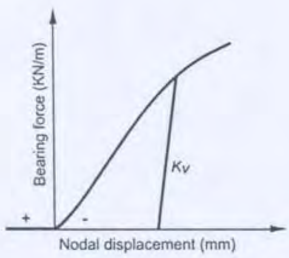

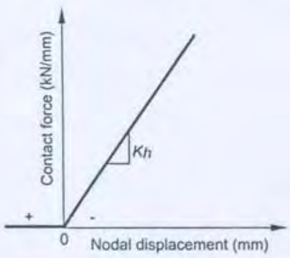

(a) Stud and base plate (b) Bearing springs (c) Contact springs

Fig. 5. Constitutive relation of different materials

The material properties such as Young's modulus (E) and Poisson's ratio (ν) are considered as 210kN/mm^2 and 0.3 respectively. Initial yield stress (σ_y) and the effective shear coefficient[8] (κ) are taken as 235N/mm^2 and 0.575 for the stud and 293N/mm^2 and 0.867 for the steel plate. The kinematic hardening parameter H is assumed as 1% of the Young's modulus E. Two stress components, one normal component in longitudinal direction and another shear component in the transverse direction are considered whereas the other components are assumed to be zero. A particular stress integrating algorithm with little modification of the return-mapping algorithm[9] is considered here for the simulation of the above plastic constitutive relation with two stress components.

4.3 Bearing spring

For the accurate numerical analysis, it is of course important to take into account the proper bearing characteristics between the stud shank and the surrounding concrete. The bearing force to relative displacement relation obtained from the bearing test is shown in Fig. 6. The ordinate shows the bearing force applied per unit length of the pipe (Fig. 4) and the abscissa shows the relative displacement between the rebar and base platform shown in Fig. 2. A fourth order polynomial curve given by the following equation (Eq. 1) is assumed to fit the envelope curve of the mechanical characteristics of the bearing springs shown in Fig. 5(b) for nonlinear hardening.

$$P=a_1\delta+a_2\delta^2+a_3\delta^3+a_4\delta^4 \tag{1}$$

where, P is the bearing force and δ is the relative displacement at any load level.

The coefficients a_1, a_2, a_3, and a_4 are determined from best fit curve and are taken as 1.43, 6.30, -8.96 and 3.45 respectively. The spring constant (K_v) per unit length along the stud shank was estimated to be $12kN/mm^2$ based on the unloading stiffness of the bearing force-relative displacement relation. The bearing force for an element is distributed equally to two nodes that belong to the element. So, the spring constants of the base and tip springs are proportionately evaluated as per contributing length. The bearing springs are considered to be active only in compression and arranged between the stud shank and the virtual fixed end. One-dimensional return-mapping algorithm[9] is employed to compute plastic effect of the bearing springs.

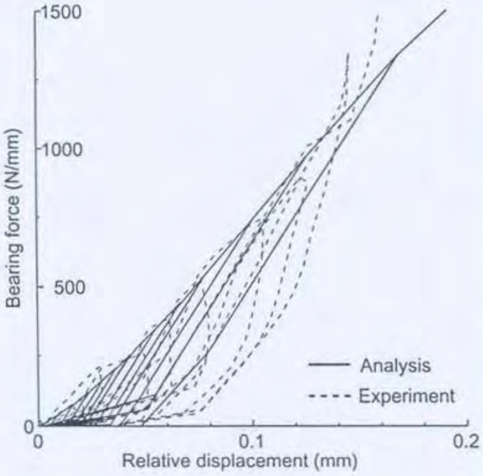

Fig. 6. Bearing force-relative displacement relation

4.4 Contact spring

The natural bond between the concrete block and base steel plate was omitted by providing craft tape and grease before placing concrete in test specimen. In numerical analysis the contact surface between the concrete block and base plate is modeled as a type of penalty[10] springs provided horizontally as shown in Fig. 4. The spring constant (K_h) of the contact springs is estimated by trial and error and its magnitude is considered sufficiently large and taken as $170kN/mm^2$. It is assumed that the spring works only in compression and constitutive relation of the contact spring is shown in Fig. 5(c).

5. Comparison of numerical and experimental responses

The numerical evaluations of the stud shear connectors obtained from two-dimensional nonlinear finite element method are discussed and compared with the experimental results for the pulsating and alternating load conditions.

5.1 Shear force-Slip relation

The relation between the shear force and slip obtained from the numerical analysis for the pipe stud is shown in Fig. 7(a) under the pulsating load condition along with the experimental value obtained from push- and pull-out test[1,2]. The same relations obtained from the alternating load condition are shown in Fig. 7(b). The solid lines stand for the result obtained from numerical analysis and the dashed lines stand for the experimental results. The ordinate indicates the shear force applied per single stud and the abscissa indicates the slip between the concrete block and the base plate. The slip is estimated by the vertical displacement at the base node A (Fig. 4) of the numerical model. According to Fig. 7(a), it is observed that the numerical results agree well with the experimental ones under the pulsating load condition. On the other hand, in Fig. 7(b), the agreement between the numerical and experimental results for compression sided loading are found to be good under the alternating load condition, but for tension side loading the estimation by the numerical analysis is somewhat less than the experimental data.

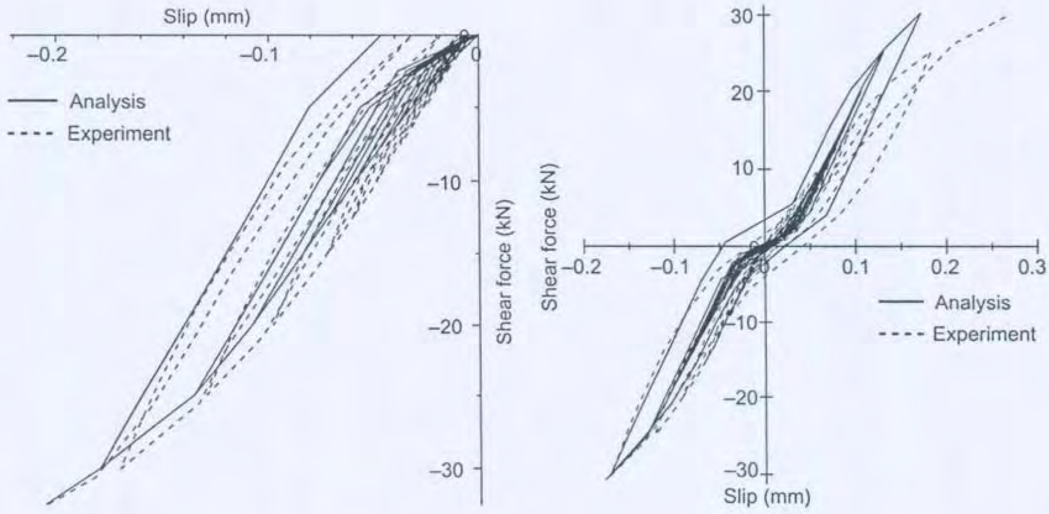

(a) Pulsating load condition (b) Alternating load condition

Fig. 7. Shear force-slip relations

5.2 Bearing force-relative displacement relation

The relation between the bearing force and the relative displacement obtained from the numerical analysis is shown in Fig. 6 by the solid line and the dashed line shows the one obtained from bearing test. Absolute values are considered for both the bearing force as ordinate and relative displacement as abscissa. In the numerical model, the relative displacement is estimated by the vertical displacement at the node B (Fig. 4). The numerical result agrees reasonably well with experimental one.

5.3 Strain behavior of stud shank

In the numerical analysis, the strain can be estimated at any point along the height of the stud shank. From experimental records, strains are available at the base and mid height of the stud shank. The strain behavior determined from numerical analysis is compared with the experimental ones at the base and mid height of the stud shank for the pulsating and alternating load conditions.

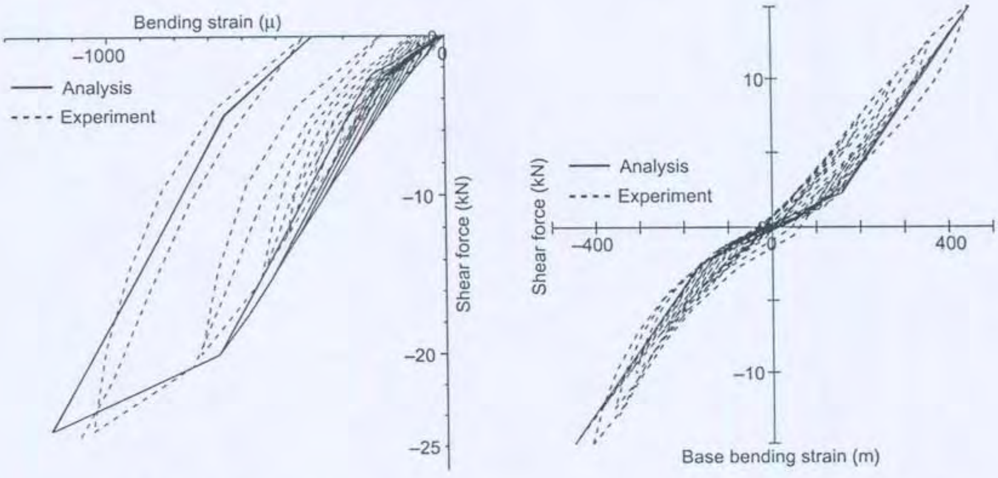

(a) Pulsating load condition (b) Alternating load condition

Fig. 8. Shear force-bending strain relations at base

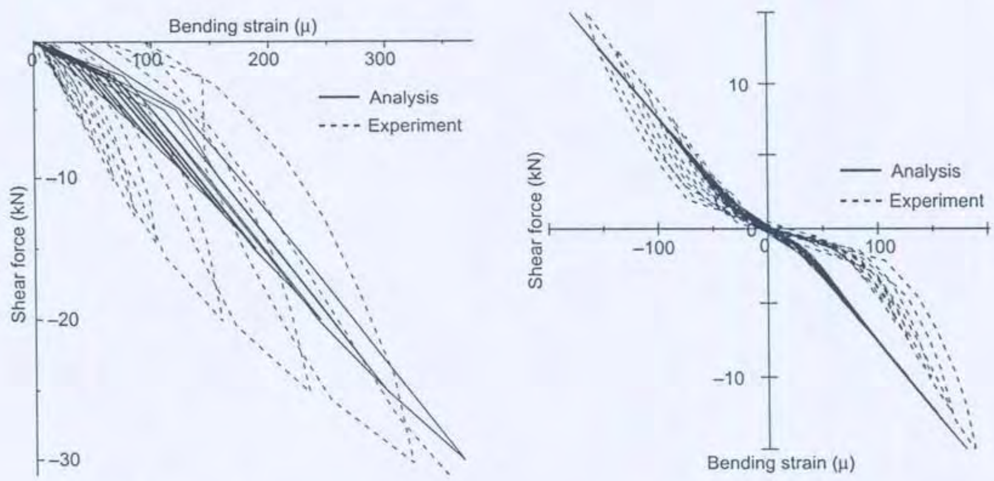

(a) Pulsating load condition (b) Alternating load condition

Fig. 9. Shear force-bending strain relations at mid height

Only the bending strains at the base and mid height levels obtained from the experimental investigation are compared with the numerical predictions. The bending strains at the base and mid height are estimated from the elementary beam theory and the corresponding relations are shown in Figs. 8 and 9 along with the experimental data. The bending strain relations obtained from the numerical analysis agrees well with the experimental responses. The agreement between the numerical and experimental results for the pulsating load condition is better than the one for the alternating load condition. In the pulsating load condition, the correlation between the numerical and experimental strain behavior at the base of the stud shank is better than those at the mid height level. The shear force-slip relations and shear force-bending strain relations play important role for the structural design and show good correlation with each other. In reality, pipe stud shear connectors are non-existent in the field of composite construction while base strains are almost impossible to measure experimentally for solid studs. However, it can be observed that the numerical results of pipe stud shear connectors predict the experimental response with fair degree of accuracy. Hence, numerical results of pipe stud and solid stud shear connector can be compared with each other to arrive at some practical solution. From numerical solution of both type of studs, shear force amplitude to bending strain amplitude relation are constructed in Fig.10 to investigate the shear force transmission for the pipe stud as well as solid stud (13mm).

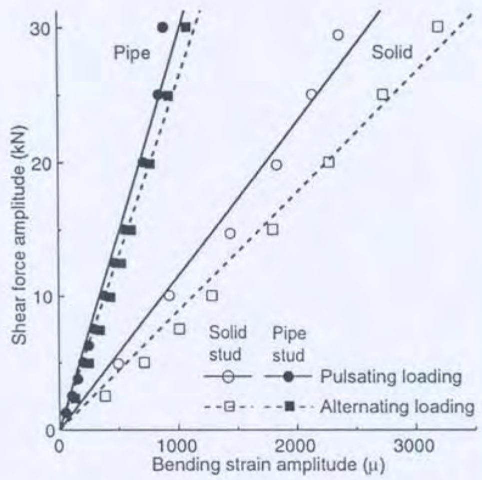

Fig. 10. Shear force amplitude-bending strain amplitude relation

Regression lines are plotted to observe the correlation among the plotted data. For shear force amplitude of 25kN, the bending strain amplitudes of the pipe studs under the alternating load condition are found to be about 10% larger than that under the pulsating load condition. This difference is over 30% for solid studs. On the other hand, the bending strain amplitudes of the solid studs are 2.5 times higher than the pipe stud shear connectors under the pulsating load and 3.0 times larger under alternating load conditions.

6. Conclusions

To evaluate the mechanical behavior like the strain and slip behavior of the stud shear connector, a numerical method has been proposed. One-dimensional bearing springs with nonlinear hardening and beam-column element with geometrical and material nonlinearity are included in this formulation. The assessment from this numerical approach agrees with the experimental results within a certain degree of accuracy ranging from 75% to 95%. Hence, the reliability of this formulation is reasonably established for predicting the behavior of the stud shear connectors.

References

1. Miah, Md. K., Nakajima, A., Saiki, I., Kadogaki, T. and Ooe, H.: Experimental study on Strain Behavior of Pipe Stud Shear Connector Subjected to Various Load Conditions, Proc. of The 5th Symposium on Research and Application of Composite Constructions, pp.231-238, 2003.

2. Nakajima, A., Miah, Md. K., Kadogaki, T., A., Saiki and Ooe, H.: Experimental evaluation of strain behavior of stud shear connector through shear transmission, Proc. of 5th Japanese-German Joint Symposium on Steel and Composite Bridge, pp.481-492, 2003.
3. Civjan, S. A. and Singh, P.: Behavior of shear studs subjected to fully reversed cyclic loading, Journal of Structural Engineering, ASCE, Vol. 129, No. 11, pp.1466-1474, 2003.
4. Salari, M.R. and Spacone, E.: Analysis of steel-concrete composite frames with bond slip, Journal of Structural Engineering, ASCE, Vol. 127, No. 11, pp.1243-1250, 2001.
5. Spacone, E. and El-Tawil, S.: Nonlinear Analysis of steel-concrete composite Structure: State of the Art, Journal of Structural Engineering, ASC}, Vol. 130, No. 2, pp.159-168, 2004.
6. Nakajima, A., Saiki, I., Kokai, M., Doi, K., Takabayashi, Y. and Ooe, H.: Cyclic shear force-slip behavior of studs under alternating and pulsating load condition, Engineering Structures, Elsevier Science Ltd.}, Vol.25, pp.537-545, 2003.
7. Miah, Md. K., Saiki, I. and Nakajima, A.: Numerical evaluation of static behavior of stud shear connectors, JSCE Journal of Applied Mechanics, Vol.7, pp.571-578, 2004.
8. Hutchinson, J.R.: Shear coefficients for Timoshenko Beam Theory, ASME Journal of Applied Mechanics, Vol.68, pp.87-92, 2001.
9. Simo, J.C. and Hughes, T.J.R.: Computational Inelasticity, Springer, 1998.
10. Wriggers, P.: Computational Contact Mechanics, John Wiley Inc., 2002

Japan-Bangladesh Joint Seminar on Advances in Bridge Engineering
Dhaka, Bangladesh. 10 August 2005 ISBN: 984-32-2520-6

Evaluation method for bending capacity of corroded steel girder

Takeshi Mori*

Department of Civil and Environmental Engineering, Hosei University
3-7-2 Kajino-cho, Koganei-shi, Tokyo, Japan.

Abstract

Corrosion is typical damage on steel bridges, but the evaluation method for capacity of steel member with corrosion has not been established. The estimation to repair corroded steel member is usually done on the basis of corroded area and/or corrosion depth. However, it makes the estimation more reasonable that the relationship between capacity of the member and the degree of corrosion is clear. In this study, examination of corrosion configuration using actual corroded steel member has been done, and simulation method for the configuration is discussed. Furthermore, bending capacity of I-shaped beam with corrosion on the lower flange is examined by using three-dimensional elastic-plastic finite element stress analyses.

1. Introduction

It is well known that the most typical damage in the steel bridge is the corrosion and the capacity of the member lowers with increase in corrosion. The corrosion is divided roughly into local and general one from its appearance. The general corrosion, in which whole surface of steel corrodes and its thickness decreases, is apt to occur when the steel was exposed in almost uniform corrosive environment such as atmosphere and seawater. On the other hand, local corrosion, in which partially deep hole or groove occurs, is apt to occur when corrosion reaction locally occurs. Whether corrosion damage should be repaired or not is usually assessed on the basis of the degree of the corrosion (surface area and depth of the corrosion). However, more reasonable assessment could be realized if the relationship between the capacity of the corroded member and degree of the corrosion is made clear (Japanese Society of Steel Construction 2002).

In this study, the surface configuration of the corroded steel plate taken out from actual bridges has been measured, and geometrical features and the simulation method for the configuration have been examined on the basis of the measurement results. Furthermore,

* Email: mori@k.hosei.ac.jp

the bending capacity of steel I-shaped beam with the general or local corrosion on the lower flange is discussed using three-dimensional elastic-plastic finite element stress analyses.

2. Investigation on the configuration of corroded steel surface

2.1 Specimen and measuring method

Specimens were obtained from 3 bridges as shown in below.

A-bridge : This bridge was constructed in 1928, and removed in 1993. The stringer was an object.
B-bridge : It was a arch bridge which was over the river in the inland. It was rebuilt in 1992. The test piece was collected from lateral bracing.
C-bridge : It is a truss bridge which is located in the estuary. The lateral bracing was removed due to the remarkable corrosion is an object.

On the A-bridge, the data indicated in the report (Public Works Research Institute 1996) was utilized. The corrosion depth was measured at 5mm interval in the transverse direction of the flange and 50mm or 100mm interval in the longitudinal direction.

As for the B- and C-bridges, the specimens were mounted on the digital movable pedestal, and their surface configurations have been measured by the laser displacement gauge (measuring range: 15mm, laser spot diameter: 70μm, resolution: 3μm). The measurement was carried out at the intervals of 1.0 mm in both directions.

Table 1. Results of corrosion depth measurements on A-bridge

Specimen	Corrosion depth (mm)		Corroded cross-section area (mm^2)	
	maximum	average	maximum	average
No.1	12.88	4.82	72.12	57.39
No.2	8.13	3.37	69.68	56.26
No.3	15.68	2.63	48.89	30.29
No.4	9.59	2.07	21.63	9.61

2.2 Geometrical feature

The corrosion configuration of the A-bridge was measured on the upper flanges of 4 stringers, which had especially remarkable corrosion. Outline of measurement results on the each stringer is shown in Table 1. The corrosion on the specimen No.1 is the most remarkable, and the specimen No.2, No.3 and No.4 follows.

The frequency diagram of corrosion depth measured in each specimen is shown in Fig. 1(a)-(d). As for the specimen No.1 whose corrosion is the most severe, the frequency of the corrosion depth is the most remarkable where the depth is 4.0 to 5.5mm, and the histogram is similar to the normal distribution. In the specimen No.4 whose corrosion is the slightest, the frequency diagram of the corrosion depth looks the half normal

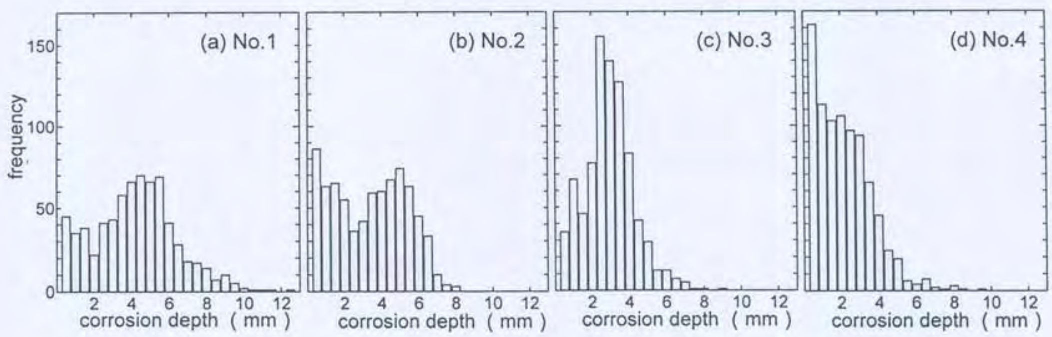

Fig. 1. Distribution of corrosion depth on the upper flange of each girder (A-Bridge)

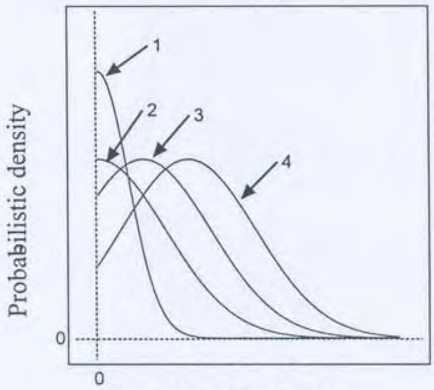

Fig. 2. Model of corrosion progress

distribution whose modal value is equal to 0. On the basis of these facts, the histogram of the corrosion depth is considered to progress at the order shown in Fig.2.

Mean value, standard deviation and largest corrosion depth in each specimen measured by the laser equipment are shown in Table 2. Fig.3(a) to (c) and Fig.4(a) to (c) show the example of frequency diagram of corrosion depth, frequency diagram of corrosion depth at the point adjacent to objective point, and the relationship between maximum, average and minimum value of corrosion depth at the adjacent point and corrosion depth at the objective point. The number of adjacent points surrounding an objective point is eight.

The solid line shown in Fig.3(a) and Fig.4(a) is normal distribution obtained from measured modal value and standard deviation. Two examples shown here almost correspond with the normal distribution. Other data also corresponded with the normal distribution. From Fig.3(b) and Fig.4(b), it can be understood that corrosion depth of the adjacent point is also followed by the normal distribution whose modal value is equal to the depth at the objective point.

Fig.3(c) and Fig.4(c) indicate that the average corrosion depth of adjacent point is almost the same as that of the objective point. The maximum and minimum corrosion depth at the adjacent point is almost parallel to the average corrosion depth. This fact means that the (gradient) restriction of the corrosion depth at adjacent point to the depth of the objective point exists. That is, the corrosion depth does not change suddenly and corrosion configuration is comparatively smooth.

Table 2. Results of corrosion depth measurements of B- and C-bridge

Specimen		Average corrosion depth	Standard deviation	Maximum corrosion depth
B-bridge	No.1	1.25mm	0.45mm	2.62mm
	No.2	1.23mm	0.52mm	3.03mm
	No.3	0.58mm	0.29mm	1.88mm
C-bridge	No.1	1.44mm	0.68mm	2.69mm
	No.2	1.97mm	0.77mm	3.56mm
	No.3	1.40mm	0.66mm	3.36mm
	No.4	1.39mm	0.69mm	2.77mm

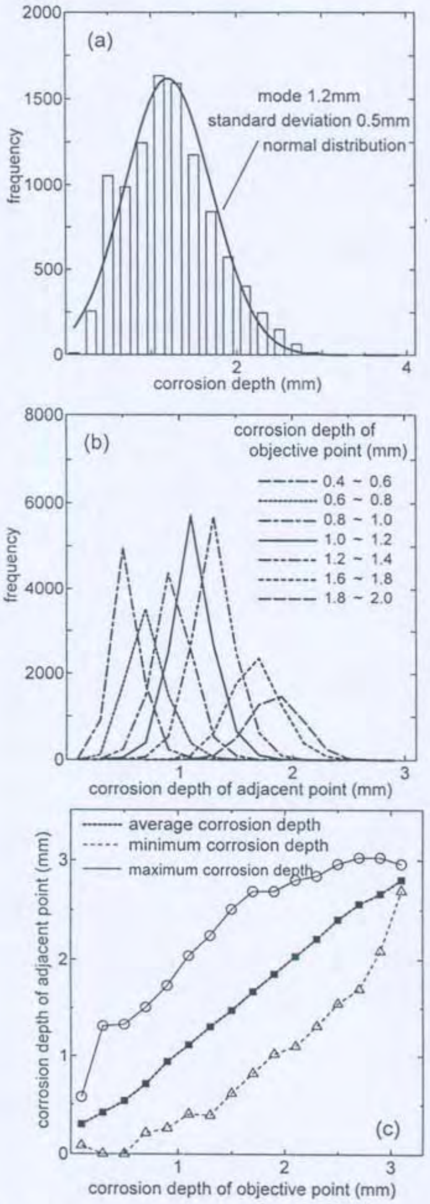

Fig. 3. An example of measured results of corrosion depth in the B-bridge

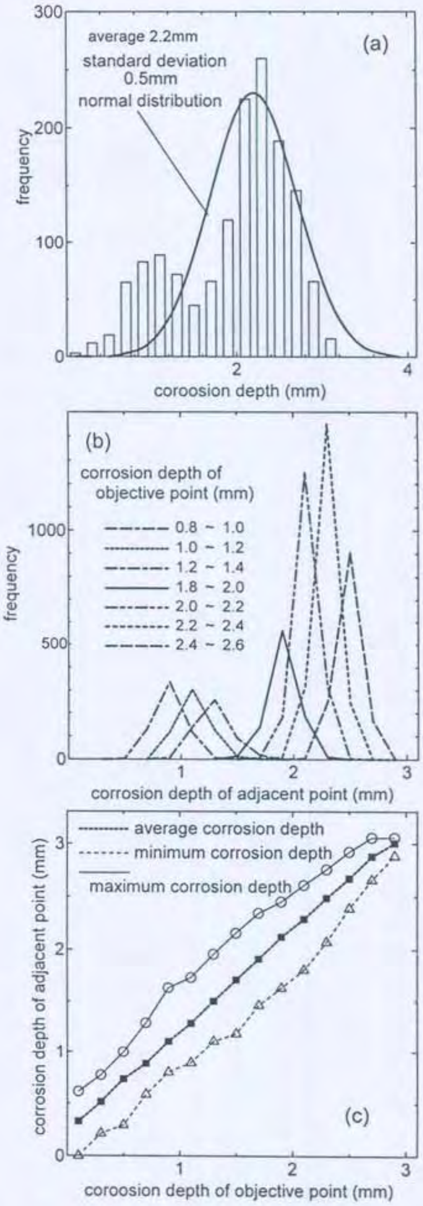

Fig. 4. An example of measured results of corrosion depth in the C-bridge

2.3 Simulation of surface configuration

On the basis of results indicated in the former section, the technique to simulate the configuration of corroded steel plate surface has been developed as follows.

(a) The steel plate surface is divided into grid of perfect square, and the numbering for each node of the grid is randomly carried out using uniform random number.
(b) The permutation of corrosion depth is prepared, which follows fixed normal distribution (mode, standard deviation, maximum value, minimum value) using the normal random number.
(c) The first corrosion depth in the permutation specified in the step (b) is given to the No.1 node determined in the step (a). This corrosion depth is deleted from the permutation.
(d) Whether the No.2 node is adjacent to the No.1 node is judged. If adjacent, whether the first corrosion depth in the permutation has satisfied the condition that corrosion depth of the adjacent point follows the normal distribution with the modal value equal to the depth at the objective node is assessed. If it has been satisfied, this value is adopted as the corrosion depth at the No.2 node, and it is deleted from the permutation. When it is not satisfied, the depth satisfying the condition is searched in the order of corrosion depth in the permutation, and it is defined as the corrosion depth at No.2 node, then it is deleted from the permutation.
(e) Corrosion depth of all nodes is determined by doing repeatedly the work of the step (d).

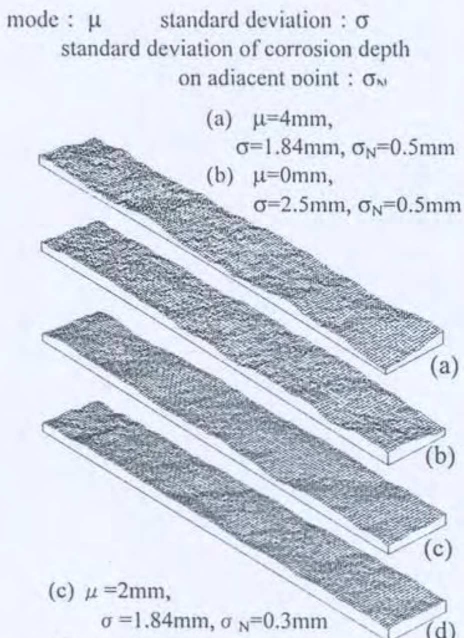

Fig. 5. Examples of simulated corrosion surface

2.4 *Results of simulation*

The configuration of the corroded steel plate surface simulated using the technique described in the former section has been obtained. Some examples of simulated configurations are shown in Fig.5. The conditions of the simulation are also indicated in Fig.5.

3. Analyses of bending capacity

In this chapter, the bending capacity of corroded steel beam is analyzed using three-dimensional elastic-plastic finite element stress analyses, and bending capacity evaluation method is discussed.

3.1 *Analytical model*

Analytical object is the steel I-shaped beam whose cross-section is shown in Fig.6. The length of the beam is assumed to be 800mm. The existence of the general corrosion was assumed in a range of 500mm in span center on the upper surface of lower flange, and the local corrosion is assumed to exist at the span center. The configuration of general corrosion and local corrosion consists of 6 types and 6 types, respectively. In addition to the above models, the sound beam (without corrosion) was also the analytical object. The example of the finite element model is shown in Fig.7 in order to indicate the surface configuration of each corrosion model.

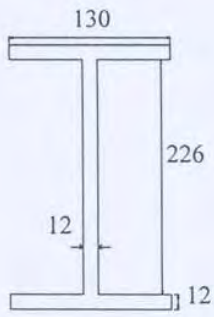

Fig. 6. Cross section of beam

3.2 *General corrosion model*

Longitudinal wave (LW) model and transverse wave (TW) model simulate the corrosion configuration by sine wave, and corrosion depth of the deepest point is set at 1, 2, 4, 6 and 8mm (the minimum corrosion depth is set at 0), and the wave length is assumed to be 6 times of the depth. The double wave (DW) model simulates the corrosion configuration by double sine wave, and the wave length is set at 40mm, and the depth of the deepest point is assumed to be 2, 4, 6 and 8mm.

The uniform distribution (UD) model simulated the corrosion configuration using the uniform random number. The corrosion depth was set so that the average is equal to 1, 2, 3, 4, and 5mm (a range of random number 0-2, 0-4, 0-6, 0-8 and 0-10mm). The normal distribution (ND) model simulated the corrosion configuration using the normal random number. The modal value and the standard deviation of normal distribution is set as shown in Table 3.

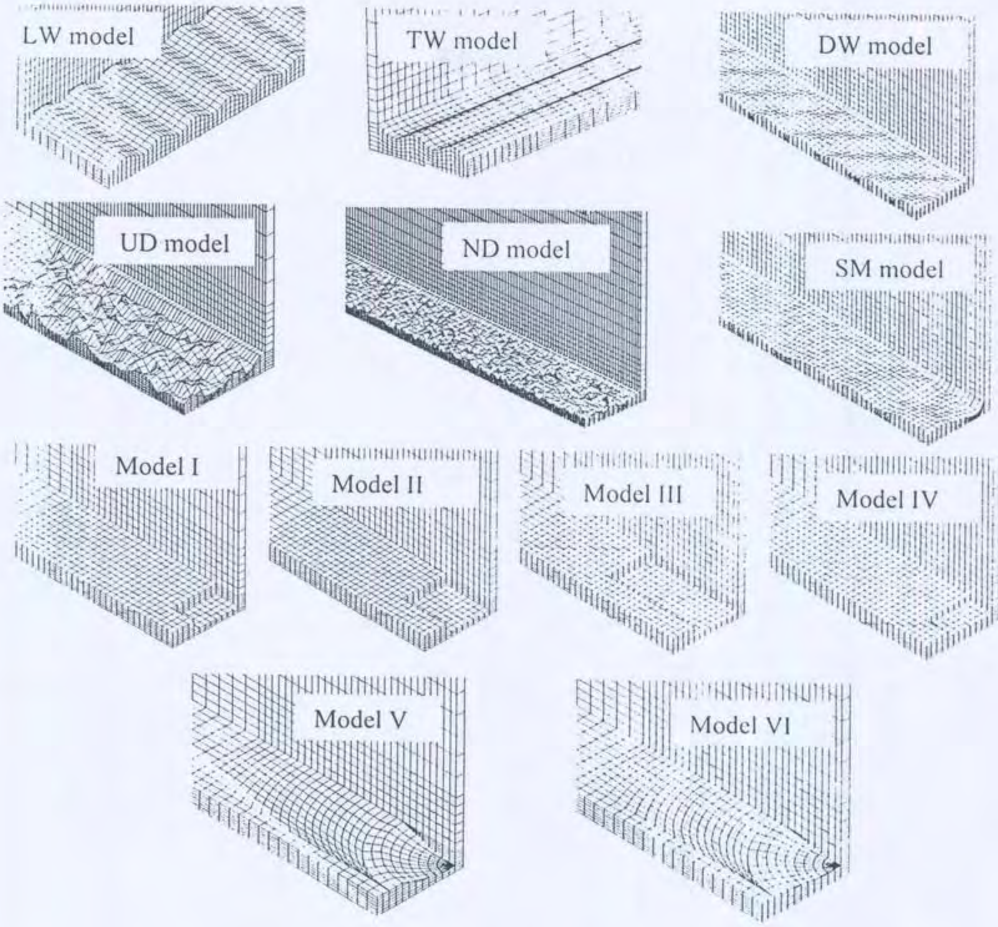

Fig. 7. Finite element of each corrosion model

Table 3 Normal distribution model

ND	Mode	Standard deviation
1	0	1.84mm
2	2.0mm	1.84mm
3	4.0mm	1.84mm
4	0	1.0mm
5	0	1.5mm
6	0	2.5mm

The simulation (SM) model simulated the corrosion configuration using the method described in the former chapter. The modal value and the standard deviation of the normal distribution is set as shown in Table 4. The standard deviation of corrosion depth at the adjacent point has been set at 0.3mm or 0.5mm.

3.3 Local corrosion model

Model I to IV simulate the local corrosion by square groove. In the model I, corrosion depth is set at 2, 4, 6, 8 and 10mm, and the width and length are assumed to be 5 times of the depth. In the model II, the length and width of the groove is set at 10 times and 5 times of the depth, respectively. As for the model III and IV, the length (width) is 20 times (5 times) and 10 times (10 times) of the depth, respectively.

Table 4. Simulation model

SM	Mode	Standard deviation	Standard deviation*
1	0	1.0mm	0.3mm
2	0	1.5mm	0.3mm
3	0	1.8mm	0.3mm
4	0	2.5mm	0.3mm
5	2.0mm	1.8mm	0.3mm
6	4.0mm	1.8mm	0.3mm
7	0	1.0mm	0.5mm
8	0	1.5mm	0.5mm
9	0	1.8mm	0.5mm
10	0	2.5mm	0.5mm
11	2.0mm	1.8mm	0.5mm
12	4.0mm	1.8mm	0.5mm

* *adjacent point*

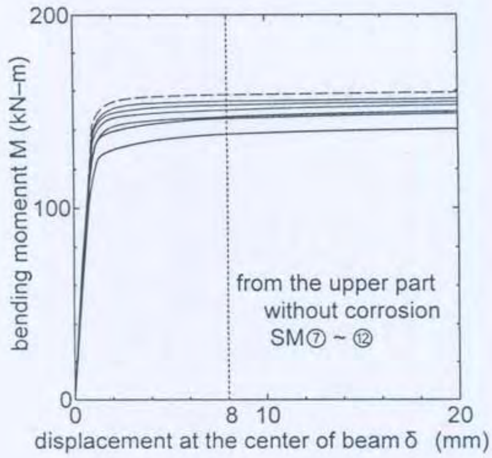

Fig. 8. An example of M-δ relationship

Model V and VI simulated the corrosion configuration by a quarter ellipsoidal groove. In the model V, the corrosion depth is equal to 2, 4, 6 and 8mm and the diameter is set at 5 times of the depth. As for the model VI, the depth is 2 and 4mm, and the width and length is equal to 10 times and 20 times of the depth, respectively.

3.4 *Analytical method*

Steel for the model is assumed to be JIS SM400, and its yield stress is set at 294N/mm^2, Young's modulus is 2.06x10^{5}N/mm^2 and Poisson's ratio is 0.3. Considering the symmetrical shape of the analytical object, finite element elastic-plastic stress analyses have been carried out using quarter models. The element size is basically set at 5x5x2mm (2mm in thickness direction). The relationship between stress and strain is assumed to be bi-linear, and the gradient after the yield is set at $4.66 \times 10^{-3} N/mm^2$. Von-Mises criterion has been employed for assessment of yielding.

3.5 Analytical results

An example of the relationships between bending moment M and deflection δ at the span center, which were obtained from the analyses on SM models, is shown in Fig.8. The bending capacity was assumed to be a bending moment as the deflection reached one-hundredth of the span length (8mm).

Fig.9(a) shows the bending capacity ratio arranged by maximum corroded cross-section ratio. The bending moment ratio is the ratio of bending capacity of the beam with the corrosion to one of the beam without corrosion. The maximum corroded cross-section ratio is an amount of the loss in cross-section area due to corrosion in which the largest corrosion occurs normalized by the original flange cross-section area. The bending capacity ratio decreases as the maximum corroded cross-section ratio increases in either corrosion model. However, the lowering rate of bending capacity with increase in the maximum corroded cross-section ratio has significant difference among the corrosion model. Fig.9(b) indicates the relationship obtained from local corrosion model. The relationship also large difference among the corrosion model in this case. These facts mean that the maximum corroded cross-section ratio is not suitable parameter to arrange the bending capacity of the corroded steel member.

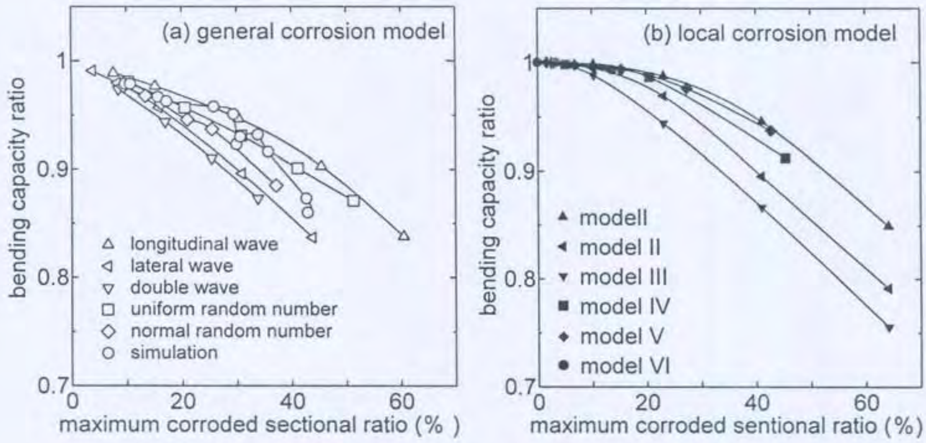

Fig. 9. Bending capacity ratio arranged by maximum corroded sectional ratio

Bending capacity ratio of the beam with general corrosion has been tried to be arranged by the average corroded cross-section ratio. The average corroded cross-section ratio is the average ratio in all cross-sections with the corrosion, and it is equal to the volume defect ratio in the objective part. The results are shown in Fig.10. The difference of bending capacity ratio due to corrosion model also exits in the case that the average corroded cross-section ratio is utilized.

3.6 Estimation of bending capacity using modified corroded cross-section ratio

The bending capacity can be defined as a bending moment when a cross-section receives large plastic deformation. Such plastic deformation does not occur in the whole region of the beam, and it is considered to occur in some part of the beam. If this region (length) can be defined, the average corroded cross-section ratio in the region may be powerful parameter to arrange the bending capacity. Here, the length (F_L) being 0.5, 1.0 and 1.5 times of the flange width (F_W) is taken up in the direction of longitudinal axis of the beam, the average corroded cross-section ratio is regularly calculated in each region, and the bending capacity is tried to be arranged by the largest one of the average corroded cross-section ratio calculated. This average corroded cross-section ratio is called the modified corroded cross-section ratio.

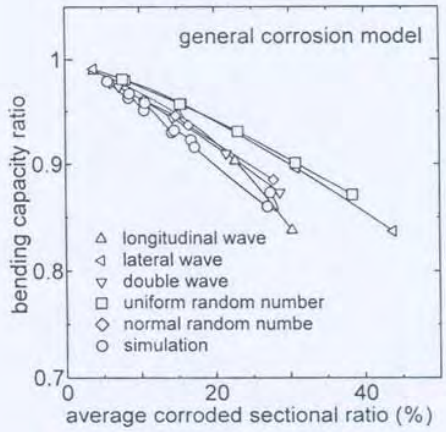

Fig. 10 Bending capacity ratio arranged by average corroded sectional ratio

Fig.11(a) to (c) shows the bending capacity ratio arranged by the modified corroded cross-section ratio in case of F_L=0.5F_W, F_L=1.0F_W and F_L=1.5F_W. As for the general corrosion model, the bending capacity ratio is well arranged by the modified corroded cross-section ratio regardless of corrosion model in each value of F_L. In the local corrosion model, the bending capacity is also arranged well by the modified corroded cross-section ratio regardless of corrosion model in each value of F_L. However, the bending capacity of the local corrosion model is higher than one of the general corrosion model in case of F_L=0.5F_W and lower in case of F_L=1.5F_W. When F_L is assumed to be equal to 1.0F_W, the bending capacity is not influenced by corrosion type. Therefore, the modified corroded cross-section ratio in a region of F_L=1.0F_W is considered to be adequate parameter to evaluate the bending capacity of the beam with corrosion.

3.7 Estimation method of bending capacity

Bending capacity of corroded beam is tried to be evaluated by plastic moment (Mp) which can be obtained from simple calculation. In order to obtain the value of Mp of corroded beam, thickness of flange with corrosion is uniformly reduced by the modified corroded cross-section ratio. The value of Mp can be calculated by following equation using the symbols shown in Fig.12.

$$M_p = \sigma_{ys}\left(\int_{y_2}^{y_1} w_l y \cdot dy + \int_0^{y_2} t_w y \cdot dy - \int_{-y_3}^{0} t_w y \cdot dy - \int_{-y_4}^{-y_3} w_u y \cdot dy\right) \quad (1)$$

Solid line in Fig.11 indicates the relationship between bending capacity ratio and the corroded cross-section ratio, which was obtained from Eq.(1). This line has represented well the data shown in Fig.11(b).

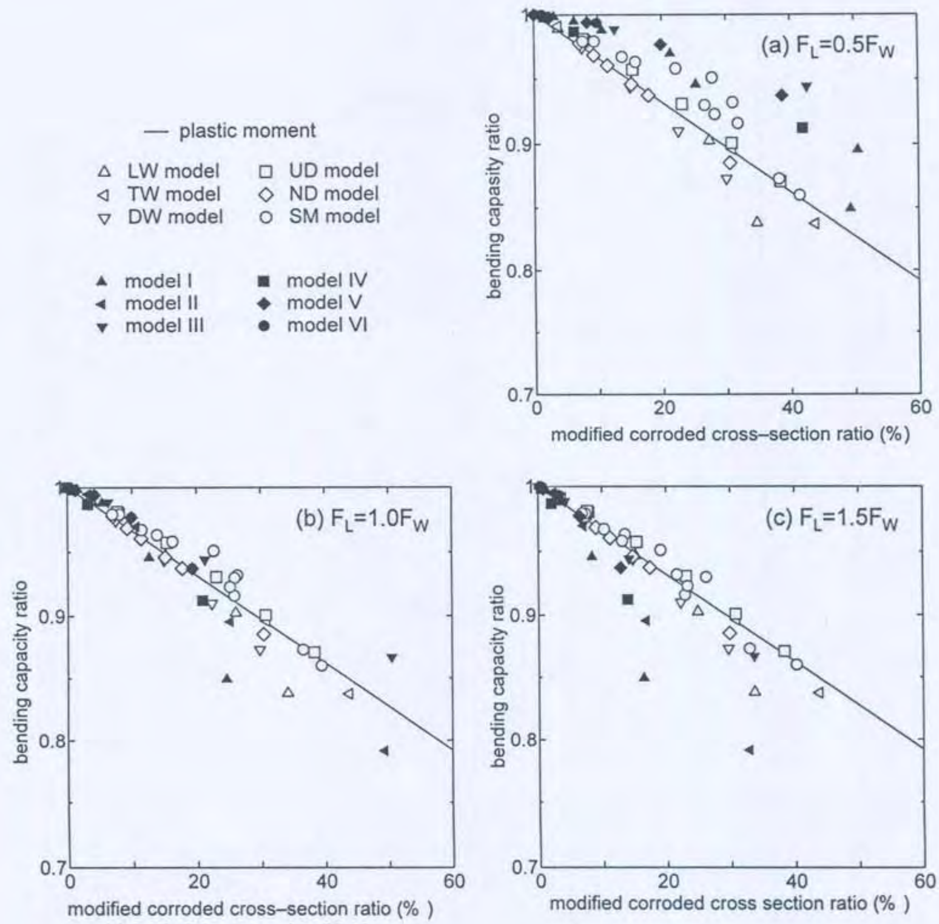

Fig. 11. Bending capacity ratio arranged by modified corroded cross-section ratio

4. Conclusions

(1) The corrosion depth of corroded steel plate follows the normal distribution.

(2) The corrosion depth of the adjacent point to the objective point follows the normal distribution whose modal value is equal to the corrosion depth of the objective point.

(3) The method for simulating the configuration of corroded steel plate surface has been proposed using the conclusions (1) and (2).

(4) The bending capacity of steel I-shaped beam with corrosion in the lower flange can be arranged by the maximum value of volume defect ratio due to corrosion in a region where length of flange is equal to flange width (modified corroded cross-section ratio).

(5) The bending capacity of steel I-shaped beam with corrosion in the lower flange can be evaluated by plastic moments of the beam in which the thickness of the lower flange is uniformly reduced by the modified corroded cross-section ratio.

References

Japanese Society of Steel Construction, "Reports of Estimation on capacity and endurance and repair method of exiting steel bridge members", *JSSC Report*, No.51, 2002.

Public Works Research Institute, "Experiments on capacity of corroded steel bridge members", 1996.

Japan-Bangladesh Joint Seminar on Advances in Bridge Engineering ISBN: 984-32-2520-6
Dhaka, Bangladesh. 10 August 2005

Highway bridge specifications and recent development of steel-concrete composite bridges in Japan

Masatsugu Nagai*

Department of Civil and Environmental Engineering, Nagaoka University of Technology 1603-1, Kami-tomioka, Nagaoka 940-2188, Japan

Abstract

Highway Bridge Specifications in Japan is introduced, which covers all the national roadway bridges. After shifting the technical standards based on specifications to those based on performance in 2002, next revision is now under consideration. Shift to LSD with partial safety factor format, explicit statement of lifetime, strengthening specifications for enhancing durability, addition of provisions that meet newly developed composite girder bridges with very simple transverse stiffening system and so on are expected. In order to reduce the bridge construction cost, new technology has been developed and being used, and they are introduced in detail. For further reduction of the construction cost, the importance of introduction of innovative design concept is emphasized.

1. Introduction

This paper deals with three topics. The first one is Highway Bridge Specifications in Japan (JHBS)[1] and the second one is recent development of steel-concrete composite bridges for reducing the construction cost and enhancing durability. Finally, future subjects for further reducing the construction cost are presented.

Design Specifications for Highway Bridges was revised in 2002. The basic concept is to shift the technical standards based on specifications to those based on performance. In addition, several provisions were added in order to meet new requirements for constructing economical bridge systems. The next revision is now under consideration. Since the work for revision has just started, at the present moment, the contents of new version is not clear. However, shift from Allowable Stress Design method (ASD) to Limit State Design method (LSD) with partial safety factor format is expected.

* E-mail: nagai@nagaokaut.ac.jp

The new bridge technology developed for reducing the construction cost is explained. Under the leadership of Japan Highway Public Corporation (JH), the revival of continuous composite girder bridges and the structural reform from multi-girder to two- or three-girder bridge system with very simple stiffening system have been made. Based on economical evaluation made by JH, when the span length is from 30 to 60 meters, these newly developed steel-concrete composite girder bridges are the most competitive solution and have been widely used now in Japan. For attaining further reduction of construction cost, since the newly developed bridge system is too simple to reform, it is recommended to incorporate the design innovation.

2. Design specifications for highway bridges

The Design Specifications for Highway Bridges in Japan (JHBS)[1] was issued from Japan Road Association (JRA) around 100 years ago and have been revised many times. Recent main revision was made in 1993 and 1996. In 1993, specifications related to live load was revised in order to meet the increasing size of vehicle and the improvement of durability. In 1996, after the Hyogo-ken Nanbu earthquake, the seismic design method was revised. JHBS covers all the national roadway bridges whose span length is less than 200 meters. Besides the above Specifications, there are a number of guidelines, such as Specifications for steel, composite and concrete structures issued by Japan Society of Civil Engineers (JSCE), and have been used as a reference. For long-span highway bridges such as the Honshu Shikoku Connecting Bridge Project, Design Specifications issued by the Honshu Shikoku Bridge Authorities are available.

JHBS consists of 5 parts; Common rules for design, Design of Steel bridges, Concrete bridges, Sub-structures and Seismic design. Basically, stability of the structures has been checked based on the Allowable Stress Design method (ASD). Fatigue problems have not been dealt with except for designing the steel deck plate. However, in view of increasing fatigue damage in steel bridges, Guidelines for Fatigue Design was newly issued in 2002. In the 2002 edition, performance based design concept was also introduced.

The next revision of the Design Specifications for Highway Bridges is now under consideration. Introduction of Limit State Design method (LSD) is expected, in which ultimate, serviceability and fatigue limit states of the bridge will be checked by employing the partial safety factor format.

Hereafter, we introduce the revision of the Specifications made in 2002 and an outline of the next revision now under consideration.

2.1 Recent revision of specifications for highway bridges

The design standards were revised in 2002. The basic concept is to shift the existing technical standards based on specifications to those based on performance, and to give consideration for improving durability of the bridges. In addition, new provisions were added to meet requirements for designing newly developed economical bridge system, which will be introduced later in this paper.

2.2 Revision in the common section

The followings are main revised items.

1. Performance required for designing a bridge has been clearly indicated.
2. Required items for materials and regulations on wire rope and parallel strand have been added.
3. Required performance for bearing shoes and expansion joints have been defined and their design procedures have been also prescribed.
4. Installation of water-preventing layer between asphalt pavement and concrete slab has been obliged, and checking items for enhancing durability of the slab have been listed.

2.3 Revision in section on steel bridges

The followings are the main revised items.

1. Design code for checking fatigue strength has been added in order to enhance durability. In view of increasing fatigue damage in steel bridges, fatigue check has been obliged.
2. Available upper limit of the plate thickness has been increased from 50 to 100 millimeters, including weathering steel. In Japan, in order to reduce the construction cost, instead of multi-girder system, construction of two-girder bridge has been increasing. This results in the use of larger thickness of the lower flange plate exceeding 50 millimeters. To meet this requirement, upper limit of the available thickness has been increased.
3. Use of tension-type bolt connection has been increasing. New specifications on tension-type bolt connection has been added.
4. As mentioned in above 2), construction of two-girder bridge has been increasing. In this bridge system, instead of RC slab, pre-stressed concrete (PC) slab has been used to meet the wide span. Hence, specifications on PC slab have been added.
5. Since a thick plate exceeding 50 millimeters is welded, detecting inner defect at the welding points becomes very important. Hence, the regulations on non-destructive testing such as ultrasonic testing of welds have been strengthened.
6. In view of increasing fatigue damage in steel deck plate, regulations on fabrication of the steel deck plate have been added.

2.4 Revision now under consideration

Discussions on next revision have started. First meeting was held on July 2004. Final revised version is expected to issue in 2007. New revised version may consist of 3-level document; Level-1 is basic of design (definition of required performance), Level-2 is standard specifications (measures to satisfy the required performance) and Level-3 is reference materials (theory, technical information and examples etc.) .
Although not finalized at all, the issues would be

1. Introduction of limit state design with the partial safety factor format which meets ISO
2. Clear definition of performance of bridge and its component
3. Specifications related to maintenance of existing bridges
4. Specifications for durability and explicit statement of lifetime of bridges
5. Specifications for composite structures and members
6. Specifications for new structural type such as steel girders with less stiffeners
7. Specifications for structural analysis and modeling

2.5 *Design code for steel and composite structures by Committee of Steel Structures of JSCE*

Committee of Steel Structures of JSCE has just started the project to publish Standard Specifications for Steel and Composite Structures. It is based on LSD and partial safety factor format will be employed. Design code for steel structures was issued in 1987 and revised in 1997. These versions were based on LSD. Design code for composite structures was also issued in 1989, however, it was incorporated in Guidelines for Performance-Based Design of Steel-Concrete Hybrid Structures and was issued by Committee of Structural Engineering of JSCE in 2002.

New Standard Specifications for Steel and Composite Structures consists of 5 parts: Basic planning, Performance-based Design, Fabrication, Maintenance and Seismic design, and will be published in 3 or 4 years, which includes latest research fruits. Furthermore, the design format will meet ISO format.

3. Recent development of steel-concrete composite bridges

In order to reduce the bridge construction cost, instead of multi-girder system, recently the bridge with two or three main girders has been increasing. It is natural to consider, when we design plate girder bridges, that the employment of smaller number of girder leads to economical solution. In such system, since the slab span becomes wider, pre-stressed concrete slab or steel-concrete composite slab with higher durability is inevitable. This practice is completely different from that of European engineers. They have been using RC slab until the span length reaches 8 or 10 meters.

In the followings, newly developed composite I-girder and box-girder bridges are introduced. Regarding the economical evaluation of various types of bridges, we followed the estimation made by JH.

3.1 *I-girder bridges*

For bridges with a width from 10 to 11 meters (2-lane), PC slab is supported by two girders and, for bridges with the width around 18 meters (3-lane), PC slab is supported by two or three girders. These are shown in Figure 1. The main girders are connected with small-sized rolled cross beams only installed at a distance from 5 to 10 meters. The main role of the cross beam is to support the erection facilities and to prevent lateral torsional buckling instability of the main girder at intermediate supports. This bridge system is very simple, which has a slab, two or three I-girder and small-sized rolled cross beams.

By employing this system, fabrication cost is drastically reduced and painting area is also reduced, resulting in the reduction of construction cost and enhancement of the ease of inspection and maintenance. It has been reported, when the span length is from 30 to 60 meters, this type of bridge is very competitive and, in many competitions, it beats the strong competitor, PC box girder bridges. However, depending on the site conditions, segmental PC box girder bridges sometimes beat the composite two I-girder bridges.

3.2 *Box girder bridges*

When the span length exceeds 60 meters or so, it has been reported that PC box girder bridges having the web of concrete or of corrugate steel become competitive. To compete with this solution, a two-box girder bridge system with narrow width box section was developed. It will be applied to the bridge with a relatively wide width. If we employ a box section with narrower width, thicker flange is requisite, which leads to less number of longitudinal stiffeners mainly used for preventing buckling instability of the steel plate subjected to compressive force. By this means, we can reduce labor cost for fabrication.

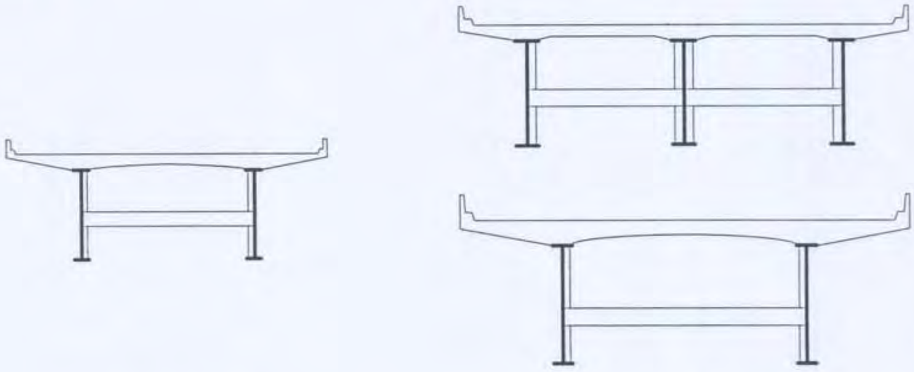

\- 2-lane bridge -   - 3-lane bridge -

Fig. 1. I-girder bridge

This bridge system is also simple. It has a slab, two box girders with thick flange plate and cross beam at supports only. Intermediate cross beams are removed. Figure 2 shows the cross section.

When the bridge width is relatively narrow, for example the bridge with two-lane, a top-opened box girder bridge shown in Figure 3 has been constructed. At the erection stage, since the slab is not installed, the bridge has an open section, hence, safety against lateral torsional buckling instability has to be checked carefully. After casting concrete slab, closed section with high torsional rigidity is obtained. When steel-concrete composite slab is used, if the bottom steel plate in composite slab is attached atop the upper steel flange in advance, high torsional rigidity is ensured, and no possibility of lateral torsional buckling is predicted during construction.

At the present moment, when the span exceeds 60 meters, it has been evaluated that these bridges are less competitive compared to PC box girder bridges.

3.3 Development of competitive steel solutions for longer-span bridge

As explained above, it has been reported, when the span length exceeds 60 meters, that PC box girder bridges, PC box girder bridges with steel corrugated web plate and PC box girder bridges suspended by diagonal cables from relatively lower tower (so called extradosed-type PC bridges) are very competitive (see Figure 4). This evaluation on economics is made by JH, and its judgment has a strong influence on selecting bridge type in Japan. In fact, if the span exceeds 60 meters, we can see many PC bridges in a new highway bridge construction. For example, when the span length is from 60 to 100 meters, PC box girder bridges with web of concrete or of corrugated steel and, when the span length exceeds 100 meters, PC box girder with corrugated steel web, hybrid truss girder (upper and lower chord members are concrete and web member is steel truss) and extradosed PC box girder bridges have been constructed.

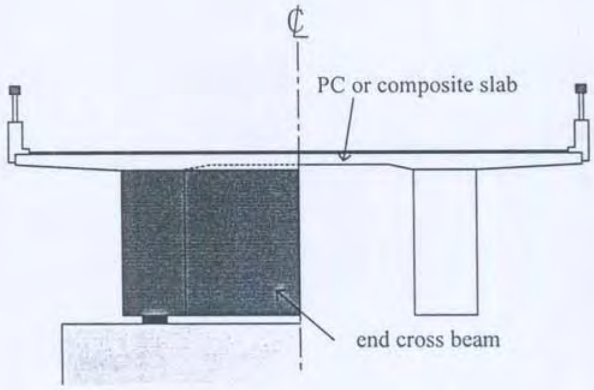

Fig. 2. Two-box girder bridge

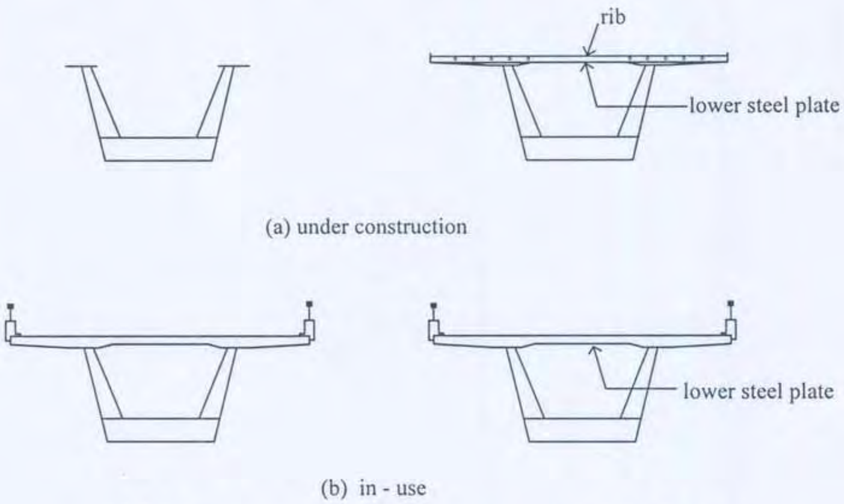

Fig. 3. Top-opened single box girder

A composite truss girder bridge and box girder bridge with steel deck are steel solutions against the above. However, except for the construction site with very bad soil condition, these types have not been realized.

To compete with above PC bridges with a span exceeding 60 meters, the composite two I-girder bridge is recommended, in which lower two steel flanges are connected with concrete slab at intermediate supports. This type of bridge shown in Figure 5 has been called "double composite girder bridges", and a lot of examples can be seen in Germany. However, if elastic design method is adopted, the effectiveness of this type of bridge will not be obtained. Because, at intermediate supports subjected to hogging bending moment, the yield moment of the "double composite type" and "conventional type" will be nearly the same (see Figure 6). In order to utilize this system efficiently, taking into account the fact that buckling instability of compressed thin web plate is prevented by concrete slab, ultimate bending strength should be full plastic moment, which is 30 to 40% higher than yield moment.

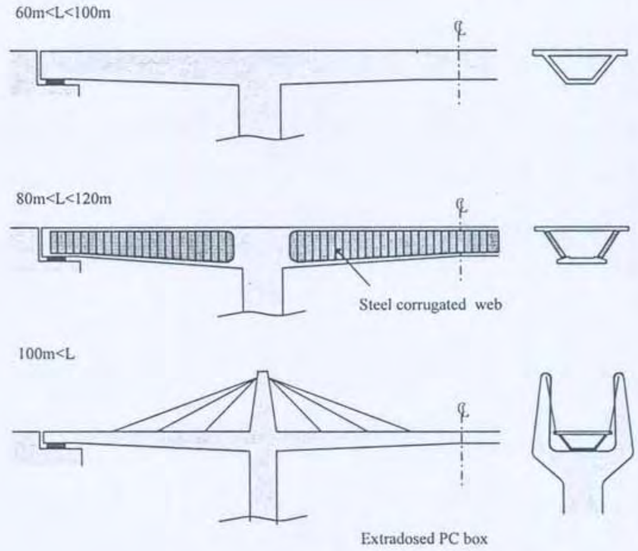

Fig. 4. Competitive PC bridge solutions

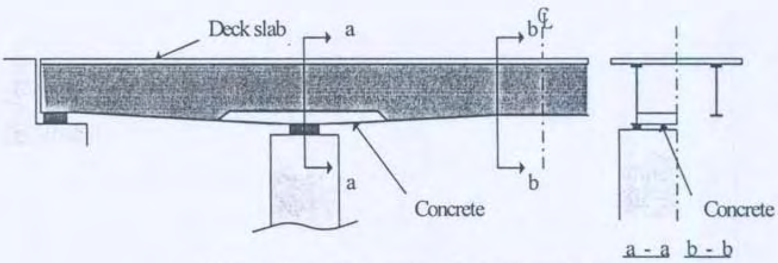

Fig. 5. Double composite girder bridge

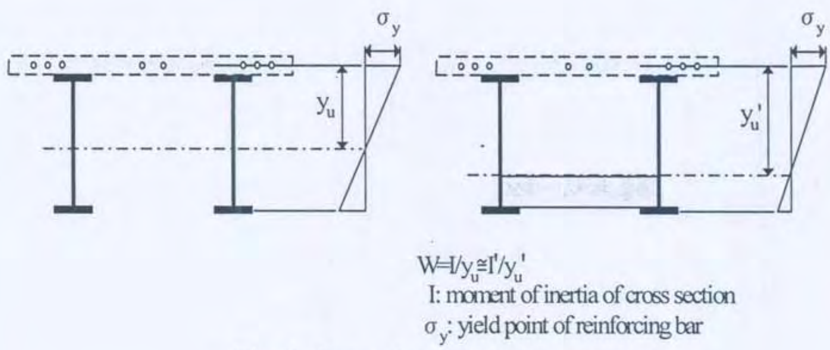

Fig. 6. Comparison of yield moment

Furthermore, since both open and closed sections are used, safety against aerodynamic instability has to be examined. Even though there is a lot of subjects to be resolved, the structural characteristics and economical evaluation of this type of bridge is now under survey by our research group sponsored by the Japan Iron and Steel Federation.

4. Future subjects

The revival of continuous composite bridge together with structural reform from complicated to simple had been carried out from 1995 to 2000 under the leadership of JH. From this research project, economical solutions for the bridge with a span length from 30 to 60 meters has been developed, namely, continuous composite two-I-girder bridge with a simple transverse stiffening system. So far, construction of this type of bridge has been limited to bridges owned by JH. Recently, in spite of the fact that some parts of design procedure violate the provisions stipulated in JHBS for national roadway bridges, the adoption has been gradually increasing. This verifies an economical advantage of this type of bridge.

In my opinion, since a newly developed bridge system is very simple, we will face difficulty in developing further simple bridge system. Hence it is recommended to incorporate design innovation. The followings are design innovations to be considered.

4.1 Thin web with large aspect ratio without horizontal stiffeners

Normally, buckling strength of the web is estimated under the condition that four sides are simply supported. Identification of the degree of rotational constraint obtained from flange plate and vertical stiffeners at four sides of the web is very difficult, so that the simply support condition has been commonly used. However, it is clear, when the composite girder is subjected to sagging bending moment, that fixed condition is expected at the upper side of the web, and enhances the buckling strength of the web. Based on this fact, we can use more slender web compared with web thickness stipulated in JHBS.

We carried out the experimental research[2] and the new web design method[3] was proposed. A maximum aspect ratio is set to be 3.0, which is larger than the maximum aspect ratio of 1.5 stipulated in JHBS. In addition, relatively thin web can be used. For example, in case of the web (yield point = 355MPa) with a height of around 3,000 millimeters and without horizontal stiffeners, JHBS requires a minimum thickness of 23 millimeter. However, we used the thickness of 18 millimeters at the design of actual bridge of JH. This resulted in less steel weight and the reduction of the fabrication cost.

4.2 Evaluation of ultimate strength by 3D finite element analysis

When estimating ultimate strength of the girder or bridge system under bending, shear and combined bending and shear, computer calculation, that is to say, elasto-plastic finite displacement analysis using solid and/or shell element, will give us precise strength. Because, conservative assumptions related to the boundary conditions can be avoided.

Introduction of computer-aided design "Design by Analysis" to the practical design is the future subject to be examined. Precise estimation of ultimate strength will lead to more economical solution.

4.3 Introduction of compact section design

Based on ASD, maximum strength is yield point of the material or buckling strength of the member, which has been stipulated to be less than yield point.

When the composite girder is subjected to sagging bending moment, as has been stipulated in ASSHTO-LRFD[4] and EC[5], if PNA (Plastic Neutral Axis of the composite section) falls in the concrete slab or compressed web height-to-thickness at full plastic moment is less than specified values, plastic moment is expected, and it is around from 30 to 40% larger than the yield moment.

PNA of most of recent composite two I-girder bridges is predicted to fall in the concrete slab. Furthermore, since the relatively high depth of the girder has been used, crash of the concrete slab before reaching plastic moment of the section can be avoided. Hence, introduction of compact section is important.

4.4 Double composite 2-I-girder bridges

The double composite girder bridge was explained. At intermediate supports, when the full plastic moment is expected, the ultimate bending strength will be full plastic bending moment throughout the bridge length. This behavior is also seen at the design of the rolled beam. This makes possible to design the bridge with less steel volume.

5. Codification of design innovation

In order to obtain economical solutions with high durability, which can reduce the construction cost, the structural reform from multi-girder to two-girder system was proposed by JH. The two-I-girder bridge requires relatively thick lower flange plate exceeding 50 millimeters and wide span concrete deck. To meet these requirements, in 2002, JHBS allowed using maximum plate thickness up to 100 millimeters and pre-stressed concrete slab.

The lower lateral bracing members were removed and, instead of cross bracing members and/or large-sized cross beams, small-sized shape-steel cross beams at a distance from 5 to 10 meters were recommended. However, above structural simplifications violate the related regulations stipulated in JHBS.

In the former chapter, innovative design methods leading to further reduction of construction cost were proposed. However, these means also violate the provisions in JHBS. In the next revision, specifications for new structural type and composite structures will be added, and the design by analysis will also be discussed.

6. Concluding remarks

JHBS was introduced, which covers all the national roadway bridges with a span length less than 200 meters in Japan. Revision in 2002 and revision now under consideration were also introduced. In the revised version in 2002, shift to technical standards based on performance was made and new provisions meeting design procedures for newly developed simple structural form were added. The content of revision now under consideration is not clear at this moment. However, the shit from ASD to LSD with partial safety factor format is expected.

Reduction of construction cost is a key factor for promoting public works. To cope with the subjects, JH carried out structural reform from multi-girder to two- or three-girder system depending on the number of vehicle lanes. In addition, continuous composite girder design was revived and very simple transverse stiffening system was also employed. To push the construction of such bridge system, JH established their own design manual, in which several provisions violate JHBS. However, the validity of new design procedures had been confirmed through analytical and experimental researches.

Hence, these provisions should be included in JHBS. Finally, in order to attain further reduction of construction cost, incorporating design innovation explained is recommended and inevitable.

References

1. Japan Road Association (JRA): Specifications for Highway Bridges, 2002 (in Japanese)
2. Ohgaki, K., Kawaguchi, Y., Isoe, A., Takahashi, S., Kawashiri, K. and Nagai, M, "Experimental study on stiffening design method for main girder of composite two plate-girder bridges, " Jour. of Structural Engineering, JSCE, Vol.44A, pp.1229-1239, 1998 (in Japanese)
3. Expressway Technical Center: Design and construction manual for continuous composite two girder bridges with PC slab, 2002 (in Japanese)
4. AASHTO: AASHTO LRFD Bridge design specifications, The third edition, 2004
5. CEN: Eurocode 3: Design of steel structures, Part 1-1: General rules and rules for buildings (prEN 1993-1-1: 2003), 2003

Japan-Bangladesh Joint Seminar on Advances in Bridge Engineering
Dhaka, Bangladesh. 10 August 2005

ISBN: 984-32-2520-6

Analytical study on steel-concrete composite girders

Yoshiaki Okui *

Department of Civil & Environmental Engineering, Saitama University
255 Shimo Okubo, Saitama 338-8570, Japan

Abstract

Analytical study on steel-concrete composite girders is introduced in this contribution. The load-carrying capacity of the composite girders and designing shear connectors are mainly discussed. A finite element model that accounts for partial interaction between a concrete slab and a steel girder in composite beams is introduced. The model takes into account material non-linearity in concrete and steel, and shear-slip behavior in shear connectors as well as geometric non-linearity due to large displacements. It is shown that the model can simulate reasonably well the load-deflection and interfacial slip in composite beams. Parametric studies are carried out on a continuous composite girder bridge to investigate the effect of the shear-slip characteristics of shear connectors. Installing flexible shear connectors near an interior support is effective for reduction of extension strain in a concrete slab, but reduces the load-carrying capacity.

Keywords: composite girder, shear connector, partial interaction

1. Introduction

Recent design codes for continuous composite girders allow tensile cracking in a concrete slab near internal supports due to negative bending. Of course, the crack width must be limited within an allowable level to ensure durability of the concrete slab. An amount of reinforcement in the concrete slab is commonly increased to reduce the crack width. In structural analysis, concrete within the crack region is neglected, and only steel girder and reinforcement in the concrete slab are considered as an effective member. One of the issues in designing continuous composite girder is the functionality as well as a rational design method for shear connectors embedded in the cracked concrete slab. To clarify the function and to establish the design method, it is necessary to consider the effect of relative slip between the concrete slab and steel girder on mechanical behavior of composite girders.

* E-mail: okui@post.saitama-u.ac.jp

Other examples where the slip effects become important are flexible shear connectors and precast concrete slabs. The flexible shear connectors are installed at internal supports in order to reduce tensile stress and accordingly cracking in concrete slab. In composite girder bridges with precast concrete slabs, due to the limit of the spacing for in-situ concrete casting, it is not always possible to accommodate enough studs for full interaction.

In this contribution, a two-dimensional nonlinear finite element program for load-carrying capacity of steel-concrete composite beams with partial interaction has been developed. The program considers geometrical non-linearity due to large displacement and material non-linearity for steel and concrete. In order to take into account partial interaction effects, additional degree of freedoms representing the slip at an interface between the concrete deck and steel girder is introduced.

2. Fiber model for partial interaction

In this section, the proposed finite element model is briefly introduced; see Peckley (1998) and Peckley & Okui (2000) for a detailed formulation. A composite beam is modeled as two fiber beam elements and an interfacial spring, which connects the beam elements. Figure 1 illustrates the modeling a composite beam by means of these beam elements and the interfacial spring as well as definitions of coordinates and symbols for displacements. The upper beam represents the concrete slab, and the lower beam the steel girder. The effect of local buckling in a steel section is neglected in this modeling.

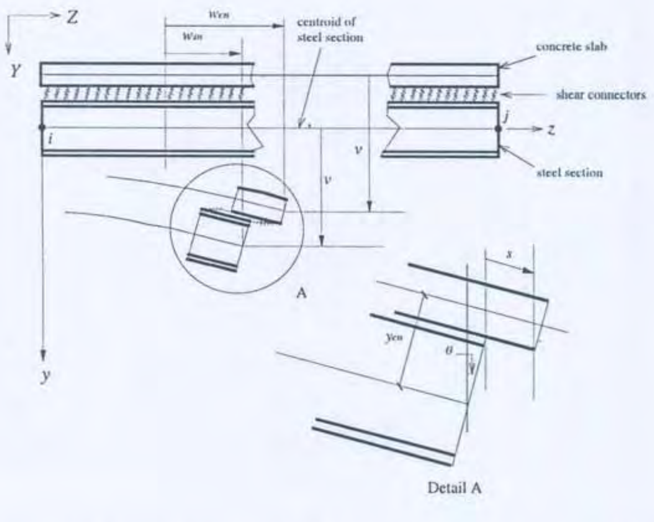

Fig. 1. Composite beam element and definition of coordinates and displacements.

Since the vertical displacements, rotations, and curvatures of these two beams are assumed to be identical, the displacements of both concrete and steel section can be expressed in terms of the axial and transverse displacements at the steel section centroid w_{sn}, v, and slip at the interface s. These displacements in an element are interpolated in terms of the shape function $\mathbf{H}$ and the nodal displacements:

$$w_{sn} = \mathbf{Hw}, \quad v = \mathbf{Hv}, \quad s = \mathbf{Hs} \tag{1}$$

where $\mathbf{w} = \{w_i, w'_i, w_j, w'_j\}^T, \mathbf{v} = \{v_i, \theta_i, v_j, \theta_j\}^T, \mathbf{s} = \{s_i, s'_i, s_j, s'_j\}^T$ and the prime stands for differentiation with respect to z; the Hermite function is employed as a shape function:

$$\begin{aligned} \mathbf{H} = [&1 - 3(z/l)^2 + 2(z/l)^3, 1 - 2z^2/l + z^3/l^2, \\ &3(z/l)^2 - 2(z/l)^3, z^2/l + z^3/l^2] \end{aligned} \tag{2}$$

where l = the length of an element.

Furthermore, fiber beam elements are employed for modeling the concrete slab and the steel girder to account for material nonlinearity. In each beam element, cross sections are considered to consist of thin steel or concrete layers subject to a different stress as shown in Fig. 2. The tangential stiffness of the beam element is evaluated in accordance with the tangential Young's modulus of the nonlinear stress-strain relation

The element stiffness matrix is evaluated by using the finite element method and the nonlinear strain-displacement equation including the finite displacement effect. An updated Lagrangian formulation is employed. The tangent stiffness matrix is obtained by integrating over the volume of an element including nonlinear stress-strain relations for steel and concrete, and slip-shear force relation at the interface. In the current formulation, effects of shear stress on the nonlinear stress-strain relations are neglected, and a simple fiber model with a uniaxial stress-strain relation is employed.

Finally, we have an incremental equilibrium equation for the nodal displacement and applied force:

$$[\mathbf{K} + \mathbf{K}_G]\Delta\mathbf{u} = \Delta\mathbf{P} \tag{3}$$

where $\Delta\mathbf{u} = \{\Delta\mathbf{w}, \Delta\mathbf{v}, \Delta\mathbf{s}\}^T$ and $\mathbf{K}$ = the tangential stiffness matrix due to material nonlinearity, $\mathbf{K}_G$ = the geometric stiffness matrix. Eq. (3) is solved for displacement increment $\Delta\mathbf{u}$ in an iterative manner until the unbalanced forces are within allowable tolerance.

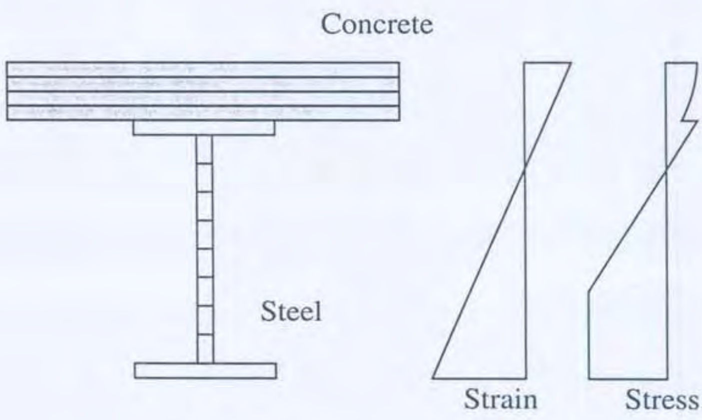

Fig. 2 Fiber beam element

3. Comparison with experimeant

To check the proposed model and program, comparison has been made with the test data reported by Nakajima & Ikegawa (1996). Figure 3(a) illustrates the experimental set up, and Fig. 3(b) shows the cross section of a specimen. This test specimen is designed to behave as a girder with partial interaction. The relative slip between the concrete slab and the steel girder on the shorter shear span is measured with clip-type gages. In addition, Nakajima & Ikegawa (1996) carried out push out tests of the same studs as the load-carrying test shown in Fig. 3. The reported slip-shear curve is used in the numerical analysis.

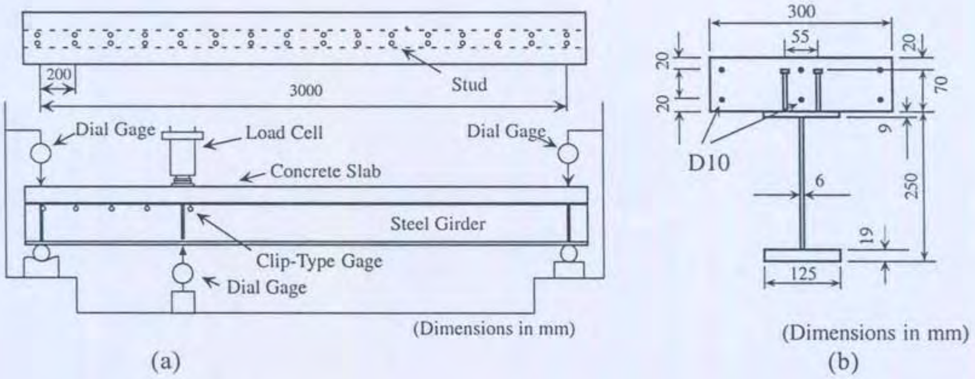

Fig. 3. (a)Test set-up; (b) Cross section of specimen from Nakajima et al. (1996).

Figure 4 shows the comparison of the load-deflection curves, and Fig. 5 is that of the load-slip curve. In both load-displacement and load-slip behavior, the numerical results are in good agreement with experiment ones.

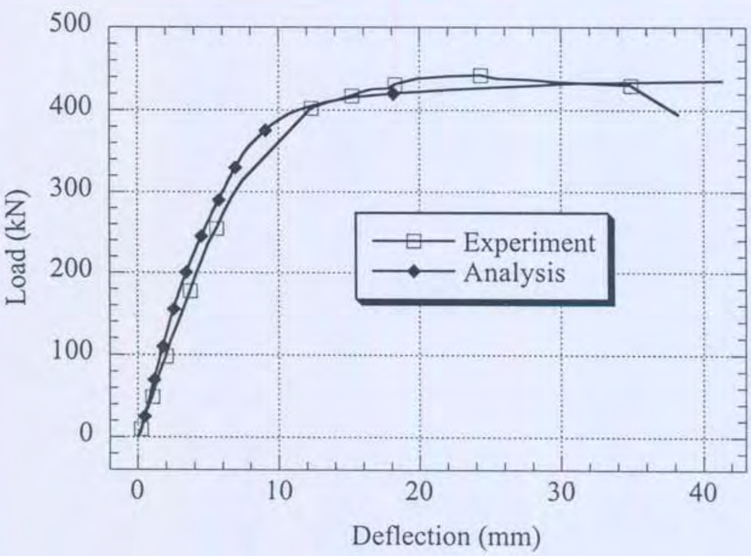

Fig. 4. Load-deflection curves.

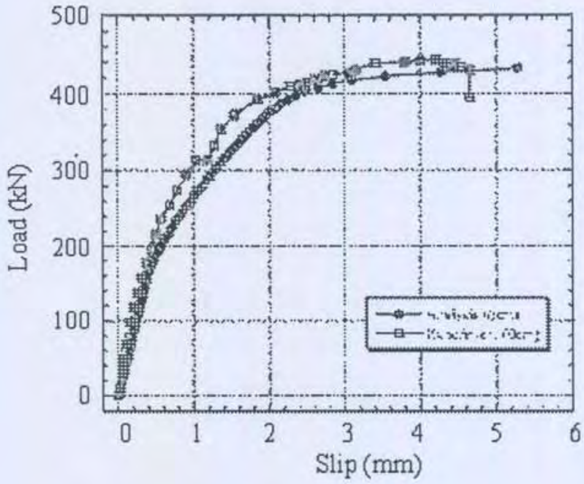

Fig. 5. Load-slip curves.

4. Parametric study for continuous bridge model

4.1 Structural model

In this section, we apply the proposed analytical method to the two-span continuous composite bridge shown in Fig. 6 (Japan Association of Steel Bridge Construction, 1995). The cross section of the model is shown in Fig. 7. The dimensions and yield stresses of the flange and web plates of the steel section are listed in Table 1. In designing this model bridge, cracking of the concrete slab near the internal support is assumed.

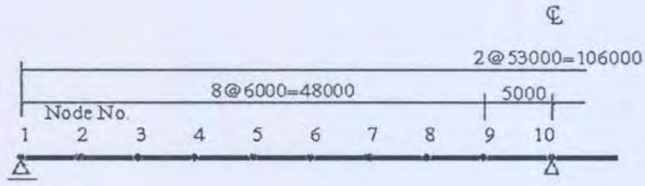

Fig. 6. Two-span continuous composite girder model (53+53 m) and dimensions of the steel girder (unit: mm).

For the stress-strain relation of steel, the simple elastic-perfectly-plastic model is used, while for concrete a parabolic-linear model (Fig. 8) is implemented in the program. The parabolic-linear model is given as

$$\sigma = \begin{cases} \sigma_{cm}\left[\dfrac{2\varepsilon}{\varepsilon_{cm}} - \left(\dfrac{\varepsilon}{\varepsilon_{cm}}\right)^2\right] & \text{for } (0 < \varepsilon < \varepsilon_{cm}) \\ \sigma_{cm}\left[1 - \dfrac{\varepsilon - \varepsilon_{cm}}{\varepsilon_{cu} - \varepsilon_{cm}}\right] & \text{for } (\varepsilon_{cm} < \varepsilon < \varepsilon_{cu}) \end{cases} \quad (4)$$

where the concrete strength σ_{cm}=35 MPa is used in the following analysis.

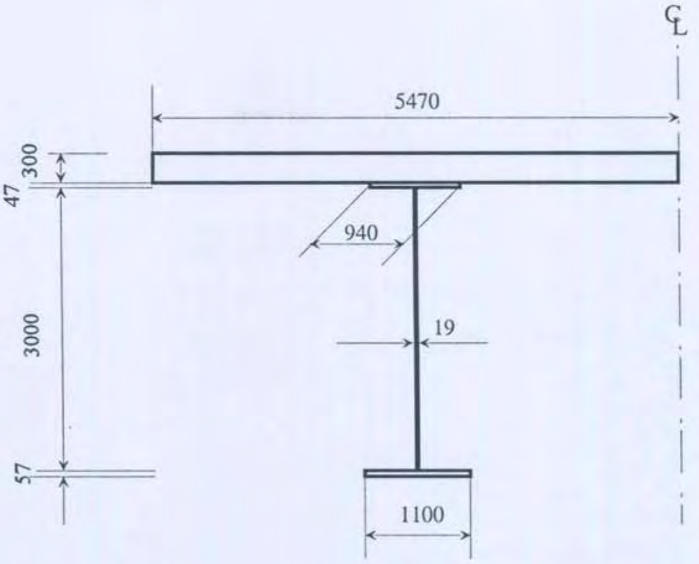

Fig. 7. Cross section near the interior support.

Table 1. Dimensions and yield stress of upper and lower flange plates

Position node-node	flanges			web	
	upper mm	lower mm	yield stress MPa	thickness mm	yield stress MPa
1-2	430x22	640x40	215	13	215
2-3	430x22	650x43	325	13	325
3-4	430x28	760x45	325	12	325
4-5	430x28	760x45	325	12	325
5-6	430x28	760x45	325	12	325
6-7	350x18	580x40	325	12	325
7-8	371x18	880x46	325	13	325
8-9	640x33	910x47	420	17	420
9-10	940x47	1100x57	420	19	420

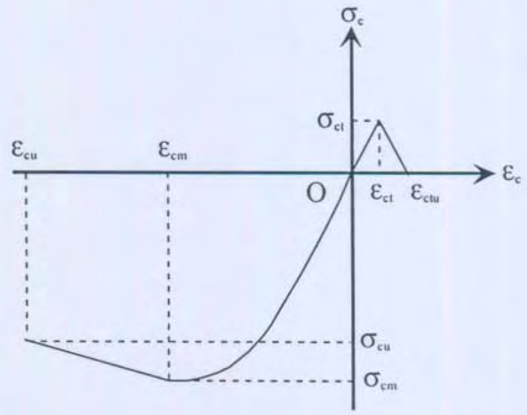

Fig. 8. Stress-Strain relation of concrete in compression.

Note that Eq. (4) is only valid in compression. The concrete in tension is neglected, but reinforcement steel in the RC slab is accounted as effective structural members. The tension stiffening effect in cracked RC members is also neglected in this treatment of concrete. The cross-sectional area ratio of reinforcement to the RC section is assigned to 1.5% in a negative bending region.

4.2 Shear connector

Two types of shear connectors are considered, namely conventional stud type connectors and a flexible shear connector proposed by Abe et al. (1989). The flexible shear connector is made of W-shapes (called H-shapes in Japan), whose web plate is covered with expanded polystyrene to enhance flexibility when it is embedded in a concrete slab. This flexible shear connector is specially designed to reduce tensile stress in the concrete slab near interior supports in continuous composite bridges. The flexible shear connectors have been installed in a railway bridge (Okuda et al., 1990).

The shear-slip relationships of these shear connectors are shown in Fig. 9, which is based on the push-out test results reported by Hosaka et al. (1998). Since it is seen that the tangential stiffness of the flexible shear connector after yielding is smaller than that of the shear studs, the flexible shear connector is more effective after the first yielding. Two cases for arrangement of shear connector are considered in the numerical analysis.

Figure 10 shows the distribution and types of shear connectors for both cases. In Case A, stud type connectors are used, and the pitch of shear studs is determined based on an elastic analysis following Japanese "Specification for Highway Bridges" (1992). On the other hand, in Case B, the flexible shear connectors are installed in the negative bending moment region near the interior support, and their pitch is determined according to that of slab anchors in non-composite bridges.

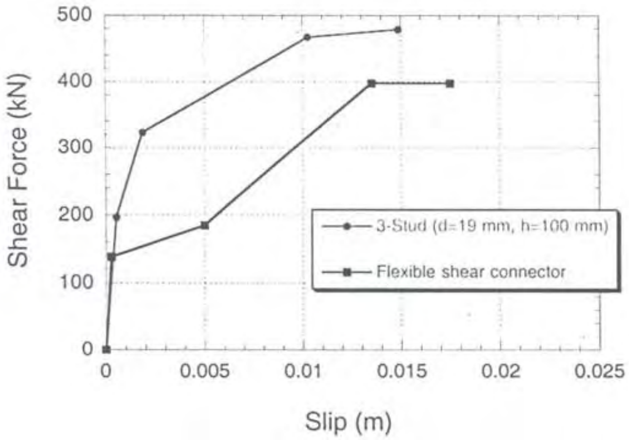

Fig. 9. Shear force-slip relationships of studs and flexible shear connector.

4.3 Load cases

In the following numerical analysis, the unshored construction is assumed. The dead load corresponding weight of steel girder and concrete (D_1=69.3 kN/m) is applied to the steel girder only, and then the superimposed dead load (D_2=13.7 kN/m) and the live load is applied to the composite section. In the following, the magnitude of the load is expressed in terms of the load factor α. The total load TL is given as

$$TL = \alpha(D + L) \quad (6)$$

where $D = D_1 + D_2$ = Dead load, and L = Live load. Figure 11 shows considered loading cases in the numerical analysis. The intensity of the live and dead loads are 13.7 and 83.0 kN/m, respectively.

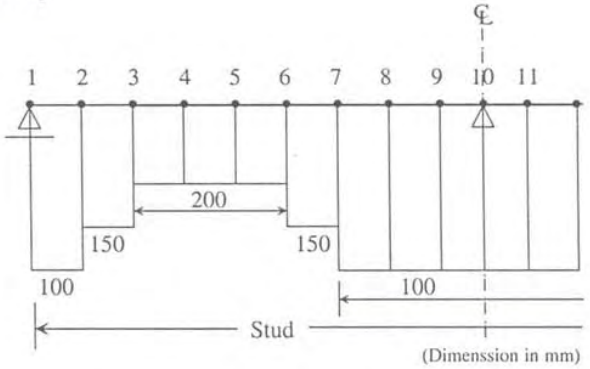

Fig. 10. Distribution of stud pitches and shear connector type; (a) Case A. (continue)

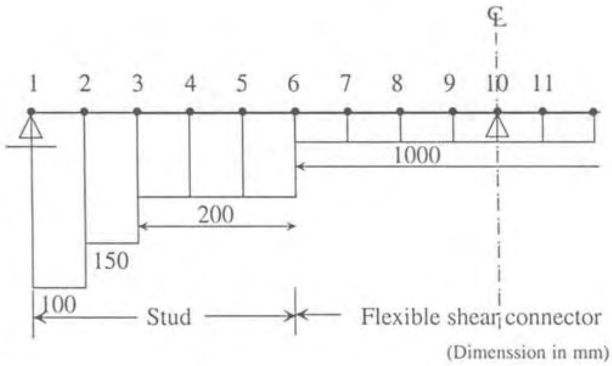

Fig. 10. Distribution of stud pitches and shear connector type; (b) Case B.

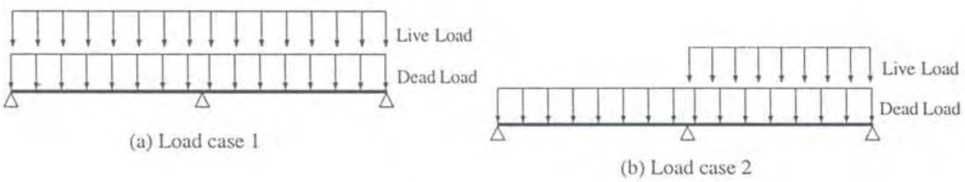

Fig. 11. Load cases; Dead and live load combination.

4.4 *Effect of shear connector*

Figures 12 shows the load-displacement curves for Load Case 1 and 2. The "Stud Case 1" stands for the original arrangement of studs defined in Fig. 10(a). The "Stud Case 2" and "Stud Case 3", etc. mean 2 times and 3 times stud pitch of "Stud Case 1", respectively. In these figures, open circles and squares denote the ultimate points in the corresponding load-displacement curve. The circles express failure due to concrete crushing, while the squares due to failure of shear connector. By reducing shear connector, the failure mode changes from concrete crushing to failure of shear connector.

The distributions of the relative slip along the bridge length at the maximum loading states are shown in Figs. 13 and 14 for Load Case 1 and 2, respectively. In the "Stud Case 1", the maximum slip for both cases are less than 0.005 mm, and the "Stud Case 1", in which studs arrangement is designed on the basis of the current Japanese Specification for Highway Bridges, is almost full interaction behavior. Even though the studs pitch is increased to twice of Case 1, the ultimate load-carrying capacity is governed by the concrete crushing and accordingly this situation is classified into full shear connection.

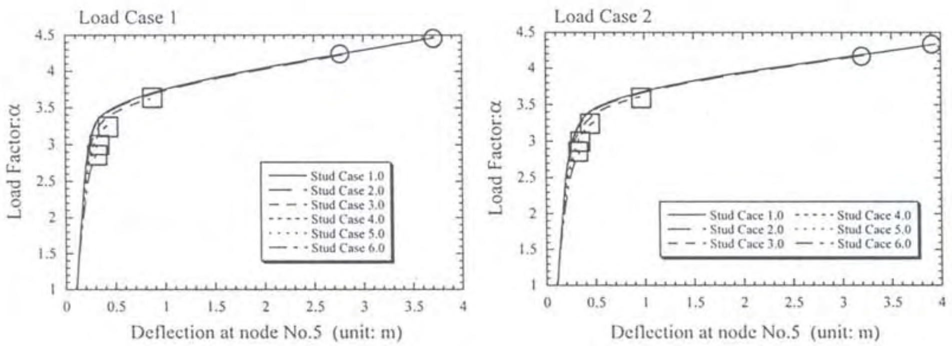

Fig. 12. Load-deflection curve for Load Case 1and 2.

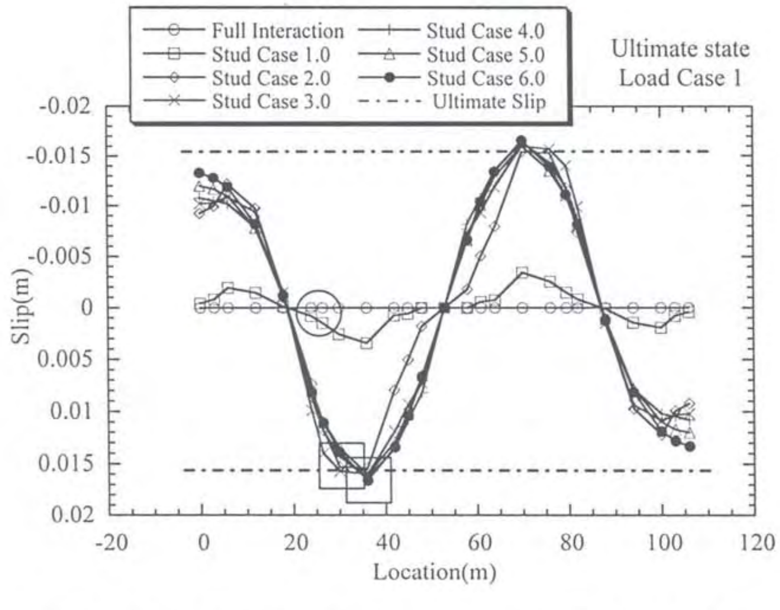

Fig. 13. Slip distribution along bridge at maximum loading for Load Case 1.

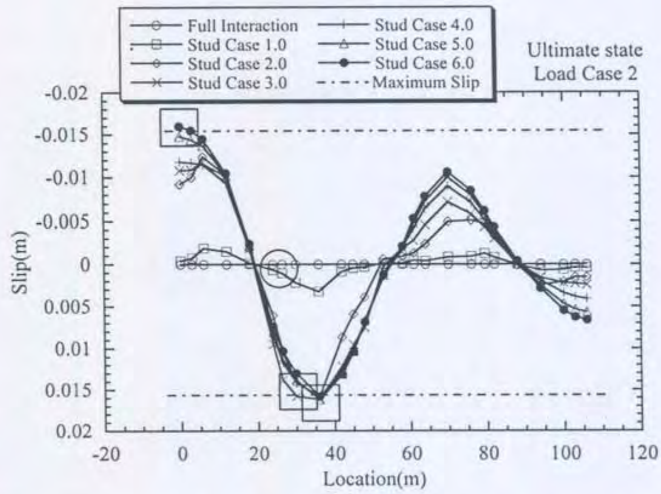

Fig. 14. Slip distribution along bridge at maximum loading for Load Case 2.

4.5 Flexible shear connector

Fig. 15 shows the bending moment diagram of both shear-connector cases at a service load of $D+L$. For these two cases, the difference of the maximum negative bending moments at the interior support is only 4%. Under service level loading, the reduction of negative bending moment at interior supports is not expected in spite of installing the flexible shear connector. However, it can be said that the increase in the maximum positive bending moment by installing the flexible shear connector is negligibly small as well.

To ensure durability of continuous composite bridges, it is important to control tensile cracks in a concrete slab owing to the negative bending moment. One objective for installing the flexible shear connector is to reduce crack width in a concrete slab. To check this aspect, the normal strain variations in the composite section at the interior support are plotted in Fig. 16, where the vertical axis stands for the vertical distance from the top of a concrete slab. In the shear-connector Case A, there is a slight strain jump at the interface between the concrete slab and steel girder. However, the behavior in Case A is practically full-interaction behavior. On the other hand, in Case B (flexible shear connector case) a considerable strain jump due to the slip occurs at the interface. Furthermore, the maximum strain in the concrete slab is reduced to 40 % of the strain in Case A. It is shown that the flexible shear connector is effective to reduce tensile strain, and accordingly tensile crack width in concrete slab.

5. Summary

In this contribution, a finite element model for load-carrying capacity of composite beams with partial interaction was introduced. The proposed model was applied to a two-span continuous composite bridge with two types of shear connectors. The numerical analysis shows that:

1. By installing flexible shear connectors, the load carrying capacity is decreased.
2. However, tensile strain at the internal support decreases, which is preferable from a crack-width control point of view.

3. The bending moment distribution at the service load level is not significantly affected by the flexible shear connector.

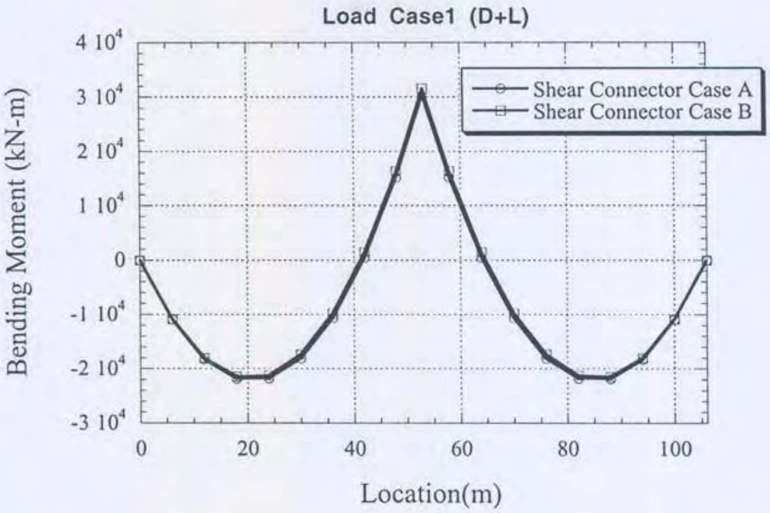

Fig. 15. Bending moment diagram for Load Case 1 at a service load level: Effect of shear connector cases on bending moment.

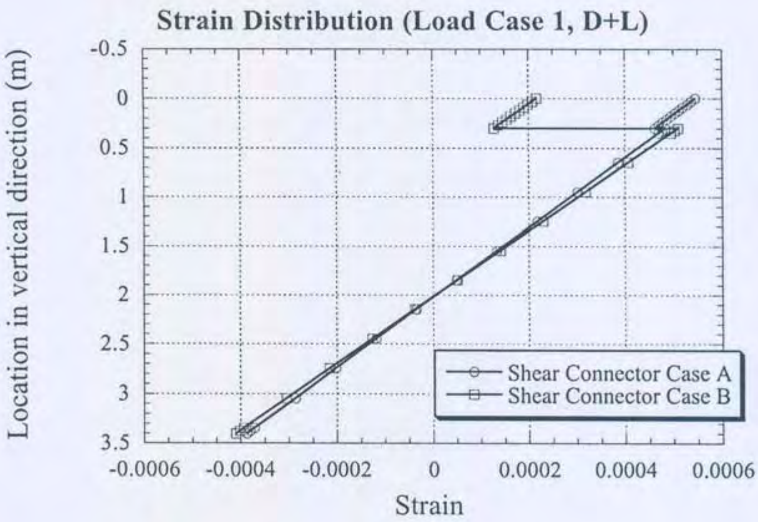

Fig. 16. Normal strain distribution in a plane at the interior support (profile view) for Load Case 1 at the service load.

References

Abe, H., Nakajima, A. & Horiuchi H., 1989. Effect of division of slab in composite girder and development of flexible connectors, *J. Structural Eng., JSCE*. 35A:1205-1214. (in Japanese)

CEN, 1996. EUROCODE4: Design of composite steel and concrete structures, Part 2: Bridge, 2nd draft.

Hosaka, T., Hiragi, H., Korda, Y., Tachibana, Y. & Watanabe, H. 1998. An experimental study on characteristics of shear connectors in composite continuous girder for railway bridges, *J. Structural Eng., JSCE*. 44A:1497-1504. (in Japanese)

Japan Road Association (JRA) 1992. Specification for high way bridges. Tokyo: Maruzen. (in Japanese)

Japan Association of Steel Bridge Construction (JASBC) 1995, Report on design of continuous composite bridges. (in Japanese)

Nakajima, A & Ikegawa, M. 1996. Elasto-plastic analysis of composite girder with inelastic behavior of shear connectors, *J. of Structural Mechanics & Earthquake Engineering, JSCE.* 43(591):97-106. (in Japanese)

Okuda, M., Satou, T., Yamaki, Y., Iseki, J. & Sasaki, H. 1990. Design and construction of Tokeidou3.4.20 viaduct in Hokusou line, *Bridge & Foundation.* 12: 13-22. (in Japanese)

Peckley Jr., D.C. 1998. Nonlinear analysis and ultimate strength of composite beams with partial interaction, Master thesis, Saitama University.

Peckley Jr., D.C & Okui, Y. 2000. A finite element model of steel-concrete composite beams and girders for near-collapse analysis, *Proc. Int. Conf. Concrete Art, Science and Technology, CAST2000, Manila*: Theme E: 1-17.

Okui Y., Seki K., Peckley D.C. 2001. Nonlinear analysis of load-carrying capacity for composite beams with partial interaction,., Proc. 1st Int. Structural Engineering and Construction Conf., pp.963-968.

Japan-Bangladesh Joint Seminar on Advances in Bridge Engineering
Dhaka, Bangladesh. 10 August 2005 ISBN: 984-32-2520-6

Scope of application of composite materials in bridge construction from Bangladesh perspective

M.A. Sobhan*

Design Planning & Management Consultants Limited
House 4/1, Road 4, Dhanmondi R/A, Dhaka 1205, Bangladesh

Abstract

The paper after giving a brief review of the current practices of composite bridge construction in the country, discusses on the scope of using the new materials e.g. GFRP, CFRP, AFRP, etc. side by side with the traditional materials e.g. concrete, steel, etc. It then discusses how the innovative structural concept including hybrid forms using the composite high strength but light weight material may enable to construct elegant medium to long span bridges. Further, the country needs to avoid close spacing piers in its river crossing structures from consideration of the river hydraulics and the morphology. Thereafter, the scope of using these new materials in strengthening, repair & rehabilitation of bridge decks, girders, railings, and pier columns is discussed. The initial cost might be high but the whole life cost considering the indirect benefit of aesthetics, and environmental friendliness might justify its use. The essential R&D needs are highlighted in the end.

Abbreviations

AFRP	-	Aramit fiber reinforced polymer
BWDB	-	Bangladesh Water Development Board
CFRP	-	Carbon fiber reinforced polymer
CRC	-	Compact reinforced composite
FRP	-	Fiber reinforced polymer
GFRP	-	Glass fiber reinforced polymer
HPC	-	High performance concrete
IABSE	-	International Association of Bridge and Structural Engineering
LGED	-	Local Government Engineering Department
PC	-	Prestressed concrete
RC	-	Reinforced concrete
R&D	-	Research & development
RHD	-	Roads & Highways Department
RPC	-	Reactive Powder Concrete
f_c'	-	28 days compressive strength in cylinder
MPa	-	Mega Pascal

* E-mail: mas@dpm.com.bd

1. Introduction

In the bridge structures of Bangladesh, composite construction is related to its superstructure only. It's in the following form: cast-in-situ RC deck shear-connected to the steel or precast RC/PC girders or steel trusses. A few of the composite steel truss and concrete deck bridges are: 133 m Lamakagazi Bridge on Sylhet-Sunamganj Road, Sherpur Bridge on Sylhet-Dhaka Highway. Recently one arch bridge has been constructed across Crescent lake connecting ZIA Musoleum in the Dhaka Metropolitan city, using Glass block panels as deck.

Besides, several long continuous span PC box girder bridges have been constructed in the country namely, Meghna and Meghna Gumti Japan Bangladesh Friendship Bridges, Jamuna Multi-purpose Bridge, Bhairab Bridge, Pakshi Bridge and Gabkhan Bridge. Segmental free cantilever method of construction using traditional materials e.g. concrete, high yield reinforcing bars, high strength prestressing steel, etc. were used for these bridges. These are modern bridges but can't be categorised as composite bridges.

Further, plenty of the country's permanent bridges are located on the rural roads, which are constructed by LGED. Most of these bridges are traditional RC deck girder bridges, and some are PC girder bridges. The construction uses cast-in-situ deck shear-connected to the precast PC girders. These are also categorised under composite construction as noted earlier.

The traditional material and the structural forms are being used beneficially in the country's bridge construction. It's necessary now to examine whether new materials and concepts can modernise our bridge construction technology further.

The subsequent sections discuss on this aspect of bridge engineering.

2. What are the new/composite materials?

2.1 General

Nowadays different types of FRPs e.g. GFRP, CFRP, AFRP, etc. are being used as engineering materials. In Bangladesh some of these materials are being used in boating industry for example, in making speed boats; in furniture industries, in wrapping gas pipes, etc. and there is one example of retrofitting building structure using poly-carbon fibre. Globally in bridge engineering these materials are used in deck slabs, girders, and in repair and rehabilitation of structures.

The traditional concrete used in the country is in the strength range $f_c' = 18 \sim 35$ MPa. The recently developed HPC may be of very high strength say, $f_c' > 80$ MPa. Other types of fibre concrete also have been developed having $f_c' > 200$ MPa. In addition to compressive strength their direct and flexural tensile strength are also be very high. This type of concrete may also be categorised in the new material group.

2.2 FRPs

FRP elements are normally made of both metallic and non-metallic fibers. The FRPs made by using glass, carbon and aramid fibers impregnated in polymer matrices e.g. polyester, epoxy, etc. are called GFRP, CFRP, and AFRP respectively. The FRPs impregnated in cement matrix is called FRP reinforced concrete. This may contain short fibers, textile or bar reinforcement or may even be prestressed.

The non-metallic FRPs impregnated in polymer matrices are used for making tension elements e.g. strips, straps, bars, cables, sheets, shell elements, etc.; and also stiff elements e.g. profiles, sandwiches, sensors, etc.. The profiles may be of innumerable shapes e.g. U-sections, box sections, I-sections. At present different manufacturers make shapes of the profiles identical to the standard steel sections. Some of the tension elements mentioned above are popularly used for repair and strengthening of columns, beams, and deck slab. The hybrid structures and all-composite new structures may be designed using both the tension and stiff elements.

Two types of polymers are available namely, thermoset and thermoplastics. Currently thermosets are mostly used. For thermosets after hardening or polymerization reaction, their shapes cannot be changed, and these cannot be welded also. But thermoplastics have advantages of easily moulding into different shapes, and it's also easy for bonding together. This is making it increasingly popular. The commonly used thermosets are unsaturated polyester (UP resins), vinylester (VE resins), and epoxy resins (EP resins). The tensile strength of UP and EP resins ranges from 20-70 MPa and 60-80 MPa respectively [1].

The patented strand cables, anchorages, shear plates, etc. are also available now from different manufacturers. Exhibit-1 shows the available forms of reinforcing fibers [1].

2.3 RPC

This reactive powder concrete (RPC) has been newly developed in Korea. This is formed of HPC, reinforced with steel fibers, and it allows to build slender long span bridge structures of high durability. This concrete minimises micro cracks and pore spaces in concrete. A typical composition for 200 MPa concrete as given in RPC200 is as follows: Using the mix composition having fiber 200 μm 161 kg/m^3, fine sand 310 μm 1066 kg/m^3, cement 10 μm 746 kg/m^3, quartz powder 12 μm 224 kg/m^3, super plasticizer 9 kg/m^3, and water 142 kg/m^3 the manufacturer obtained the compressive strength of the mix 170 – 230 MPa, flexural strength 30 – 60 MPa, Young's Modulus 50 -60 GPa [2].

In Seoul, Korea the symbolic new millennium structure the Sun-Yu Pedestrian Arch Bridge crossing Han River has been constructed using this RPC. The main arch span of the bridge is 120 m long. The bridge has been opened in May 1995). Exhibit-2 shows the overview of the bridge [2].

2.4 CRC

Chalmers University of Technology, Sweden has developed this high performance concrete CRC [3]. The goal was to design a joint which will make the surrounding concrete continuous. It's a silica-fume-based concrete, formed by fine and ultra fine particles in combination with steel fiber reinforcement. Its water/binder ratio is about 0.16 and the silica fume content is 20-25%. Quartz sand with particle diameters up to 4 mm is used as aggregates. Its characteristic compressive strength at 28 days is normally about 150 MPa. The fiber content is normally about 6% by volume or more than 450 kg per m^3 of joint concrete. This compound is used in moment stiff joints between precast modules.

Exhibit - 3 shows the moment stiff high performance joints for prefabricated RC deck panels made of CRC side by side with the conventional joint [3].

3. One example of an all-composite GFRP bridge

This is located at about 2 km from the city of Leida in Spain. This cable suspended bridge crosses a roadway, and a railway line. Another new high speed railway line connecting Madrid and Barcelona will be added in near future. The footbridge has been opened in October 2001. Exhibit -4 shows the bridge overview and details[4].

The double-tied arch of 38 m span length with a rise of 6.2 m was selected as the structural form of this 3 m wide footbridge. This dimension was selected to suit the properties of the GFRP profiles. The arch configuration minimised the serviceability problems likely to be arisen due to the low modulus of elasticity (E=23-27 GPa) of the profiles. The total weight of the bridge was only 19 metric ton. All of the profiles were made of E-glass fibers and woven and complex mats with a minimum glass fiber content of 50%. The tensile or compressive strength of the profiles in the longitudinal direction was 240 MPa and in the transverse direction 50 to 70 MPa. Both arches and the tied longitudinal members were rectangular hollow sections of two U300 x 90 x 15 mm profiles joined with glued flat plates of 180 x 12 mm (Ref. Exhibit – 4).

GFRP pultruded profiles used in the deck panel of this 38 m long bridge has the advantages that it has no magnetic interaction with the adjacent electrified railway line, it has minimum maintenance cost and it's easy to build [2]

4. Strengthening of structures

In the tropical humid climate of Bangladesh concrete deteriorates faster particularly in the cover zone. This is truer particularly when the concrete isn't dense. For strengthening of deck slab and even for new deck, the light weight GFRP panels are beneficial.

Fiber Composites e.g. FRP plates and fabrics are used for strengthening RC columns, beams, masonry walls, etc. They can be formed in place to any complicated shapes. They are significantly lighter than steel plates of equivalent strength; it doesn't need temporary support for the plates while the adhesive gains strength. They are stronger than steel and so they can be applied in much thinner sections, which can be fitted in curved sections.

Exhibit – 5 shows wrapping fabrics winding around columns for its strengthening. This may be used for rehabilitation of the columns also [1].

5. Use of GFRP panels in temporary structures

The light weight GFRP panels may be used as a permanent or temporary/removable formwork for constructing deck slab of bridges. Photo 1 shows the photograph of the under construction Hazrat Shah Paran Bridge. The photograph shows the precast concrete slab which was used by the contractor as temporary shutter of the deck concrete, supported over the adjacent precast PC girder flange. The light weight GFRP panels would have been more appropriate for this purpose.

Photo 1. Under construction Sylhet Shah Paran Bridge showing precast deck forms

6. Making of FRP products

The FRP products are made mainly by pultrusion process as shown in Exhibit – 6. The VARTM technique using vacuum pumps for intake of resins are also used. Besides, hand laminated technique is also used. For example, some of the FRP manufacturers located at Pagla, Dhaka producing FRP products for boating industries. .

7. R&D need

R&D is needed on two issues namely, on the behaviour of the composite material e.g. FRPs, artificial concretes, etc., and their products; and concept R&D to develop the areas and the structural forms where these can be beneficially used.

FRP products are susceptible to deterioration when exposed to the ultra violet (UV) rays. R&D should be done on the climatic conditions including the sun shine prevalent in Bangladesh. Research is needed to develop the design and construction guidelines on achieving adequate ductility of the FRP structures against wind and earthquake loading given in BNBC'93.

The R&D may include pilot structures using the FRP products, where its deformational behaviour against sustained and environmental loading may be monitored by readings from sensors. In FRP structures particularly using thermoplastics, installing FRP sensors made of optical fibers is easy.

9. Conclusions

The use of FRP in composite bridges is till now in the infant stage. In 2002 only 36 bridge structures were constructed using the FRP panels [1]. In 2005 about 175 vehicular bridges and 160 pedestrian bridges have been constructed using FRPs [5].

The composite construction using traditional and new materials along with the hybrid construction, if found feasible by further R&D on our environmental conditions, and if found cost effective will be immensely beneficial. FRP being high strength but lighter material its use in the medium and long span bridges should be advantageous. Besides it needs less maintenance.

For structural strengthening particularly of the bridge deck this appears to be efficient and time saver as regards construction/erection time. For deck construction its use as deck form, permanent or temporary, should be tried. Use of GFRP as deck form appears to be a feasible option both from practical and economic consideration.

The country's both public and private sectors are weak in R&D. The country's research organizations always lack adequate funds, and also lack initiative. Appropriate measures should be taken to develop the R&D sector in this regard. Also manufacturer and material independent standards and guidelines will be necessary.

This R&D should be done in the country's research laboratories. HBRI's scope may be extended to conduct this R&D. It may be done developing the partnership with the academic institutions and the private sectors.

References

[1] Thomas Keller, Use of Fiber Reinforced Polymers in Bridge Construction, Structural Engineering Documents Nr 7, IABSE-AIPC-IVBH, 2003.

[2] Sun-Bum Huh & Yoon-Joo Byun, Sun-Yu Pedestrian Arch Bridge, Seoul, Korea, Structural Engineering International, IABSE, SEI Vol. 15, Nr 1, February 2005, pp. 324.

[3] Peter Harryson, High Performance Joints for Concrete Bridge Applications, Structural Engineering International, IABSE, SEI Vol. 13, Nr 1, February 2002, pp. 69-75.

[4] Juan A. Sabrino, M Dolores G. Pulido, Towards Advanced Composite Material Footbridges, Structural Engineering International, IABSE, SEI Vol. 12, Nr 2, May 2002, Pg. 84-86.

[5] Sara Black, How are Composite Bridges Performing?, December 2003, High Performance Composites Source Book 2005, Internet

Appendices

Exhibits 1-6

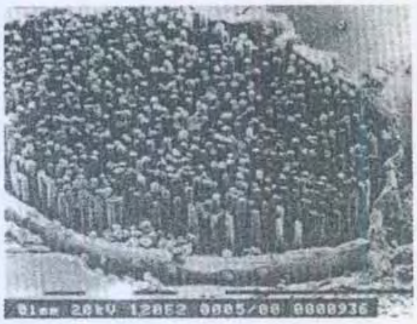

Exhibit - 1a Roving

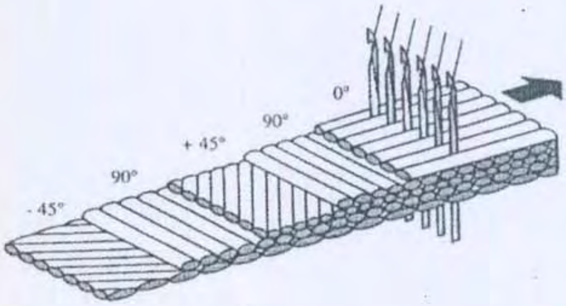

Exhibit - 1b .Multiaxial non-woven fabric

Exhibit - 1c Hybrid fabric of carbon and aramid fibers

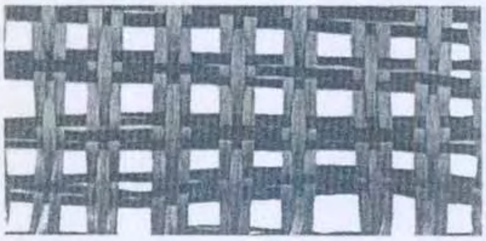

Exhibit – 1d Grid fabric

Exhibit – 1e Mat of continuous fabric

Exhibit – 1f Fleece of chopped glass

Exhibit – 1. FRP fibre elements

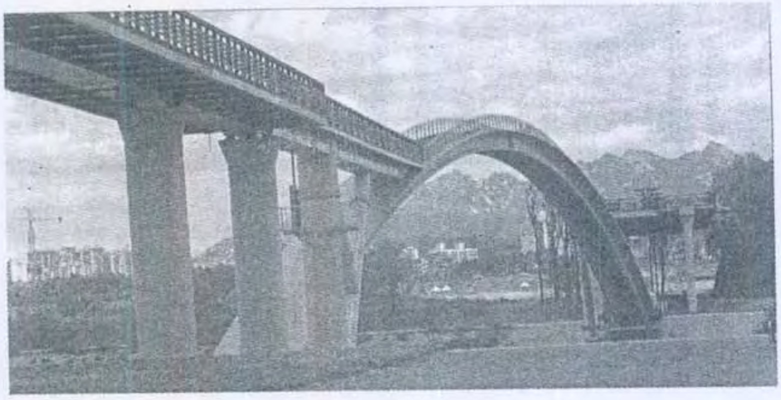

Exhibit – 2. Sun-Yu pedestrian arch bridge, Seoul, Korea [2]

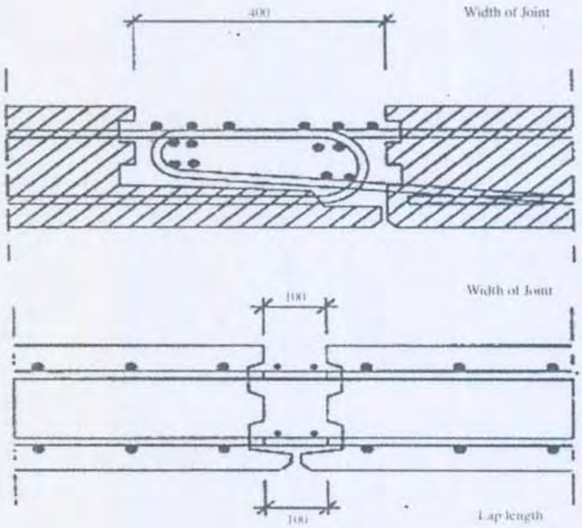

Exhibit – 3. Conventional joint (top) and the CRC filled joint (bottom) [3]

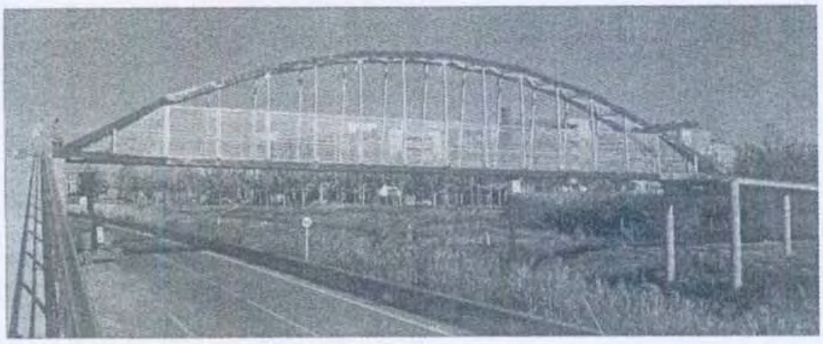

Exhibit – 4a General view of the GFRP footbridge, Leida, Spain

Exhibit – 4b Floor system Exhibit – 4c GFRP profile

Exhibit – 4. GFRP Bridge at Leida, Spain

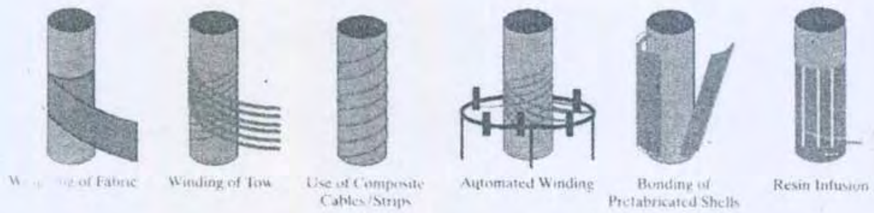

Exhibit – 5. Wrapping fabrics [1]

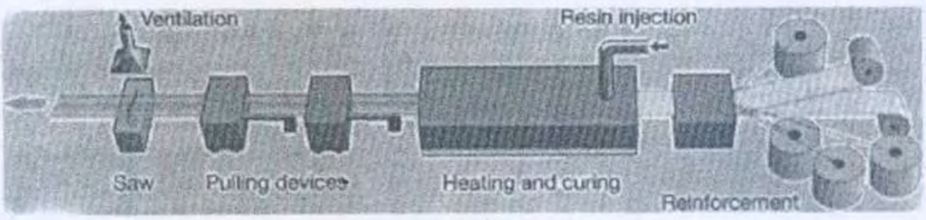

Exhibit – 6. Pultrusion process for making FRP products

Japan-Bangladesh Joint Seminar on Advances in Bridge Engineering
Dhaka, Bangladesh. 10 August 2005

ISBN: 984-32-2520-6

Geotechnical problems of bridge construction in Bangladesh

A.M.M. Safiullah*

Department of Civil Engineering
Bangladesh University of Engineering and Technology, Dhaka 1000, Bangladesh.

Abstract

The paper deals with various foundations used in Bangladesh for river crossing bridge structures. Some of the problems of construction and design of these foundations are highlighted. Because of the fact that most alluvial deposits of Bangladesh contain significant percentage mica, their effect need to be assessed in the interpretation of foundation design and slope stability calculations. The existing correlations using SPT values should be verified for these soils and there is a need for research in this area. For three large bridges in Bangladesh Osterberg (O-cell) cell tests have been performed. It has been observed that use of base grouting and skin grouting can significantly increase pile load carrying capacity.

1. Introduction

Bangladesh is a low-lying country crisscrossed by numerous rivers. Communication network has been a great challenge for road and rail-line construction, as most road or rail-line links require building of numerous river crossings. Three large rivers: the Padma, the Jamuna and the Meghna divide the country. Most of these rivers have braided characteristics that make the banks unstable and variable soil condition exist across the crossings. Geotechnical conditions for foundation construction for bridges has been challenging for many reasons. Distribution of soils across crossings is complex and are usually heterogeneous both in vertical and horizontal direction. Soils consist of wide varieties of material ranging from poorly graded sand to silt and clay. In general there is a predominance of silt-sized materials and most often sandy soils contain significant percentage of mica. The presence of mica itself provides some unique characteristics to these soils that have been little studied in geotechnical literature.

Most of the older bridges built in this country are founded on well or caisson foundations. Because these well foundations were open caissons, it did not require any

* E-mail: safi@ce.buet.ac.bd

heavy or specialized equipment to construct them except for equipment for grubbing soil from within the well. But there have been frequent problems of undesirable sinking or difficulty in sinking of these caissons that delayed the construction time. Some case studies of such problems are described in this paper. With the development of bored pile construction in this country, the current tendency is to build bridge piers founded on large diameter bored piles. Driven piles are seldom used for bridges in Bangladesh except for very small brides where scouring is not significant and driving is not a problem. The only major bridge built in Bangladesh that is founded on large diameter tubular steel piles is the Jamuna Bridge. Foundation for this bridge lies on 2.5 m and 3.2m diameter battered piles of about 80m long driven in medium dense granular micaceous sand. Obviously such driving required very heavy driving equipment that very few contractors own globally.

This paper reviews some bridge foundation design and construction practice followed in Bangladesh and reflects some case studies of the type of geotechnical problems that needs to be overcome to develop towards advancement of bridge construction in Bangladesh.

2. Caisson foundations

Caisson foundation have been very popular in Bangladesh for a long time because of the ease with which these could be built without use of any heavy or sophisticated machinery or equipment. Some of the large bridges have been founded on this type of foundation.

Before starting construction of a caisson within riverbed, the local practice is to build a sand island. Since the sand islands are temporary structures these are usually built of sheet pile enclosure filled with sand. In deep waters where scour is a problem often stability of the sand island requires critical examination. In shallow waters, sometimes wooden piles (shal-bolli) are driven closely with some bamboo mattress inside that retains sand for Sand Island. There have been instances where Sand Island has been washed out, tilted or displaced the caisson built inside it, which, necessitated either change in alignment or readjustment of the bridge spans. Often there are considerable problems with sinking of caissons by overcoming skin-friction. Sinking in conditions where skin friction is considerable lateral jetting becomes essential along with use of drilling fluid (usually bentonite). This requires thoughtful arrangement of internal piping and mud circulation, which is seldom followed by our contractors resulting in delay in construction, uneven sinking and even collapse of caisson.

2.1 Problem with construction of 2nd Buriganga bridge

The 2nd Buriganga Bridge over river Buriganga connects heart of Dhaka city at Nayabazar with Jinjira on the other side. The total length of the bridge within the limit of contract is 1479 m while the span within the river portion is 304 m and founded on five caisson foundations. The depth of these caisson foundations varied between 30.5 m and 32.5 m. Each caisson is oval shaped with external dimensions of 6 m by 13.4 m. The construction of the bridge commenced on 29th August 1994.

During middle of September 1996, difficulties developed during construction of the caisson foundation for pier no. 17. After the caisson was sunk to a depth of about 16 m. there was difficulty in further sinking although grubbing and soil removal from inside of the caisson was in progress. Some 4 to 4.5m of soil were removed from inside the caisson but the caisson did not sink by its own weight. There were no inbuilt outer jetting arrangements within the caisson walls. At this stage the contractor used a 1.5-inch GI pipe 18 m long to inject water close to the caisson wall and this jetting continued at one-foot interval. When half the diameter of the caisson was covered, water suddenly oozed out from the caisson and the caisson sank to a depth of 6.7 m and the level of soil inside the caisson raised to a depth of about 7 m above excavated ground inside the well. The top of the caisson went under river water level. Fig. 1 shows the condition of the caisson before and after sinking. It can be seen from the figure that before sinking the caisson had a grip length of about 16 m (52 feet). Fortunately because of this grip length there was no tilting of the caisson and the sinking could be continued to desired depth despite the fact that top of the caisson went below river water level. Two important lessons were learnt from Buriganga. Adequate internal jetting arrangements should be provided for caissons where significant skin friction is likely to develop. If external jetting is to be used it should be done symmetrically so that uniform sinking takes place. One need not go for excessive removal of soil from within the open caisson without releasing skin frictional resistance in uniform manner.

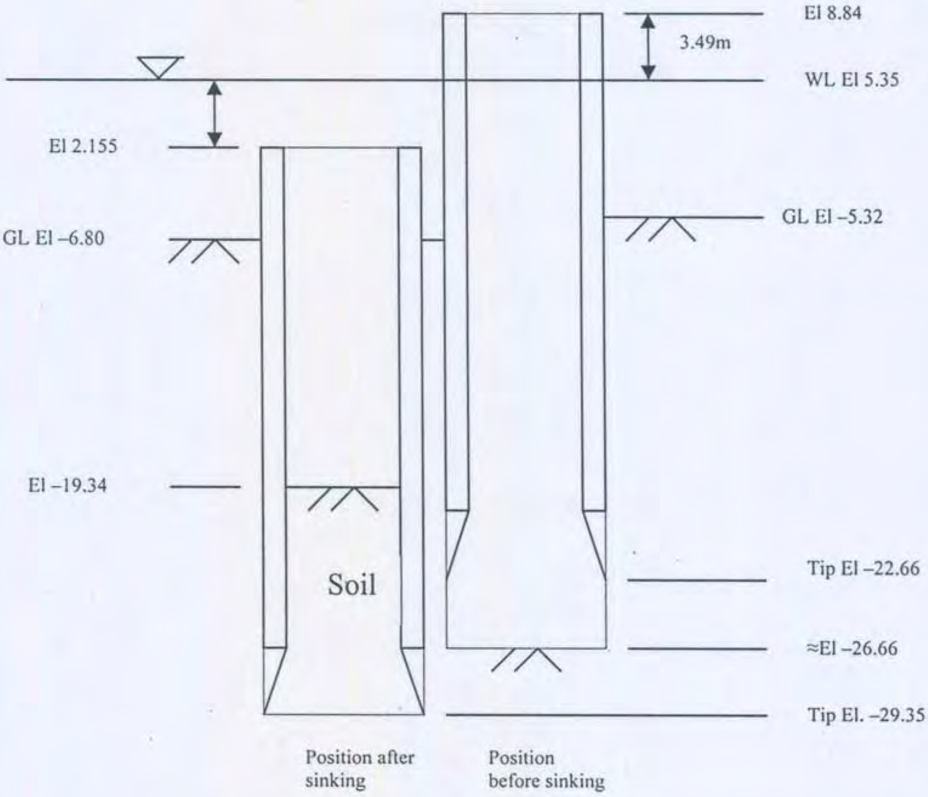

Fig. 1. Position of caisson on Pier 17 of the Buriganga bridge before and after sudden sinking on September 1996.

2.2 *Failure of caisson on Kalidash-Pahalia Khal Bridge on Feni-by-pass*

It may be recalled that in 1976 during installation of a caisson for the bridge on Kalidash Pahalia Khal on Feni-by-pass road, due to heavy inrush of water of the flashy river the caisson tilted and failed. The reason for failure was investigated and found to be due to inadequate depth of embedment and resulting scour at the time of high river flow (Hossain et al, 1983[1]). Therefore due importance should be given to the grip length of the caisson at the time of construction.

3. Bored pile foundation

Although this type of foundation induces more turbulence and scour at the riverbed level it is becoming popular due to development of technical capability to built very large diameter piles, faster construction and better construction techniques and also due to elimination of the need to construct sand island. Large diameter bored piles are gradually replacing caisson foundation in bridge construction in Bangladesh.

The Japan-Bangladesh Friendship Bridge over river Meghna is built on piers founded on bored piles. The construction of foundation at riverbed level required construction of a watertight cofferdam built with steel pipe piles (diameter: 1.016 m, length: 28.5 m) with vertical interlocking system. The cofferdam had to be braced with heavy steel pipes to resist external water pressure when inside is drained out. After installation of bored piles within the cofferdam, the inside had to be dewatered for excavation and preparation of bed for pile cap and pier. Fig. 2 shows pile head treatment for construction of pier within the cofferdam. Cast-in-situ concrete piles of 1.5m in diameter were constructed by using reverse circulation drilling method. Special measuring system was adopted for the vertical accuracy of the boreholes. The lengths of these piles are variable ranging from 40.0 m to 58.0 m depending on the level of the bearing strata for the piles.

Fig. 2. Pile head treatment for construction pier foundation inside the cofferdam.
(Courtesy: Roads and Highway Department, Bangladesh)

Most of the bored pile foundations used for smaller bridges use Sand Island instead of the type of cofferdam used for the Meghna Bridge. Because the pile tops are placed at the surface of the sand island, which is above river water level, bottom of pile caps are above riverbed, creating turbulence and excessive scour at riverbed level. Some times

[1] Hossain, A.S.M.M; Salahuddin, M and Hasan, A (1983): A case study on Kalidas Khal Bridge caisson failure. Unpublished undergraduate thesis, Department of Civil Engineering, BUET.

piles develop defect due to bad construction practice that relates to borehole formation, borehole cleaning and underwater or tremie concreting. Fig. 3 shows an example of bad concreting that developed within the piles just below pile cap for one of the pier of Dhaleshwari-1 Bridge. From the photograph it can be observed that there is discontinuity in the top casing where the concreting was affected.

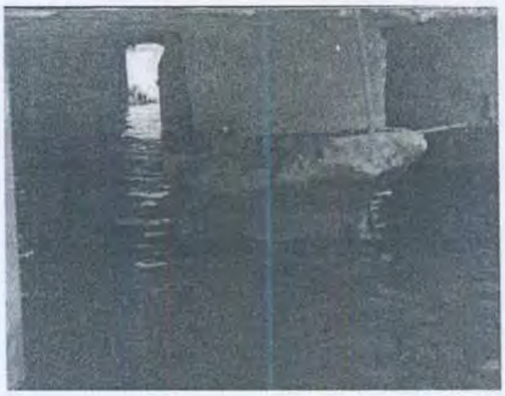

Fig. 3. Photograph shows defective concrete work in the piles for Dhaleshwari-I Bridge.

One of the major problems faced by the engineers in Bangladesh is the estimation of pile capacity for bored piles installed in riverbed for bridge structures by using static formulas. Since most of the riverbed formations are of granular deposits no undisturbed samples are usually collected. Design is normally based on field test such as standard penetration test N-values. The N values are correlated to angle of internal friction (ϕ) values, that is normally required in static analysis. For granular soils it usual to use ϕ –N value relations proposed by various authors such as Peck et al (1974)[2] and Kishida (1967)[3]. Here N is the Standard Penetration Test value corrected for field conditions and normalized for overburden pressure. Unfortunately, due to presence of large quantity of mica in the riverbed, there is uncertainty as to the applicability of these correlations for granular deposits of Bangladesh. Besides it is not possible to collect undisturbed granular deposits from riverbed and test these in the laboratory for shear strength and deformation parameters for field condition. Tests at BUET have indicated that sands containing mica can have significantly lower ϕ values and lower density during sedimentation process.

3.1 Load test of piles

Because of the uncertainty with estimation of pile capacity from static formula, it is better to evaluate pile capacity from static load tests. Since large diameter piles are commonly used for bridge foundations it is a formidable task to perform field pile load test using normal pile load test practice, which uses load platform or anchor piles. Because of the huge loading platform that would be required for such test, it is not practicable. Besides normal load test procedure, followed for bored piles, furnish

[2] Peck, R.B.; Hanson, W.E; and Thornburn, T.H.(1974): Foundation Engineering; 2nd Edition; Wiley Eastern limited.
[3] Kishida, H.(1967): Ultimate bearing capacity of piles driven into loose sand; "Soils and Foundations", vol. 7, no.3:20-29.

insufficient information on skin friction and end bearing components separately. Such information is required in applying appropriate factor of safety in pile capacity at various deformation stages. For the large diameter bored piles in Bangladesh, much of the soil parameters for design related to estimation of skin frictional resistance and end bearing is estimated from 'Bi-directional Osterberg Cell Load Testing' or O-cell testing.

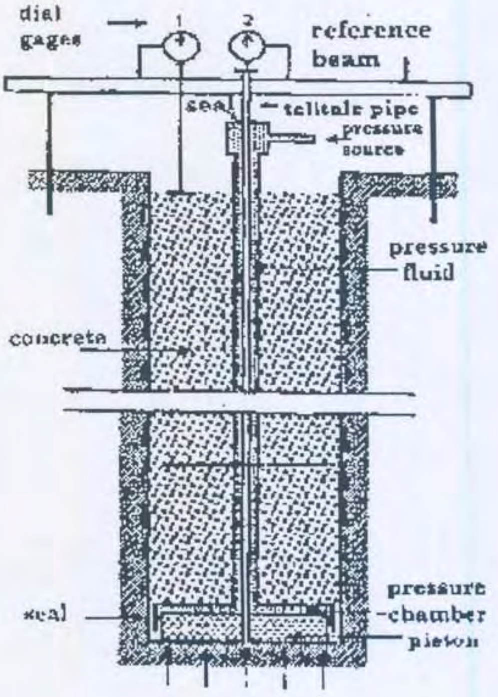

Fig. 4. Osterberg cell schematic

Invented and developed by Dr. J. Osterberg of Northwestern University, O-cell test for testing high capacity piles has changed the way foundation load tests are designed, performed and interpreted. The Osterberg Load Cell (also called O-cell) consists of a specially designed hydraulic jack capable of exerting very large loads at high internal pressures. Fig. 4 is a schematic diagram illustrating how the load cell works. A small amount of concrete is placed on the bottom of a bored pile hole after which the O-cell is lowered into the hole, which is then filled with concrete. A pipe welded to the top of the center of the cell extending to above ground surface acts as a conduit for applying fluid pressure to the previously calibrated cell. Inside the pipe is a smaller pipe connected to the bottom with an open end. It extends to the surface and emerges form the large pipe through an O-ring seal. This pipe acts as a telltale to measure the downward movement of the bottom of the cell as load is applied. The fluid for applying pressure can be oil or water. The liquid most often used is water with a small amount of miscible oil added to keep pump equipment from rusting. After the concrete has reached its desired strength, the cell is pressurized internally creating an upward force on the bottom of the shaft and an equal but opposite force in end bearing. As the pressure increases, the telltale moves downwards as the load in the end bearing increases and the shaft moves upward as the side shear on the shaft is mobilized. It should be noted that at all times the total side shear resistance above the O-cell is equal to the end bearing. Because of this no reaction load or hold down piles with a frame is needed as in the conventional test where the load is applied downward on the pile head.

The downward movement is measured by dial gage 2, and the upward movement of the top of the concrete is measured by dial gage 1. Not shown on the figure is a pipe extending from top of the of the load cell to above the surface in which telltale rod that measures the upward movement of the top of the cell. Thus the difference between the measurement of this rod and dial gage 1 gives the compression of the concrete. From data obtained as the load is increased, the load-upward movement curves and the load-downward movement curves can be plotted. After the test is completed, the area below the bottom of the O-cell and the cell chamber can be grouted if the pile is to be used as a working pile.

For the largest capacity size O-cell (three feet diameter) the maximum force, which can be applied, is 3,000 tons up and 3,000 tons down. Details of testing procedure and interpretation of results can be referred to Osterberg (1999)[4].

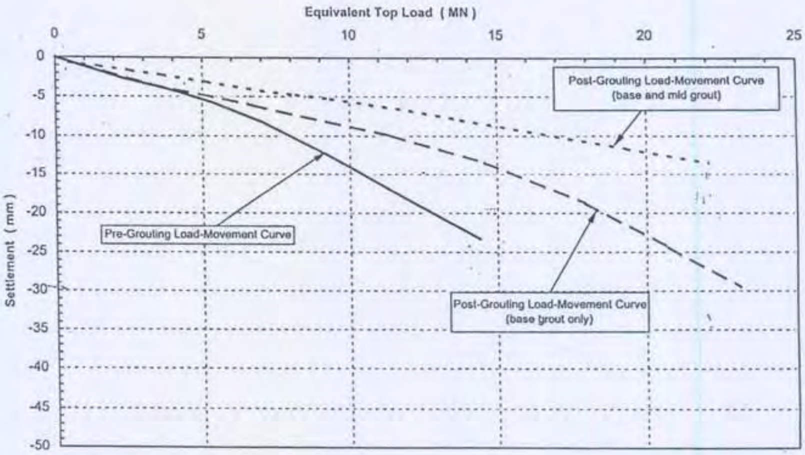

Fig. 5. Comparison of pre and post grouting capacity of test piles for Paksey Bridge as obtained by O-cell tests.

O-cell tests have been very useful in interpretation of skin-friction and end-bearing characteristics of large diameter bored piles used in three major bridges in Bangladesh such as the Bhairab Bridge, the Paksey Bridge and the Rupsa Bridge. It may be recalled that pile capacity in these bridges had to be increased by skin and base grouting as the un-grouted piles did not provide desired capacity required for deign. Fig. 5 shows load-settlement relations for test piles used in Paksey bridge using O-cell test for condition of (1) no grouting, (2) base grouting only and (3) combination of skin and base grouting. The diameter for these piles was 1.6 m and the embedded length was about 70m. Using O-cell, load tests could be performed to a very high capacity. It can be seen from the test results that significant improvement in pile capacity in bored piles is possible in the granular deposits of Bangladesh. A specialist pile load-test contractor 'Load Test Inc.' performed all these tests.

---

[4] J.O. Osterberg (1999): What has been learned about drilled shafts from Osterberg test. Paper presented at the Deep Foundation Institute Annual Meeting- October 1999.

4. Large diameter pipe or tubular piles

Small displacement tubular or pipe piles are not much in use in bridge construction in Bangladesh because of lack of driving equipment required for such piles. But these piles have the advantage that they can be easily spliced and welded to achieve significant depth of penetration sometimes required due to scour. Also these piles can be driven in battered position to resist lateral loads. Development of offshore technology introduced heavier pile driving hammers that are capable to drive large diameter piles to considerable depth within a very short time. It is for such reason large diameter (2.5 m and 3.2 m) driven tubular piles were selected for use in the Bangabandhu Bridge (Jamuna Bridge) over river Jamuna.

Fig. 6 shows typical 2-pile arrangement for pier support of the Bangabandhu Bridge. The tubular structural steel piles were originally supposed to be left empty inside, but later, the inside had to be removed of soil and filled with concrete except for bottom 5 m. of the tube. Grouting pipes were installed within the filled concrete and when the concrete had hardened, pressure grouting was done to improve the base soil inside the tube against any possible loose condition. Tappin et al (1998)[5] has described the construction of the Jamuna Bridge in Bangladesh.

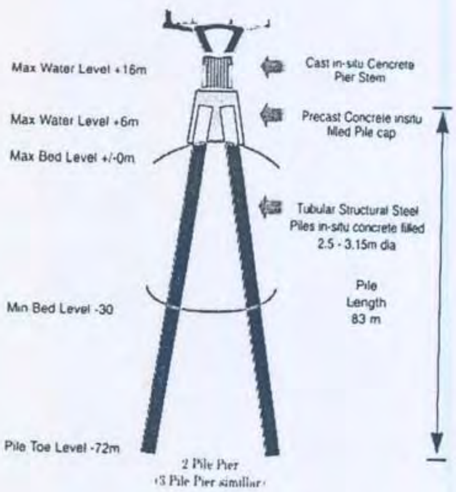

Fig. 6. Typical 2-pile arrangement for Jamuna bridge piers.

5. River training works and guide bunds

Guide bunds are essential to confine the river flow within the bridge length. Guide bunds require bank protection from waves, bed scour and stability of the slope. In Bangladesh all the river courses are in loose alluvial soil and are prone to rapid scour, which can significantly change the cross-section and course of the river. Hydraulic and soil conditions determine the stability condition of the channel.

Scour depth around piers and guide bunds should be determined from estimation of general scour, constriction scour and local scour. Bridge Engineers' Hand Book

[5] Tappin, R.G.R, Duivendijk, J.V. & Haque, M. (1998): The design and construction of Jamuna Bridge, Bangladesh; Proc. Instn. Civ. Engng, 126, Nov., paper 11704:150-162.

published by the Roads and Highway Department is normally used for these computations.

Stability of riverbanks, which contains mainly sandy silts and mica in loose state, is a serious problem for stability analysis in Bangladesh. Lessons learned from the construction of the Jamuna Bridge are of great significance in designing guide bunds and bank protection works. In the Jamuna Bridge, important elements of the construction were the West and East Guide Bunds, designed to control the flow of the river. The guide bunds, which comprise heavily protected sand slopes, are 3.3 km long, with the northern tip 2.5 km north of the bridge site. To enable slope protection materials to be placed, a trench, varying in depth from 27 to 30 m below original ground level, was excavated below water by cutter-suction dredgers. The trench comprised of the permanent protected slope and a temporary unprotected slope. The temporary slope had to remain sufficiently stable during construction so as not to interfere with the formation of the permanent slope and to maintain a barrier to the river flow, so to ensure current free condition for placement of the protective mattresses.

The West Guide Bund was constructed at the site of a rapidly formed island. The materials forming the dredged slopes consisted of young, rapidly deposited sand sediments. During its construction, a number of slips occurred in both the permanent and temporary unprotected slopes. A plan of the location of interest where the slips had occurred in both the permanent and temporary slopes while it was being dredged at original design slope of 1 in 3.5 are shown in Fig. 7. These slips represented approximately 50 % of the constructed length. At this time, the temporary slope being dredged at 1 in 3 slope was affected almost 100% of the dredged length. After the incidence a modification into the original designed slope was made which is shown in Fig.8. After the modification in the design profile was made, only three minor slips, representing less than 5% of the constructed length, occurred in the permanent slope when it was being dredged at 1 in 6 slope. In contrast, slips continued apace in temporary slopes, which was now at 1 in 5; these slips were associated with dredging, with storm activity, and draw down of river level. It is important to note marked difference in performance of the two slops, at 1 in 6 and 1 in 5. Hight and Leroueil (2003)[6] provided a detailed account of this difference in behavior, which is described below.

The slips had the characteristics of underwater flow slides. Bathymetric surveys showed that, in plan, the slips had a classic hourglass shape, comprising a bowl-shaped depression from which the materials have been removed and an alluvial fan, where the slipped materials collected. In cross-section, the post failure profile was stepped and had a slope between 1 in 10 and 1 in 20. The failures took several hours to develop and involved between 50,000 and 100, 000 m^3 of material.

The slopes were being dredged in micaceous sands. The mica comprised thin sand-sized plates, generally biotite. The quantity of mica, its distribution and its orientation varied. Grain counting indicated mica contents of 5-10%. SPT tests at the site suggested that relative density of these micaceous sands was between 40 and 60%, values that would not normally be associated with flow slides.

[6] Hight, D.W., & Leroueil, S. (2003): Characteization of soils for engineering purposes. Characterization and Engineering Properties of Natural Soils; Tan et al (eds), Vol.1, A.A. Balkema Publishers: 255-360.

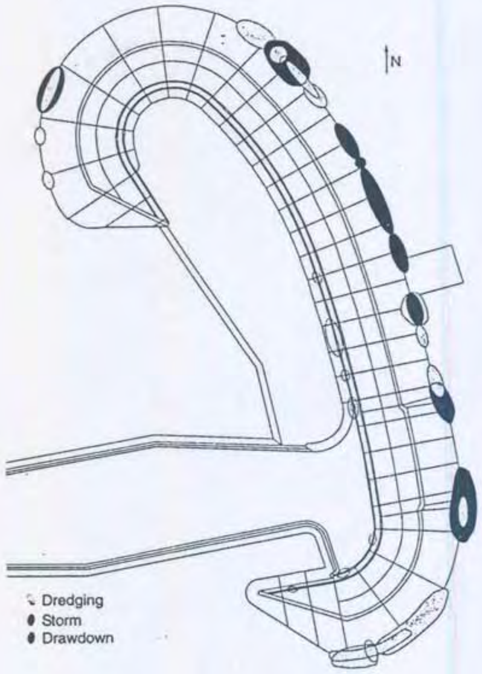

Fig.7. Plan on west guide bund to Jamuna bridge, showing locations of flow slides and trigger (Hight et al, 1999)

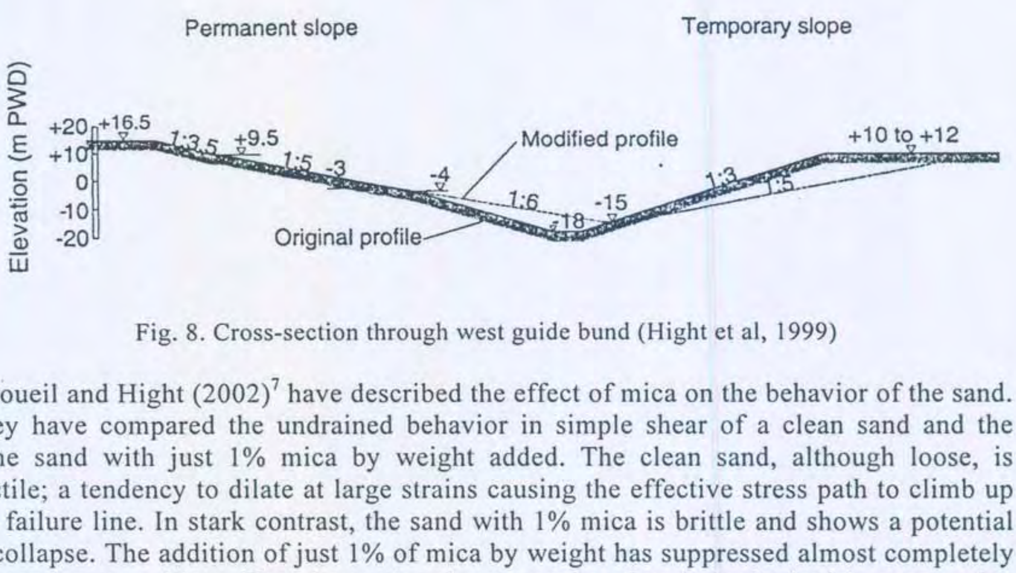

Fig. 8. Cross-section through west guide bund (Hight et al, 1999)

Leroueil and Hight (2002)[7] have described the effect of mica on the behavior of the sand. They have compared the undrained behavior in simple shear of a clean sand and the same sand with just 1% mica by weight added. The clean sand, although loose, is ductile; a tendency to dilate at large strains causing the effective stress path to climb up the failure line. In stark contrast, the sand with 1% mica is brittle and shows a potential to collapse. The addition of just 1% of mica by weight has suppressed almost completely the tendency to dilate. They have also shown results of undrained triaxial compression and extension tests on samples from one batch of natural materials, prepared by dry spooning at relative densities of 58% and 55%, respectively. In compression, the material is ductile and has an undrained strength in excess of 180 kPa. In undrained extension, the mateial is brittle and has a strength of only 10 kPa.

[7] Leroueil, S.,& Hight, D.W. (2002): Mechanical behaviour and properties of natural soils and soft rocks Proc. Int. Workshop on Characterization and Engineering Properties of Natural Soils, Singapore.

The key points of their study may be summarized as follows:

- The presence of sand sized mica in a sand leads to an increase in void ratio, to extreme levels of undrained anisotropy and extreme sensitivity to fabric. Volume change characteristics are modified and a collapse potential may exist for certain loading directions and for certain quantities, distribution and orientations of the mica. In terms of brittleness and collapse potential, small quantities of mica, less than 2.5 % by weight, are probably critical.
- Micaceous sands appear to be particularly weak in extension loading and most vulnerable to collapse when under low stress. These conditions apply just beyond the toe of an underwater slope subject to unloading by dredging or scour.
- In evaluating flow potential, anisotropy and principal stress directions of potential perturbation must be taken into account.
- Current design approaches that rely on triaxial compression tests on reconstituted samples are not valid because they implicitly assume that steady state is isotropic and independent of stress path and initial fabric.

The case study emphasizes the importance of considering quantity, distribution and orientation of mica particles in a sand, its full stress path including possible rotation of principal stress direction, and the range of drainage conditions that may apply.

6. Conclusions

Bridge design and construction in Bangladesh involves a very good understanding of the local soil conditions. At present due to lack of understanding and research on the geotechnical parameters to be used for river borne granular deposits containing mica application of existing parametric correlations remains questionable. The SPT-ϕ correlations suggested in most literatures need to be validated for Bangladesh soils.

Three types of deep foundations are now in use for bridge construction in riverbeds: caissons, cast-in-situ bored piles and tubular bored piles with or without concrete infill. Construction of most of these foundations requires Sand Island whose stability is critical to hydraulic flow and scour during construction. Some case studies presented in the paper demonstrate that quality control and monitoring during construction stage should be carefully performed to avoid development of unwanted situations like failure, delay in construction or modification of the design.

Use of large diameter bored piles for three major bridges in Bangladesh has revealed that considerable improvement in pile capacity can be achieved by skin and base grouting techniques. Use of O-cell test has been very useful in interpreting pile capacity and deriving skin frictional resistance and base resistance of large diameter piles.

Case study of guide bund failure for Jamuna bridge has revealed that slope stability analysis during dredging can be very critical which requires considerations for relative density of soil, quantity, distribution and orientation of mica particles in the soil, its full stress path including possible rotation of principal stress direction, and the range of drainage conditions that may apply

References

Hight, D.W., Georgiannou, V.N.,Martin, P.L. & Mundegar, A.K. (1999): Flow slides in micaceous sands. Proc. Of the Int. Symposium on Problematic Soils, IS Tohoku, Sendai, Japan. Balkema, Rotterdam, Vol.2:945-598.

Hight, D.W., & Leroueil, S. (2003): Characteization of soils for engineering purposes. Characterization and Engineering Properties of Natural Soils; Tan et al (eds), Vol.1, A.A. Balkema Publishers: 255-360.

Hossain, A.S.M.M; Salahuddin, M and Hasan, A (1983): A case study on Kalidas Khal Bridge caisson failure. Unpublished undergraduate thesis, Department of Civil Engineering, BUET.

Kishida, H.(1967): Ultimate bearing capacity of piles driven into loose sand; "Soils and Foundations", vol. 7, no.3:20-29.

Leroueil, S.,& Hight, D.W. (2002): Mechanical behaviour and properties of natural soils and soft rocks Proc. Int. Workshop on Characterization and Engineering Properties of Natural Soils, Singapore.

Peck, R.B.; Hanson, W.E; and Thornburn, T.H.(1974): Foundation Engineering; 2nd Edition; Wiley Eastern limited.

Tappin, R.G.R, Duivendijk, J.V. & Haque, M. (1998): The design and construction of Jamuna Bridge, Bangladesh; Proc. Instn. Civ. Engng, 126, Nov., paper 11704:150-162.

Japan-Bangladesh Joint Seminar on Advances in Bridge Engineering
Dhaka, Bangladesh. 10 August 2005

ISBN: 984-32-2520-6

Recent topics in the wind engineering

Hitoshi Yamada*

Faculty of Environment and Information Sciences, Yokohama National University
79-1 Tokiwadai, Hodogaya-ku, Yokohama 240-8501, Japan.

Abstract

Wind resistant design is of great importance for large scale projects of bridges as well as buildings. However comparing the seismic effect, it is apt not to understand it well, because the contribution in the structural design increase rapidly as its scale and most of the wind-action include various vibration such as the self-excited vibration and the random vibration. In this paper importance of the wind resistant design is demonstrated referring history of the modern long span bridges and method of the wind resistant design is also illustrated.

Keywords: wind resistant design, long span bridges

1. Introduction

The wind action on structures is very usual phenomena in daily life, which everyone can experience. However it is also true that it is not only one of severe natural disasters but also it is hard to understand how large its effect can be. It is well known that there is a long list of structural damages due to the wind action and history of development of the suspension bridges coincides with history of the wind accident. According to these lessons, main key issues in the structural responses against the wind actions are extracted and illustrated in Figure 1. Shortly those actions can be explained as a chain ling of structural dynamics, aerodynamics and atmospheric exposures. It means that the wind action on structures and its wind resistant design should be discussed from those combined viewpoints. In this paper, examples of the wind induced vibrations of bridges is reviewed and some new trends in the wind resistant design are introduced.

2. Significance of the wind action

A part of bridge damages, which are publicly reported, are listed in Table 1. Referring the fact the modern suspension bridge was proposed around 1800 after the industrial revolution, reports of structural damage of bridges increased simultaneously after 19th

* Email: yamada@cvg.ynu.ac.jp

century. Besides it can be found that main counter majors were to give additional stiffness to the structure by adding some members, such as stay-cables and truss reinforcement. From a viewpoint of modern wind resistant design, stiffening the whole structure is one of ways to suppress the vibration but it is neither easy nor efficient in comparison with aerodynamic improvement, because it must dissipate the kinetic energy of the self-induced vibration.

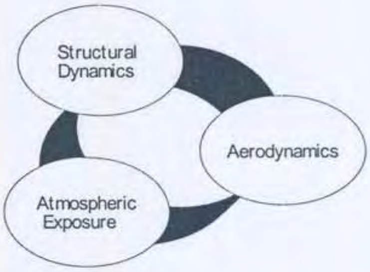

Fig. 1. Link of wind action on structures

Table 1. List of monumental failure of long-span bridges

Due to Wind force

1879 Tay Bridge / short wind force and derailment

Due to Aero elastic vibration

1823	Brighton Chain Pier Bridge(UK) / torsional vibration
1826	Menai Strait Bridge(UK) / reparation of deck system
1830	Nassau Bridge(D) / broken chain
1850	Niagara-Lewiston Bridge(US) / collapsed
1932	George Washington Bridge(US) / bending vibration, truss reinforcement
1937	Golden Gate Bridge(US) / reinforcement of the trussed deck, change from open truss to closed truss
1938	Thousand Island Bridge(US) / bending vibration, installation of stay-cables
1939	Deer Isle Bridge(US) / bending vibration, installation of stay-cables
1939	Bronx Whitestone Bridge(US) / truss reinforcement
1940	Tacoma Narrows Bridge(US) / collapsed due to torsional vibration

2.1 Tay Bridge, UK

The Tay Bridge, a 85 span trussed high girder bridge of 3,160m, is well known as its collapse on December 28, 1879, as in Figures 2 and 3. Reason of this collapse has been widely understood as lack of the lateral stiffness of the truss girder due to too small wind load specification. It can be proved by the fact that the steam locomotive was found in the truss frame in the water and salvaged. However according to many reports on it, tight schedules of big bridge projects, change of the structure redesign due to lack of foundation support capacity and maintenance process seem to have been importance keys in this collapse. In the wind load its designer Thomas Bouch decided 12lb/ft^2 (~5MPa) for the sever storm as the wind load referring an advice of the Astronomer Royal. After this accident, the wind load specification was changed to 56 lb/ft^2 (~20MPa) for the Force Railway Bridge. On the other hand Japanese Road design code specifies 30MPa for the deck girder.

Fig. 2. Artist drawing of the collapse

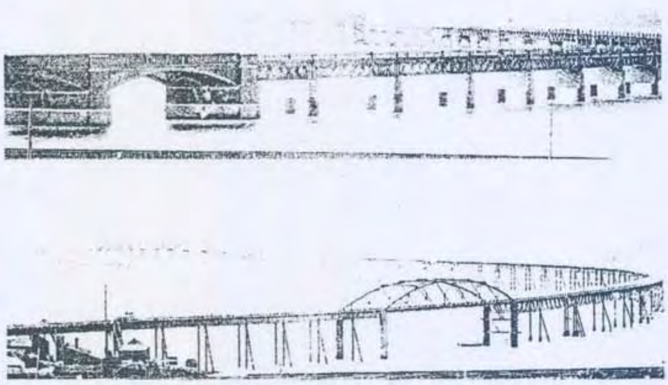

Fig. 3. Old and new Tay bridge

2.2 Tacoma Narrows Bridges, USA

The Old Tacoma Narrows bridge was one of technically advanced bridges at the completion, which is designed basing on the flexure theory. It is also very famous that its collapse occurred in only few months after its opening ceremony, as in Figure 4. It is understood its reason was lack of knowledge in bridge aerodynamics and poor aerodynamic performance of the stiffening deck. According to the flexure theory, the main cable system can support all of loads and the deck stiffness can be decreased to the minimum. The extreme shape of the deck under this idea is the plate-girder as illustration in Figure 5. Only demerit of this type was aerodynamics.

After the collapse, many investigations were made to clarify the reason. Among them a wind tunnel for a full bridge model was constructed and full bridge wind model testings were conducted at University of Washington, USA by Prof. Farquharson[1]. In Figure 6, one of their results is illustrated and the observation is also plotted. Important findings of this testings were as follows

1. Responses occur as order of the natural modes from the lowest.
2. Possibility of destructive vibration in the torsional mode was found.

Fig. 4. Vibration of the Tacoma Narrows bridge

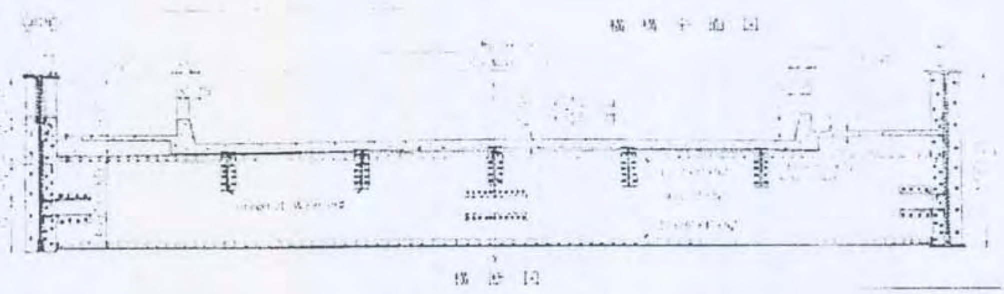

Fig. 5 Cross section of the Old Tacoma Narrows bridge

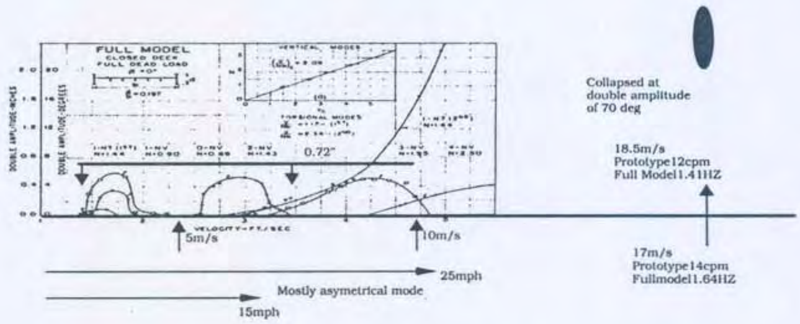

Fig. 6 Full bridge model test and observation

Comparing the observation (horizontal solid line and black eclipse in the figure), the response at low wind speed range shows reasonable agreement but in the flutter occurrence only qualitative coincide was found More than 50 years have passed, but this is very rare example to make a comparison between wind tunnel testings and the field observation even from the modern viewpoint.

2.3 Kessock bridge, UK

Kessock bridge with 240m in main span and 1056m in total length, completed in 1982, is a cable stayed bridge near Inverness in Scotland UK (in Figure 8). This bridge is one of bridges with TMDs (in Figure 7) to suppress the vortex-induced vibration. Vibration of 90-200mm in the amplitude due to vortex shedding was observed in wind only from Moray Firth[2]. To suppress this vibration of the vertical fundamental mode eight TMDs were installed (as in Figure 7),

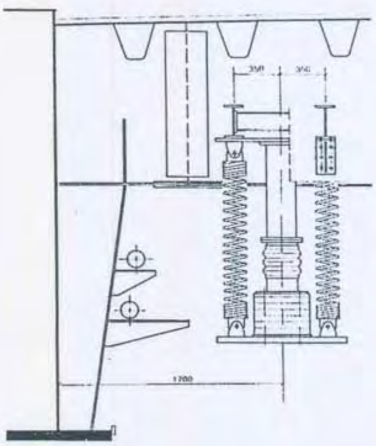

Fig. 7. TMD of Kessock bridge

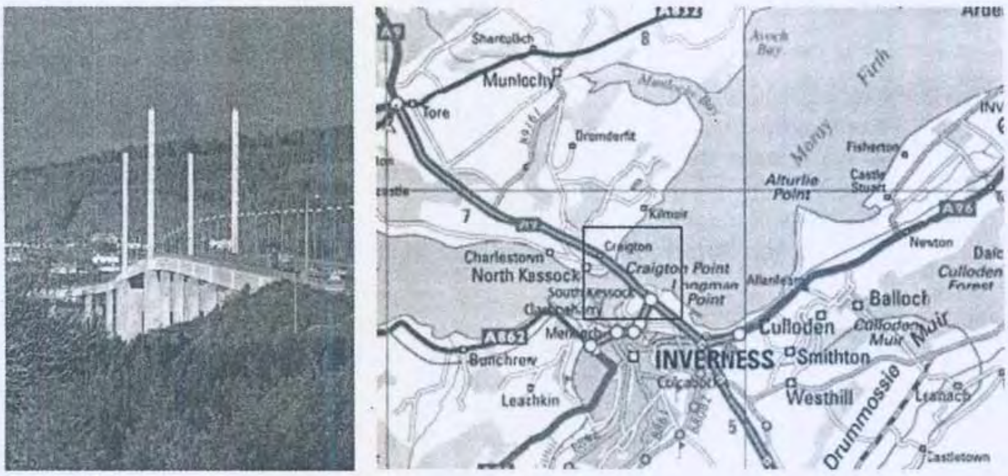

Fig. 8. The Kessock bridge

2.4 Trans-Tokyo Bay highway bridge, Japan [3]

Trans-Tokyo Bay Highway in Figure 9 is a 10-span continuous steel box girder bridge, completed in 1995 ,that is 1,630 m in total length including 240 m spans in maximum length. In the wind tunnel examination, it was reported that two or more vertical bending vibration modes would occur due to vortex-induced oscillation Before the opening, vibration with the amplitude of±50 cm was observed at a wind of 15 to 16 m/s. It is also reported that the logarithmic decrement of 0.028 - 0.044 were observed by the field dynamic testing. Comparison between the wind tunnel testings and observation is illustrated in Figure 10.

It can be found that the response of this bridge is almost same with the wind tunnel test. Looking at this fact some TMDs were installed to suppress vortex-induced vibration for some vibration modes.

Fig. 9. Trans-Tokyo Bay bridge

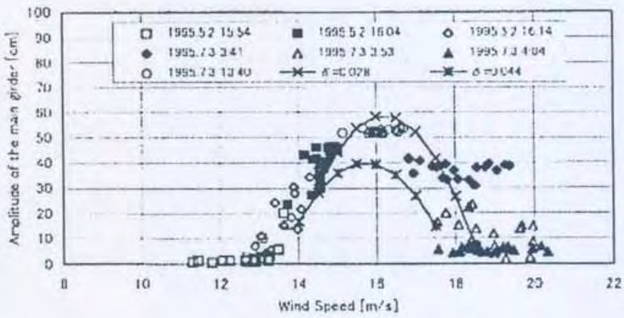

Fig. 10. Observation vs. response in wind tunnel test[3]

3. Aerodynamics and structural dynamics

3.1 Wind tunnel testing

For long time the wind tunnel test has been only tool to investigate aerodynamic characteristics of structures. Although CFD is improved quickly, the wind tunnel testing under well adjusted similitude in the modeling is believed as the most reliable approach for the verification of stability of structures against the wind action.

Roughly wind tunnel test can be classified into the full bridge model test and the section model test. Literally in the full bridge model test, the model should be scaled down at specified scale in detail. From a viewpoint of similarity law, the full bridge model is optimum and it will be easy to understand the result of the testing. However when the scaling ratio is not small enough to ensure the detail modeling, size of the model must be huge. In case of the Akashi Kaikyo bridge, length of its 1/100 scale full bridge model is 40m. It required the world largest wind tunnel, which accommodate the whole model (in Figure 11). The section model has scaled section but it does not have the mode shape(in Figure 12).

Fig. 11. Full bridge model for the Akashi Kaikyo Bridge and wind tunnel for it

Fig. 12. A section model and test section of a wind tunnel

Strictly speaking, this is not a model, which satisfies the similarity law, and it cannot show behavior of the prototype directly. To understand output of the testing, interpretation must be required basing on some assumptions. Although there is this limitation, this model is very convenient to know aerodynamic characteristics of the section of the deck, such as aerodynamic derivatives, aerodynamic forces, pressure distributions and so on. Besides large wind tunnel facility will not be required, because the model is just a section. This is a reason why this testing method is widely used for slender structure with similar section shape from one end to another, such as suspension bridges and airfoils.

3.2 One example of similarity for elastic/locking partial model

One example which is out of usual similitude is safety verification of a tower of suspension bridge in completion. It is usually required to investigate wind induced vibration of a tower of a suspension bridge not only during construction but also after completion (possible vibration mode shapes in Figure 13). In case of a free standing tower it will be very easy to model it as elastic mode. However the vibration after completion is a part of a global vibration of the whole system. When only the tower model is used because of limitation of the size of a wind tunnel, the whole structure and the modeled tower must be equivalent. This discussion is similar to equivalent modeling of the section model. In the section model following formulations is applied.

Looking at one natural mode and assuming only velocity component of the wind force the equation of motion can be as follows;

$$m\ddot{u} + c\dot{u} + ku = \frac{1}{2}\rho U^2 C^* A\left(\frac{\dot{u}}{\omega L}\right) \tag{1}$$

When longitudinally uniform deck under wind action can be assumed and one dominant vibration mode is looked at, equation (1) can be rewritten as equation (2).

$$\begin{aligned}
&\int_s m\phi^2 dx\ddot{q} + \int_s c\phi^2 dx\dot{q} + \int_s k\phi^2 dxq \\
&\quad = \frac{1}{2}\rho U^2 C^* A\left(\frac{\dot{q}}{\omega L}\right)\int_{wind}\phi^2 dx
\end{aligned}$$

$$\begin{aligned}
&\frac{\int_s m\phi^2 dx}{\int_{wind}\phi^2 dx}\ddot{q} + \frac{\int_s c\phi^2 dx}{\int_{wind}\phi^2 dx}\dot{q} + \frac{\int_s k\phi^2 dx}{\int_{wind}\phi^2 dx}q \\
&\quad = \frac{1}{2}\rho U^2 C^* A\left(\frac{\dot{q}}{\omega L}\right)
\end{aligned} \tag{2}$$

where suffixes of integration, "a" and "wind", mean integral areas of the whole structure and the exposed part of the structure to the wind respectively.

Mass parameter $\dfrac{\int_s m\phi^2 dx}{\int_{wind}\phi^2 dx}$ in equation (2) is called as the "equivalent mass", and similarity of this equivalent mass can make two different system equivalent in the equation of motion with the wind induced force. This is an essential idea to realize the section model testing.

This equivalent mass can be a solution for the similarity of the tower model as a part of the global structural system. When spans of a cable stayed bridge are not symmetrical (one example in Figure 14), similar discussion can be applied to design the wind tunnel model of its tower.

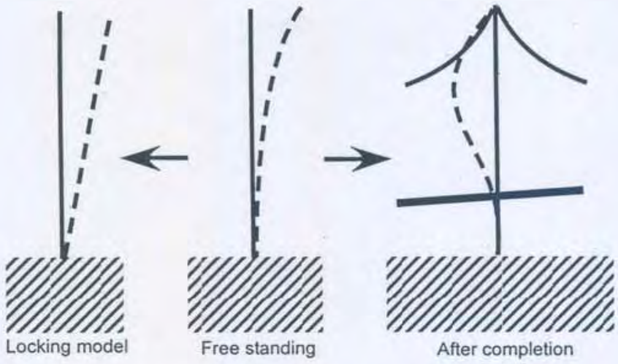

Fig. 13. Images of vibrations of towers

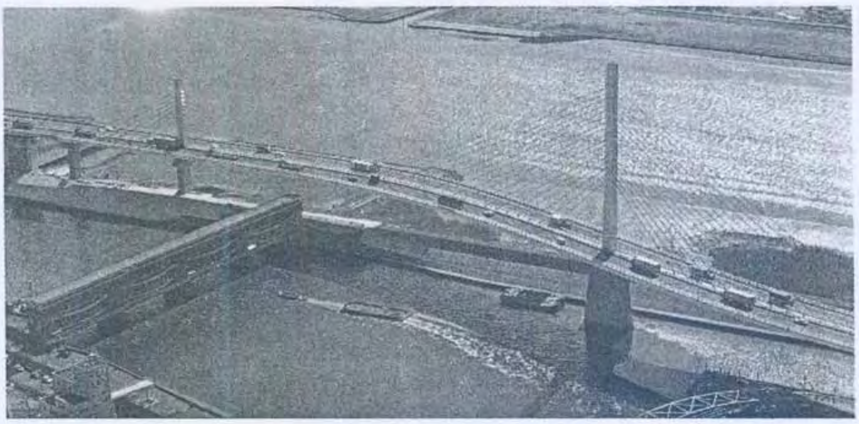

Fig. 14. Katsushika Harp Bridge, Japan

3.3 *Aerodynamic countermeasures*

To suppress the wind induced vibrations, aerodynamic devices to control the air flow are sometimes applied. Double flaps are illustrated in Figure 15 as one example of aerodynamic countermeasures. On the other hand to control stay-cable's vibration installation of dampers or/and helical strakes are very common, like in Figure 16.

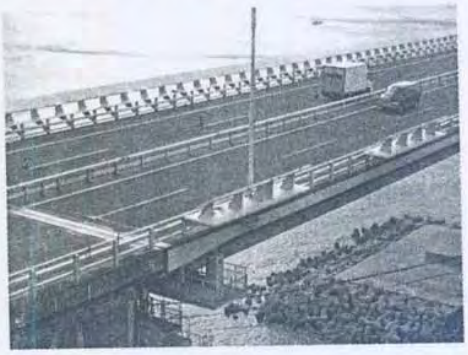

Fig. 15. Tozaki Viaduct of the Honshu-shikoku bridges,Japan

Fig. 16. Cable dampers and helical strakes of Brotonne Bridge, France

4. Aero-elastic investigation

4.1 Natural frequency analysis

Structural dynamic analysis of a carefully prepared structural model is very essential as the first step in the wind resistant design. Especially it is always required to evaluate the natural frequencies, the natural mode shapes and the equivalent masses, which are calculated using detailed structure models (in Figure 17). For examples, sometimes mass contribution of structurally coupled vibration becomes great. This happens in coupled vibration of a deck in lateral and torsional directions, due to discrepancy in location of the gravity center and the stiffness center (in Figure 18).

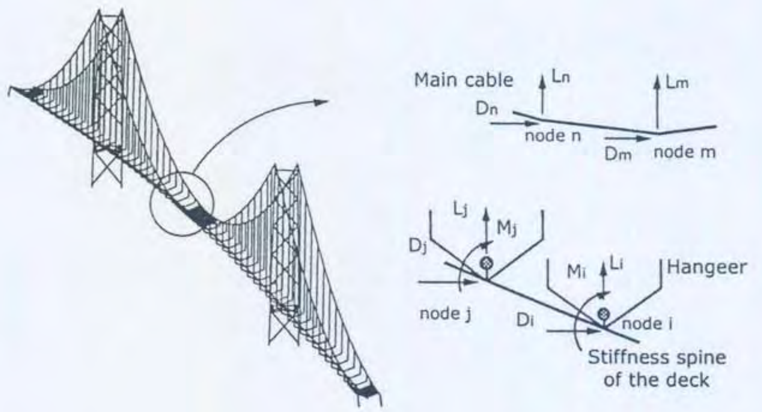

Fig. 17 Structural frame model for the Akashi Kaikyo bridge

4.2 Numerical response analysis

When unsteady aerodynamic forces are extracted in the wind tunnel experiments and applied to FEM structural model as in Figure 17, solutions of those equations of motion as Equation (3) give aero-elastic behavior of the structure due to the wind action.

$$[M]\ddot{u}+[C]\dot{u}+[K]u=[F_A]\ddot{u}+[F_V]\dot{u}+[F_D]u \qquad (3)$$

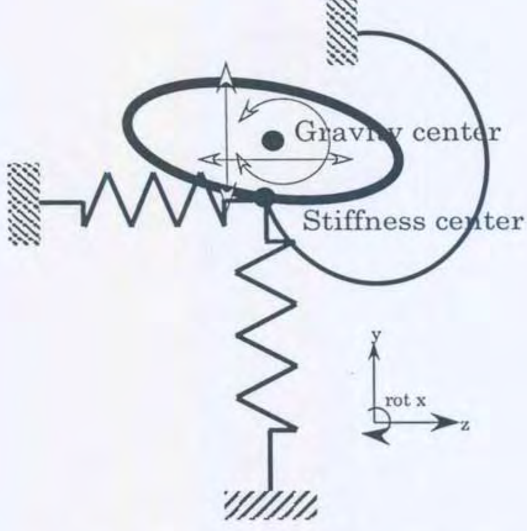

Fig. 18 Coupling mechanism of a deck

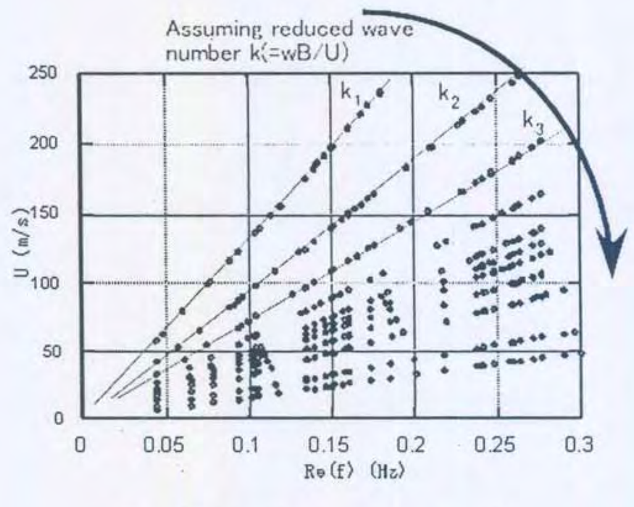

Fig. 19. Tracking aero-elastic roots

The unsteady aerodynamic forces at every nodes are formulated as in Figures (4,5) [4,5]

$$\begin{Bmatrix} L \\ M \\ D \end{Bmatrix} = \frac{1}{2}\rho U^2 \begin{bmatrix} B & 0 & 0 \\ 0 & B^2 & 0 \\ 0 & 0 & B \end{bmatrix} \left\{ \begin{bmatrix} kP_1^* & kP_2^* & kP_5^* \\ kH_1^* & kH_2^* & kH_5^* \\ kA_1^* & kA_2^* & kA_5^* \end{bmatrix} \begin{Bmatrix} \dot{y}/U \\ B\dot{\theta}/U \\ \dot{z}/U \end{Bmatrix} + \begin{bmatrix} k^2P_4^* & k^2P_3^* & k^2P_6^* \\ k^2H_4^* & k^2H_3^* & k^2H_6^* \\ k^2A_4^* & k^2A_3^* & k^2A_6^* \end{bmatrix} \begin{Bmatrix} y/B \\ \theta \\ z/B \end{Bmatrix} \right\} \tag{4}$$

$$\begin{Bmatrix} L \\ M \\ D \end{Bmatrix} = \pi\rho\omega^2 \begin{bmatrix} B^3 & & 0 \\ & B^4 & \\ 0 & & B^3 \end{bmatrix} \left\{ \begin{bmatrix} L_{yI} & L_{\theta I} & L_{zI} \\ M_{yI} & M_{\theta I} & M_{zI} \\ D_{yI} & D_{\theta I} & D_{zI} \end{bmatrix} \begin{Bmatrix} \dot{y}/\omega B \\ \dot{\theta}/\omega \\ \dot{z}/\omega B \end{Bmatrix} + \begin{bmatrix} L_{yR} & L_{\theta R} & L_{zR} \\ M_{yR} & M_{\theta R} & M_{zR} \\ D_{yR} & D_{\theta R} & D_{zR} \end{bmatrix} \begin{Bmatrix} y/B \\ \theta \\ z/B \end{Bmatrix} \right\} \tag{5}$$

where U, B, ω, ρ, L, M, D, y, θ, z, k are the wind speed, width of the model, circular frequency, density of the air, the lift force, the aerodynamic moment, the drag force, the vertical displacement , the twisting displacement the horizontal displacement respectively and the reduced wave number(= ωB/U). One of ways to get solution is to track eigenvalues as reduced wave number-damping plain and reduced wave number – frequency plain [5] as illustrated in Figure 19. Refereeing comparison among experiment and analysis in Figure 20, analytical results can explain the experiment but there still remains room for improvement.

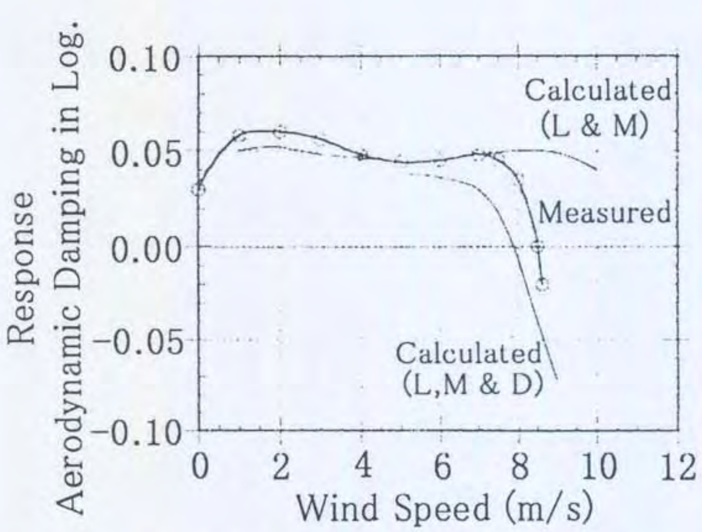

Fig. 20. Behavior of the Akashi Kaikyo bridge

5. Atmospheric exposure

5.1 Design wind speed

Atmospheric exposure will be classified into 3 categories for the structure-wind engineering as meso-scale exposure for motion of mostly low/high pressure system, micro-scale exposure for development atmospheric turbulence and local exposure for local topography's contribution. Although various contributions exist, primary interest for the wind resistant design is the design wind speed, which specifies the upper boundary of the wind action. In many examples of wind resistant design codes this design wind speed is given as a map after correction of the fundamental wind speed due to the topographical effect at the site and various safety factors, which is specifies on a map(one example in figure 21) as assumed common topography. The vertical wind speed profile is also a key for the wind speed correction, which is decided on appropriate ground roughness (in Figure 22). In the aeronautical engineering and the bridge wind engineering, the smooth flow has been used to the reference wind of the wind tunnel testing. Main reason of use of this smooth flow is that it can give the safe side evaluation and it will be possible to make wind tunnel experiments more equal condition than in some turbulent flow at various wind tunnel facilities. However it is clear that effect of the boundary layer turbulence play an essential role to interpret measurements in laboratories and observations of real bridges. Introduction of this effect in evaluation of the wind –induced response is understood to increase its importance.

Topographies of the roughness I,II,III,IV are on water, open terrain, suburb and down town/mountainous area respectively.

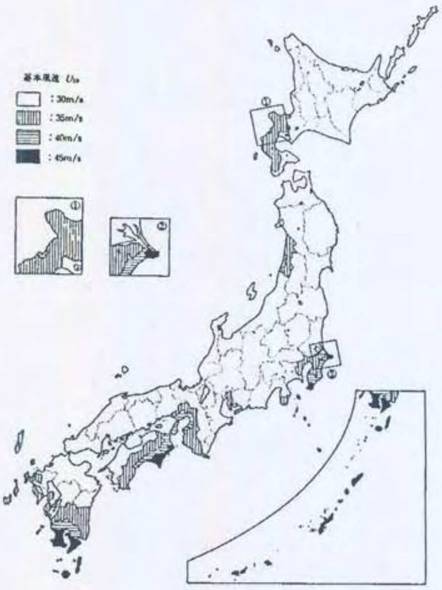

Fig. 21. Wind speed map in the wind resistant design manual, Japan[6]

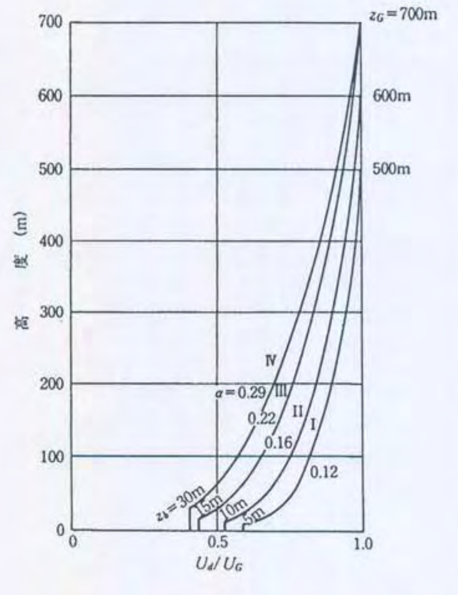

Topographies of the roughness I,II,III,IV are on water, open terrain, suburb and down town/mountainous area respectively.

Fig. 22. Vertical wind speed profile in the wind resistant design manual, Japan

5.2 Utilization of meteorological stations and statistical typhoon simulation

The design wind speed will be decided referring wind speed observations at meteorological stations and extreme value statistical analysis of their annual maxima. However it will be easily understandable that those observations will already include effects of continuous change of their topography and difference of adopted anemometers. In Figure 23 and 24, annual maxima of the strong wind for these years are plotted.

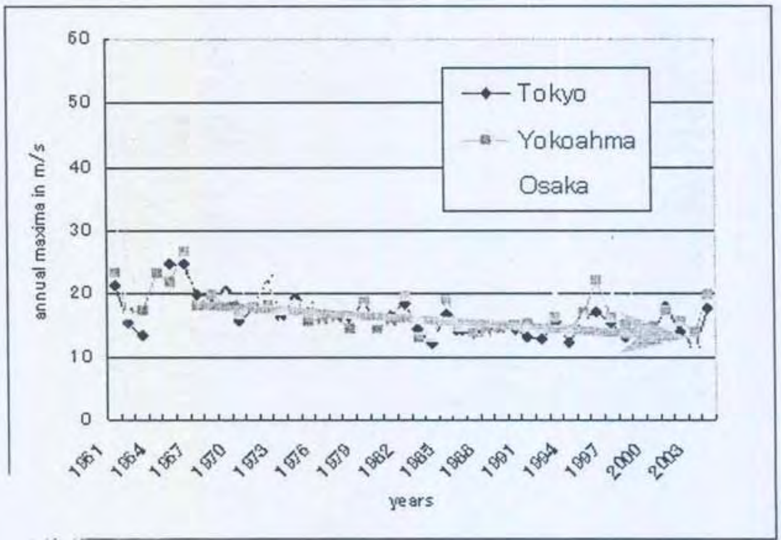

Fig. 23. Annual maxima of observed wind speed in urban areas

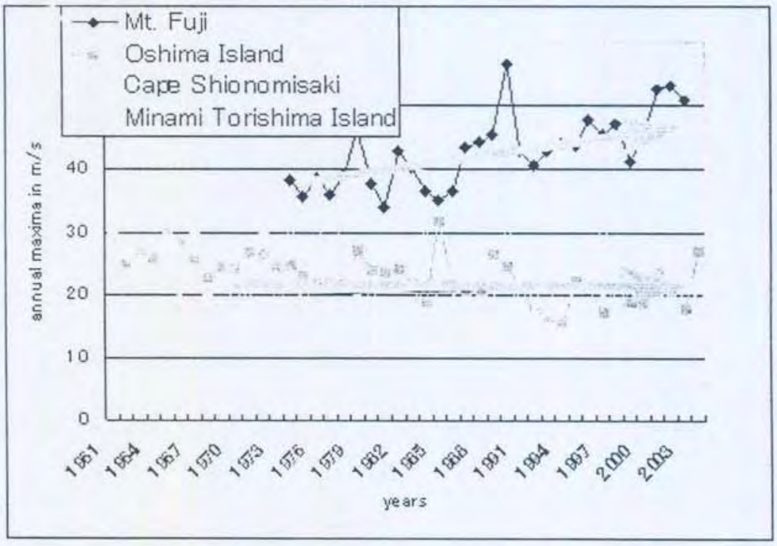

Fig. 24. Annual maxima of observed wind speed at cape, islands and Mt. Fuji

In Figures 23 and 24 it can be found that observations in urban are decrease slightly as years, although situations seems to be different at capes, islands and Mt. Fuji. Although it is not clear what this reason is, it is obvious that there exist some issues to disturb statistical homogeneity in the population of annual maxima of strong wind. Referring this fact, the statistical typhoon simulation is introduced as one of methods to realize many-year's homogeneous sampling. This is a method to simulate typhoon tracks basing on statistical information in every latitude and longitude meshes in occurrence, development or decay, direction of movement and speed of movement of virtual typhoons [7]. Although this is only one of many methods to get the design wind speed, both of typhoon simulation by CFD and this statistical approach will come to be widely applied.

6. Concluding remarks

Although there are many occasions to discuss structural aerodynamics at wind tunnels, the chain link of structural response in Figure 1 is very important point in the wind resistant design. To realize its balanced development, continuous investigations are carried out and some new approaches are introduced in this paper. To construct long-span bridges, it is very important to introduce careful wind resistant design backed up by reliable wind tunnel experiment, careful structural analysis and meteorological discussions. More reasonable the long-span structure design becomes, more frequently wind resistant design works will be required.

Reference

[1] Farquharson, F.B. et. al., Aerodynamic stability of suspension bridges with special reference to the Tacoma Narrows Bridge, Bulletin of Univ. of Washington Engineering. Exp. Station No. 116, 1949-1954.

[2] Wallace, A.A.C., Wind influence on Kessock Bridge, Eng. Struct., vol.7, Jan. 1985.

[3] Katsuura, H., Makuta, H., Sato, H., Y.Yoshida, Honda, A., Fujino,Y., Vortex-induced Oscillation of Trans-Tokyo Bay Highway Bridge, Proceedings of the 8th U.S. National conference on wind engineering, on CDROM, June 1997.

[4] Simiu, E., Scanlan, R. H., Winds Effects on Structures: Fundamentals and Applications to Design, 3rd Edition, Wiley, August 1996

[5] Miyata, T., Fujisawa, N. and Yamada H., Long-span bridges and aerodynamics, Springer, March 1999.

[6] Japan Road Association, Wind Resistant Design Manuals for Highway Bridges, Maruzen, March 1992.

[7] Miyata, T. Yamada, H. Katsuchi H. And Nishiwaki, M., Incorporation of sea-temperature to typhoon simulation, Proc. of 17th National Symposium on Wind Engineering, pp. 29-34, December 2002.

Japan-Bangladesh Joint Seminar on Advances in Bridge Engineering
Dhaka, Bangladesh. 10 August 2005

ISBN: 984-32-2520-6

A method for observing weights of trucks running on a bridge

Eiki Yamaguchi*, Kazushi Matsuo

Department of Civil Engineering
Kyushu Institute of Technology, Kitakyushu, Fukuoka 804-8550, Japan

Abstract

The development of the weigh-in-motion techniques that give the weights of running trucks without disturbing traffic flow has attracted many researchers. We employ herein a technique based on the deformation of a steel girder. For the accuracy of this technique, the usage of a short simply-supported straight steel bridge is preferred. However, that kind of bridge is not always available. Actually, the highway of our interest does not have steel bridges except a continuous skew steel-plate-girder bridge. Because of this, we conduct running tests with three trucks of known weights very carefully. The present technique then proves to be satisfactory, yielding the weights of running trucks with about 11% error at most. Thus, we may conclude that a continuous skew steel-plate-girder bridge can be used for the weigh-in-motion.

1. Introduction

For carrying out a good maintenance work of an existing bridge, it is important to know actual traffic loads acting on the bridge. To this end, a technique to measure the weight of a running truck without disturbing traffic flow is needed. Such a technique is known as the weigh-in-motion and various efforts have been made. One of the weigh-in-motion techniques is based on the deformation of a bridge and is called the bridge-weigh-in-motion. The technique was developed by Moses (1979) and is relatively inexpensive so that it has been explored much in Japan (Matsui & El-Hakim 1989, Ojio et al. 2001, Miki et al. 2001, Ikeda et al. 2002, Ishio et al. 2002).

For a good accuracy in the bridge-weigh-in motion, it is essential to use a bridge whose deformation is not so small and not complicated either, and on which multiple trucks do not run at the same time. Thus, a short, simply-supported steel bridge is idealistic. However, this type of bridge is not always available in the highway of interest.

* E-mail: yamaguch@civil.kyutech.ac.jp

We have encountered such a situation actually when we initiated a project to figure out actual truck loads in a national highway near Fukuoka City, Japan. There is only one steel bridge in the area and it is a continuous skew steel-plate-girder bridge, far from an ideal structure. To the best knowledge of authors, the accuracy of the weigh-in-motion using such a type of bridge has not been known well. Therefore, we first study the accuracy that we can achieve by this bridge. In this paper, we present the result of this study.

2. Bridge-weigh-in-motion

The truck weight is evaluated from the deformation of a bridge due to a truck running upon it. The technique used herein follows specifically the one employed by Miki et al. (2001). The outline of their method is described in what follows.

When the location of an axle of a truck at time t is denoted by x_n, strain at Point i at this time is given by

$$\varepsilon_i(t) = \sum_{n=1}^{N_A} A_n\, I_i\big(x_n(t)\big) \tag{1}$$

where N_A is the number of axles, A_n is the weight of the axle at x_n, and I_i is the influence line corresponding to $\varepsilon_i(t)$ that is the normal strain in the direction of the bridge axis at the bottom flange at Point i at time t.

Letting $\varepsilon_i^*(t)$ denote the measured strain, the following equation can be set up:

$$E = \sum_{i=1}^{N_M} \sum_{j=1}^{N_S} \left[\varepsilon_i(j\Delta t) - \varepsilon_i^*(j\Delta t)\right]^2 \tag{2}$$

where N_S is the number of strain measurements for each of which the location of the axle is different; N_M is the number of strain-measuring points; Δt is the time difference between two consecutive strain measurements. The values of A_n that minimize E would give the axle weight we look for. To be specific, the stationary condition of $\partial E/\partial A_n = 0$ yields the values of A_n. It may be understood from Equations (1) and (2) that the final equations to be solved would be a set of simultaneous equations for A_n. Once the axle weights are obtained, we can compute the gross weight of the truck by simply summing up the axle weights.

For this method to be effective, the influence lines and the positions of the axles must be known. The influence line is determined by running a truck of known axle weight on the bridge. For the determination of the positions of the axles, we measure the strains at several vertical stiffeners in addition to the strains at the bottom flanges. The strain at the vertical stiffener is sensitive to the axle load, so that without much difficulty we can identify when the truck passes right above the vertical stiffener. Knowing the distance between stiffeners, then we can evaluate the speed of the truck and the distance between the axles. Thus the position of the truck at any time can be estimated.

3. Outline of bridge and strain measurement

The bridge used in this study is presented schematically in Figure 1. The bridge is a two-span continuous steel bridge, having 5 main plate girders. The bridge axis is not straight but skewed. Therefore, the deformation of the bridge may be quite complicated. The bridge carries two traffic lanes, one for each direction. A sidewalk exists above the G5 girder.

Figure 1(b) shows the positions of the strain measurements: the circles indicate the positions in the bottom flange while the solid circles correspond to the positions in the vertical stiffeners.

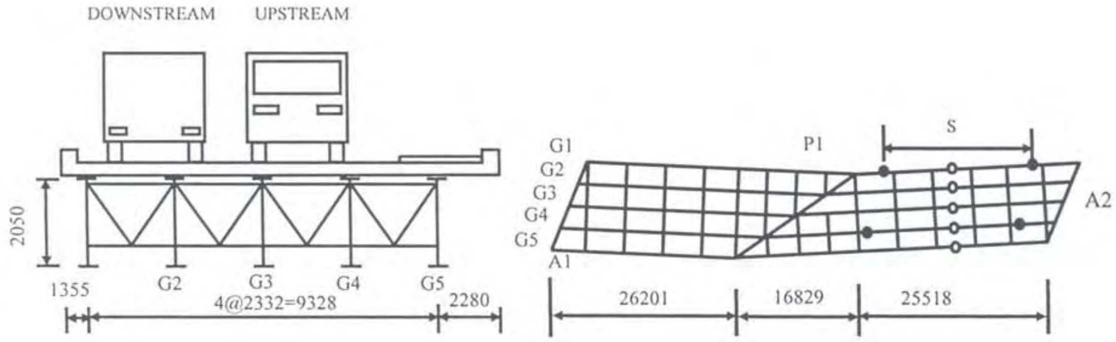

(a) Cross section (b) Top view

Fig.1. Schematic of bridge

4. Running tests

We conduct running tests with three trucks of known weights: Truck A-C are 20.35 tf, 20.00 tf and 16.39 tf in weight, respectively. The following five running patterns are employed:

- Pattern 1: Only one truck runs
- Pattern 2: One truck runs right after the other
- Pattern 3: Two trucks run in different directions
- Pattern 4: One truck runs right after another while the other runs in the opposite direction
- Pattern 5: A truck runs in an ordinary traffic flow

Patterns 1 to 4 are illustrated in Figure 2. For Pattern 1 to 4, the traffic is controlled so that no traffic except our trucks runs on the bridge during the test.

The influence of the speed is also investigated. Multiple tests are conducted under the same condition, since the scatter of the measured data is expected in this kind of test. Altogether the number of the running tests amounts to 76.

5. Evaluation of truck weights

Based on the strain measurement of Pattern 1, the influence lines are constructed. There are several sets of measurements even for Pattern 1, but they yield the influence lines very similar to each other. The strain measured in the G5 girder is much smaller than those in the other girders. Hence, the strain in the G5 girder is ignored.

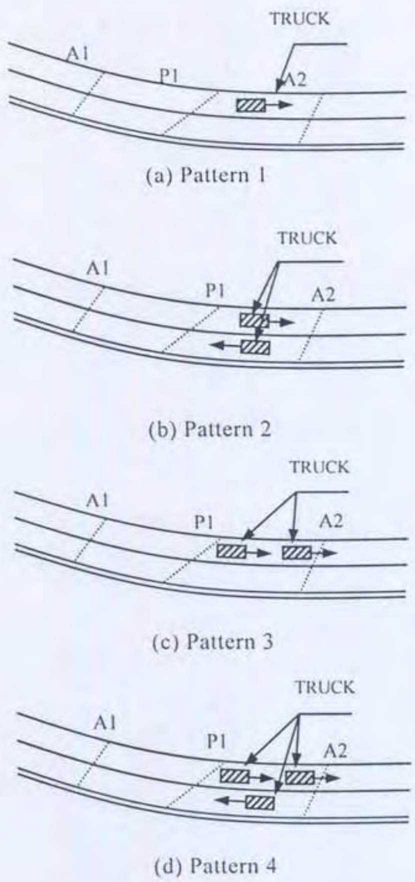

Fig. 2. Running test patterns

Figure 3 (a) presents the result of the bridge-weigh-in-motion for Pattern 1. The accuracy varies, but the error is no more than 5.4%. It can be also observed that the influence of speed is insignificant. Figures 3 (b) to (d) give the result of the bridge-weigh-in-motion for Patterns 2 to 4. In most cases, the error is less than 10%. In 2 tests of Pattern 2 and one test of Pattern 3 the error exceeds 10%: the maximum error is found to be11.6%. In all the tests of Pattern 5, the error is less than 10%. Therefore, we may conclude that the accuracy of the bridge-weigh-in-motion by the present bridge is satisfactory in all the practical situations.

6. Concluding remarks

The bridge-weigh-in-motion technique is applied to a continuous skew steel-plate-girder bridge. Through quite a few running tests, we have made sure that the technique works satisfactorily for all practical purposes. Hence, we may conclude that the bridge-weigh-in-motion can be applied even when we have no other choice but to use a complicated bridge such as this continuous skew steel-plate-girder bridge.

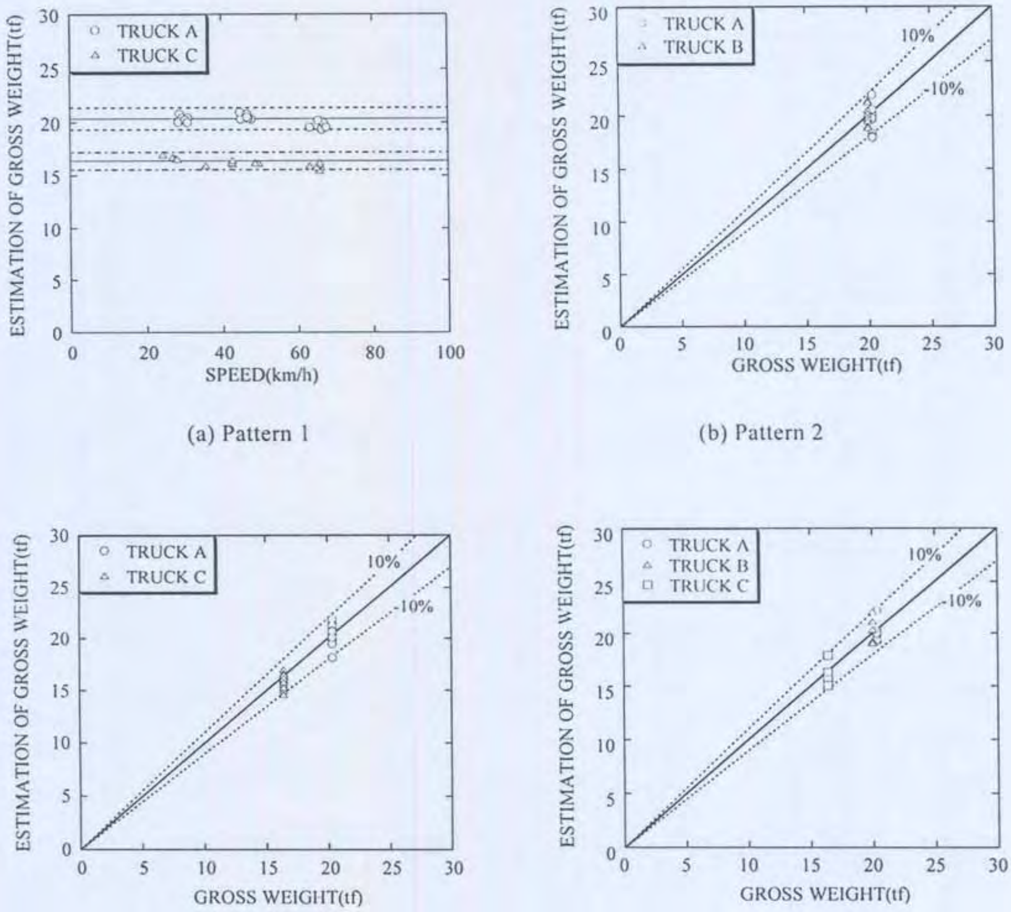

(a) Pattern 1

(b) Pattern 2

(c) Pattern 3

(d) Pattern 4

Fig. 3. Evaluation of truck weight

Acknowledgements
The present research was partially supported by the Ministry of Education, Science, Sports and Culture of Japan, Grant-in-Aid for Scientific Research (A) (No. 13355020). The support is gratefully acknowledged.

References

Ikeda, K., Yoneda, M., Kimura, T. & Edamoto, K. 2002. A fundamental study on traffic load monitoring system using genetic algorithm on highway bridges. Proc. of 57th Annual Conference of The Japan Society of Civil Engineers: 1101-1102.

Ishio, M., Nakatani, S., Tamakoshi, T. & Nakasu, K. 2002. About the WIM system using the influence line. Proc. of 57th Annual Conference of The Japan Society of Civil Engineers: 1447-1448.

Matsui, S. & El-Hkim, A. 1989. Estimation of axle loads of vehicles by crack opening of RC slab. Journal of Structural Engineering 35A: 407-418.

Miki, C., Mizunoue, T. & Kobayashi, Y. 2001. Monitoring system of bridge performance with fiber-optic communications, Journal of Construction Management and Engineering, 686/VI-52: 31-40.
Mose, F. 1979. Weigh-In-Motion system using instrumented bridges. Transportation Engineering Journal of ASCE 105 (TE3): 233-249.
Ojio, T., Yamada, K. & Kobayashi, N. 2001. Development of bridge weigh-in-motion system using stringers of steel plate girder bridge. Journal of Structural Engineering 47A: 108-1092.

ISBN 984-32-2520-6